

The Sensitivity of The Measurement Of Pollution In The Troposphere
(MOPITT) Retrievals of Carbon Monoxide to the Lowermost
Troposphere

Thesis submitted for the degree of
Doctor of Philosophy
at the University of Leicester

by

Vijay Punjaji Kanawade BSc MSc MTech
Department of Physics and Astronomy
University of Leicester, England

January 2010



Dedication

This thesis is dedicated to my lovely wife (Shilpa) for her boundless love and support.
This thesis is also dedicated to my supervisors for their continuous support and encouragement.

Vijay Kanawade

January 2010

© Vijay Kanawade, January 2010

This thesis is copyright material and no quotation from it may be published
without proper acknowledgement.

Declaration

I hereby declare that no part of this thesis has been previously submitted to this or any other University as part of the requirement for a higher degree. The work described herein was conducted by the undersigned except for contributions from colleagues as acknowledged in the text.

Vijay Kanawade

January 2010

The Sensitivity of The Measurement Of Pollution In The Troposphere (MOPITT)
Retrievals of Carbon Monoxide to the Lowermost Troposphere

Vijay Kanawade

ABSTRACT

In this thesis, the measurements of carbon monoxide (CO) obtained from an nadir sounding Measurement Of Pollution In The troposphere (MOPITT) instrument are used. Atmospheric CO is one of the most abundant and widely distributed air pollutant and is a very important indirect greenhouse gas via its reaction with the OH radical which in turn controls the oxidising capacity of the troposphere. In this thesis, the MOPITT Level 2 Version 3 (L2V3) retrieved CO data is primarily used and compared with recently released (April 2009) Level 2 Version 4 (L2V4) retrieved CO data to examine the potential of the MOPITT instrument to differentiate emission features in the lowermost troposphere including mega-cities. This study develops a novel robust methodology using day-night difference profile simulations to examine the ability of the instrument to identify CO enhancements in the lowermost layer of the atmosphere using ‘typical’ averaging kernels. More realistic CO profiles from the TOMCAT model are then used to validate this methodology. The day-night difference simulations are performed for the Indian subcontinent. It is shown that for L2V3, the daytime and nighttime degrees of freedom for a signal (DOFS) exhibit a bi-modal distribution for all selected Indian regions. The L2V3 simulation study clearly demonstrates, for higher DOFS, that $\text{day}_{700}\text{-night}_{700}$ differences give a closer differentiation of lowermost CO than other measures for MOPITT data, the first time that this has been processed. For L2V4, similar DOFS distributions are observed for the Indian subcontinent. The L2V4 simulation study also demonstrates for the first time that $\text{day}_{850}\text{-night}_{700}$ CO differences give a closer differentiation of lowermost CO by taking account of L2V4 day and night a priori mixing ratios. Finally, the methodologies developed in chapter 3 and 4 are applied to identify spatially isolated signals of lowermost CO for one year of data i.e. 2007. Features associated with nearly 100 cities are identified, the use of thresholds for higher DOFS retrievals and the use of non-surface retrieval levels with less tie to a priori. The significant step forward being consistent day-night differences for two different analyses (L2V3, L2V4).

ACKNOWLEDGEMENTS

Firstly and foremost, I would like to thank my supervisors Prof. John J. Remedios and Prof. Paul S. Monks for giving me the opportunity to conduct this work and for their support, encouragement, unwavering dedication and thoughtful input during the course of this study. Special thanks must go to my immediate supervisor, Prof. John J. Remedios, for many insightful discussions and for his contribution to this work and much appreciated guidance.

My immense gratitude also goes to the SPARTAN Programme (Centre of Excellence for Space, Planetary and Astrophysics Research Training and Networking), which provided the fellowship for this doctorate study, through the European Commission Maire Curie Actions (Contract number MEST-CT-2004-007512).

I also would like to thank the Earth Observation Science (EOS) crew for making me feel part of the team. A special mention must go to Dr. Gary Corlett, Dr. Dave Moore, Dr. Hartmut Boesch, Dr. Roland Leigh, and Dr. Harjinder Sembhi who all have been an incredibly useful source of information for topics specifically related to this study as well as for general advice. I also would like to thank Dr. Robert Parker and Mr. Samuel Illingworth for their help on my unique IDL programming queries, and there are a few other past and present members of the EOS group that I would like to thank, including Dr. Lizzie Noyes, for her excellent IDL programming lectures in EOS group meetings, and also my fellow EOS PhD students.

A very special acknowledgement goes to my brothers Satish and Prakash for being there with me always. I also would like to thank my lovely parents for their continual help, support and encouragement towards their children forever.

And to all of those who have contributed, either directly or indirectly, to the successful completion of this thesis, I say God bless you all. Finally, I thank God for life, excellent health, peace and a sound mind.

Vijay Kanawade

Table of Contents

Table of Contents	I
1 Measuring Carbon Monoxide in the Troposphere	1
1.1 Introduction	1
1.2 The Importance of CO in the Troposphere	2
1.2.1 CO Sources	3
1.2.1.1 Fossil Fuel and Biofuel Burning	3
1.2.1.2 Biomass Burning	3
1.2.1.3 Oxidation of Methane and Non-methane Hydrocarbons (NMHC)	4
1.2.1.4 Oceans	5
1.2.1.5 Plants	6
1.2.2 CO Sinks	6
1.2.2.1 Hydroxyl Radical (OH) Chemistry	6
1.2.2.2 Soil Uptake	6
1.2.3 Global Budget of CO	7
1.3 CO Observations in the Troposphere	9
1.3.1 Ground-based Measurements of CO	9
1.3.2 Satellite Sensing of Tropospheric CO	14
1.4 Summary and Objectives of Thesis	18
2 The MOPITT Instrument	20
2.1 Introduction	20
2.2 Observational Techniques	21
2.2.1 Thermal Infrared Techniques	21
2.3 The Radiative Transfer Equation	22
2.3.1 Nadir Infrared Sounding	26
2.4 The MOPITT Concept	27
2.4.1 The MOPITT Technique	28
2.4.2 Gas Correlation Radiometry	29
2.4.3 Retrieval Theory	32
2.4.3.1 The State and Measurement Vectors	32
2.4.3.2 The Forward Model	33
2.4.3.3 The Weighting Function Matrix	33

2.4.4	MOPITT L2V3 Operational Retrievals	34
2.4.4.1	Forward Modelling	34
2.4.4.2	Retrieval Algorithm Formulation	36
2.4.4.3	MOPITT V3 A Priori	38
2.4.4.4	Standard Averaging Kernels	40
2.4.4.5	Degrees Of Freedom for a Signal (DOFS)	41
2.4.4.6	Percent A Priori CO Mixing Ratio	43
2.5	MOPITT Level 2 Version 3 (L2V3) Product Validation	44
2.6	Summary of Chapter 2	49
3	Sensitivity of MOPITT Observations of Tropospheric CO	51
3.1	Introduction	51
3.2	The Methodology	52
3.3	Understanding MOPITT Sensitivity to Tropospheric CO	53
3.3.1	The Role of Thermal Contrast	54
3.3.1.1	Thermal Contrast Over India	54
3.3.2	MOPITT L2V3 Diagnostics Analysis	57
3.3.2.1	Retrieved CO Errors	57
3.3.2.2	Percent Apriori CO Mixing Ratios	58
3.3.2.3	Averaging Kernels	61
3.3.2.4	Degrees of Freedom for a Signal	63
3.3.3	Selection Criteria for a ‘Typical’ Averaging Kernel	67
3.4	Examination of Day-Night Differences in MOPITT L2V3 CO Data	69
3.4.1	Day-Night Difference CO Maps	69
3.4.2	L2V3 Profile Simulation - A Case Study of Bihar	75
3.4.2.1	Mean L2V3 CO Profile	75
3.4.2.2	L2V3 Simulation	77
3.4.2.3	TOMCAT Model CO Profile Simulation	85
3.4.3	L2V3 Profile Simulation - A Case Study of Delhi	88
3.4.3.1	Mean L2V3 CO Profile	88
3.4.3.2	L2V3 Simulation	89
3.4.3.3	TOMCAT Model CO Profile Simulation	96
3.4.4	L2V3 Profile Simulation - A Case Study of Mumbai	98
3.4.4.1	Mean L2V3 CO Profile	98
3.4.4.2	L2V3 Simulation	100
3.4.4.3	TOMCAT Model CO Profile Simulation	107
3.4.5	L2V3 Profile Simulation - A Case Study of Coimbatore	110
3.4.5.1	Mean L2V3 CO Profile	110
3.4.5.2	L2V3 Simulation	111
3.4.5.3	TOMCAT Model CO Profile Simulation	117
3.5	CO Over Indian Subcontinent	120
3.5.1	Spatial Distribution of CO	120
3.5.2	Correlation Results	125
3.6	Evaluation of a Robust Methodology	128
3.7	Summary of Chapter 3	132

4	MOPITT CO Profile Information Content: Comparison Between L2V3 and L2V4 Retrievals	134
4.1	Introduction	134
4.2	MOPITT Level 2 Products	135
4.2.1	Review of L2V3 Product	135
4.2.2	Features of L2V4 Product	136
4.3	L2V4 Product Diagnostics	138
4.3.1	L2V4 A Priori CO	138
4.3.2	L2V4 Retrieval Averaging Kernels	142
4.3.3	L2V4 Degrees Of Freedom for a Signal	143
4.4	Methodology	144
4.5	Examination of Day-Night Differences : MOPITT L2V3 Vs L2V4 . .	144
4.5.1	Day-Night Difference CO Maps	144
4.5.2	A Case Study of Bihar	150
4.5.2.1	L2V3 and L2V4 Simulations	150
4.5.2.2	TOMCAT Model CO Profile Simulation	161
4.5.3	A Case Study of Delhi	166
4.5.3.1	L2V3 and L2V4 Simulations	166
4.5.3.2	TOMCAT Model CO Profile Simulation	176
4.5.4	A Case Study of Mumbai	180
4.5.4.1	L2V3 and L2V4 Simulations	180
4.5.4.2	TOMCAT Model CO Profile Simulation	190
4.6	Spatial Distribution of CO	194
4.7	Summary of Chapter 4	199
5	Signatures of CO from Megacities	200
5.1	Introduction	200
5.2	Methodology	202
5.3	Global Distribution of CO	204
5.4	CO from Urban Centres	208
5.4.1	A City-Specific Analysis	208
5.4.2	Global Analysis	213
5.5	Summary of Chapter 5	218
6	Conclusions and Future Scope	220
6.1	Conclusions	221
6.1.1	Chapter 3: Sensitivity of MOPITT Observations of Tropospheric CO	221
6.1.2	Chapter 4: MOPITT L2V3 and L2V4 Simulation Comparison Study	223
6.1.3	Chapter 5: Signature of CO from Megacities	225
6.2	Future Scope	227

7	Appendix-I	228
7.1	A Case Study of Mexico City	238
7.1.1	L2V3 and L2V4 Simulations	238
7.1.2	TOMCAT Model CO Profile Simulation	246
7.2	A Case Study of Johannesburg	249
7.2.1	L2V3 and L2V4 Simulations	249
7.2.2	TOMCAT Model CO Profile Simulation	256

List of Figures

1.1	The current WMO WDCGG global CO observation network [WMO, March 2009].	10
1.2	Average seasonal cycles for each 30° latitudinal zone from which the long-term trends were subtracted [WMO, March 2009].	11
1.3	Top panel: Variation of zonally averaged monthly mean CO mixing ratios, middle panel: deseasonalised CO mixing ratios, and bottom panel: CO Growth rates [WMO, March 2009].	12
1.4	Near-global distribution of MAPS CO mixing ratios averaged over 5° latitude \times 5° longitude areas during (a) April 1994 and (b) October 1994 (Adapted from Conrad et al. [1999]).	16
2.1	Configuration of the optical path and thickness	25
2.2	MOPITT instrument scanning the atmosphere in nadir modes (Image: NASA).	27
2.3	Showing (a) the MOPITT instrument layout, (b) calibration photo, (c) Terra space-craft showing onboard instruments including MOPITT, and (d) the MOPITT instrument scan pattern [Drummond, 1992].	28
2.4	Schematic diagram of the spectral bands used for MOPITT instrument [Drummond, 1992].	29
2.5	A basic gas correlation radiometry	30
2.6	Operation of a correlation spectrometer in spectral space. Panel (a) shows low cell pressure ($\tau\mu_l$) and high cell pressure ($\tau\mu_h$) curves. The filter profile is illustrated by the EDT curve in (b), which is the difference of the system transmission at low cell pressure and at high cell pressure. Panel (c) shows the advantage of gas correlation in discriminating against interference spectral lines [Drummond, 1992].	31

2.7	Shows weighting functions for the different cell pressures of the 6 CO channels used in operational retrievals [Deeter et al., 2003].	35
2.8	MOPITT L2V3 a priori profile.	39
2.9	Mean averaging kernels obtained by averaging all daytime and nighttime averaging kernels separately on May 01, 2006 (a) in the box defined by 20°N, 30°N, 10°E, and 25°E (over Libyan desert) and (b) in the box defined by 15°S, 30°S, 5°W, and 20°W (over South Atlantic).	40
2.10	Degrees Of Freedom for Signal for September, 2006 for (a) Daytime and (b) Nighttime observations.	42
2.11	Percent a priori CO mixing ratio gridded on 1.0 deg. at 350 hPa for September, 2006 for (a) Daytime and (b) Nighttime observations.	43
2.12	Left panel shows NOAA routine sampling sites and field campaigns and right panel shows individual profile locations and regional groupings (Adapted from Emmons et al. [2009]).	47
2.13	Right panel: Bias between MOPITT and aircraft in situ measurements for the 700 hPa retrieval for each year, sorted by NOAA site, Field Campaign or MOZAIC geographical region. Each symbol and error bar indicates the mean and standard deviation of the biases for each site or region; Left panel: Same as right panel, for the column retrieval (Adapted from Emmons et al. [2009]).	48
3.1	(a) MOPITT L2V3 mean standard (dashed lines) and grid-normalised averaging kernels (solid lines) for May 2004 over 24 to 27°N and 75 to 85°E; (b) Distribution of the surface value of MOPITT grid-normalised averaging kernel at 850 hPa for May 2004. (Adapted from Kar et al. [2008]).	53
3.2	(a) Monthly averaged thermal contrast derived from ECMWF temperature fields, over India, at 06 UTC and 18 UTC, for May 2007 (left) and December 2007 (right); (b) same as (a) except for PBL height.	55
3.3	Monthly mean spatial distribution of the thermal contrast derived from ECMWF temperature fields over India at (a) 06 UTC and (b) 18 UTC; (c) and (d) shows mean temporal variation of the thermal contrast for each selected region over Indian subcontinent at 06 UTC and 18 UTC.	56

3.4	(a) MOPITT L2V3 850 hPa retrieved 0.5 degree gridded daytime CO mixing ratio errors, over India, for May 2007; (b) same as (a) except for December 2007; (c) Histogram of daytime CO mixing ratio errors, over Bihar box (shown by rectangle), for May 2007; (d) same as (c) except for December 2007.	58
3.5	(a) MOPITT L2V3 850 hPa retrieved 0.5 degree gridded daytime Percent a priori CO mixing ratio, over India, for May 2007; (b) same as (a) except for December 2007; (c) Histogram for 850 hPa retrieved daytime Percent a priori CO mixing ratio, over Bihar box, for May 2007; (d) same as (c) except for December 2007.	59
3.6	MOPITT L2V3 retrieved errors versus percent a priori CO mixing ratio, over Bihar box, for May 2007.	60
3.7	Same as Fig. 3.6 except for December 2007.	60
3.8	(a) MOPITT retrieved Averaging Kernel profiles as a function of DOFS, over Bihar region, for May 2007; (b) Same as (a) except for December 2007.	62
3.9	(a) MOPITT L2V3 0.5 degree gridded daytime DOFS, over India, for May 2007; (b) same as (a) except for December 2007; (c) Histogram for daytime and nighttime DOFS, over Bihar box, for May 2007; (d) same as (c) except for December 2007.	64
3.10	(a) MOPITT L2V3 DOFS versus percent a priori CO mixing ratio at 7 retrieval levels, over Bihar region, for May 2007; (b) Same as (a) except for December 2007.	66
3.11	(a) MOPITT L2V3 Selected daytime ‘typical’ AK profile, over Bihar box, for May 2007; (b) Same as (a) except for December 2007; (c) Selected nighttime ‘typical’ AK profile, over Bihar box, for May 2007; (d) Same as (c) except for December 2007.	67
3.12	(a) SCIAMACHY 0.5 degree gridded NO ₂ total column, over India, for May 2007; (b) Same as (a) except for December 2007.	70

3.13	(a) MOPITT L2V3 0.5 degree gridded daytime 850 hPa CO mixing ratios for May 2007; (b) MOPITT L2V3 0.5 degree gridded nighttime 850 hPa CO mixing ratios for May 2007; (c) MOPITT L2V3 0.5 degree gridded 850 hPa day-night CO mixing ratio differences for May 2007; (d) Same as (a) except for December 2007; (e) Same as (b) except for December 2007; (f) Same as (c) except for December 2007.	71
3.14	(a) MOPITT L2V3 0.5 degree gridded daytime CO total column for May 2007; (b) MOPITT L2V3 0.5 degree gridded nighttime CO total column for May 2007; (c) MOPITT L2V3 0.5 degree gridded day-night CO total column differences for May 2007; (d) Same as (a) except for December 2007; (e) Same as (b) except for December 2007; (f) Same as (c) except for December 2007.	73
3.15	Correlation results, over India, in the month of (a-c) May and (d-f) December.	74
3.16	(a) MOPITT L2V3 retrieved mean daytime and nighttime CO profiles, over Bihar box, for May 2007; (b) Mean day-night difference CO profile, over Bihar box, for combination of LDD and HDD; (c) Same as (a) except for December 2007; (d) Same as (c) except for December 2007.	76
3.17	(a) MOPITT L2V3 ‘simulated’ daytime and nighttime CO profiles for HDD _{peak} , over Bihar, for May 2007; (b) Same as (a) except for December 2007. The green, black, cyan, blue, and red line indicates the considered sample CO profile, perturbed CO profile, a priori CO profile, ‘simulated’ day CO profile, and ‘simulated’ night CO profile. The green, black, cyan, blue, and red triangles show calculated total column values for corresponding CO VMR profiles (shown on upper horizontal scale).	79

3.18	MOPITT L2V3 ‘simulated’ day-night difference CO profiles for LDD_{peak} and HDD_{peak} , over Bihar, for May 2007; (b) Same as (a) except for December 2007. The diamond solid and dash-dotted lines indicates day and night CO ratio (850/350) term respectively. The ratio scale shown as top x-axis. The dark grey coloured lines represents day_{850} - $night_{700}$ CO difference profiles for LDD_{peak} and HDD_{peak} . Note that the key result is depicted in Fig. 3.19.	81
3.19	Key result from Fig. 3.18.	82
3.20	MOPITT L2V3 calculated total column values for i) a priori CO profile (cyan), ii) 7 individual sample profiles (green), iii) 7 individual perturbed sample profile (black), and iv) 7 individual simulated day (blue) and night (red) CO profiles, over Bihar, for May 2007; (b) Same as (a) except for December 2007. Note that these are not considered as profiles. For proper understanding the total column values plotted at corresponding perturbed retrieval level (layer) for each CO vmr profile.	84
3.21	MOPITT L2V3 calculated total column tests for day and night simulated profiles in the month of (a) May and (b) December. Note that these are not considered as profiles and are in arbitrary unit.	84
3.22	Selected TOMCAT model CO profiles, over Bihar box, for May 2004 (blue) and December 2004 (red).	86
3.23	‘Simulated’ daytime and nighttime CO profiles for TOMCAT model selected base CO profile, over Bihar, for May (top panel) and December (bottom panel) 2007.	87
3.24	(a) MOPITT L2V3 ‘simulated’ day-night difference CO profile for HDD_{peak} , over Bihar for TOMCAT, for May 2007; (b) Same as (a) except for December 2007.	87
3.25	(a) MOPITT L2V3 retrieved mean daytime and nighttime CO profiles, over Delhi box, for May 2007; (b) Mean day-night difference CO profile, over Delhi box, for combination of LDD and HDD; (c) Same as (a) except for December 2007; (d) Same as (b) except for December 2007.	89

3.26	(a) MOPITT L2V3 Selected daytime ‘typical’ AK profile, over Delhi box, for May 2007; (b) Selected nighttime ‘typical’ AK profile, over Delhi box, for May 2007; (c) Same as (a) except for December 2007; (d) Same as (b) except for December 2007.	90
3.27	(a) MOPITT L2V3 ‘simulated’ daytime and nighttime CO profiles for HDD_{peak} , over Delhi, for May 2007; (b) Same as (a) except for December 2007. The green (black, cyan, blue, and red) line indicates the considered sample CO profile (perturbed CO profile, a priori CO profile, ‘simulated’ day CO profile, and ‘simulated’ night CO profile). The green (black, cyan, blue, and red) triangles show calculated total column values for considered sample profile (perturbed sample profile, a priori profile, ‘simulated’ daytime profile, and ‘simulated’ nighttime profile).	91
3.28	MOPITT L2V3 ‘simulated’ day-night difference CO profiles for LDD_{peak} and HDD_{peak} , over Delhi, for May 2007; (b) Same as (a) except for December 2007. The diamond solid and dash-dotted lines indicates day and night CO ratio (850/350) term respectively. The ratio scale shown as top x-axis. The dark grey coloured lines represents day_{850} - $night_{700}$ CO difference profiles for LDD_{peak} and HDD_{peak} . Note that the key result is depicted in Fig. 3.29.	93
3.29	(a)Key result from Fig. 3.28 for May 2007; (b) Same as (a) except for December 2007.	94
3.30	(a)MOPITT L2V3 calculated total column values for May 2007; i) a priori CO profile (cyan), ii) 7 individual sample profiles (green), iii) 7 individual perturbed sample profile (black), and iv) 7 individual simulated day (blue) and night (red) CO profiles, over Delhi, for May 2007; (b) Same as (a) except for December 2007. Note that these are not considered as profiles. For proper understanding the total column values plotted at corresponding perturbed retrieval level (layer) for each CO vmr profile.	95
3.31	MOPITT L2V3 calculated total column tests for day and night simulated profiles in the month of (a) May and (b) December.	96

3.32	Selected TOMCAT model CO profiles, over Delhi box, for May 2004 (blue) and December 2004 (red) for the given latitude and longitude co-ordinate.	97
3.33	(a)‘Simulated’ daytime and nighttime CO profiles for TOMCAT model selected base CO profile, over Delhi, for May (top panel) 2007; (b) Same as (a) except for December (bottom panel) 2007.	98
3.34	(a) MOPITT L2V3 ‘simulated’ day-night difference CO profile for HDD _{peak} , over Delhi, for May 2007; (b) Same as (a) except for December 2007.	99
3.35	(a) MOPITT L2V3 retrieved mean daytime and nighttime CO profiles, over Mumbai box, for May 2007; (b) Mean day-night difference CO profile, over Mumbai box, for combination of LDD and HDD; (c) Same as (a) except for December 2007; (d) Same as (b) except for December 2007.	100
3.36	(a) MOPITT L2V3 Selected daytime ‘typical’ AK profile, over Mumbai box, for May 2007; (b) Same as (a) except for December 2007; (c) Selected nighttime ‘typical’ AK profile, over Mumbai box, for May 2007; (d) Same as (c) except for December 2007.	101
3.37	(a) MOPITT L2V3 ‘simulated’ daytime and nighttime CO profiles for HDD _{peak} , over Mumbai, for May 2007; (b) Same as (a) except for December 2007. The green (black, cyan, blue, and red) line indicates the considered sample CO profile (perturbed CO profile, a priori CO profile, ‘simulated’ day CO profile, and ‘simulated’ night CO profile). The green (black, cyan, blue, and red) triangles show calculated total column values for considered sample profile (perturbed sample profile, a priori profile, ‘simulated’ daytime profile, and ‘simulated’ nighttime profile).	102

3.38	MOPITT L2V3 ‘simulated’ day-night difference CO profiles for LDD_{peak} and HDD_{peak} , over Mumbai, for May 2007; (b) Same as (a) except for December 2007. The diamond symbol solid and dash-dotted lines indicates day and night CO ratio (850/350) term respectively. The ratio indicated by top x-axis. The dark grey coloured lines represents day_{850} - $night_{700}$ CO difference profiles for LDD_{peak} and HDD_{peak} . Note that the key result is depicted in Fig. 3.39.	103
3.39	Key result from Fig. 3.38.	105
3.40	MOPITT L2V3 calculated total column values for i) a priori CO profile (cyan), ii) 7 individual sample profiles (green), iii) 7 individual perturbed sample profile (black), and iv) 7 individual simulated day (blue) and night (red) CO profiles, over Mumbai, for May 2007; (b) Same as (a) except for December 2007. Note that these are not considered as profiles. For proper understanding the total column values plotted at corresponding perturbed retrieval level (layer) for corresponding perturbed or simulated profile.	106
3.41	MOPITT L2V3 calculated total column tests for day and night simulated profiles in the month of (a) May and (b) December.	107
3.42	Selected TOMCAT model CO profiles, over Mumbai box, for May 2004 (blue) and December 2004 (red) for the given latitude and longitude co-ordinate.	107
3.43	(a) ‘Simulated’ daytime and nighttime CO profiles for TOMCAT model selected base CO profile, over Mumbai, for May 2007; (b) Same as (a) except for December 2007.	108
3.44	(a) MOPITT L2V3 ‘simulated’ day-night difference CO profile for HDD_{peak} , over Mumbai, for May 2007; (b) Same as (a) except for December 2007.	109
3.45	(a) MOPITT L2V3 retrieved mean daytime and nighttime CO profiles, over Coimbatore box, for May 2007; (b) Mean day-night difference CO profile, over Coimbatore box, for combination of LDD and HDD; (c) Same as (a) except for December 2007; (d) Same as (b) except for December 2007.	111

3.46	(a) MOPITT L2V3 Selected daytime ‘typical’ AK profile, over Coimbatore box, for May 2007; (b) Same as (a) except for December 2007; (c) Selected nighttime ‘typical’ AK profile, over Coimbatore box, for May 2007; (d) Same as (c) except for December 2007.	112
3.47	(a) MOPITT L2V3 ‘simulated’ daytime and nighttime CO profiles for HDD_{peak} , over Coimbatore, for May 2007; (b) Same as (a) except for December 2007. The green (black, cyan, blue, and red) line indicates the considered sample CO profile (perturbed CO profile, a priori CO profile, ‘simulated’ day CO profile, and ‘simulated’ night CO profile). The green (black, cyan, blue, and red) triangles show calculated total column values for considered sample profile (perturbed sample profile, a priori profile, ‘simulated’ daytime profile, and ‘simulated’ nighttime profile).	113
3.48	MOPITT L2V3 ‘simulated’ day-night difference CO profiles for LDD_{peak} and HDD_{peak} , over Coimbatore, for May 2007; (b) Same as (a) except for December 2007. The diamond symbol solid and dash-dotted lines indicates day and night CO ratio (850/350) term respectively. The ratio indicated by top x-axis. The dark grey coloured lines represents $day_{850}-night_{700}$ CO difference profiles for LDD_{peak} and HDD_{peak} . Note that the key result is depicted in Fig. 3.49.	114
3.49	Key result from Fig. 3.48.	115
3.50	MOPITT L2V3 calculated total column values for i) a priori CO profile (cyan), ii) 7 individual sample profiles (green), iii) 7 individual perturbed sample profile (black), and iv) 7 individual simulated day (blue) and night (red) CO profiles, over Coimbatore, for May 2007; (b) Same as (a) except for December 2007.	116
3.51	MOPITT L2V3 calculated total column tests for day and night simulated profiles in the month of (a) May and (b) December. Note that these are not considered as profiles and are in arbitrary unit.	116
3.52	Show selected TOMCAT model CO profiles, over Coimbatore box, for May 2004 (blue) and December 2004 (red) for the given latitude and longitude co-ordinate.	117

3.53	((a)MOPITT L2V3 ‘Simulated’ daytime and nighttime CO profiles for TOMCAT model selected base CO profile, over Coimbatore, for May 2007; (b) Same as (a) except for December 2007.	118
3.54	(a) MOPITT L2V3 ‘simulated’ day-night difference CO profile for HDD_{peak} , over Coimbatore, for May 2007; (b) Same as (a) except for December 2007.	119
3.55	(a) MOPITT L2V3 0.5 degree gridded daytime 700 hPa CO mixing ratios, over India, for May 2007; (b) MOPITT L2V3 0.5 degree gridded nighttime 700 hPa CO mixing ratios, over India, for May 2007; (c) MOPITT L2V3 0.5 degree gridded 700 hPa day-night CO mixing ratio differences, over India, for May 2007; (d) Same as (a) except for December 2007; (e) Same as (b) except for December 2007; (f) Same as (c) except for December 2007.	122
3.56	(a) MOPITT L2V3 0.5 degree gridded daytime CO ratio (850hPa/350hPa), over India, for May 2007; (b) MOPITT L2V3 0.5 degree gridded $day_{850}-night_{700}$ CO mixing ratio differences, over India, for May 2007; (c) Same as (a) except for December 2007; (d) Same as (b) except for December 2007.	123
3.57	Top panel: show spatial distribution of the (a) daytime and (b) nighttime surface value of the MOPITT L2V3 700 hPa averaging kernel for May 2007; (c) and (d) same as (a) and (b) respec. except for December 2007. Bottom panel: (e) and (f) same as (a) and (b) respec. except for surface value of the 850 hPa averaging kernel; (g) and (h) same as (c) and (d) respec. except for for surface value of the 850 hPa averaging kernel.	124
3.58	(a) and (b) show correlation plots between the thermal contrast and surface value of 700 hPa averaging kernels in May 2007 for 06 UTC and 18 UTC respectively; (c) and (d) show correlation plots between the boundary layer height and surface value of 700 hPa averaging kernels in May 2007 for 06 UTC and 18 UTC respectively. Note TC refer to thermal contrast and BLHt refer to boundary layer height.	125
3.59	Correlation results, over India, in the month of May 2007.	126
3.60	Correlation results, over India, in the month of Dec 2007.	127

3.61	Correlation results, over India, in the month of May 2007.	127
3.62	Top panel (a-d): MOPITT L2V3 ‘simulated’ using mean averaging kernel key day-night difference CO profiles for HDDpeak, over Bihar and Delhi, for May and December 2007; Bottom panel (e-h)): Same as top panel except for ‘simulated’ using selected ‘typical’ averaging kernel.	130
3.63	Top panel (a-d): MOPITT L2V3 ‘simulated’ using mean averaging kernel key day-night difference CO profiles for HDDpeak, over Mumbai and Coimbatore, for May and December 2007; Bottom panel (e-h): Same as top panel except for ‘simulated’ using selected ‘typical’ averaging kernel.	131
4.1	Difference in the MOPITT L2V3 and L2V4 retrieved number of profiles on global scale for the year 2007.	138
4.2	(a) MOPITT L2V4 retrieved 800 hPa 0.5 deg. gridded a priori CO mixing ratios during daytime and nighttime for September 2006; (b) Same as (a) except for 300 hPa level.	139
4.3	MOPITT L2V4 a priori CO mixing ratio profiles as a function of DOFS, for global case (left panel), and IG basin (right panel) on 01 May 2006.	141
4.4	MOPITT L2V4 mean averaging kernels obtained by averaging all daytime and nighttime averaging kernels separately on 01 May 2006. (a) in the box defined by $20^{\circ}N$, $30^{\circ}N$, $10^{\circ}E$, and $25^{\circ}E$ (over Libyan desert) and (b) in the box defined by $15^{\circ}S$, $30^{\circ}S$, $5^{\circ}W$, and $20^{\circ}W$ (over South Atlantic).	142
4.5	Degrees Of Freedom for Signal for September, 2006 for (a) daytime and (b) Nighttime MOPITT L2V4 data	143
4.6	(a) MOPITT L2V3 0.5 deg. gridded 700 hPa daytime CO mixing ratios, over India, for May 2007; (b) MOPITT L2V3 0.5 deg. gridded 700 hPa day-night difference CO mixing ratios, over India, for May 2007; (c) Same as (a) except for December 2007; (d) Same as (b) except for December 2007; (e) Same as (a) except for L2V4; (f) Same as (b) except for L2V4; (g) Same as (c) except for L2V4; (h) Same as (d) except for L2V4.	146

4.7	(a) MOPITT L2V3 0.5 deg. gridded (850hPa/350hPa) daytime CO mixing ratios, over India, for May 2007; (b) Same as (a) except for December 2007; (c) MOPITT L2V4 0.5 deg. gridded (800hPa/400hPa) daytime CO mixing ratios, over India, for May 2007; (d) Same as (c) except for December 2007.	147
4.8	Correlation results, over India, in the month of May 2007.	148
4.9	Correlation results, over India, in the month of December 2007.	149
4.10	(a) MOPITT L2V3 and L2V4 a priori CO mixing ratio profile(s), over Bihar region, in the month of May 2007; (b) Same as (a) except for December 2007.	150
4.11	(a) MOPITT L2V3 and L2V4 DOFS histogram plot, over Bihar region, in the month of May 2007; (b) Same as (a) except for December 2007.	151
4.12	(a) MOPITT L2V3 selected daytime ‘typical’ averaging kernel, over Bihar region, in the month of May 2007; (b) Same as (a) except for nighttime; (c) MOPITT L2V4 selected daytime ‘typical’ averaging kernel, over Bihar region, in the month of May 2007; (d) Same as (c) except for nighttime; (e-f) Same as (a-d) except for December 2007.	152
4.13	(a) MOPITT L2V3 retrieved mean daytime and nighttime CO profiles, over Bihar box, for May 2007; (b) Mean day-night difference CO profiles, over Bihar box, for combination of LDD and HDD; (c) Same as (a) except for MOPITT L2V4; (d) Same as (b) except for MOPITT L2V4; (e) Same as (a) except for December 2007; (f) Same as (b) except for December 2007; (g) Same as (c) except for December 2007; (h) Same as (d) except for December 2007;.	154
4.14	(a) MOPITT L2V3 ‘simulated’ daytime and nighttime CO profiles for HDD_{peak} , over Bihar, for May 2007; (b) Same as (a) except for MOPITT L2V4. The green, black, cyan, blue, and red line indicates the considered sample CO profile, perturbed CO profile, a priori CO profile, ‘simulated’ day CO profile, and ‘simulated’ night CO profile. The green, black, cyan, blue, and red triangles show calculated total column values for corresponding CO VMR profiles.	156

4.15	(a) MOPITT L2V3 ‘simulated’ daytime and nighttime CO profiles for HDD _{peak} , over Bihar, for December 2007; (b) Same as (a) except for MOPITT L2V4. The green, black, cyan, blue, and red line indicates the considered sample CO profile, perturbed CO profile, a priori CO profile, ‘simulated’ day CO profile, and ‘simulated’ night CO profile. The green, black, cyan, blue, and red triangles show calculated total column values for corresponding CO VMR profiles.	157
4.16	(a) MOPITT L2V3 ‘simulated’ key day-night difference CO profiles for HDD _{peak} , over Bihar, for May 2007; (b) Same as (a) except for MOPITT L2V4. The diamond solid and dash-dotted lines indicates day and night CO ratio (L2V3: 850hPa/350hPa and L2V4: 800hPa/400hPa) terms respectively. The ratio scale shown as top x-axis. The red coloured line represents day ₈₅₀ -night ₇₀₀ (for L2V3) and day ₈₀₀ -night ₇₀₀ (for L2V4) CO difference profiles for HDD _{peak}	159
4.17	(a) MOPITT L2V3 ‘simulated’ key day-night difference CO profiles for HDD _{peak} , over Bihar, for December 2007; (b) Same as (a) except for MOPITT L2V4. The diamond solid and dash-dotted lines indicates day and night CO ratio (L2V3:850hPa/350hPa and L2V4: 800hPa/400hPa) terms respectively. The ratio scale shown as top x-axis. The red coloured line represents day ₈₅₀ -night ₇₀₀ (for L2V3) and day ₈₀₀ -night ₇₀₀ (for L2V4) CO difference profiles for HDD _{peak}	160
4.18	MOPITT L2V3 and L2V4 retrieval calculated total column values for i) a priori CO profile (cyan), ii) 7 individual sample profiles (green), iii) 7 individual perturbed sample profile (black), and iv) 7 individual simulated day (blue) and night (red) CO profiles, over Bihar, for May (top panel) and December (bottom panel) 2007; Note that these are not considered as profiles. For proper understanding the total column values plotted at corresponding perturbed retrieval level (layer) for each CO VMR profile.	161
4.19	Selected TOMCAT model CO profiles, over Bihar box, for May 2004 (blue) and December 2004 (red).	162

4.20	(a)MOPITT L2V3 ‘Simulated’ daytime and nighttime CO profiles for TOMCAT model selected base CO profile, over Bihar, for May 2007; (b) Same as (a) except for MOPITT L2V4; (c) Same as (a) except for December 2007; (d) Same as (a) except for MOPITT L2V4 and for December 2007.	163
4.21	(a) MOPITT L2V3 ‘simulated’ day-night difference CO profile for HDD _{peak} , over Bihar, for May 2007; (b) Same as (a) except for MOPITT L2V4.	164
4.22	(a) MOPITT L2V3 and L2V4 retrievals a priori CO mixing ratio profile(s), over Delhi region, in the month of May 2007; (b) Same as (a) except for December 2007.	166
4.23	(a) MOPITT L2V3 and L2V4 DOFS histogram plot, over Delhi region, in the month of May 2007; (b) Same as (a) except for December 2007.	167
4.24	(a) MOPITT L2V3 selected daytime ‘typical’ averaging kernel, over Delhi region, in the month of May 2007; (b) Same as (a) except for nighttime; (c) MOPITT L2V4 selected daytime ‘typical’ averaging kernel, over Delhi region, in the month of May 2007; (d) Same as (c) except for nighttime; (e-f) Same as (a-d) except for December 2007. .	168
4.25	(a) MOPITT L2V3 retrieved mean daytime and nighttime CO profiles, over Delhi box, for May 2007; (b) Mean day-night difference CO profiles, over Delhi box, for combination of LDD and HDD; (c) Same as (a) except for MOPITT L2V4; (d) Same as (b) except for MOPITT L2V4;(e) Same as (a) except for December 2007; (f) Same as (b) except for December 2007; (g) Same as (c) except for December 2007;(h) Same as (d) except for December 2007;.	170
4.26	(a) MOPITT L2V3 ‘simulated’ daytime and nighttime CO profiles for HDD _{peak} , over Delhi, for May 2007; (b) Same as (a) except for MOPITT L2V4. The green, black, cyan, blue, and red line indicates the considered sample CO profile, perturbed CO profile, a priori CO profile, ‘simulated’ day CO profile, and ‘simulated’ night CO profile. The green, black, cyan, blue, and red triangles show calculated total column values for corresponding CO VMR profiles.	172

4.27	(a) MOPITT L2V3 ‘simulated’ daytime and nighttime CO profiles for HDD _{peak} , over Delhi, for December 2007; (b) Same as (a) except for MOPITT L2V4. The green, black, cyan, blue, and red line indicates the considered sample CO profile, perturbed CO profile, a priori CO profile, ‘simulated’ day CO profile, and ‘simulated’ night CO profile. The green, black, cyan, blue, and red triangles show calculated total column values for corresponding CO VMR profiles.	173
4.28	(a) MOPITT L2V3 ‘simulated’ key day-night difference CO profiles for HDD _{peak} , over Delhi, for May 2007; (b) Same as (a) except for MOPITT L2V4. The diamond solid and dash-dotted lines indicates day and night CO ratio (L2V3: 850hPa/350hPa and L2V4: 800hPa/400hPa) terms respectively. The ratio scale shown as top x-axis. The red coloured line represents day ₈₅₀ -night ₇₀₀ (for L2V3) and day ₈₀₀ -night ₇₀₀ (for L2V4) CO difference profiles for HDD _{peak}	174
4.29	(a) MOPITT L2V3 ‘simulated’ key day-night difference CO profiles for HDD _{peak} , over Delhi, for December 2007; (b) Same as (a) except for MOPITT L2V4.	175
4.30	MOPITT L2V3 and L2V4 retrieval calculated total column values for i) a priori CO profile (cyan), ii) 7 individual sample profiles (green), iii) 7 individual perturbed sample profile (black), and iv) 7 individual simulated day (blue) and night (red) CO profiles, over Delhi, for May (top panel) and December (bottom panel) 2007.	176
4.31	Selected TOMCAT model CO profiles, over Delhi box, for May 2004 (blue) and December 2004 (red).	177
4.32	(a)MOPITT L2V3 ‘Simulated’ daytime and nighttime CO profiles for TOMCAT model selected base CO profile, over Delhi, for May 2007; (b) Same as (a) except for MOPITT L2V4; (c) Same as (a) except for December 2007; (d) Same as (a) except for MOPITT L2V4 and for December 2007.	178
4.33	(a) MOPITT L2V3 ‘simulated’ day-night difference CO profile for HDD _{peak} , over Delhi, for May 2007; (b) Same as (a) except for MOPITT L2V4.	179

4.34	(a) MOPITT L2V3 and L2V4 retrievals a priori CO mixing ratio profile(s), over Mumbai region, in the month of May 2007; (b) Same as (a) except for December 2007.	180
4.35	(a) MOPITT L2V3 and L2V4 DOFS histogram plot, over Mumbai region, in the month of May 2007; (b) Same as (a) except for December 2007.	181
4.36	(a) MOPITT L2V3 selected daytime ‘typical’ averaging kernel, over Mumbai region, in the month of May 2007; (b) Same as (a) except for nighttime; (c) MOPITT L2V4 selected daytime ‘typical’ averaging kernel, over Mumbai region, in the month of May 2007; (d) Same as (c) except for nighttime; (e-f) Same as (a-d) except for December 2007.	182
4.37	(a) MOPITT L2V3 retrieved mean daytime and nighttime CO profiles, over Mumbai box, for May 2007; (b) Mean day-night difference CO profiles, over Mumbai box, for combination of LDD and HDD; (c) Same as (a) except for MOPITT L2V4; (d) Same as (b) except for MOPITT L2V4;(e) Same as (a) except for December 2007; (f) Same as (b) except for December 2007; (g) Same as (c) except for December 2007;(h) Same as (d) except for December 2007;.	184
4.38	(a) MOPITT L2V3 ‘simulated’ daytime and nighttime CO profiles for HDD_{peak} , over Mumbai, for May 2007; (b) Same as (a) except for MOPITT L2V4. The green, black, cyan, blue, and red line indicates the considered sample CO profile, perturbed CO profile, a priori CO profile, ‘simulated’ day CO profile, and ‘simulated’ night CO profile. The green, black, cyan, blue, and red triangles show calculated total column values for corresponding CO VMR profiles.	186
4.39	(a) MOPITT L2V3 ‘simulated’ daytime and nighttime CO profiles for HDD_{peak} , over Mumbai, for December 2007; (b) Same as (a) except for MOPITT L2V4. The green, black, cyan, blue, and red line indicates the considered sample CO profile, perturbed CO profile, a priori CO profile, ‘simulated’ day CO profile, and ‘simulated’ night CO profile. The green, black, cyan, blue, and red triangles show calculated total column values for corresponding CO VMR profiles.	187

4.40	(a) MOPITT L2V3 ‘simulated’ key day-night difference CO profiles for HDD _{peak} , over Mumbai, for May 2007; (b) Same as (a) except for MOPITT L2V4. The diamond solid and dash-dotted lines indicates day and night CO ratio (L2V3: 850hPa/350hPa and L2V4: 800hPa/400hPa) terms respectively. The ratio scale shown as top x-axis. The red coloured line represents day ₈₅₀ -night ₇₀₀ (for L2V3) and day ₈₀₀ -night ₇₀₀ (for L2V4) CO difference profiles for HDD _{peak}	188
4.41	(a) MOPITT L2V3 ‘simulated’ key day-night difference CO profiles for HDD _{peak} , over Mumbai, for December 2007; (b) Same as (a) except for MOPITT L2V4. The diamond solid and dash-dotted lines indicates day and night CO ratio (L2V3:850hPa/350hPa and L2V4: 800hPa/400hPa) terms respectively. The ratio scale shown as top x-axis. The red coloured line represents day ₈₅₀ -night ₇₀₀ (for L2V3) and day ₈₀₀ -night ₇₀₀ (for L2V4) CO difference profiles for HDD _{peak}	189
4.42	MOPITT L2V3 and L2V4 retrieval calculated total column values for i) a priori CO profile (cyan), ii) 7 individual sample profiles (green), iii) 7 individual perturbed sample profile (black), and iv) 7 individual simulated day (blue) and night (red) CO profiles, over Mumbai, for May (top panel) and December (bottom panel) 2007; Note that these are not considered as profiles. For proper understanding the total column values plotted at corresponding perturbed retrieval level (layer) for each CO VMR profile.	190
4.43	Selected TOMCAT model CO profiles, over Mumbai box, for May 2004 (blue) and December 2004 (red).	191
4.44	(a)MOPITT L2V3 ‘Simulated’ daytime and nighttime CO profiles for TOMCAT model selected base CO profile, over Mumbai, for May 2007; (b) Same as (a) except for MOPITT L2V4; (c) Same as (a) except for December 2007; (d) Same as (a) except for MOPITT L2V4 and for December 2007.	192
4.45	(a) MOPITT L2V3 ‘simulated’ day-night difference CO profile for HDD _{peak} , over Mumbai, for May 2007; (b) Same as (a) except for MOPITT L2V4.	193

4.46	(a) MOPITT L2V3 0.5 degree gridded daytime 700 hPa CO mixing ratios, over India, for May 2007; (b) MOPITT L2V3 0.5 degree gridded nighttime 700 hPa CO mixing ratios, over India, for May 2007; (c) MOPITT L2V3 0.5 degree gridded 700 hPa day-night CO mixing ratio differences, over India, for May 2007; (d) MOPITT L2V4 0.5 degree gridded daytime 800 hPa CO mixing ratios, over India, for May 2007; (e) MOPITT L2V4 0.5 degree gridded nighttime 800 hPa CO mixing ratios, over India, for May 2007; (f) MOPITT L2V4 0.5 degree gridded day ₈₀₀ -ngt ₇₀₀ CO mixing ratio differences, over India, for May 2007.	195
4.47	(a) MOPITT L2V3 0.5 degree gridded daytime 700 hPa CO mixing ratios, over India, for December 2007; (b) MOPITT L2V3 0.5 degree gridded nighttime 700 hPa CO mixing ratios, over India, for December 2007; (c) MOPITT L2V3 0.5 degree gridded 700 hPa day-night CO mixing ratio differences, over India, for December 2007; (d) MOPITT L2V4 0.5 degree gridded daytime 800 hPa CO mixing ratios, over India, for December 2007; (e) MOPITT L2V4 0.5 degree gridded nighttime 800 hPa CO mixing ratios, over India, for December 2007; (f) MOPITT L2V4 0.5 degree gridded day ₈₀₀ -ngt ₇₀₀ CO mixing ratio differences, over India, for December 2007.	196
4.48	Correlation results, over India, in the month of May 2007.	197
4.49	Correlation results, over India, in the month of December 2007.	198
5.1	(a) SCIAMACHY 0.25 deg. gridded NO ₂ total column ($\times 10^{15}$ molecules.cm ⁻²); (b) MOPITT L2V3 0.5 degree gridded daytime 700 hPa CO mixing ratios; (c) MOPITT L2V3 0.5 gridded 700 hPa day-night difference CO mixing ratios; (d) Same as (a); (e) MOPITT L2V4 0.5 degree gridded daytime 800 hPa CO mixing ratios; (f) MOPITT L2V4 0.5 gridded day ₈₀₀ -ngt ₇₀₀ difference CO mixing ratios.	205
5.2	Correlation results for (a) L2V3 700 hPa daytime CO Vs L2V4 700 hPa daytime CO; (b) Same as (a) except for nighttime; (c) L2V3 700 hpa day-night difference Vs day ₈₀₀ -ngt ₇₀₀ difference; (d) L2V3 CO column Vs L2V4 CO column, for the year 2007.	207

5.3	SCIAMACHY NO ₂ , MOPITT L2V3 daytime 700 hPa CO mixing ratios, MOPITT L2V3 700 hPa day-night difference CO mixing ratios, MOPITT L2V4 daytime 800 hPa CO mixing ratios, and MOPITT L2V4 day ₈₀₀ -ngt ₇₀₀ difference CO mixing ratios, over striking cities. Houston (top row), Florida(middle row), Cairo(bottom row).	209
5.4	SCIAMACHY NO ₂ , MOPITT L2V3 daytime 700 hPa CO mixing ratios, MOPITT L2V3 700 hPa day-night difference CO mixing ratios, MOPITT L2V4 daytime 800 hPa CO mixing ratios, and MOPITT L2V4 day ₈₀₀ -ngt ₇₀₀ difference CO mixing ratios, over Birmingham and Wales.	210
5.5	Correlation results for (i) L2V3 CO diff. vs L2V4 CO diff.; (ii) SCIAMACHY NO ₂ vs L2V3 CO diff.; and (iii) SCIAMACHY NO ₂ vs L2V4 CO diff. for (a-c) Houston, (d-f) Florida, (g-i) Cairo, (j-l) Birmingham respectively.	211
5.6	SCIAMACHY NO ₂ , MOPITT L2V3 daytime 700 hPa CO mixing ratios, MOPITT L2V3 700 hPa day-night difference CO mixing ratios, MOPITT L2V4 daytime 800 hPa CO mixing ratios, and MOPITT L2V4 day ₈₀₀ -ngt ₇₀₀ difference CO mixing ratios, over striking cities. Delhi(top row), Norilsk(middle row), Tokyo(bottom row).	214
5.7	SCIAMACHY NO ₂ , MOPITT L2V3 daytime 700 hPa CO mixing ratios, MOPITT L2V3 700 hPa day-night difference CO mixing ratios, MOPITT L2V4 daytime 800 hPa CO mixing ratios, and MOPITT L2V4 day ₈₀₀ -ngt ₇₀₀ difference CO mixing ratios, over striking cities. Johannesburg(top row), Teheran(middle row), Lagos(bottom row). .	215
5.8	SCIAMACHY NO ₂ , MOPITT L2V3 daytime 700 hPa CO mixing ratios, MOPITT L2V3 700 hPa day-night difference CO mixing ratios, MOPITT L2V4 daytime 800 hPa CO mixing ratios, and MOPITT L2V4 day ₈₀₀ -ngt ₇₀₀ difference CO mixing ratios, over striking cities. Toronto(top row), Los Angeles(middle row), Guatemala(bottom row). .	216

5.9	SCIAMACHY NO ₂ , MOPITT L2V3 daytime 700 hPa CO mixing ratios, MOPITT L2V3 700 hPa day-night difference CO mixing ratios, MOPITT L2V4 daytime 800 hPa CO mixing ratios, and MOPITT L2V4 day ₈₀₀ -ngt ₇₀₀ difference CO mixing ratios, over striking cities. Bologna(top row), Moscow(bottom row).	217
5.10	Map showing large cities found in this analysis.	218
7.1	(a)Histogram for daytime and nighttime DOFS, over Delhi box, for May 2007; (b) Same as (a) except for December 2007; (c) Same as (a) except for Mumbai; (d) Same as (a) except for Mumbai and December 2007; (e) Same as (a) except for Coimbatore; (f) Same as (a) except for Coimbatore and December 2007.	229
7.2	Histogram of DOFS and thermal contrast calculated for Northern Hemisphere tropical region for each month of the year 2007.	230
7.3	Correlation results between MOPITT L2V3 retrieved CO data and considered diagnostics in this study in the month of May 2007.	231
7.4	Correlation results between MOPITT L2V3 retrieved CO data and considered diagnostics in this study in the month of December 2007.	232
7.5	Correlation between DOFS and percent a priori CO mixing ratio, over Delhi region, in the month of May and December 2007.	233
7.6	Correlation between DOFS and percent a priori CO mixing ratio, over Mumbai region, in the month of May and December 2007.	234
7.7	Correlation between DOFS and percent a priori CO mixing ratio, over Coimbatore region, in the month of May and December 2007.	235
7.8	Correlation between DOFS and percent a priori CO mixing ratio for global land data in the month of May 2007.	236
7.9	Correlation between DOFS and percent a priori CO mixing ratio for global land data in the month of Dec 2007.	237
7.10	(a) MOPITT L2V3 and L2V4 retrievals a priori CO mixing ratio profile(s), over Mexico region, in the month of May 2007; (b) Same as (a) except for December 2007.	238

7.11	(a) MOPITT L2V3 and L2V4 DOFS histogram plot, over Mexico region, in the month of May 2007; (b) Same as (a) except for December 2007.	239
7.12	(a) MOPITT L2V3 selected daytime ‘typical’ averaging kernel, over Mexico region, in the month of May 2007; (b) Same as (a) except for nighttime; (c) MOPITT L2V4 selected daytime ‘typical’ averaging kernel, over Mexico region, in the month of May 2007; (d) Same as (c) except for nighttime; (e-f) Same as (a-d) except for December 2007.	240
7.13	(a) MOPITT L2V3 retrieved mean daytime and nighttime CO profiles, over Mexico box, for May 2007; (b) Mean day-night difference CO profiles, over Mexico box, for combination of LDD and HDD; (c) Same as (a) except for MOPITT L2V4; (d) Same as (b) except for MOPITT L2V4;(e) Same as (a) except for December 2007; (f) Same as (b) except for December 2007; (g) Same as (c) except for December 2007;(h) Same as (d) except for December 2007;.	241
7.14	(a) MOPITT L2V3 ‘simulated’ daytime and nighttime CO profiles for HDD_{peak} , over Mexico, for May 2007; (b) Same as (a) except for MOPITT L2V4. The green, black, cyan, blue, and red line indicates the considered sample CO profile, perturbed CO profile, a priori CO profile, ‘simulated’ day CO profile, and ‘simulated’ night CO profile. The green, black, cyan, blue, and red triangles show calculated total column values for corresponding CO VMR profiles. The total column has unit 10^{18} molecules.cm ⁻²	242
7.15	(a) MOPITT L2V3 ‘simulated’ daytime and nighttime CO profiles for HDD_{peak} , over Mexico, for December 2007; (b) Same as (a) except for MOPITT L2V4. The green, black, cyan, blue, and red line indicates the considered sample CO profile, perturbed CO profile, a priori CO profile, ‘simulated’ day CO profile, and ‘simulated’ night CO profile. The green, black, cyan, blue, and red triangles show calculated total column values for corresponding CO VMR profiles. The total column has unit 10^{18} molecules.cm ⁻²	243

7.16	(a) MOPITT L2V3 ‘simulated’ key day-night difference CO profiles for HDD _{peak} , over Mexico, for May 2007; (b) Same as (a) except for MOPITT L2V4.	244
7.17	(a) MOPITT L2V3 ‘simulated’ key day-night difference CO profiles for HDD _{peak} , over Mexico, for December 2007; (b) Same as (a) except for MOPITT L2V4.	244
7.18	MOPITT L2V3 and L2V4 retrieval calculated total column values for i) a priori CO profile (cyan), ii) 7 individual sample profiles (green), iii) 7 individual perturbed sample profile (black), and iv) 7 individual simulated day (blue) and night (red) CO profiles, over Mexico, for May (top panel) and December (bottom panel) 2007; Note that these are not considered as profiles. For proper understanding the total column values plotted at corresponding perturbed retrieval level (layer) for each CO VMR profile.	245
7.19	Selected TOMCAT model CO profiles, over Mexico box, for May 2004 (blue) and December 2004 (red).	246
7.20	(a)MOPITT L2V3 ‘Simulated’ daytime and nighttime CO profiles for TOMCAT model selected base CO profile, over Mexico, for May 2007; (b) Same as (a) except for MOPITT L2V4; (c) Same as (a) except for December 2007; (d) Same as (a) except for MOPITT L2V4 and for December 2007.	247
7.21	(a) MOPITT L2V3 ‘simulated’ day-night difference CO profile for HDD _{peak} , over Mexico, for May 2007; (b) Same as (a) except for MOPITT L2V4.	248
7.22	(a) MOPITT L2V3 and L2V4 retrievals a priori CO mixing ratio profile(s), over Johannesburg region, in the month of May 2007; (b) Same as (a) except for December 2007.	249
7.23	(a) MOPITT L2V3 and L2V4 DOFS histogram plot, over Johannesburg region, in the month of May 2007; (b) Same as (a) except for December 2007.	250

7.24	(a) MOPITT L2V3 selected daytime ‘typical’ averaging kernel, over Johannesburg region, in the month of May 2007; (b) Same as (a) except for nighttime; (c) MOPITT L2V4 selected daytime ‘typical’ averaging kernel, over Johannesburg region, in the month of May 2007; (d) Same as (c) except for nighttime; (e-f) Same as (a-d) except for December 2007.	251
7.25	(a) MOPITT L2V3 retrieved mean daytime and nighttime CO profiles, over Johannesburg box, for May 2007; (b) Mean day-night difference CO profiles, over Johannesburg box, for combination of LDD and HDD; (c) Same as (a) except for MOPITT L2V4; (d) Same as (b) except for MOPITT L2V4;(e) Same as (a) except for December 2007; (f) Same as (b) except for December 2007; (g) Same as (c) except for December 2007;(h) Same as (d) except for December 2007;.	252
7.26	(a) MOPITT L2V3 ‘simulated’ daytime and nighttime CO profiles for HDD _{peak} , over Johannesburg, for May 2007; (b) Same as (a) except for MOPITT L2V4.	253
7.27	(a) MOPITT L2V3 ‘simulated’ daytime and nighttime CO profiles for HDD _{peak} , over Johannesburg, for December 2007; (b) Same as (a) except for MOPITT L2V4.	254
7.28	(a) MOPITT L2V3 ‘simulated’ key day-night difference CO profiles for HDD _{peak} , over Johannesburg, for May 2007; (b) Same as (a) except for MOPITT L2V4.	255
7.29	(a) MOPITT L2V3 ‘simulated’ key day-night difference CO profiles for HDD _{peak} , over Johannesburg, for December 2007; (b) Same as (a) except for MOPITT L2V4.	255
7.30	Selected TOMCAT model CO profiles, over Johannesburg box, for May 2004 (blue) and December 2004 (red).	256
7.31	(a)MOPITT L2V3 ‘Simulated’ daytime and nighttime CO profiles for TOMCAT model selected base CO profile, over Johannesburg, for May 2007; (b) Same as (a) except for MOPITT L2V4; (c) Same as (a) except for December 2007; (d) Same as (a) except for MOPITT L2V4 and for December 2007.	257

7.32 (a) MOPITT L2V3 ‘simulated’ day-night difference CO profile for
HDD_{peak}, over Johannesburg, for May 2007; (b) Same as (a) except
for MOPITT L2V4. 258

List of Tables

1.1	Global CO budget derived from non-inversion and inversion techniques (adapted partly from Duncan et al. [2007]).	8
1.2	Near and thermal-IR nadir sounding missions capable of measuring CO in the troposphere.	17
2.1	Characteristics of MOPITT CO and CH ₄ channels. The nominal PMC and LMC cell pressure, temperature, and length are listed [Wang et al., 1999].	32
2.2	Absolute and percentage biases (mean and standard deviation) for each retrieval level and column, Averaged over all comparisons [Emmons et al., 2004].	46
5.1	L2V3 and L2V4 DOFS limit and equivalent L2V3 percent a priori CO mixing ratio for selected regions.	203

Chapter 1

Measuring Carbon Monoxide in the Troposphere

1.1 Introduction

In 'Climate Change 2007', Solomon et al. [2007] highlighted that

"As a result of anthropogenic forcing from greenhouse gases, aerosols and land surface changes, it is extremely likely that human activities have exerted a substantial net warming influence on climate since 1750. It has been observed that discernible human influences extend beyond average temperature to other aspects of climate".

There is an increasing awareness in both the science and policy communities to the climate change, predicted global warming [e.g., Houghton et al., 1992] due to changes in the atmospheric abundance of direct greenhouse gases (e.g. carbon dioxide) and indirect greenhouse gases (e.g. carbon monoxide) that alter the energy balance of the climate system. For example, the radiative forcing for the tropospheric ozone (O_3) changes due to emissions of O_3 forming chemicals (nitrous oxide (N_2O); CO; hydrocarbons) is of the order of $+0.35$ [$+0.25$ to $+0.65$] $W.m^{-2}$ [IPCC, 2007]. The major greenhouse gases and minor constituents with implications for climate change include carbon dioxide (CO_2), methane (CH_4), and N_2O and CO, sulphur dioxide (SO_2), chlorofluorocarbons (CFCs), and hydrocarbons respectively. Their concentrations have been shown to increase sharply since the industrial revolution [Etheridge

et al., 1988; Gulluk et al., 1998]. These both have an effect on the chemistry of the entire troposphere, directly impacting on the quality of the air we breathe, as well as also playing a key role in the greenhouse effect [Wang et al., 1998]. Thus, improved understanding of greenhouse gases and trace gases influences on the global scale is a major aspect of tropospheric chemistry research with implications for climate studies [e.g., Mickley et al., 1999; Jacob et al., 1999; Wang et al., 1998].

This thesis focuses on the indirect greenhouse gas, CO which is mainly produced from incomplete combustion. Considering air pollutant, CO is an important component in urban and indoor air pollution because of its short-term harmful health effects. Scientifically, atmospheric CO is important for several reasons: i) it plays a vital role in the tropospheric chemical system via its effect on hydroxyl radical (OH) concentration, ii) Via OH it largely influences the abundance of numerous trace species including several greenhouse gases, iii) it is a very good tracer and indicator of pollution, because the lifetime of CO allows major pollution source regions and subsequent transport in the atmosphere to be identified.

1.2 The Importance of CO in the Troposphere

Atmospheric CO is an important in relation to tropospheric chemistry and climate. Of equal significance is the fact that the study of CO and its budget greatly enables us to fingerprint anthropogenic activities by providing a strong signal from fossil-fuel use and biomass burning. Human perturbations on the earth system are directly reflected in changes in atmospheric composition including CO concentration. CO thus provides a way to evaluate our existing knowledge of the patterns of human activities.

Atmospheric CO acts as a precursor to tropospheric O₃ production [Crutzen, 1973], is a good tracer of long-range pollution transport [Jacob et al., 2003; Jaffe et al., 2004] due to its relatively long lifetime of about 2 to 3 months, and plays an important role in the tropospheric chemistry, through its reaction with OH [Logan et al., 1981], accounting for about 75 % of the removal of OH. For example, the 1997 Indonesian fires alone have been estimated to have lowered global OH levels by 6 % in late-1997, due to very large CO enhancements [Duncan et al., 2003]. Additionally, the increased tropospheric CO concentrations also hinders the removal

of other greenhouse gases and pollutants such as CH_4 and SO_2 [Brasseur and Solomon, 1986] and in turn increases the global warming potential of these gases. CO has recently been explicitly recognised as an important indirect greenhouse gas for the first time at high level [IPCC, 2007]. Our ability to understand CO concentrations and its effects on the Earth system depends on how well we understand global CO sources and sinks, and their spatio-temporal distribution. Most of the significant sources and sinks of CO have been identified, but there are large areas of uncertainty in the global CO budget [IPCC, 2007].

1.2.1 CO Sources

1.2.1.1 Fossil Fuel and Biofuel Burning

CO is produced in large quantities by the incomplete combustion of carbonaceous materials used as fuels such as coal, oil, gasoline and wood. The transportation sector (automobiles) accounts for the majority of the production of CO from combustion of fossil fuel. The other large source is due to energy (e.g. boilers, ovens, industrial engines, residential and cracking of crude oil). Wood and charcoal are also widely used in developing countries for domestic use and cooking. Several studies have focused on CO sources in Asia in general, and East Asia in particular (recent fast growing and developing countries). The fossil fuel and biofuel burning CO source is estimated to be 115 Tg CO/year in the most up-to-date inventory for this region [e.g. Streets et al., 2003]. Recently, Kar et al. [2008] estimated that the total CO emissions in India are 27 Tg CO for the period from May through December, with fossil fuel combustion, biomass burning, and biofuel combustion accounting for 15 %, 22 % and 63 % of the total respectively.

1.2.1.2 Biomass Burning

Biomass burning is the burning of living and dead vegetation and is a significant global source of gaseous and particulate matter emissions to the troposphere. Ninety percent of all biomass burning events are thought to be human initiated. Human induced fires are used for a variety of applications such as agricultural expansion, deforestation, bush control, weed and residue burning, and harvesting practices. Lightning can trigger mid and high latitude natural fires and in tropical regions, convective systems

can ignite the dry vegetation, mainly grassland and forest fires. Biomass burnings is important mainly for two reasons: first for a large number of compounds, biomass burning is one of the largest single sources in the troposphere, especially in the tropics; secondly biomass burning emissions play an important role in the biogeochemical cycles of carbon and nitrogen. Several studies have documented that biomass burning is a large source of CO in the troposphere [e.g. Crutzen and Andreae, 1990; Levine, 1991, 1996], for example, the large increase in CO concentrations in the Northern Hemisphere (NH) associated with anomalously large forest fires in 1998, 2002, and 2003.

1.2.1.3 Oxidation of Methane and Non-methane Hydrocarbons (NMHC)

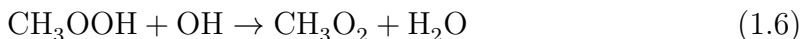
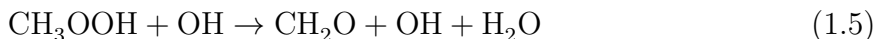
In the troposphere, the oxidation of CH₄ by OH is one of the major natural chemical sources of CO. In a high-NO_x environment, oxidation of CH₄ leads rapidly to production of CH₂O without involving relatively long lived intermediates. The CH₂O is then likely to photolyse or to react with OH, leading to formation of CO. In contrast, in a low-NO_x environment, oxidation leads to the production of CH₂O via CH₃OOH, a relatively long lived intermediate. It can then photolyze or react with OH, producing CH₂O, and CO. This can be generalised by the following photochemical reactions viz,



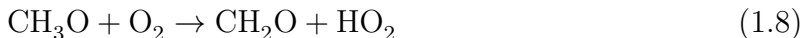
The CH₃O₂ molecule (methylperoxy radical) is analogous to HO₂. Its dominant sinks in the atmosphere are reactions with HO₂ and NO:



Similarly to H₂O₂, methylhydroperoxide (CH₃OOH) may either react with OH or photolyze



The methoxy radical CH_3O produced by (1.4) and (1.5) reacts rapidly with O_2 :



Formaldehyde produced by (1.5) and (1.8) may either react with OH or photolyze (two photolysis branches):



Reactions (1.9) and (1.10) produce the CHO radical, which reacts rapidly with O_2 to yield CO:



Other non-methane hydrocarbons (NMHC), emitted by vegetation, react with OH or O_3 are converted to oxygenated compounds and then partly to CO. It is likely that the hydrocarbon chemistry is not trivial. A small but significant anthropogenic source of CO comes also from non-biogenic hydrocarbons. These hydrocarbons are released mostly in automobiles and use of organic solvents. Logan et al. [1981] estimated the global source for CO is 4.5×10^8 tons C yr⁻¹ derived from combustion of fossil fuel (15%) and oxidation of atmospheric CH_4 (25%), with the balance from burning from vegetation and oxidation of hydrocarbons. Most recent chemical transport models can provide detailed calculations on the fate of these hydrocarbons.

1.2.1.4 Oceans

A source of CO in the oceans has been suggested in early studies of the CO cycle [e.g. Seiler and Junge, 1970]. The surface waters of the oceans are ubiquitously supersaturated with CO relative to CO in the atmosphere resulting in a net flux from oceans to the atmosphere. The photo-oxidation of dissolved organic matter is an important mechanism in the production of CO in the oceans. The flux of CO has been estimated using air-sea exchange flux equations, which are dependent on gas transfer velocity (parameterised using wind speed/sea surface temperature information) and latitudinal and seasonal dependent CO concentration in the surface waters. The relative contribution of the ocean to the total source is rather negligible and uncertain [Bates et al., 1995].

1.2.1.5 Plants

It has been suggested that there exist a net production of CO from plants, which is linearly dependent on light intensity and proportional to leaf area but independent on season [Bauer et al., 1974]. The mechanism of the production is not well understood. The estimate remains uncertain and there is no firm evidence that it is a significant source.

1.2.2 CO Sinks

1.2.2.1 Hydroxyl Radical (OH) Chemistry

A complete discussion of tropospheric chemistry involving OH radical, and the references for the chemistry that follows, can be found in [Crutzen, 1973; Ehhalt et al., 1994; Logan et al., 1981; Warneck, 1988; Wayne, 1991; Wofsy, 1976]. Here it is noted that OH initiates the most important oxidation reactions in the troposphere. It is important to understand the chemical role played by the OH radical to assess CO abundances in the troposphere. In the troposphere, OH oxidises CO to form hydroperoxy radicals (HO_2) [Levy II, 1971];



As shown by [Crutzen and Zimmermann, 1991], in a NO_x -rich environment, reactions following 1.13a and 1.13b produce ozone. Otherwise, reactions of ozone with HO_2 radicals destroy ozone. Either reaction chain is a CO sink, producing CO_2 . The fast reaction 1.13a does not depend on temperature [DeMore et al., 1994]; it leads to a global-average CO lifetime of two months in the current atmosphere, and is the most significant OH sink in the troposphere. It is, thus, generally accepted that the reaction of CO with OH is the major sink for CO [Levy II, 1971].

1.2.2.2 Soil Uptake

Early studies of CO suggested that soil consumption of CO is a biological process and the consumption rate is proportional to the organic carbon content of the soil. There are large uncertainties on the types of microorganisms responsible for the CO

loss [Conrad and Seiler, 1985]. Soil uptake is not related to microorganisms but from oxidation of organic compounds in the soil humus. This emission is temperature dependent and mainly occurs in the tropics and desert soils. Field studies have estimated that the global consumption is about 100-300 Tg.year⁻¹ [King, 2000; King and Crosby, 2002; Potter et al., 1996].

1.2.3 Global Budget of CO

Over the last decade, the knowledge of CO in the troposphere has been improved significantly. However, due to its significantly strong spatial and temporal variability and uneven distribution of individual sources, the estimates of the global CO budget in the troposphere is still uncertain.

The sources of CO are usually categorised by underlying process by which they are produced in the environment (see section 1.2.1). An up-to-date summary of the recent estimates of global CO budget is given in Table 1.1, derived from inversion techniques by using atmospheric models and datasets. In addition to these, several other studies have also estimated global CO budget in the troposphere [e.g., Bates et al., 1995; Crutzen and Zimmermann, 1991; Kanakidou et al., 1999]. It is most likely that anthropogenic (human-made) activities are responsible for more than half of the CO emissions while natural processes account for the remaining fractions. The contribution of anthropogenic and natural emissions of CO have been subject of debate for several decades. This is partly due to issues in delineating the nature of anthropogenic origin (i.e. not all methane are produced from natural processes, causes of biomass burning - could be human initiated or lightning flash, hydrocarbons may be also produced from combustion, etc.). However due principally to the strong spatial and temporal variability of CO sources, the estimation of the global total CO budgets in the troposphere remains uncertain. Specific estimation studies are required either "bottom-up" from inventories or via inverse modelling. Either require observation in one form or another.

Table 1.1: Global CO budget derived from non-inversion and inversion techniques (adapted partly from Duncan et al. [2007]).

References	[Khalil and Rasmussen, 1990]	[Bergamaschi et al., 2000] ^a	[IPCC, 2001]	[Petron et al., 2004]	[Muller and Stavrakou, 2005] ^b	[Arellano and Hess, 2006]
Model		TM2 ^c		MOZART	IMAGES ^e	GEOS-Chem
Data Constraint		ESRL GMD		MOPIITT ^d	ESRL GMD	MOPIITT ^d
Year		1993-1995		Apr00 - Mar01	1997	Apr00 - Apr01
Sources						
Fossil-fuel combustion	400 - 1000	639 ± 23	650	375 - 475	760	841
Biomass burning ^f	335 - 1400	772 ± 65	700	675 - 700	359	501
Oxidation of CH ₄	400 - 1000	771 ± 24	800	720 - 845	870	820
Oxidation of Isoprene	-	287 ± 41	270	-	-	-
Oxidation of Terpene	-	135 ± 12	~0	-	-	-
Oxidation of industrial NMHC	300 - 1400	206 ± 26	110	-	-	-
Oxidation of biomass NMHC	-	-	30	-	774	394
Oxidation of Acetone	-	-	20	-	-	-
Vegetation	50 - 200	-	150	-	-	-
Oceans	20 - 80	51 ± 4	50	0 - 185	23	-
Sinks						
Surface deposition	-	250 - 640			203	-
OH chemistry	-	1500 - 2700			-	2618

∞

^a S2 base scenario, CH₄ was fixed in inversion.

^b Case A, inverted for CO only.

^c TM2 model is a three-dimensional atmospheric transport model [Heimann, 1996].

^d MOPIITT CO column data used in inversion.

^e IMAGES model is a global three-dimensional chemical transport model [Muller and Brasseur, 1995].

^f From agricultural, deforestation, savannah and waste burning

1.3 CO Observations in the Troposphere

A number of different techniques can be used to measure the complex spatial and temporal variations in CO distribution. These include mainly ground based remote measurements, in-situ air sampling, and remote sensing from space. Each has its own strengths and weaknesses and is useful for looking at a particular aspect of the CO distribution. It is likely that an integrated observing system which includes a combination of some or all of these methods is required to give a more comprehensive understanding.

1.3.1 Ground-based Measurements of CO

CO was first identified as a trace constituent in the atmosphere in the late 1940s by measuring with fair accuracy its total column abundance using solar spectroscopy. Extensive measurements of CO began however in early 1970s when, coincident with new theoretical developments in tropospheric chemistry, gas chromatographic methods were developed to measure discrete samples of CO. These early studies showed that CO mixing ratios varied with latitude and season and provided evidence of anthropogenic signature in the atmosphere [Singer, 1970; Seiler and Junge, 1970; Seiler, 1974]. And in conjunction with modeling activities and flux measurements, the global CO cycle has been studied in more detail to enhance our understanding of tropospheric CO burden and its variability.

Atmospheric CO concentrations are currently measured by a series of ground stations spread across the globe. Specifically, the Global Atmosphere Watch (GAW) programme is a global network for monitoring the atmospheric environment. Currently, there are about 150 sites complemented by continuous flux tower, balloon, aircraft, and ship observations (Fig. 1.1). CO concentrations are reported by WMO World Data Centre for Greenhouse Gases (WDCGG) in WMO [March 2009] that is run by the Atmospheric Environment Division in Japan Meteorological Agency. Measurements can either be made continuously by infrared analyzers (sampled at a rate of ≥ 1 min) or from air samples captured in flasks which are later analyzed in the laboratory. From these observations it is possible to construct monthly mean time-series, at each station accurate to within about ≥ 10 ppb [WMO, March 2009]. Unfortunately, the uneven geographical spread of the networks hampers understanding of the

CO global distribution, as flux estimates can only really be made at continental and ocean basin scales. Other ground based techniques for measuring the atmospheric concentration of CO are available (e.g. [Clerbaux et al., 2008] and references therein), but only on an intermittent and sparse basis and will not provide the dense sampling needed to improve the knowledge of surface CO spatial distribution.

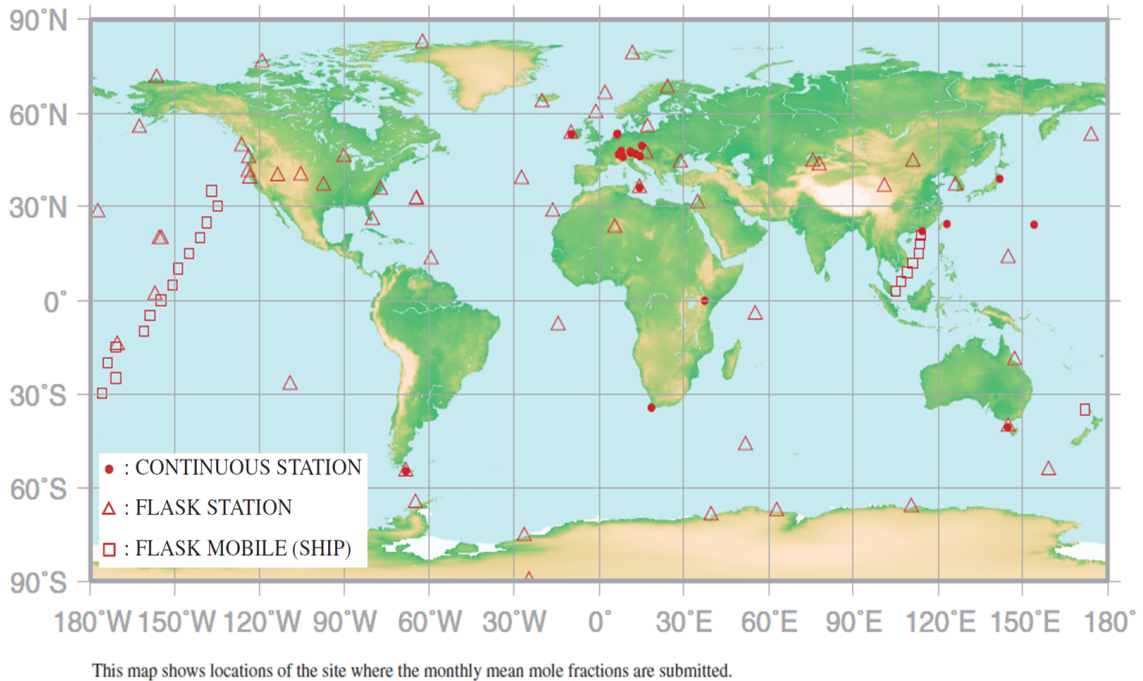


Figure 1.1: The current WMO WDCGG global CO observation network [WMO, March 2009].

Figure 1.2 shows average seasonal cycle in the CO concentrations for each 30° latitudinal zone. The seasonal cycle of CO is mainly driven by variations in OH abundance. Additional factors include emission and oxidation from CO sources and large-scale transportation of CO, despite a relatively weak seasonality in emission and oxidation compared with OH abundance. This seasonality and a short lifetime of about a few months produce a sharp decrease in early summer followed by a relatively slow increase in autumn. Biannual peaks evident in the southern low latitudes may be attributed to the transportation of CO from the tropical to extratropical SH [Bowman, 2006]. Novelli et al. [1998b] showed seasonal cycles that are strongly affected by changes in emission from biomass burning in both hemispheres, using a

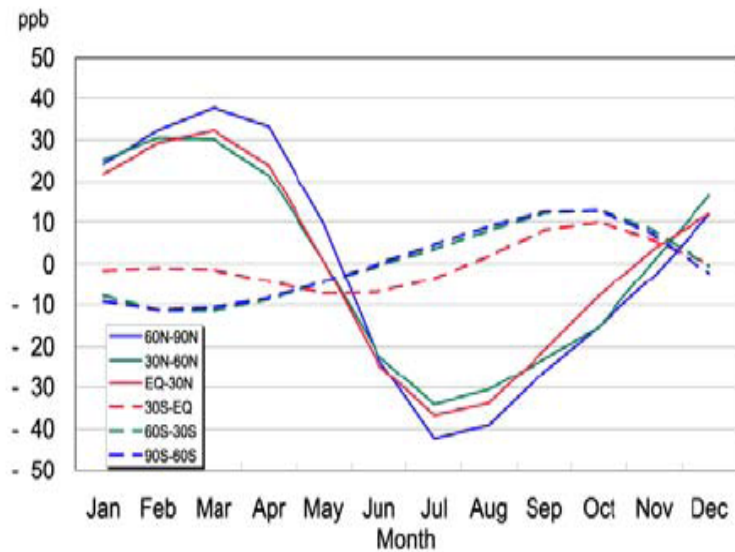


Figure 1.2: Average seasonal cycles for each 30° latitudinal zone from which the long-term trends were subtracted [WMO, March 2009].

model of two boxes representing the well-mixed northern layer and southern boundary layer. According to model simulations of global CO distribution, seasonal variations in regional distribution reflect the strength of regional sources, including biomass burning [Bergamaschi et al., 2000; Holloway and Kasibhatla, 2000].

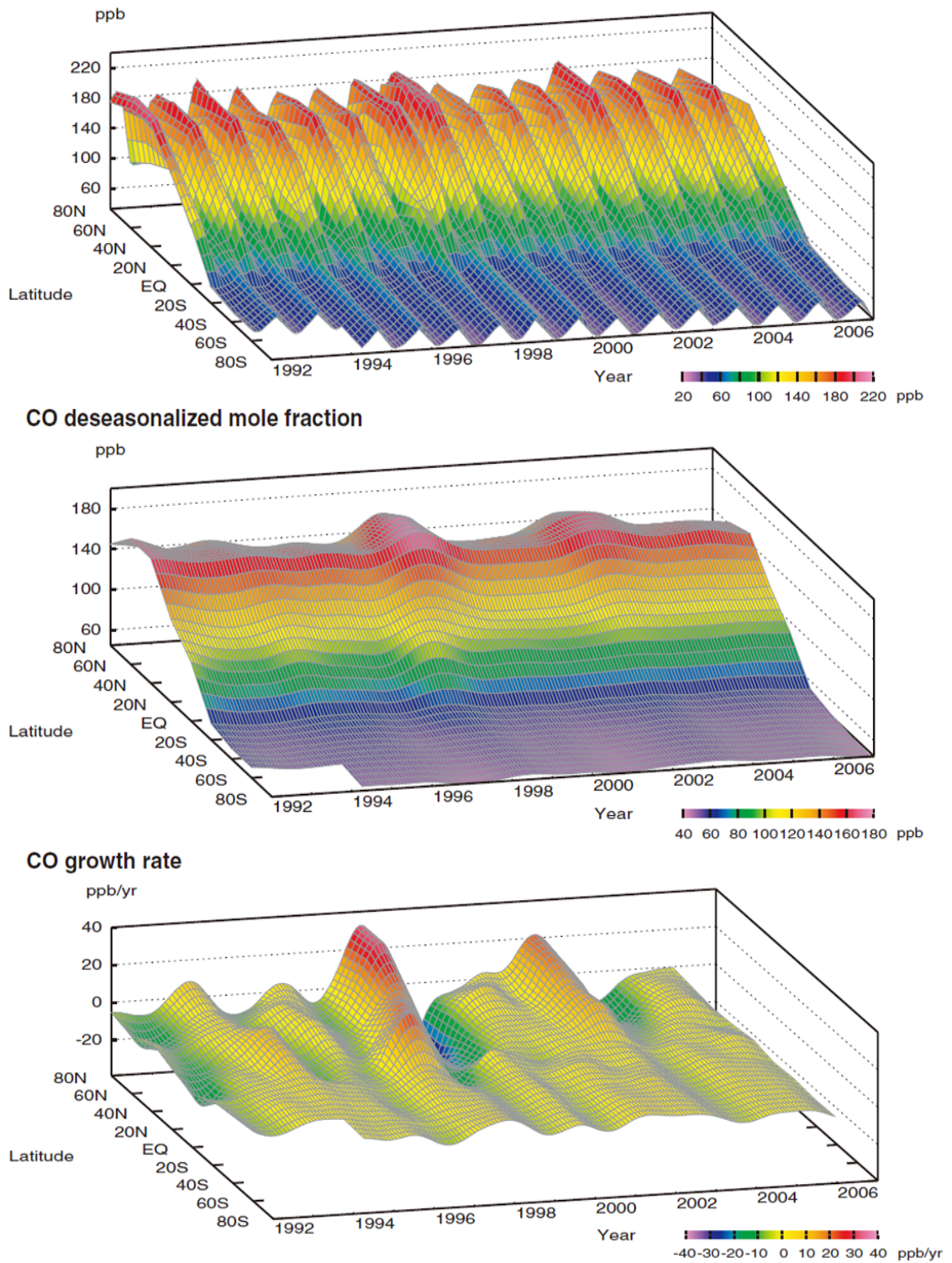


Figure 1.3: Top panel: Variation of zonally averaged monthly mean CO mixing ratios, middle panel: deseasonalised CO mixing ratios, and bottom panel: CO Growth rates [WMO, March 2009].

Fig. 1.3 shows variation of zonally averaged monthly mean CO mixing ratios, deseasonalised CO mixing ratios, and CO growth rates. Zonally averaged CO concentrations are calculated for each 20° zone. CO concentrations exhibit a distinct seasonal pattern (with highest levels observed in winter and lowest in summer). The monthly mean CO concentrations show seasonal variations, with large amplitudes in the NH and small amplitudes in the SH. The seasonal cycle is driven by industrial emissions, biomass burning, large-scale transportation, greater production from hydrocarbons (including CH_4), and variations in the OH radical, which acts as a sink. Although annual variations in the atmospheric flow can influence CO [Allen et al., 1996], a negative growth rate was seen in 1992 in all latitudes. Novelli et al. [1998b] showed a obvious decline in CO from late 1991 through mid-1993, with a subsequent recovery from mid-1993 through mid-1994. The decline in CO concentrations generally coincided with a decrease in the growth rate of CH_4 , most likely due to variations in their common sinks. The enhanced stratospheric ozone depletion due to increased volcanic aerosols following the eruption of Mt. Pinatubo in 1991 may have increased OH radicals, which react with both CO and CH_4 [Dlugokencky et al., 1996]. Increases in CO concentrations were observed from 1997 to 1998 in northern mid latitudes and in southern low latitudes. These enhancements were attributed to large biomass burnings around Indonesia in late 1997 and around Siberia in the summer and autumn of 1998 [Novelli et al., 2003]. Duncan et al. [2003] estimated CO emission of 133 Tg in 1997 from biomass burning in Indonesia and Malaysia, nearly a quarter of their estimate of the global emission for biomass burning. The CO concentrations returned to background values after 1999, but the growth rates in the NH increased substantially again in 2002. The latter might also be attributed to large biomass burning events. Large-scale boreal forest fires occurred in Siberia and North America from 2002 to 2003. The CO emission from these boreal forest fires was estimated to be 142 Tg [Simmonds et al., 2005].

In addition to strong seasonal variations, examination of time series of tropical CO surface measurements [Langenfelds et al., 2002; Novelli et al., 2003] show significant interannual variability that appears to be driven primarily by biomass burning. An increase in the growth rate of both CO and CO_2 has been observed in those years in which strong El Nino-Southern Oscillation (ENSO) warming events, such as 1997-98, resulted in tropical drought conditions that increased fire frequency and intensity

[Edwards et al., 2004]. The correlation between CO variability and variations in the CO₂ growth rate may help to distinguish fire and biogenic sources of CO₂ [Palmer et al., 2006].

The distribution of CO within the atmosphere is determined by short to long-range transport processes, and by spatio-temporal variation of natural and anthropogenic sources and sinks at the surface. For the NH, there are reports suggesting that CO concentration increased from the early 1950s to mid-1980s at a rate of about 1 % yr⁻¹ [Khalil and Rasmussen, 1988; Zander et al., 1989; Yurganov, 1993]. A negative trend started in the late 1980s [Khalil and Rasmussen, 1994; Mahieu et al., 1997]. The sharpest decrease occurred in 1992 [Novelli et al., 1994] and another small decrease in 1995 [Novelli et al., 1998a]. These recent decreases in CO have been attributed to decreased emissions, particularly from biomass burning, and an increased OH sink due to the thinning of the stratospheric ozone layer [Khalil and Rasmussen, 1994; Lowe et al., 1994; Novelli et al., 1994; Mahieu et al., 1997] by increased ultra-violet radiation. For the SH, no trend is detected across these years at Cape Point, South Africa and at Cape Grim, Tasmania [Fraser et al., 1986a, 1994; Brunke et al., 1990; Scheel et al., 1990, 2001]. The different trend recorded here, compared to that of the Northern Hemisphere, may reflect the high spatial variability of CO due to enormous irregular biomass burning emissions.

In general, the high degree of interannual variability illustrates the need for continuous monitoring since observations over the months of a single year, or even the climatological seasonal variation derived from many years of data, will not necessarily be representative of the emissions of any given year.

1.3.2 Satellite Sensing of Tropospheric CO

Along with in situ measurements from aircraft and ground-based measurements, CO can be potentially identified by satellite sensing techniques. Satellite measurements provide the opportunity to achieve global distribution of CO on a daily basis over long periods of time and are needed in conjunction with ground and airborne sensors to give a complete picture of CO in the atmosphere. Currently CO is measured by various satellite instruments in different wavelength ranges. Conceptually, the near infrared (NIR) observations sense the attenuation (by CO molecules) of solar

radiation reflected from the Earth's surface, whereas the thermal infrared (TIR) observations detect CO signatures in thermally emitted radiation from the Earth's surface and atmosphere. In principle, the NIR radiances provide information with respect to the CO total column with very weak sensitivity to the vertical distribution of CO, whereas the TIR radiances are sensitive to differences in CO concentrations over broad layers in the troposphere [Deeter et al., 2009].

Ludwig et al. [1974] first suggested the possibility of remotely measuring CO profiles in the troposphere from space-borne platform observations of thermal IR emission or absorption. Success of the Measurement of Air Pollution from Satellite (MAPS) on the second Space Transport System engineering test flight (STS-2) of the shuttle on 12-14 November 1981 proved the feasibility of inferring CO profiles from measurements by a nadir-viewing instrument. The instrument employed is a gas filter radiometer operating in the 4.7 μm region of the CO fundamental band with a passband from 2080 to 2220 cm^{-1} . At the surface the instantaneous field of view is approximately 20 by 20 km. Successive MAPS experiment provided global picture of tropospheric CO and further demonstrated the importance and feasibility of CO measurements from space. Specifically, the first results from this flight were reported by Reichle et al. [1986]. The instrument was flown again on the space shuttle during October 1984, and these measurements were reported by Reichle et al. [1990]. Figure 1.4 shows CO mixing ratios observations were made by the MAPS experiment during April 9-19 and September 11 to October 11, 1994 from the STS-2 shuttle [Conrad et al., 1999]. In Fig. 1.4a the April CO mixing ratios was fairly uniform with longitude with a distinct latitudinal gradient. The highest CO mixing ratios were at the high northern latitudes with values of about 120 ppb and lowest to the south of the equator with uniform values about 45 to 60 ppb in the southern latitudes. The controlling process for this northern spring distribution is mainly an enhanced lifetime of CO in the northern hemisphere (with low availability of hydroxyl radicals). Figure 1.4b shows a remarkably different distribution. The CO mixing ratios at the southern latitudes in October are highest due to extensive biomass burning in South Africa and South America and significantly low CO mixing ratios compared to Spring at the high northern latitudes as a result of the increased photochemical destruction of CO in the summer and early fall.

However, the MAPS dataset was limited and only weighted total column CO and

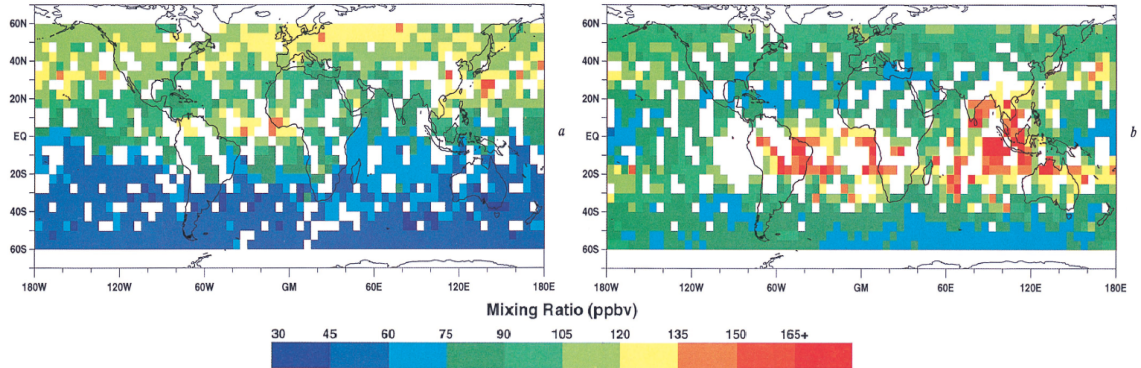


Figure 1.4: Near-global distribution of MAPS CO mixing ratios averaged over 5° latitude \times 5° longitude areas during (a) April 1994 and (b) October 1994 (Adapted from Conrad et al. [1999]).

average mid-tropospheric CO mixing ratios were derived from the one-channel correlation radiometer measurements and, therefore, could not provide tropospheric CO profile information. In order to improve our understanding of vertical differentiation of tropospheric CO and its impact on overall tropospheric chemistry, measurements that are sensitive to different layers of the atmosphere are ideally needed. The Measurement Of Pollution In The Troposphere (MOPITT) is a gas correlation radiometer designed to meet this requirement [Drummond, 1992].

The possibility of using satellite-derived observations to monitor pollution sources and transport are important because satellites can sample the whole planet and could complement the in-situ ground stations network. Unlike NO_2 , which is a good tracer of urban pollution due to its short lifetime [Wang et al., 2004], the medium lifetime of CO makes it difficult to distinguish uneven distribution of sources using in-situ ground based networks. It is worth noting that new space-borne missions are currently being designed for air quality measurements in support of policy decisions. As a result, satellite CO measurements are vital for carbon budget studies, and provide insight into the reasons for the high interannual variability of the CO_2 growth rate [Edwards et al., 2006] which has implications for climate studies. Table 1.2 lists some of the current near and thermal infrared missions that have been deployed in space to measure CO in the troposphere.

Table 1.2: Near and thermal-IR nadir sounding missions capable of measuring CO in the troposphere.

Instrument	Platform	Launch	Measurement Window
MOPITT	The EOS-TERRA satellite (NASA)	Dec-1999	Nadir sounding (2.3 and 4.7 μm)
SCIAMACHY	The European Space Agency (ESA) ENVironmental SATellite (ENVISAT)	Mar-2002	Nadir sounding (0.24 to 2.38 μm)
TES	The EOS-AURA satellite (NASA)	Jul-2004	Nadir sounding (3.2-15.4 μm)
IASI	The ESA's METOP-A	Aug-2007	Nadir sounding (3.62-15.5 μm)

Measurements from satellite instrument can be made in downwards (nadir) direction or along a horizontal direction (limb). In this thesis, retrievals from thermal-IR measurements of nadir emission are discussed. To do this, remotely sensed MOPITT instrument on NASA's EOS Terra satellite measurements are considered in this thesis and are used to study CO concentrations in the troposphere.

The MOPITT instrument provides the first opportunity to routinely obtain regular global observations of the horizontal and vertical distribution of CO in the troposphere. The MOPITT instrument was launched on December 18, 1999 aboard NASA's Terra satellite and continues to provide data to the scientific community to the present time. The MOPITT CO data is now available for almost a decade of observations and has been extensively used in scientific analyses. Signatures of industrial activity, biomass burning and forest fires are readily discernable in the data and significant variations of these over the last 10 years have been found. In addition, the transport processes e.g. trans-continental or vertical transport have been extensively studied. Lastly, the retrieved CO profile data is reported with an anticipated 10% precision.

However, satellite remote sensor i.e. MOPITT data are still uncertain for several reasons (e.g. vertical sensitivity, insufficient signal due to reflection from the ocean, etc.). It is therefore of crucial importance to understand how satellite data can be used

to identify and determine various natural and anthropogenic sources contributing to the tropospheric CO distribution, and to enhance knowledge of vertical differentiation of CO in the troposphere.

1.4 Summary and Objectives of Thesis

Atmospheric CO is a major tropospheric air pollutant, which is strongly influenced by anthropogenic activities (e.g. fossil-fuel and biomass burning) and photochemical processes (e.g. oxidation of CH_4), affecting air quality from local to global scales. It is an important compound in tropospheric chemistry both through its direct influence on the oxidizing capacity of the troposphere and through its indirect role as a precursor to tropospheric ozone (O_3) production. It hinders the removal of greenhouse gases and pollutant such as CH_4 and SO_2 respectively.

The distribution of CO is complex due to uneven distribution of its sources and sinks. Further, due to its lifetime of about 2 to 3 months, both short and long range transport complicates its distribution. Several studies have shown that there are a number of factors which need to be understood to characterise CO in the troposphere. The principal factor in these is better monitoring of the CO emissions.

Space-borne measurements are crucial in conjunction with ground-based and aircraft measurements to give a complete and accurate picture of CO in the atmosphere. Satellite-borne instruments provide us with global coverage over a long period of time, provided the measurements are of suitable precision. The MOPITT instrument has provided the first opportunity to routinely obtain regular global observations of the horizontal and vertical distribution of CO in the troposphere. The MOPITT remote sensor data could be useful for climatic research over last decade.

The overall scientific objectives of this thesis are:

- to investigate whether MOPITT CO retrievals are able to differentiate emission features in the lowermost atmosphere, including cities.
- to develop and apply a methodology for identifying likely CO enhancements in the lowermost troposphere.

Primarily, this thesis will address the following questions:

1. Are thermal-IR measurements sensitive to CO enhancements in the lowermost troposphere?
2. How do we examine the case for vertical differentiation of CO in the lowermost troposphere using MOPITT retrieved CO data?
3. Can we use information content diagnostics to evaluate CO vertical profile better?
4. Are there 'typical' CO averaging kernels which can be used to simulate CO response to elevated mixing ratio?
5. Can we systematically analyze MOPITT CO retrieved data over source emission regions and infer the presence of strong source?
6. Can we use MOPITT retrieved CO data to detect the CO signatures coming from urban areas (i.e., mega-cities)?

Chapter 2

The MOPITT Instrument

2.1 Introduction

This chapter describes the observational capabilities of the MOPITT IR satellite sensor that exploit the long-wave earth and atmospheric radiation to monitor tropospheric composition of CO (i.e. MOPITT). The MOPITT instrument was launched onboard the NASA EOS Terra Satellite on December 18th, 1999. Terra is in a 705 km, Sun-synchronous orbit with a 10:30 a.m. equator crossing time. MOPITT is a nadir sounding instrument, which makes measurements by scanning across the satellite flight track to +/- 26.1 degrees from nadir in 13 seconds, with a sampling frequency of 0.45 seconds. Each of these measurements is called a 'stare' and consists of four 22 km by 22 km pixels. As a result the MOPITT instrument has a swath width of approximately 600 km and thus achieves global coverage in approximately 3 days [Drummond, 1992]. The main scientific objective of the MOPITT experiment is long-term measurement of global distribution of tropospheric CO and CH₄ (not discussed in this thesis). These measurements are useful to enhance our knowledge of tropospheric chemistry, particularly how it interacts with the surface/ocean/biomass systems, transport processes, and the carbon cycle. A more complete description of the MOPITT instrument can be found in the MOPITT mission description document [Drummond, 1996]. This chapter reviews the current theory of the propagation of radiation through the atmosphere (radiative transfer) and the MOPITT instrument technique. The MOPITT operational retrieval algorithm, data validation and errors is also been discussed briefly here.

2.2 Observational Techniques

2.2.1 Thermal Infrared Techniques

The investigation of infrared radiation emitted by the earth-atmosphere system is important for mainly two reasons: (1) investigation of the spectral content of the emitted radiation can give information about the distribution of atmospheric temperature and composition and (2) investigation of the spatial distribution of the emitted radiation in certain spectral regions enables clouds or surface characteristics to be mapped [Houghton et al., 1986].

The thermal-IR radiance $I(\lambda)$ reaching a satellite instrument is governed by both the composition and temperature of the atmosphere directly beneath it. This can be represented using the Schwarzschild equation:

$$I(\lambda) = \varepsilon_s B(\lambda, T_s) \cdot \tau(\lambda, \infty) + \int_{z=0}^{\infty} B(\lambda, T_z) \cdot \frac{d\tau(\lambda, p, T_z)}{dz} dz + R_s I_{Down}(atm) \tau(\lambda, \infty) \quad (2.1)$$

where ε_s is the surface emissivity, $B(\lambda, T_z)$ is the Planck function, τ is the atmospheric transmission (equal to $e^{-\tau_\lambda}$, where τ_λ is the optical depth) and where p , T and λ indicate the pressure, temperature (the subscript s denotes the surface temperature) and wavelength respectively. The first term represents the contribution from the surface whilst the second represents the atmospheric contribution. The third term is the radiation emitted by the atmosphere towards the surface and reflected back towards space. For the IR wavelengths, the last term is usually small and can be neglected. The atmospheric component is equal to the integral, from the surface to the top of the atmosphere (i.e. $z = \infty$), of the Planck function weighted by the corresponding derivative of the transmission for each individual height layer within the atmosphere. The derivative of the transmission, otherwise known as the weighting function, determines how much each height layer, of thickness dz , contributes to the total radiance leaving the top of the atmosphere. Through careful selection of different wavelengths, it is possible to choose "channels" which are sensitive to different altitude regions (i.e. where the weighting function peaks). Since the transmission depends on the concentrations of the absorbing gases present, if the temperature profile and the profiles of other interfering trace gases (e.g. ozone or water vapour) are known accurately,

a modelled radiance can be calculated and the difference to the measurement then attributed to the corresponding local target gas concentration e.g. CO.

Most molecules that play an important role in environmental problems have a spectral signature in the thermal-IR, although the information is easier to extract for those combining high atmospheric variability with large infrared absorption. In this regard, water vapour, ozone, and carbon monoxide are the more suitable molecules to be monitored using IR techniques. The advantage of using the thermal-IR is that measurements can be performed both day and night and additionally over the oceans where the use of NIR measurements, unless in a sun-glint viewing geometry, are questionable because of low albedo. Studies by Deeter et al. [2003] (e.g. MOPITT), Rinsland et al. [2006] (e.g. Tropospheric Emission Spectrometer, TES), Clerbaux et al. [2009] (e.g. Infrared Atmospheric Sounding Interferometer, IASI), and Wang et al. [1999] have all utilised thermal-IR spectra for the retrieval of atmospheric CO. Nevertheless, in this thesis, the thermal-IR MOPITT instrument retrieved CO data are used to examine better vertical differentiation of CO in the troposphere by quantitative analysis of retrieval information content and latter to enhance knowledge of CO in the troposphere.

2.3 The Radiative Transfer Equation

Understanding how radiation influences atmospheric properties requires a quantitative description of radiative transfer, which is complicated by its three dimensional nature and its dependence on wavelength and directionality. This is mostly due to the fact that scattered light can propagate in any direction and can undergo further scattering and absorption processes. Radiative transfer studies the propagation of radiation through a medium and its interactions with the surrounding environment. The propagation of radiation in a planetary atmosphere is affected by the distribution of atomic and molecular species. Any molecules that actively participate in the propagation of radiation impart their own signature onto the radiation field and subsequent analysis permits retrieval of the molecular species. In addition, the atmospheric state parameters of temperature and pressure play a significant role in atmospheric radiative transfer.

Consequently, remote sensing observations are only possible due to the transfer

of radiation through the atmosphere to the instrument. The energy of radiation propagating through the atmosphere will be modified by emission, absorption, and scattering. These effects are described by emission coefficients (those which increase the energy) and extinction coefficients (those which decrease the energy in the radiation field by either scattering or absorption) in which absorption is the physical process by which photons are removed from the radiation field. If an atmospheric layer has a number density of molecules, n , and each of these molecules presents an effective cross sectional area, $\hat{\sigma}_{a\lambda}$, to the ray of light propagating through the medium, then the probability of a photon being absorbed by one of these molecules along the differential path, ds , is given as,

$$\boxed{\frac{dI_\lambda}{I_\lambda} = -n\hat{\sigma}_{a\lambda}ds} \quad (2.2)$$

where the absorption cross section $\hat{\sigma}_{a\lambda}$ is referred to an individual particle and has dimension of area. This equation is known as the Beer-Lambert Law, which states that the variation of the intensity of the incident beam (radiation) as it passes through a sample is proportional to the concentration of that sample and its thickness (path length). The absorption coefficient then becomes:

$$\boxed{\beta_{a\lambda} = \rho\sigma_{a\lambda} = n\hat{\sigma}_{a\lambda}} \quad (2.3)$$

Thermal emission is the physical process by which new photons are added to a radiation field. The thermal emission of a gas in thermal equilibrium is given by the Planck function,

$$\boxed{B(\nu, T) = \frac{2hc^2\nu^3}{\exp\frac{hc\nu}{kT} - 1}} \quad (2.4)$$

where h is Planck's constant, c is the speed of light, ν is the wavenumber, T is the temperature of the source and k represents the Boltzmann constant.

The principle of detailed balance states that for a gas in thermal equilibrium, the emission and absorption will be equal at all wavenumbers. This provides the mechanism to calculate the thermal emission of a gas under thermal equilibrium [Reif, 1965]. Assuming that the atmospheric layer is in local thermodynamic equilibrium (LTE) at a given temperature, then

$$\boxed{\epsilon_\lambda = a_\lambda} \quad (2.5)$$

With Eq. 2.5, the fractional energy emitted along an incremental distance ds can be expressed as the Beer-Lambert law):

$$\boxed{\frac{dI_\lambda}{B_\lambda} = d\epsilon_\lambda = da_\lambda = \rho\sigma_{a\lambda}ds} \quad (2.6)$$

Then at a given temperature, T , we have

$$\boxed{dI_\lambda = \rho\sigma_{a\lambda}J_\lambda ds} \quad (2.7)$$

where,

$$J_\lambda = B_\lambda(T) \quad (2.8)$$

Eq. 2.8 holds under LTE condition of Kirchoff's law. Otherwise, the contribution to the source function from emission is more complex.

Extinction and emission coefficients must combine to give a change in radiance. Hence, the equation of transfer may be written as:

$$\boxed{\frac{dI_\lambda}{k_\lambda\rho ds} = -I_\lambda + J_\lambda} \quad (2.9)$$

Which is the radiative transfer equation in general form. In the absence of scattering, Eq. 2.9 reduces to

$$\boxed{\frac{dI_\lambda}{k_\lambda\rho ds} = -I_\lambda + B_\lambda(T)} \quad (2.10)$$

This equation is called Schwarzschild's equation. The first term in the right hand side of Eq. 2.10 denotes the reduction of radiant intensity due to absorption, whereas the second term represents the increase of the radiant intensity arising from blackbody emission of the material.

To apply the radiative transfer Eq. 2.10 to remote sensing problems firstly consider the optical path of radiation from source to the instrument (Fig. 2.1). The optical depth τ_λ of a medium is a dimensionless quantity related to the absorption coefficient (or opacity) that gives a measure of how much radiation is attenuated as it passes through it along a geometrical path, between two points S and S_1 (Fig. 2.1) and is defined by:

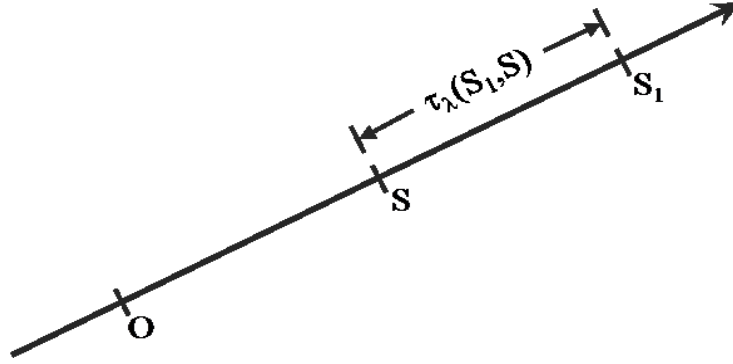


Figure 2.1: Configuration of the optical path and thickness

$$\tau_\lambda(S_1, S) = \int_S^{S_1} k_\lambda \rho ds' \quad (2.11)$$

Eq. 2.10 becomes

$$-\frac{dI_\lambda(S)}{d\tau_\lambda(S_1, S)} = -I_\lambda(S) + B_\lambda[T(S)] \quad (2.12)$$

As Eq. 2.12 is a linear first-order differential equation with constant coefficients, upon multiplying by a factor $e^{-\tau_\lambda(S_1, S)}$, and integrating the thickness ds from O to S_1 , we get,

$$-\int_O^{S_1} d \{ I_\lambda(S) e^{-\tau_\lambda(S_1, S)} \} = \int_O^{S_1} B_\lambda [T(S)] e^{-\tau_\lambda(S_1, S)} d\tau_\lambda(S_1, S) \quad (2.13)$$

Consequently,

$$I_\lambda(S_1) = I_\lambda(O) e^{-\tau_\lambda(S_1, O)} + \int_O^{S_1} B_\lambda [T(S)] e^{-\tau_\lambda(S_1, S)} k_\lambda \rho ds \quad (2.14)$$

The first term in Eq. 2.14 represents the absorption attenuation of the radiant intensity by the medium. The second term represents the emission contribution from the medium along the path from O to S_1 . If the temperature and density of the medium, and the associated absorption coefficient along the path of the beam are known, Eq. 2.14 can be integrated numerically to yield the intensity at the point

S_1 . Thus, the radiance leaving the earth-atmosphere system sensed by a satellite borne radiometer is the sum of radiation emissions from the earth-surface and each atmospheric level that are transmitted to the top of the atmosphere. Eq. 2.14 can be applied then to IR radiative transfer and to remote sounding of atmospheric temperature profiles and composition, in particular for CO, for orbiting satellite.

2.3.1 Nadir Infrared Sounding

As previously stated, measurement from satellite instrument can be made in downwards (nadir) direction or along a horizontal direction (limb). The atmospheric volume directly beneath the instrument is observed in nadir measurement mode. This observational mode have been applied successfully by other space-based instruments (e.g. SCIAMACHY, Bovensmann et al. [1999]).

In this thesis, thermal-IR measurements of nadir emission (MOPITT instrument) are discussed. In nadir (vertical) viewing, the altitude viewed depends partly on the spectral region used. Emission comes from a layer of the atmosphere at an altitude which depends on the absorption coefficient and the absorbed concentration. Spectral regions in which the atmospheric absorption is high provide measurements from high up in the atmosphere, spectral regions in which the absorption is low provide measurement of emission from low in the atmosphere or the surface [Houghton et al., 1986; Stephens, 1994]. The advantage of nadir viewing is that high spatial resolution can be achieved, but a disadvantage is poor vertical resolution. In particular, MOPITT is a nadir sounding instrument (Fig. 2.2), which provides a horizontal resolution of 22 km, but introduces a number of challenges, such as the need for accurately characterizing the surface contribution to the signal.

In order to retrieve any vertical information on trace gas concentrations the temperatures of the vertical layers to be retrieved must be different enough to provide distinct features in the radiation field. The atmospheric temperature profile is therefore important in determining the achievable vertical resolution of a nadir viewing instrument, and as such, the vertical resolution will be low over locations where the atmospheric temperature profile is quite flat such as high latitudes during the winter.

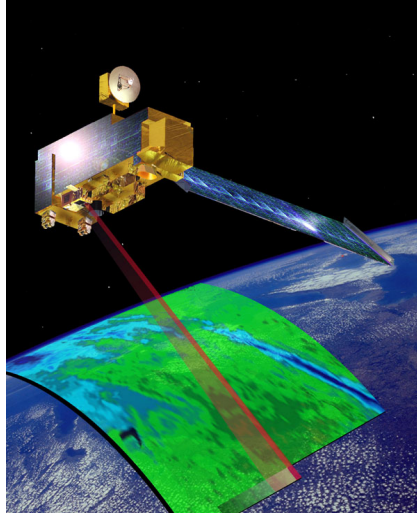


Figure 2.2: MOPITT instrument scanning the atmosphere in nadir modes (Image: NASA).

2.4 The MOPITT Concept

In this section of the thesis, a brief overview of the MOPITT instrument technique and retrieval theory used to infer CO concentrations from upwelling radiation from the atmosphere are given.

Figure 2.3 shows the MOPITT instrument layout, calibration photo, Terra spacecraft showing onboard instruments including MOPITT and the MOPITT instrument scan pattern. The MOPITT instrument makes CO measurements in two spectral regions, thermal-IR emission at $4.7 \mu\text{m}$ and reflected solar radiation at $2.3 \mu\text{m}$. A schematic of the relative thermal and solar signals is shown in Fig. 2.4. This thesis work will concentrate on the thermal-IR channels as the calibration of the solar channels has only very recently been characterised [Deeter et al., 2009]. The first retrieval results of CO are exclusively reported using NIR radiances in the $2.3 \mu\text{m}$ CO overtone band observed by MOPITT instrument. The original concept behind the design of the MOPITT instrument was to fully exploit the complementary nature of thermal-IR and NIR radiances to maximise vertical resolution, especially in the lower troposphere.

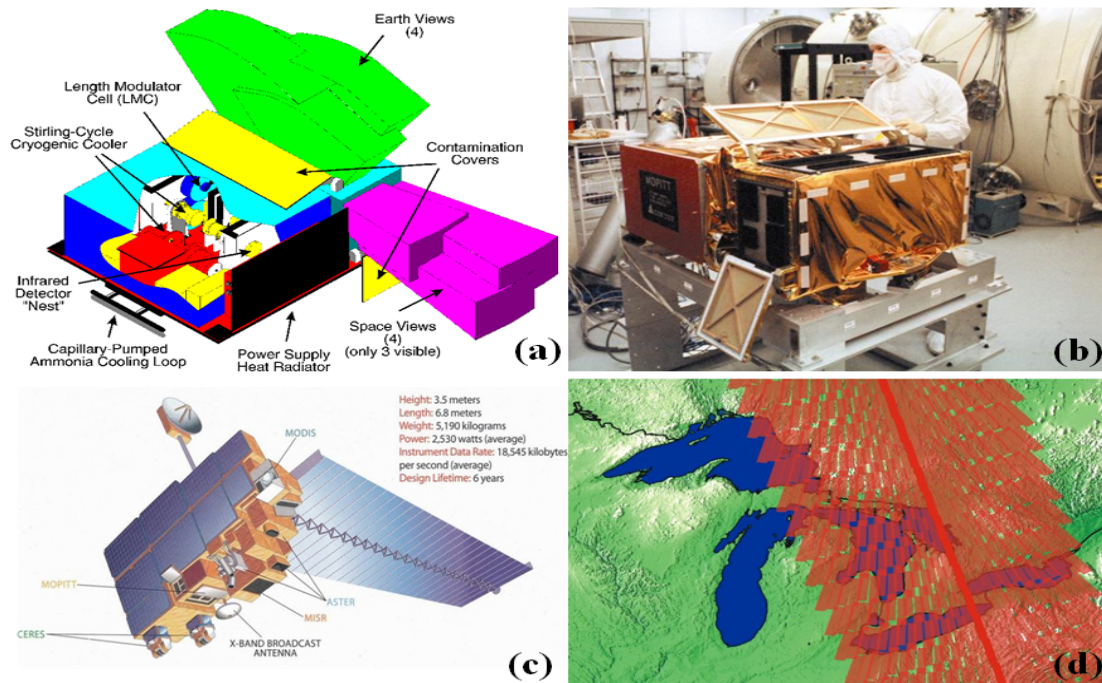


Figure 2.3: Showing (a) the MOPITT instrument layout, (b) calibration photo, (c) Terra space-craft showing onboard instruments including MOPITT, and (d) the MOPITT instrument scan pattern [Drummond, 1992].

2.4.1 The MOPITT Technique

Now that we have described some basic radiative transfer, we turn to how this transmitted and emitted atmospheric radiation is used by MOPITT to determine the atmospheric concentration of CO (target gas). The basic systems used are known as correlation radiometers. The MOPITT instrument technique has been described in publications and documents by Drummond [1992, 1993, 1996]. The key to the technique is to direct the atmospheric radiation through a gas-cell filled with the target species, CO in this case, and another identical gas-cell which is empty. The spectroscopic signature in the atmospheric signal is aligned with the absorption features of the target species in the filled gas-cell while no spectral alignment occurs in the empty cell. The difference between the signal emerging from each cell permits the spectroscopic signature of the target gas originally present in the atmospheric radiation to be determined. This is known as gas correlation radiometry. Inversion schemes can then be applied to derive concentrations of CO in the atmosphere.

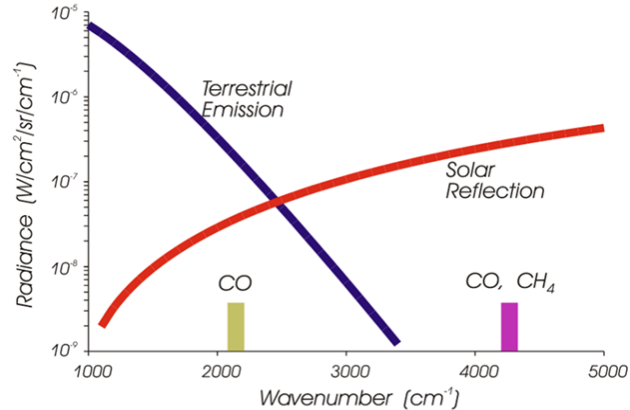


Figure 2.4: Schematic diagram of the spectral bands used for MOPITT instrument [Drummond, 1992].

2.4.2 Gas Correlation Radiometry

Since all gases in the atmosphere are emitting/absorbing simultaneously, it is essential that the effect of the gas of interest can be separated out from the overall signal. Furthermore, since the information about the vertical distribution of the gas is contained within the shape of an individual absorption/emission line, it is necessary to be able to resolve the line shape, which generally requires high spectral resolution. High spectral resolution leads to low signal to noise, which means low instrument sensitivity. Therefore, high sensitivity and high spectral resolution requirements for tropospheric trace species remote sensing are difficult to implement with conventional dispersing instruments. Correlation spectroscopy, a non-dispersing spectroscopy technique, offers the opportunity for high spectral resolution as well as high signal to noise [Wang et al., 1999]. The fundamental technique of correlation radiometry is illustrated in Fig. 2.5.

The principle of gas correlation spectroscopy is that of spectral selection of radiation emission or absorption by a gas using a sample of the same gas as the filter. In the absence of Doppler shifts, the spectral lines of a gas must align perfectly with themselves and the spectral alignment of the system will be perfect without the need for sensitive dispersive elements. The cell contains a sample of the target gas. Monochromatic radiation entering from the left (in Fig. 2.5) is filtered by the gas cell transmission function. The corresponding output as a function of spectral

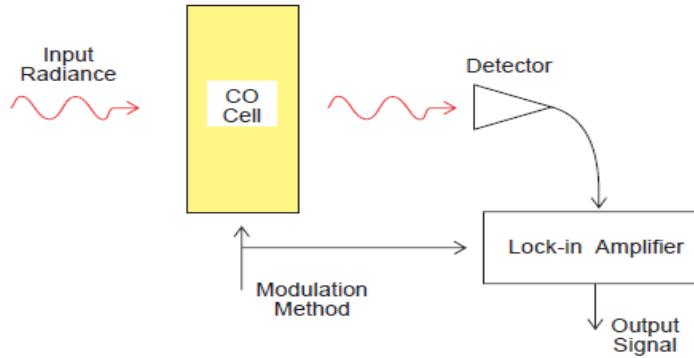


Figure 2.5: A basic gas correlation radiometry

frequency is shown in Fig. 2.6 for two different amounts of gas in the absorption cell. By cycling the amounts of gas in the absorption cell between the two states, the detector will be alternately looking through two different filters, resulting in two different signals. The difference of the two signals will be identical to the output of a system in which the gas cell and its modulator are replaced by an optical filter, with an effective difference transmission (EDT) curve in Fig. 2.6b. The EDT curve is the difference between the system transmission at low cell pressure [$\tau\mu_l$ in Fig. 2.6a] and the system transmission at high cell pressure [$\tau\mu_h$ in Fig. 2.6a]. Figure 2.6c illustrates the advantage of gas correlation in discriminating against interference spectral lines that are not correlated with the target gas spectral lines. The spectral line in the middle of the input radiance, which is not correlated with the lines of the gas in the cell, corresponds to the minimum in the EDT transmission. Hence the difference response (dashed line) is very small. Note that the average response is actually reduced at the spectral lines of the target gas and continues to include the contaminating spectral line. Therefore the difference response provides the most selective signal for the target gas whilst the average response also has some sensitivity to the target gas.

MOPITT makes use of two methods to modulate the transmittance in the gas cell. The first is by varying the cell pressure through the use of pressure-modulated cells (PMCs) that have been described in detail by Taylor [1983]. The second is by varying the amount of gas in the cell through length-modulated cells (LMCs) [Drummond, 1989]. Two PMRs with different mean pressures and four LMRs are

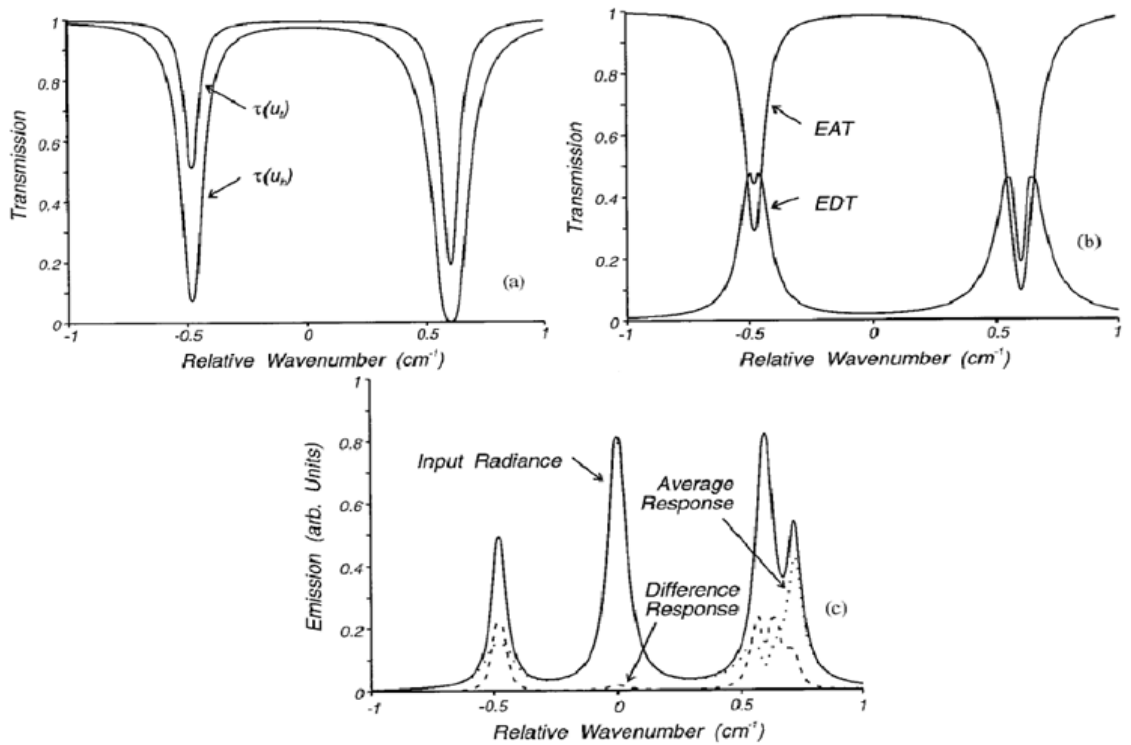


Figure 2.6: Operation of a correlation spectrometer in spectral space. Panel (a) shows low cell pressure (τ_{μ_l}) and high cell pressure (τ_{μ_h}) curves. The filter profile is illustrated by the EDT curve in (b), which is the difference of the system transmission at low cell pressure and at high cell pressure. Panel (c) shows the advantage of gas correlation in discriminating against interference spectral lines [Drummond, 1992].

used in MOPITT. Separating the 2.3 μm and 4.7 μm channels with dichroic beam splitters results in eight separate spectral channels.

Table 2.1 shows how the MOPITT instrument makes use of two PMCs and four LMCs to form eight spectral channels, six are designed to be used for CO retrievals and two for CH₄. The LMR channels contain cells with higher pressure to optimise instrument sensitivity to the lower and middle troposphere, and the PMR channels contain cells with lower pressure to optimise instrument sensitivity to the upper troposphere. Each channel produces an average signal (A), which is the average of the instrument signals corresponding to the two states of the modulating cell and a difference signal (D), which is the difference of the instrument signals corresponding to the two states of the modulating cell. For the LMC channels, the two states are defined by the two alternate cell path lengths of 2 and 10 mm. For the PMC channels,

Table 2.1: Characteristics of MOPITT CO and CH₄ channels. The nominal PMC and LMC cell pressure, temperature, and length are listed [Wang et al., 1999].

Channel no.	Primary purpose	Modulator type	Cell pressure (mb)	Cell temperature (K)	Cell length (mm)	Centre wavenumber* cm^{-1}
1	CO	LMC1	200	300	2-10	2166 (52)
2	CO	LMC1	200	300	2-10	4285 (40)
3	CO	PMC1	50-100	300	10	2166 (52)
4	CH ₄	LMC2	800	300	2-10	4430 (140)
5	CO	LMC3	800	300	2-10	2166 (52)
6	CO	LMC3	800	300	2-10	4285 (40)
7	CO	PMC2	25-50	300	10	2166 (52)
8	CH ₄	LMC4	800	300	2-10	4430 (140)

* Numbers in parenthesis are band filters full width at half maximum (FWHM).

the two states are defined by the alternate high and low cell pressures. Theoretical and experimental studies indicate that a PMC cell can be represented accurately by a two pressure system [May et al., 1988; Roscoe and Wells, 1989; Berman et al., 1993]. Radiative transfer calculations indicate that the difference signals are more sensitive to atmospheric CO (and CH₄) changes, and the average signals for MOPITT are more sensitive to earth surface and cloud characteristics.

2.4.3 Retrieval Theory

Many standard retrieval techniques can be applied to the retrieval of atmospheric trace gases and temperature profiles from measurements with gas correlation instruments. One of the widely used methods is the maximum likelihood method [Rodgers, 2000]. The general concepts underlying the MOPITT CO retrieval algorithm have been discussed in detail previously by Pan et al. [1998]. An explanation of the terminology and definitions is given in this section.

2.4.3.1 The State and Measurement Vectors

The quantities to be retrieved can be represented by a state vector, x , with n elements, x_1, x_2, \dots, x_n and the quantities actually measured in order to retrieve x can be represented by the measurement vector y , with m elements, y_1, y_2, \dots, y_m . The

aim of the retrieval is to gain as much information about x given y . Measurements are made to a finite accuracy, the associated random error of the measurements, or measurement noise, is denoted by the vector ϵ .

2.4.3.2 The Forward Model

The relationship between the state vector and the measurement vector are related to a forward model, $F(x)$, which attempts to approximate the atmospheric physics involved.

The equation relating the true atmospheric state and the measured radiances can be written as,

$$\boxed{y = F(x, b) + N_\epsilon} \quad (2.15)$$

where y is the measurement vector (i.e., the observed MOPITT radiances), x is the state vector (i.e., all the desired retrieved variables), b represents all other forward model parameters (i.e., all parameters needed to calculate the MOPITT radiances not explicitly included in the state vector), $F(x, b)$ represents the forward radiative transfer model [Edwards et al., 1999], and N_ϵ is the radiance error vector. The goal of the retrieval algorithm is to estimate the true state vector x from the measured radiances y and the associated measurement errors.

2.4.3.3 The Weighting Function Matrix

To account for the general non-linearity of the problem and to avoid interferences between strong absorbers, simplified assumptions are made to reduce the problem to a linear one, providing that $F(x)$ is linear within the bounds of the retrieval. This can be achieved by linearising Eq. 2.15 about some reference state x_0 ,

$$\boxed{y - F(x_0) = \frac{\partial F(x)}{\partial x}(x - x_0) + \epsilon = K(x - x_0) + \epsilon} \quad (2.16)$$

which defines the $m \times n$ *weighting function matrix* K . where the partial derivative $\frac{\partial F(x)}{\partial x}$ denotes the sensitivity of the forward model (i.e. the change in radiance) to a change in the state vector.

In principle, the sensitivity of MOPITT retrieved CO profiles to the actual vertical distribution of CO depends on the characteristics of the weighting functions

(see section 2.4.4). Weighting function calculations are a critical component of the MOPITT optimal estimation retrieval algorithm [Deeter et al., 2003] and generally depend on the same quantities as the radiances: profiles of CO, temperature, and water vapor, surface temperature and emissivity, and solar and satellite zenith angles [Edwards et al., 1999].

2.4.4 MOPITT L2V3 Operational Retrievals

Following a cloud-detection stage [Warner et al., 2001], an optimal estimation-based retrieval algorithm [Pan et al., 1998; Deeter et al., 2003] employing a fast radiative transfer model is used to invert the calibrated satellite radiances to determine the tropospheric CO concentrations [Deeter et al., 2004]. MOPITT is an eight-channel gas correlation radiometer; each channel generates an average (A) signal and a difference (D) signal as described in section 2.4.2. The thermal channel A-signals are sensitive primarily to emission from the surface, which depends on both the surface skin temperature and emissivity. The D-signals are sensitive to both thermal emission/reflection and solar reflection (daytime) from the surface and target gas absorption and emission for different vertical levels. The radiances used for the retrievals include the A-signal for channel 7, and the D-signals for channels 1, 3, and 7. The channel 5D-signal was excluded because of an apparent radiance bias which greatly degraded the retrievals. A-signal radiances for channels 1, 3, and 5 were excluded because of the high redundancy of the information contained in these signals with the information contained in the 7A-signal. The solar CO channels 2 and 6 were excluded from the retrievals because of low observed signal-to-noise ratios. Figure 2.7 shows weighting functions for the different cell pressures of the 6 CO channels.

In the following section of thesis, details are given about MOPITT forward modelling, retrieval algorithm formulation and operational retrieval information content.

2.4.4.1 Forward Modelling

Forward modeling of the MOPITT channel radiances must combine accuracy and precision while providing for variations in target and contaminating gases, temperature, viewing geometry and surface properties. At the same time, there must be a forward model suitable for processing at high computational speed. To achieve this,

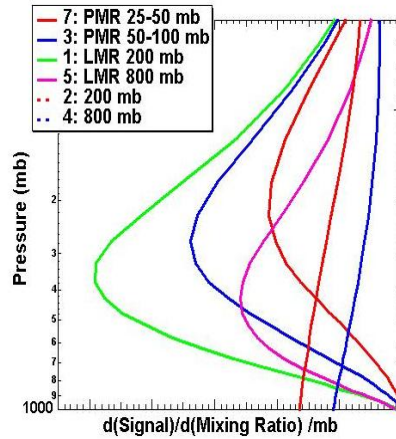


Figure 2.7: Shows weighting functions for the different cell pressures of the 6 CO channels used in operational retrievals [Deeter et al., 2003].

a set of radiation models have been developed. An expanded, though simplified, discussion can be found in Francis et al. [1999] and a detailed discussion of the MOPITT forward models is presented in Edwards et al. [1999].

The MOPITT line-by-line (LBL) calculations, described by Pan et al. [1995], were performed using the general purpose line-by-line transmittance and radiance model GENLN2 [Edwards, 1999]. The fast forward model developed for the MOPITT operational retrieval is called MOPFAS [Edwards et al., 1999]. The aim of this model is to solve the radiative transfer equation after having first performed the spectral integration off-line. It reproduces MOPITT channel signals taking into account their dependence on temperature, mixing ratios of target and contaminating gases, and satellite and solar zenith angles. A regression scheme is applied to establish a correspondence between channel-integrated transmittances and atmospheric profiles so that when given a profile MOPFAS is able to quickly infer a corresponding transmittance. The regression coefficients are pre-computed using a least squares fit over a representative atmospheric ensemble. Typically, a MOPFAS calculation is about 10^5 times faster than GENLN2 LBL calculations. This is fast enough for MOPFAS to be used in operational retrievals.

2.4.4.2 Retrieval Algorithm Formulation

In atmospheric remote sensing, the common problem of inverting a set of measured radiances to determine aspects of the atmospheric state (temperature profile, trace gas mixing ratio profiles, etc.) is often ill-conditioned, meaning that no unique solution exists without added constraints. Thus, additional information of some type is usually required to constrain the retrieval to fall within physically reasonable limits. The CO retrieval algorithm used for MOPITT exploits a nonlinear optimal estimation algorithm [Rodgers, 2000; Pan et al., 1998] and a fast radiative transfer model [Edwards et al., 1999] to invert the measured A and D-signals to determine the tropospheric CO concentrations. More precisely, the CO retrieval algorithm used for MOPITT exploits the maximum a posteriori ("MAP") solution which is a specific type of optimal estimation technique [Rodgers, 2000]. The general strategy of such techniques is to seek the solution most statistically consistent with both the measured radiances and the typical observed patterns of CO vertical profiles as represented by the a priori information. The methodology for generating the a priori (i.e., both the a priori mean profile and the a priori covariance matrix) is described in detail in section 2.4.4.3. For the thermal band signals the average and difference signals for each channel are included directly in the measurement vector. The thermal band signals are not only dependent on the CO profile being measured but also the atmospheric temperature and water vapour profiles, and the surface temperature and longwave emissivity. Therefore, good values for all these parameters must be obtained in order to produce accurate retrievals [Deeter et al., 2003]. For each MOPITT observation (i.e., a single "pixel"), the retrieval algorithm requires profiles of both temperature and water vapour. These profiles are spatially and temporally interpolated from National Centers for Environmental Prediction (NCEP) operational analysis products. Values for the surface temperature and emissivity are retrieved simultaneously with the CO profile from information contained in the thermal band signals.

The most general measurement and state vectors for a given pixel can be written, respectively, as

$$y = (y_i) = \begin{pmatrix} S_1^A \\ \cdot \\ \cdot \\ S_4^A \\ S_1^D \\ \cdot \\ \cdot \\ S_4^D \\ S_1^R \\ S_2^R \end{pmatrix} \quad x = (x_j) = \begin{pmatrix} \epsilon_{sfc} \\ T_{sfc} \\ q_1 \\ q_2 \\ \cdot \\ \cdot \\ \cdot \\ \cdot \\ q_7 \end{pmatrix} \quad (2.17)$$

where y is the measurement vector, S_A and S_D represent the average and difference signals respectively for each thermal channel, x represents the state vector which contains the surface emissivity, the surface temperature T_{sfc} and q_i which represents the CO mixing ratio at the i^{th} pressure level of the predefined retrieval grid. The seven levels in the L2V3 operational retrieval grid include the surface, 850, 700, 500, 350, 250, and 150 hPa. A Newtonian iterative form of MAP solution is found which combines the state vector, determined solely from the measurements, and the a priori state vector, inversely weighted by their respective covariances. If the error terms are neglected, the MOPITT retrieved CO profile \hat{x} can be expressed as a linear combination of the true profile x_t and an a priori profile, x_a , through the matrix relation [Rodgers, 2000].

$$\boxed{\hat{x} \approx \mathbf{A}x_t + (I - \mathbf{A})x_a} \quad (2.18)$$

where I is the identity matrix and \mathbf{A} is the averaging kernel matrix. The averaging kernels indicate the sensitivity of the retrieval to the atmospheric state $\frac{\partial \hat{x}}{\partial x}$ and provide the relative weighting between the true and a priori profile. The ideal situation would be one where \mathbf{A} equals I then from Eq. 2.18 we see that $\hat{x} \approx x_t$ and the retrieved profile reflects the true profile, generally though this is not the case and changes in the true profile result in finite changes to all elements of the retrieved profile. Thus, the averaging kernel gives some indication of the vertical resolution and sensitivity of the retrieval and the influence of the a priori. Averaging kernels are calculated from

the a priori covariance matrix (C_a) and the retrieval error covariance matrix ($C_{\hat{x}}$), determined for each retrieval:

$$\boxed{\mathbf{A} = I - C_{\hat{x}}C_a^{-1}} \quad (2.19)$$

The retrieval covariance matrix is calculated using the a priori covariance matrix, the weighting function (K), and the radiance error matrix (C_e):

$$\boxed{C_{\hat{x}} = (C_a^{-1} + K^T C_e^{-1} K)^{-1}} \quad (2.20)$$

The square roots of the diagonal elements of the retrieval error covariance matrix provide the retrieval errors for each profile retrieval. Expanding Eq. 2.19 and Eq. 2.20, the averaging kernel may be expressed as:

$$\boxed{\mathbf{A} = I - (C_a^{-1} + K^T C_e^{-1} K)^{-1} C_a^{-1}} \quad (2.21)$$

Thus, the averaging kernel is directly related to the weighting function which describes the sensitivity of the measurement to the vertical distribution of the species of interest in the atmosphere.

The MOPITT L2V3 Product consists of retrieved values and estimated uncertainties of the CO profile, CO total column, surface temperature, and surface emissivity. For the CO profile, the retrieval error covariance matrix is also provided.

2.4.4.3 MOPITT V3 A Priori

In principle, the a priori represents the expected statistical behavior (both in terms of the mean state and variability) of the state vector. For CO, seasonal and geographic patterns are well documented [Hauglustaine et al., 1998]. Therefore it might be reasonable to incorporate some degree of spatial and/or temporal dependence into the a priori. In MOPITT L2V3 operational processing, however, a fixed 'global' a priori for all CO retrievals has been chosen. This profile and its uncertainties can be seen in Fig. 2.8. A fixed a priori was chosen with mainly three motivations. First, use of a spatially-varying a priori would produce corresponding spatial features in the retrieved profiles which would not be associated with any information in the actual satellite observed radiances. Secondly, as the a priori becomes more specific (either spatially or temporally), the a priori variances and covariances would be expected to

decrease and in the retrieval scheme used would reduce the relative weight given to the measured radiances. Lastly, for practical reasons, use of a fixed a priori covariance matrix simplifies averaging kernel calculations (see section 2.4.4.4).

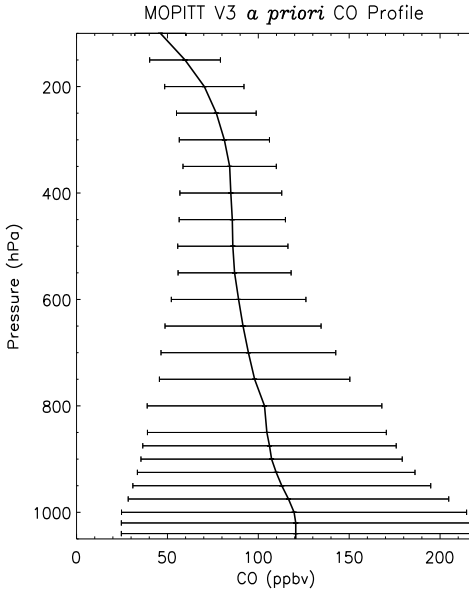


Figure 2.8: MOPITT L2V3 a priori profile.

The a priori, consisting of both the covariance matrix C_a and the mean state vector x_a , describes the statistical behavior of the CO profile, surface temperature, and emissivity. In the L2V3 product, the MOPITT a priori is generated from a master set of 525 in situ profiles measured by aircraft during eight atmospheric chemistry field campaigns (TROPOZ-II, Boissard et al. [1996]; STRAT0Z-III, Gerhardt et al. [1989]; TRACE-A, Fishman et al. [1996]; PEMWEST-A, Newell et al. [1996]; PEMWEST-B, Talbot et al. [1997]; PEMTROP-A, Hoell et al. [1999]; ABLE-3A, Harriss et al. [1992] and ABLE-3B, Harriss et al. [1994]) and at two fixed sites (Carr, Colorado, Bakwin et al. [1994] and Cape Grim, Australia, Pak et al. [1996]). Typically, these in situ profiles extend from the surface to approximately 400 hPa (the aircraft maximum flight altitude). The profiles are then extended to cover the higher MOPITT levels with monthly climatological data from the chemistry transport Model of Ozone And Related Tracers (MOZART) [Hauglustaine et al., 1998]. The a priori value of the surface temperature is interpolated from National Centre for Environmental Prediction (NCEP) reanalysis at each pixel. The longwave surface emissivity is obtained from a

surface emissivity database [Wilber et al., 1999] coupled to a geographical database of surface types [Belward and Loveland, 1996].

2.4.4.4 Standard Averaging Kernels

Averaging kernels indicate the sensitivity of the retrieval to the true observed profiles and exhibit significant variability, e.g., due to variation of the atmospheric temperature profile, surface temperature and emissivity. The more detailed analysis of L2V3 retrieval averaging kernels has been performed in chapter 3 to examine the case for better vertical structure of CO in the troposphere and to study lower tropospheric sensitivity.

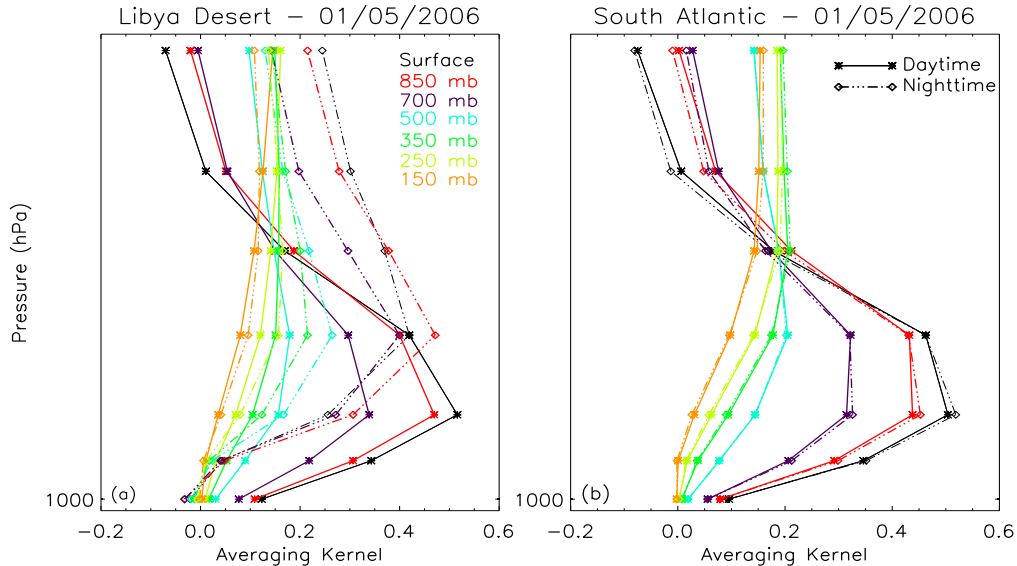


Figure 2.9: Mean averaging kernels obtained by averaging all daytime and nighttime averaging kernels separately on May 01, 2006 (a) in the box defined by 20°N, 30°N, 10°E, and 25°E (over Libyan desert) and (b) in the box defined by 15°S, 30°S, 5°W, and 20°W (over South Atlantic).

Figure 2.9 shows example averaging kernels for MOPITT retrievals conducted at day and night over the (a) Libya desert and (b) South Atlantic Ocean. Ideal averaging kernels would have a peak of one at the required pressure level (i.e., altitude) and are zero at all other levels, and good averaging kernels have elements that sum to one. It has to be noted that MOPITT operational L2V3 kernels are far from ideal and the averaging kernels for each level in the retrieved profile do not necessarily peak

at the corresponding pressure level of the true profile. Sensitivity is generally higher to CO in the middle and upper troposphere than in the lower troposphere; this is a consequence of the relatively weak thermal contrast between the surface and the lower troposphere (see section 3.3.1) and the physics of thermal-emission radiative transfer [Deeter et al., 2004]. It can be seen from Fig. 2.9 that the kernels are not sharply defined, and that averaging kernels for adjacent levels in the retrieved profile are often quite similar. For example, the strong similarity of the averaging kernels for the 850 hPa and 700 hPa levels indicates a high correlation for the retrieved values at these levels. On the other hand, a comparison of the 850 and 250 hPa averaging kernels reveals sharply contrasting vertical sensitivity. The 850 hPa averaging kernel peaks near 700 hPa whereas the 250 hPa averaging kernel peaks near 150 hPa. Thus, although the averaging kernels shown in Fig. 2.9b are not sharply defined, MOPITT retrievals should at least provide sufficient information to discriminate between mid- and upper-tropospheric CO.

Moreover, as documented by [Deeter et al., 2003], the general shapes of the MOPITT averaging kernels depend on the geophysical regime. The averaging kernels shown in Fig. 2.9b are typical for tropical oceanic scenes. The sharpest (i.e., best-separated) averaging kernels are observed in daytime scenes over land (Fig. 2.9a); these scenes provide the strongest thermal contrast between the surface and atmosphere. At the opposite extreme, the averaging kernels in polar regions and in nighttime mid-latitude winter scenes over land typically exhibit highly correlated averaging kernels at all levels and therefore much less profile shape information [Deeter et al., 2004]. The more detailed averaging kernels analysis for MOPITT operational L2V3 product is carried out in the chapter 3.

2.4.4.5 Degrees Of Freedom for a Signal (DOFS)

When experimental error is not present there are p independent pieces of information that can in principle be determined from the measurement, but with error, these p values will now be uncertain to some extent (a phenomenon called 'ill-conditioning'). A useful parameter calculated from the information about the measurement and the a priori data is the degrees of freedom for a signal (DOFS), which describes the number of independent pieces of information available in the retrieved vertical profile [Rodgers, 2000]. For the MOPITT MAP-retrieved profiles, DOFS is the sum of the

eigenvalues of \mathbf{A} , which is also the trace of \mathbf{A} . In the context of the eigenvalues and eigenvectors of \mathbf{A} , DOFS represents the number of orthogonal components in the retrieved profile which are retrieved with no contribution from the a priori profile [Rodgers, 2000; Pan et al., 1998]. In simple words, DOFS is a measure of the number of components of the retrieved CO profiles that are not constrained by the a priori. Like the averaging kernel matrix, DOFS values exhibit significant geographical variability and diurnal differences (especially over land) are strongly related to the surface temperature and emissivity [Ho et al., 2002b].

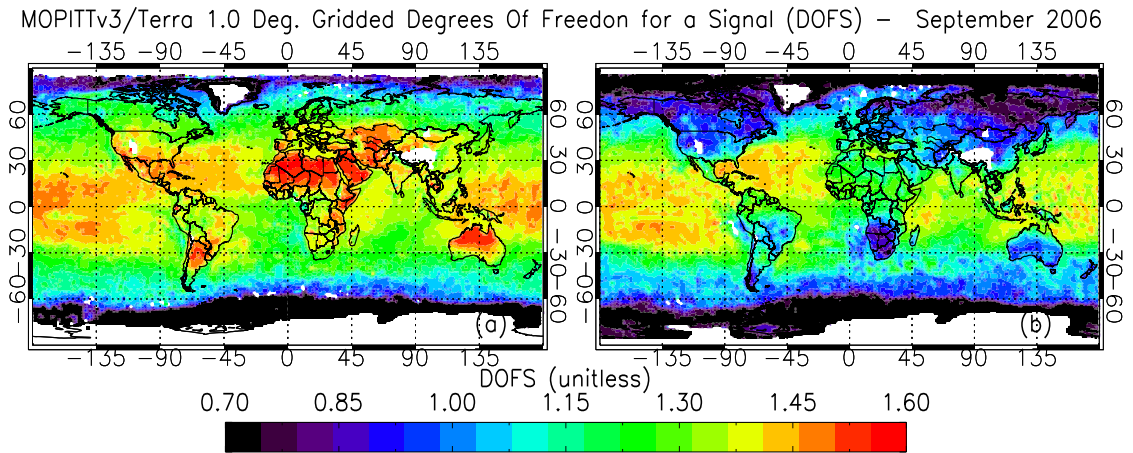


Figure 2.10: Degrees Of Freedom for Signal for September, 2006 for (a) Daytime and (b) Nighttime observations.

Figure 2.10 shows gridded MOPITT L2V3 monthly mean DOFS values for September, 2006. Values were calculated on a 1.0 by 1.0 degree grid after calculating the mean daytime and nighttime averaging kernels within each grid cell. DOFS values for daytime and nighttime observations are shown separately. White spaces in Fig. 2.10 correspond to regions of persistent cloudiness; since cloud-contaminated MOPITT observations are discarded for L2V3 operational product. Daytime DOFS values tend to be higher than nighttime values because (i) higher daytime surface temperatures (especially over land) tend to improve the thermal contrast between the surface and atmosphere, and (ii) solar radiation at $4.7 \mu\text{m}$ contributes a non-negligible component to the daytime observed radiances and therefore affects the radiance weighting functions. Latitudinally, values are highest near the Equator and decrease poleward. The highest values are observed during daytime scenes over deserts (which, as mentioned

above, are also where the averaging kernels are sharpest and/or higher thermal contrast). The smallest values occur in the polar regions and in mid-latitude nighttime scenes over land.

2.4.4.6 Percent A Priori CO Mixing Ratio

In the MOPITT L2V3 operational product, the variables "Percent a priori CO mixing ratio" and "retrieval bottom Percent a priori CO mixing ratio" give the fraction of information in each retrieval that came from the a priori profile. In order to select measurement that contain useful information about the CO content, Deeter et al. [2003] suggested use of the "percent a priori" to filter the MOPITT L2V3 data. This diagnostic is calculated (in percentage) as the ratio of the uncertainty of retrieved CO mixing ratio to the a priori variance of CO mixing ratio at same level. As this ratio tends towards zero, the retrieval is essentially perfect, and has low weighting from a priori. As this ratio tends towards unity, however, the implication is that the retrieval has not provided useful information. In other words, large percentages indicate that the retrievals were less constrained by the observations. Only those profiles having "percent a priori" less than 50% in the retrievals at retrieval pressure levels suggested to consider to ensure that the results minimally influenced by the assumed a priori profile.

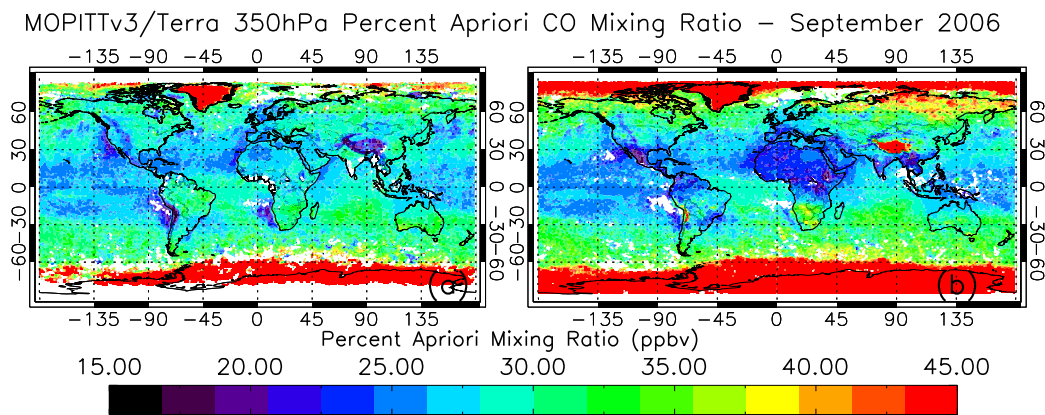


Figure 2.11: Percent a priori CO mixing ratio gridded on 1.0 deg. at 350 hPa for September, 2006 for (a) Daytime and (b) Nighttime observations.

Figure 2.11 show MOPITT L2V3 percent a priori CO mixing ratio global distribution at 350 hPa for (a) daytime and (b) nighttime observations. It is clearly evident that percent a priori has, although less significant, latitudinal variation showing a priori contribution to the retrieved CO is less at equator and increases towards poles. In this only those profiles that have percentage a priori less than 50% in the retrievals which are considered. Later, we have shown that DOFS and percent a priori CO mixing ratios are linearly correlated, in particular percent a priori CO mixing ratio retrieved at 350 hPa retrieval has best linear fit with DOFS (e.g. refer to 3.10). We, thus, define percent a priori CO mixing ratio threshold value to ensure that the profiles are not highly contaminated by retrieval artifacts. More details are discussed in Chapter 3.

2.5 MOPITT Level 2 Version 3 (L2V3) Product Validation

In this section, MOPITT retrieved L2V3 CO data, from thermal IR channel, validation for Phase I and Phase II has been discussed. The near-IR channels are not used in this version of the retrievals due to low observed signal-to-noise ratio.

The MOPITT instrument has been making global measurements of the CO distribution in the troposphere from March 2000 and continue to operate well at the present time (more than 9 years). While instrument parameters and calibration factors remain stable, validation of these products is critical to understanding their value for further scientific analyses. In May 2001, one of the two instrument coolers failed, after which only four of the eight channels were operational, requiring a change to the retrieval algorithm [Deeter et al., 2003]. The data before and after the cooler failure are therefore fundamentally different and have been termed Phase I, covering March 2000 to May 2001, and Phase II, starting from August 2001 to present. For the first year of measurements, the retrievals use the D signals from channels 1, 3, and 7 and the A signal from channel 7. After the cooler failure, channel 7 was reconfigured to improve the signal-to-noise ratio (see Deeter et al. [2004] for more details). This new configuration, using channels 5A, 5D, and 7D, results in the retrievals having a vertical resolution very similar to those of Phase I, despite the use of different signals

in the retrievals. Due to these changes in the instrument and the retrievals, Phase I and Phase II data are validated separately by Emmons et al. [2004]. In general, observations from the MOPITT spacecraft remote sensor form the basis of retrievals of tropospheric CO which have been validated by comparison with in situ aircraft measurements obtained through a regular program as well as through special field campaigns [Deeter et al., 2004; Emmons et al., 2004, 2007, 2009].

For Phase I data validation, the MOPITT CO retrievals have been compared with the in situ CO measurements (after applying the averaging kernels) at the five Climate Monitoring and Diagnostics Laboratory (CMDL, now called Earth System Research Laboratory (ESRL)) sites for each retrieval level and column. These sites include Hawaii, Rarotonga, Poker Flats, Harvard Forest, and Carr. The measurements as part of the MOPITT Validation Experiment (MOVE, Paul Novelli, CMDL) and the Southern African Regional Science Initiative (SAFARI-2000, Paul Novelli, CMDL) were made coincident with MOPITT overpasses. Furthermore, many aircraft measurements during several campaigns were also made coincident with MOPITT overpasses and comparison between the MOPITT retrieved and the in situ measured CO profile has been done. These campaigns were (i) Tropospheric Ozone Production about the Spring Equinox (TOPSE) campaign, organised by NCAR, during February-May 2000 (M. Coffey, NCAR); (ii) Biomass Burning and Lightning Experiment (BIBLE-C) campaign, organised by the Earth Observation Research Center of National Space Development Agency of Japan, during November-December 2000 (Y. Kondo, Uni. of Tokyo); (iii) CO₂ Budget and Rectification Airborne study (COBRA) organised by the University of North Dakota during August 2000. For all these validation campaign for Phase I, in general, a very good correlation between the MOPITT CO retrievals and in situ CO measurements was seen.

Similar validation comparisons have been made for the Phase II data, covering August 2001 through December 2002, using the five standard CMDL stations. The bias averaged over all of the sites for each retrieval level for Phase I and Phase II are given in Table 2.2. The bias is shown both as the absolute difference in mixing ratio and as percent. For Phase I data, in the lower troposphere MOPITT is high by 4-5 ppb (or 6-8%) whereas the bias is somewhat less in the upper troposphere. The column retrievals have an average bias of about 5%. The variability in the retrievals

attributed to uncertainties in the retrievals of surface temperature and surface emissivity [Emmons et al., 2004]. Whereas, for Phase II validation, the average bias less than ± 1 ppb (-3% to 2%) at all altitudes. In general, these results are consistent with the radiance biases found in the Level 1 validation results reported by Deeter et al. [2004].

Table 2.2: Absolute and percentage biases (mean and standard deviation) for each retrieval level and column, Averaged over all comparisons [Emmons et al., 2004].

Level	Absolute Bias ^a	Percentage Bias	Absolute Bias ^a	Percentage Bias
	Phase I		Phase II	
Surface	5.7±20.6	8.1±21.5	0.7±24.6	1.5±21.2
850 hPa	4.1±18.8	8.1±22.2	-0.6±20.9	-2.4±20.5
700 hPa	4.2±14.5	6.5±16.1	0.9±16.1	-0.2±16.3
500 hPa	2.7±9.8	3.8±10.1	0.5±9.6	0.9±10.4
350 hPa	1.7±11.9	2.6±12.3	0.7±8.9	1.6±10.1
250 hPa	0.7±11.5	1.7±13.0	0.6±7.8	1.6±9.9
150 hPa	-0.8±10.5	-0.2±15.8	-0.8±6.8	-0.2±10.8
Column	0.7±1.9	4.9±10.8	-0.2±2.2	-0.5±12.1

^a Measured in ppbv for profiles and 10^{17} molecules.cm⁻² for columns.

Later, Emmons et al. [2007] reported CO measurements made as part of three aircraft experiments during the summer of 2004 over North America for the validation of the CO retrievals from the MOPITT instrument. These campaigns were NASA’s Intercontinental Chemical Transport Experiment (INTEX-A), designed to be coincident with MOPITT overpasses, as well as the COBRA-2004 and MOZAIC (Measurement of OZone, water vapor, carbon monoxide and nitrogen oxides by Airbus In-service airCRAFT) experiments. Vertical profiles measured during these campaign provided valuable MOPITT validation results. From these comparison studies it is shown that the MOPITT CO retrievals are biased slightly high for North America locations, while the mean bias differs between the different aircraft experiments (e.g., 7.0 ppbv for MOZAIC to 18.4 ppb for COBRA at 700 hPa). This is likely due to the fact that the during INTEX-A campaign profiles were made as spirals and designed to be within one hour of the MOPITT overpass, resulting in a higher probability

that MOPITT were sampling the same air masses at all altitudes. Since the COBRA and MOZAIC-ICARTT aircraft measurements were not designed to be coordinated with MOPITT overpasses, and the vertical sampling was spread out over longer distances. On average, these results are consistent with the validation results presented by Emmons et al. [2004] and are generally within the design criteria of 10% accuracy. Moreover, these results indicate the likelihood of MOPITT CO retrievals for model evaluation and quantitative studies of the CO distributions.

Emmons et al. [2009] reported very recent and major validation results by comparing MOPITT CO retrievals to aircraft in situ measurements as part of routine sampling performed by National Oceanic and Atmospheric Administration (NOAA) at several sites, intensive field campaigns, and sampling from commercial aircraft. In particular, this work uses observations made as part of the NASA INTEX-B and National Science Foundation (NSF) Megacity Impact on Regional and Global Environment (MIRAGE) field campaigns during March-May 2006 to validate the MOPITT CO retrievals, along with routine samples from 2001 through 2006 from NOAA and the MOZAIC measurements. The details of aircraft measurements used for the MOPITT validation and the techniques used for measurements are described in Emmons et al. [2009]. The location of the measured profiles used for validation are shown in Fig. 2.12.

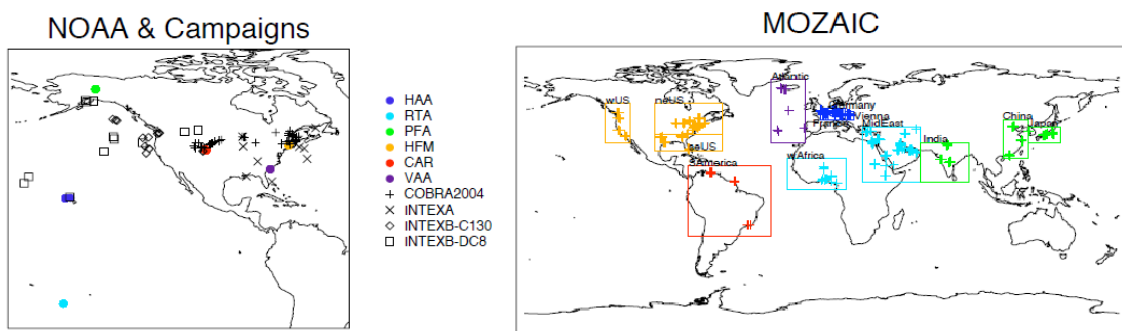


Figure 2.12: Left panel shows NOAA routine sampling sites and field campaigns and right panel shows individual profile locations and regional groupings (Adapted from Emmons et al. [2009]).

Figure 2.13 show the biases in the 700 hPa and column retrievals for the site and regional groupings for each year. In general, retrieval bias has a variety of potential

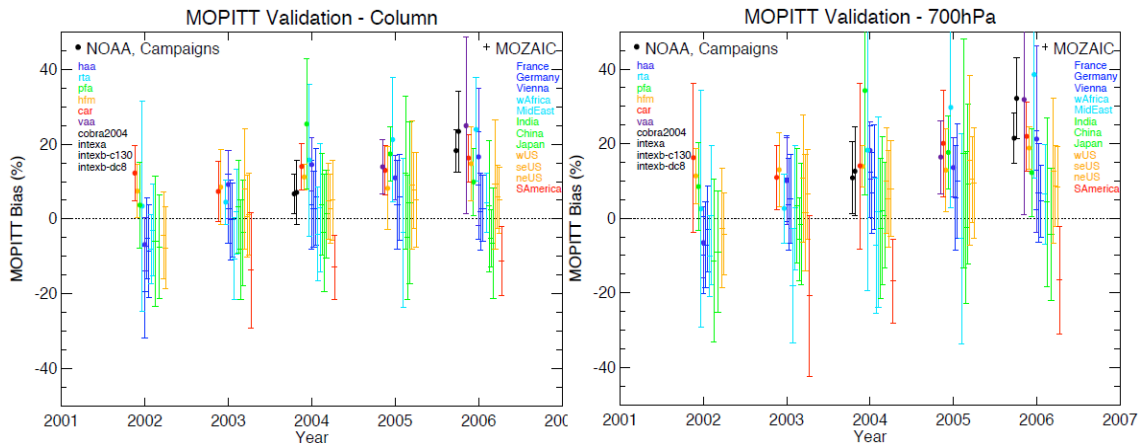


Figure 2.13: Right panel: Bias between MOPITT and aircraft in situ measurements for the 700 hPa retrieval for each year, sorted by NOAA site, Field Campaign or MOZAIC geographical region. Each symbol and error bar indicates the mean and standard deviation of the biases for each site or region; Left panel: Same as right panel, for the column retrieval (Adapted from Emmons et al. [2009]).

sources. Biases might be identified with either instrument modeling, radiative transfer modeling, biases in ancillary datasets (e.g., meteorological data) or the retrieval algorithm. Emmons et al. [2009] identified two particular sources of bias in the L2V3 product. One type of bias is associated with the assumption of Gaussian VMR variability rather than log-normal VMR variability. As shown by Deeter et al. [2007], the assumption of Gaussian VMR variability in the retrieval algorithm is inconsistent with in-situ datasets and leads to positive retrieval bias in especially clean conditions. Hence, the Version 4 (V4) retrievals, which were released in early April 2009, a state vector based on $\log(\text{VMR})$ and are therefore not be subject to this effect. A second source of potential retrieval bias in the L2V3 product occurs only in particularly polluted conditions. Retrieved profiles with CO total column values larger than the maximum value in the forward model training set (approximately 4×10^{18} molecules.cm⁻²) are rejected by the retrieval algorithm because of the inability of the forward model used in L2V3 to handle such profiles. Moreover, in the MOPITT L2V3 product, the Forward Model and retrieval processing do not account for time dependent instrument cell parameters. Hence, the changing state of the instrument could lead to a time-dependent retrieval bias, or drift.

Finally, from [Emmons et al., 2009] study, it is shown that the MOPITT operational L2V3 retrievals show a significant bias in 2006 ($\sim 20\%$ for column retrievals). Additionally, comparison of the MOPITT retrievals to the long-term records of the NOAA/GMD aircraft sampling and the MOZAIC program on commercial aircraft have revealed that the positive bias in MOPITT CO retrievals has been increasing in time. The cause of these biases in the L2V3 product were not entirely understood, but attempts were made to reduce the bias in the MOPITT L2V4 operational CO retrievals. Preliminary studies indicate that the L2V4 retrievals will have less of a drift in the bias, due in part to the use of $\log(\text{VMR})$ -based algorithms. In addition, the Forward Model in L2V4 has account for the fact that the modulation cell pressure has dropped over the mission [Emmons et al., 2009]. The silent features of MOPITT V4 operational product has been documented in chapter 4.

2.6 Summary of Chapter 2

In this thesis, CO data retrieved from the MOPITT instrument, onboard the Terra Satellite, launched in December 1999, has been used to examine CO profile information. MOPITT is a nadir viewing IR instrument which uses a combination of pressure and length modulated radiometers to provide total columns and mixing ratios of CO on 7 nominal retrieval levels (for L2V3) and 10 equivalent retrieval levels (for L2V4) starting from the surface to 100 hPa [Deeter et al., 2003; Deeter, 2009] to quantify CO in the troposphere. Note that this chapter gives a brief overview on the MOPITT L2V3 operational retrieval algorithm and data validation. The MOPITT L2V4 retrieval algorithm details are not discussed in this chapter. It is worth noting that, in this thesis, L2V3 retrieved CO data is primarily used and compared with recently released in April 2009 L2V4 retrieved CO data. A brief overview on L2V4 retrieval characteristics is given in Chapter 4.

MOPITT retrievals have limited vertical resolution but can generally distinguish between the lower and upper troposphere, and are intrinsically linked to the retrievals averaging kernels for each measured CO profile. The retrieval averaging kernels exhibit strong spatial and temporal variability and typically MOPITT is only able to obtain two pieces of independent vertical information from each measurement which strongly depend on surface and atmospheric properties.

Recent study by Emmons et al. [2009] show that there is increase in positive bias with time throughout the troposphere in MOPITT L2V3 retrieved CO data. The L2V4 data overcome some of the main reasons for positive biases in L2V3 CO data. In this thesis most work originally performed with L2V3 retrieved data and emphasis is mainly placed on identifying systematic biases in L2V3 CO data by adapting robust methodology of day/night difference in the retrieved profile. A similar approach is also applied to L2V4 retrieved data. The L2V4 has significant differences to L2V3 data and therefore, in this thesis, we also performed comparison between MOPITT retrieved L2V3 and L2V4 data to examine the case of vertical differentiation of CO in the troposphere.

Chapter 3

Sensitivity of MOPITT

Observations of Tropospheric CO

3.1 Introduction

Aside from temperature, water vapour and ozone, the usual perception is that there is little sensitivity to the surface (boundary layer) in IR measurements and further that IR data may also effectively providing a vertical column with very limited vertical resolution in many cases. However, as the averaging kernels for CO suggest (refer to section 2.4.4.4), this is not strictly true and one can generally distinguish between the lower and upper troposphere using MOPITT CO data. The sensitivity of MOPITT observations to CO concentrations in the lower troposphere varies widely as the result of variability in e.g thermal contrast conditions. Profoundly, MOPITT exhibits different vertical resolution and sensitivity between daytime and nighttime measurements, in particular, over land. Specifically, the nighttime measurements are sensitive to the mid-upper troposphere whereas the daytime measurements have higher sensitivity to the lower troposphere, especially where there is a strong temperature gradient between the surface and lower atmosphere and a large amount of CO near the surface. Therefore, for this thesis, daytime and nighttime MOPITT data have been treated separately and emphasis is placed on identifying systematic components of the day-night difference variations in the retrieved MOPITT CO profile. The separate treatment of day and night has been pointed out previously [Deeter et al., 2003, 2004; Heald et al., 2004; Kar et al., 2008]. However, Richards, N. A. D.

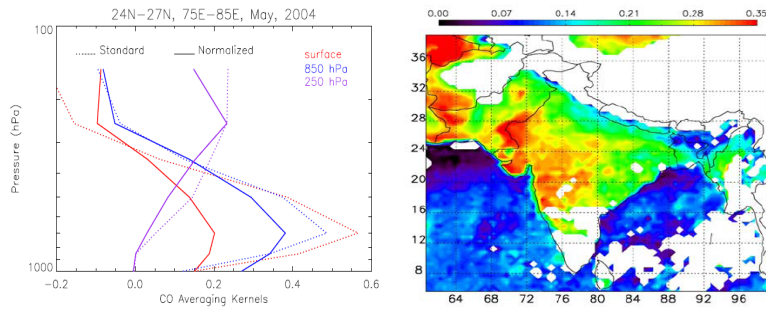
[2004] was only the first to address the issue of day-night difference and so far this quantity has not been exploited to understand vertical differentiation of CO in the troposphere using MOPITT retrieved CO data. In the succeeding sections, methodology and a case study to examine vertical differentiation of CO and specifically lower atmosphere sensitivity is presented.

3.2 The Methodology

As pointed out in chapter 2, MOPITT averaging kernels (AK) are useful to provide information on the vertical sensitivity of the MOPITT measurements and apparently shows quite large variability, in particular in the upper troposphere. The AK's depend on number of parameters, including the CO profile, the temperature profile, the surface temperature, the a priori covariance matrix, and the measurement-error covariance matrix. The a priori covariance matrix is the same for all V3 retrievals, so this would not explain any AK variability. The variability of the surface temperature or the CO profile produces the AK variability. Another possibility is the uncertainties for the Level 1 radiances which vary from pixel to pixel. Since the averaged AK for given scene may not be realistic, in this thesis the variability of the AK's are examined and a 'typical' AK selected for given set of atmospheric conditions, the degrees of freedom for a signal has been calculated, these two parameters essentially characterise the ability of the instrument to make CO profile measurements under different atmospheric and surface conditions. Using selected DOFS peak values and a 'typical' AK, one is then able to infer if it is possible for the MOPITT instrument to detect plumes or layers of enhanced CO, which have a limited vertical extent, by applying selected 'typical' averaging kernels to known profiles to simulate the effect of using MOPITT instrument to measure enhanced layers or profiles. Simulation of this kind were performed using selected 'typical' averaging kernel, over Bihar region, for daytime and nighttime measurements separately and day-night differences has been examined to detect, in particular, lower tropospheric elevated concentrations.

3.3 Understanding MOPITT Sensitivity to Tropospheric CO

The sensitivity of the MOPITT retrievals to CO in the lower troposphere can be assessed by examining MOPITT averaging kernels. However, Deeter et al. [2007] recently pointed out that interpretation of the vertical sensitivity of MOPITT retrievals have been influenced by the nonuniform thickness of the layers of the retrieval grid. They found that after normalizing for these grid effects, the averaging kernels indicate useful sensitivity to CO in the lower troposphere, particularly over daytime tropical regions with sparse vegetation [Deeter et al., 2007]. Specifically, the grid-normalised surface averaging kernels show nearly uniform sensitivity to layers from the surface to 500 hPa, in contrast to the standard averaging kernel, which apparently shows far higher sensitivity to 700 hPa level as compared to the surface (Fig. 3.1a). Moreover, the grid-normalised averaging kernel for 850 hpa also shows enhanced sensitivity to the near-surface atmosphere as compared to the standard averaging kernel.



(a) Normalised AK profiles

(b) Surface value of Normalised 850 hPa AK

Figure 3.1: (a) MOPITT L2V3 mean standard (dashed lines) and grid-normalised averaging kernels (solid lines) for May 2004 over 24 to 27°N and 75 to 85°E; (b) Distribution of the surface value of MOPITT grid-normalised averaging kernel at 850 hPa for May 2004. (Adapted from Kar et al. [2008]).

Figure 3.1(b) shows the distribution of surface values of the grid-normalised 850 hPa averaging kernels, over Indian region, for May 2004. This quantity indicates the sensitivity of the retrieved amount at the 850 hPa level to perturbations of the absorber amount of the surface layer in the true profile [Deeter et al., 2007]. Significant sensitivity to the 0-3 km altitude layer pollution can be seen over most parts of the

India region with highest sensitivity over the deserts of Rajasthan (Thar Desert) in the west. Furthermore, a pronounced minimum sensitivity over the far north-eastern states ($90 - 96^{\circ}E$) could be due to the presence of significant forested areas in this region [Kar et al., 2008]. [Deeter et al., 2007] found similar low sensitivity over the Congo and Amazon basins and attributed this to evaporation and evapotranspiration processes and possibly due to low thermal contrasts. The white areas indicate missing data for cloud contaminated pixels which are removed from the retrieval algorithm. The following section describes role of thermal contrast in IR measurements in more detail.

3.3.1 The Role of Thermal Contrast

For space instruments (e.g. MOPITT) using the thermal IR spectral range to sound the atmosphere, thermal contrast is a critical parameter for observing the planetary boundary layer (PBL), where all the pollution events occurs, which strongly depends on location, temperature, type of the surface and time of the day. Thermal contrast can be considered as the difference (in radiance) induced by the temperature difference between the surface temperature (T_{skin}) and a reference temperature in the boundary layer (T_{10m}). The earth surface heats up/cool down faster than the atmosphere and therefore, the diurnal variation of the surface is larger, and hence thermal contrast more pronounced during day than night.

3.3.1.1 Thermal Contrast Over India

In this section, the climatological variability of thermal contrast over India is examined, in order to evaluate where and when thermal IR sounders should be sensitive to the boundary layer. The surface skin temperature (T_{skin}) and temperature at 10 m (T_{10m}) as provided by the European Centre for Medium-Range Weather Forecast (ECMWF) fields on regular $1.125^{\circ} \times 1.125^{\circ}$ grid data are used to calculate thermal contrast. According to the World Meteorological Organization (WMO), the year 2007 is the second warmest on record, after 1998. The global mean surface temperatures for 2007 was estimated at $0.41^{\circ}C$ above the 1961-1990 annual average of $14.00^{\circ}C$ [WMO, 2003]. Hence 2007 may well be favourable for observations of CO in the lower atmosphere. For this study, the months of May and December are chosen as a

representative months for summer and winter seasons respectively.

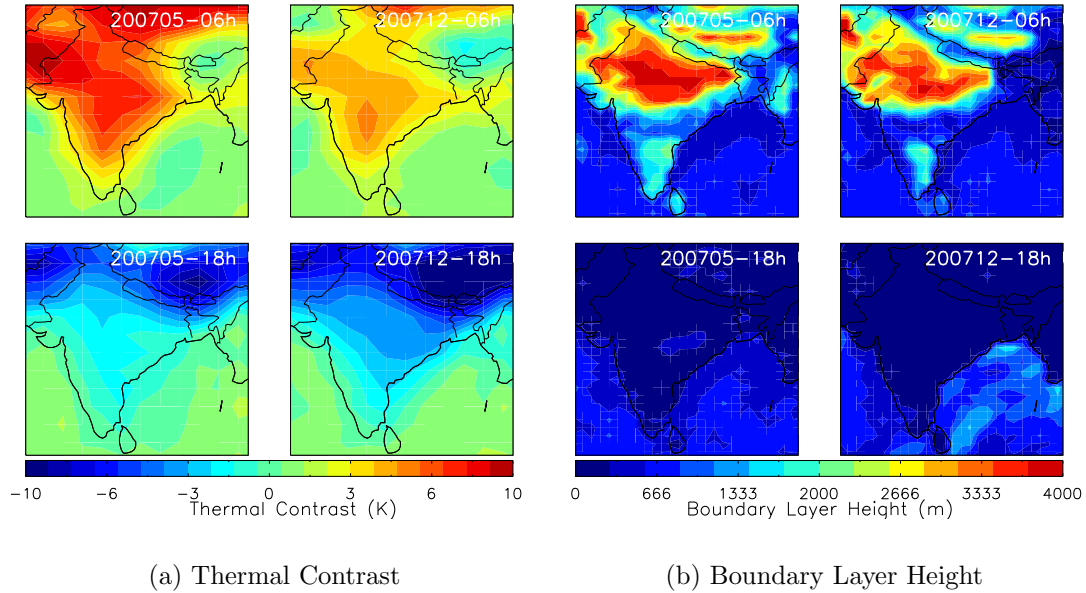
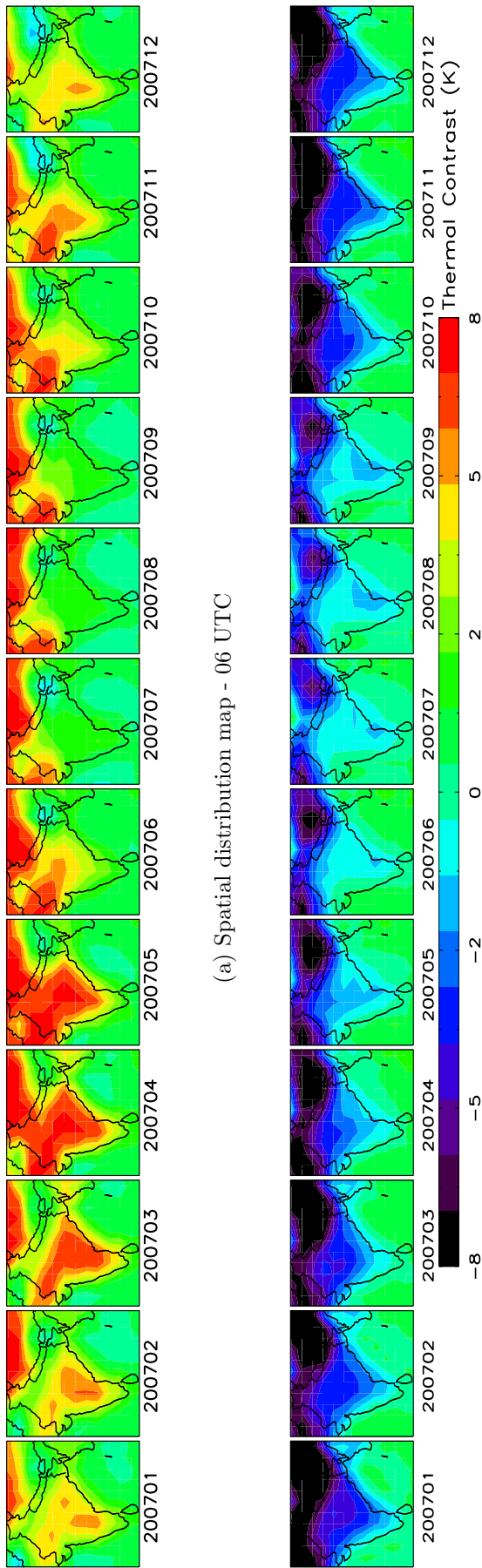


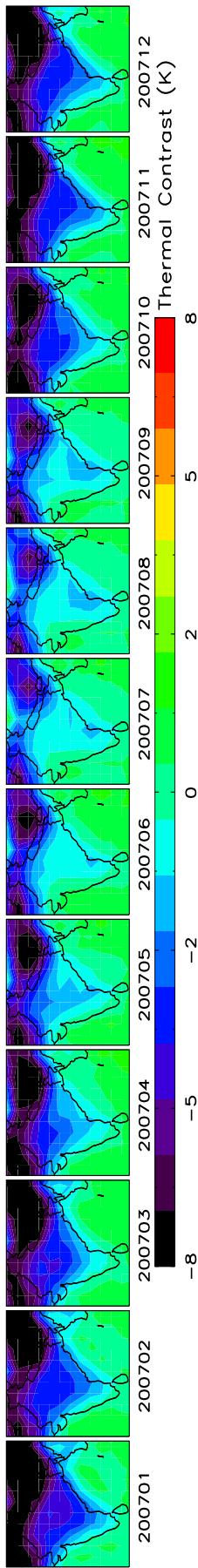
Figure 3.2: (a) Monthly averaged thermal contrast derived from ECMWF temperature fields, over India, at 06 UTC and 18 UTC, for May 2007 (left) and December 2007 (right); (b) same as (a) except for PBL height.

Figure 3.2(a) shows monthly averaged thermal contrast ($T_{skin} - T_{10m}$) for May 2007 (left) and December 2007 (right), over India, at 06 UTC (11:30 am local time) and 18 UTC (11:30 pm local time). Note that the Terra satellite is in sun-synchronous orbit with 10:30 am equator crossing local time, when daily cloud cover is typically at a minimum over land. These plots demonstrate high spatial and temporal variability of the thermal contrast. Maxima are observed during daytime (at noon local time) for May over land and are of the order of 5-10 K. The thermal contrast is comparatively lower during nighttime over India.

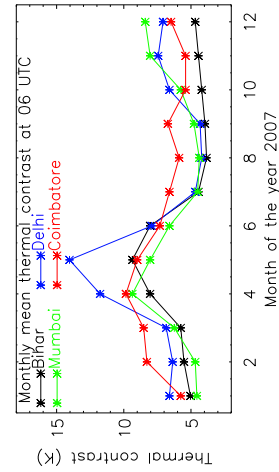
Figure 3.2(b) represents the variation of the boundary layer height over India for the same time period (May and December 2007). A fairly good correlation between the thermal contrast and the boundary layer height is observed in daytime except for central part of India. The highest thermal contrasts are associated with the elevated boundary layer height, with some delay in time. The boundary layer height variations also become more significant in May above land during daytime (at noon local time).



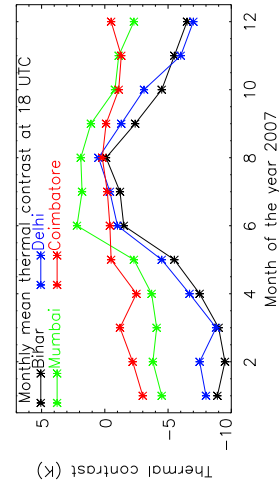
(a) Spatial distribution map - 06 UTC



(b) Spatial distribution map - 18 UTC



(c) Temporal variation - 06 UTC



(d) Temporal variation - 18 UTC

Figure 3.3: Monthly mean spatial distribution of the thermal contrast derived from ECMWF temperature fields over India at (a) 06 UTC and (b) 18 UTC; (c) and (d) shows mean temporal variation of the thermal contrast for each selected region over Indian subcontinent at 06 UTC and 18 UTC.

Figure 3.3(a, b) shows monthly mean spatial distribution of the thermal contrast over Indian subcontinent at 06 UTC (11:30 am local time) and 18 UTC (11:30 pm local time). The noon time thermal contrast is observed of the order of 10 K over Delhi region whereas 6-8 K for Bihar, Mumbai and Coimbatore regions during summer months. The thermal contrast at summer mid-nighttime found to be between 0 and -5 K, with lowest over Bihar and Delhi regions. The thermal contrast is fairly similar over water surface at 06 UTC and 18 UTC as expected. Figure 3.3(c, d) shows the temporal evolution of the thermal contrast for Bihar, Delhi, Mumbai and Coimbatore regions for local noon and mid-nighttime. The annual thermal contrast average is typically 4-6 K in daytime. The MOPITT measurements, therefore, likely to have better sensitivity to the CO in the lowermost layer during summer months in daytime when there is highest thermal contrast between the lower atmosphere and underlying surface.

3.3.2 MOPITT L2V3 Diagnostics Analysis

3.3.2.1 Retrieved CO Errors

For CO vertical profiles, estimates for CO errors are available in the error field (2nd element) of the MOPITT L2V3 CO product. The uncertainties in MOPITT retrieved CO profiles depend on the smoothing error, model parameter error, forward model error, and error due to instrument noise [Rodgers, 2000]. These uncertainties are represented by the square root of the diagonal elements of the retrieval covariance matrix. The major error is due to smoothing error [Deeter et al., 2003]. In addition, the MOPITT retrievals of CO are likely to be degraded by mainly two distinct sources of retrieval error. First, the accuracy of the operational radiative transfer model for MOPITT might be lower in conditions marked by extremely high CO loading than in more typical situations. Second, the radiative effects of aerosols, which are neglected in the operational retrieval algorithm, can potentially mask the spectral signature of CO in the upwelling radiation [Deeter et al., 2007]. In both cases, systematic differences between the calibrated radiances and model calculated radiances can lead to biases in the MOPITT CO product.

Figure 3.4 (a) and (b) show MOPITT L2V3 retrieved 850 hPa 0.5 degree gridded day CO mixing ratio errors, over India, for May 2007 and December 2007 respectively.

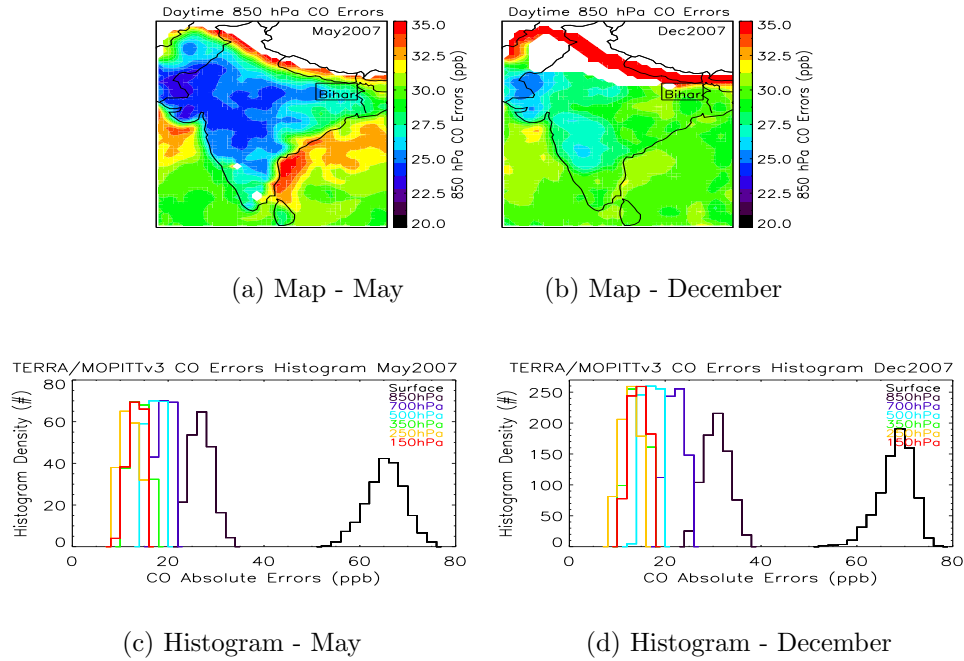


Figure 3.4: (a) MOPITT L2V3 850 hPa retrieved 0.5 degree gridded daytime CO mixing ratio errors, over India, for May 2007; (b) same as (a) except for December 2007; (c) Histogram of daytime CO mixing ratio errors, over Bihar box (shown by rectangle), for May 2007; (d) same as (c) except for December 2007.

It is clearly evident that the retrieved errors are substantially increased over Indian region during December as compared to May, due to low thermal contrast conditions in winter time (3.2a). Figure 3.4 (c) and (d) shows a histogram plot of day retrieved CO errors for selected case study region (Bihar). The retrieved errors at all pressure levels are less than 40 ppb except at surface level. The detailed analysis by Deeter et al. [2003] shows that at 500 hPa, the retrieval uncertainties are approximately 20 % in the tropics and at the mid-latitudes, and 30-40 % at high latitudes.

3.3.2.2 Percent Apriori CO Mixing Ratios

It should be noted that, in the L2V3 product, no filters are applied with regard to information content. In polar regions, for example, MOPITT CO retrievals are weighted by the a priori profile much more heavily than in other regions, and therefore contain less information. Similarly, nighttime MOPITT retrievals often contain less information than daytime retrievals (especially over land). To use accurate information content, the L2V3 product include a diagnostic ('Percent A priori CO mixing

ratio’), which describes the uncertainty of the retrieved CO (at each level in the profile) as a percentage of the a priori variability.

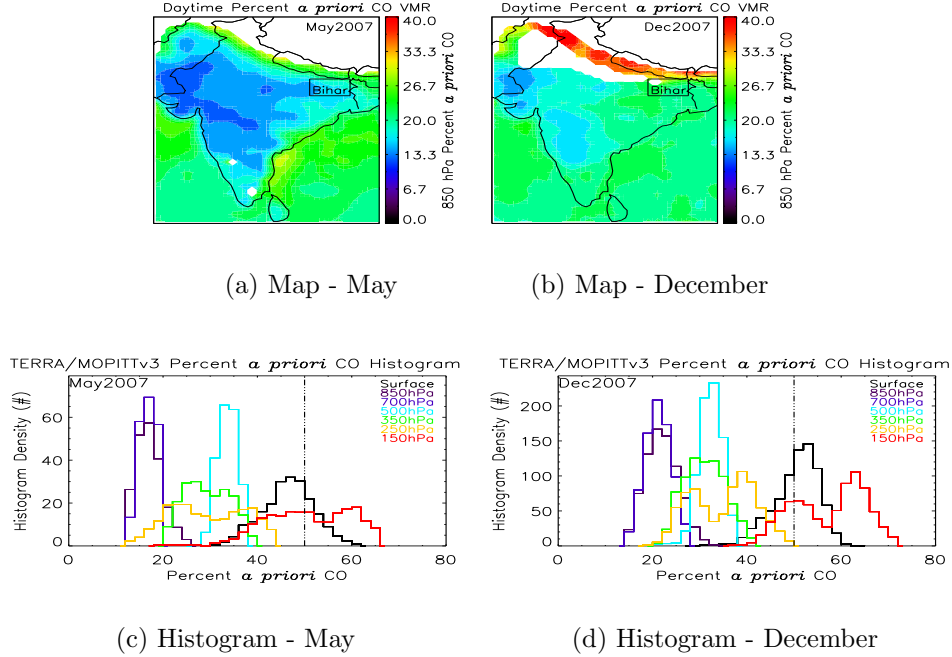


Figure 3.5: (a) MOPITT L2V3 850 hPa retrieved 0.5 degree gridded daytime Percent a priori CO mixing ratio, over India, for May 2007; (b) same as (a) except for December 2007; (c) Histogram for 850 hPa retrieved daytime Percent a priori CO mixing ratio, over Bihar box, for May 2007; (d) same as (c) except for December 2007.

Figure 3.5 (a) and (b) shows MOPITT 850 hPa retrieved 0.5 degree gridded daytime percent a priori CO mixing ratio, over India, for May and December 2007 respectively. In general, percent a priori CO mixing ratios are less than 40% over land except over Himalayan cold surfaces. The white gaps indicate the cloud contaminated pixels which are removed from retrieval algorithm. It is clearly evident that the MOPITT CO retrievals are weighted by the a priori profile information more heavily in December than in May. Figure 3.5 (c) and (d) shows a histogram plot for percent a priori CO mixing ratios, over the Bihar box, for May and December 2007 respectively. The dash dotted line indicates that the retrieved CO profiles are filtered for percent a priori CO mixing ratio values greater than 50 %. Figure 3.6 and 3.7 shows a scatter plot of MOPITT instrument retrieved errors against percent a priori CO mixing ratios at each retrieval level, over Bihar box, for summer (May) and winter (December) month respectively. It is obvious that there is a strong correlation between percent a

priori CO mixing ratio and retrieved CO errors as expected from optimal estimation. It can also be seen that the correlation is approximately linear. For both seasons, it can be seen that errors in the retrieval increase with increase of a priori contribution to the true profile. It is important to use percent a priori CO mixing ratio diagnostic to filter out profiles containing less information.

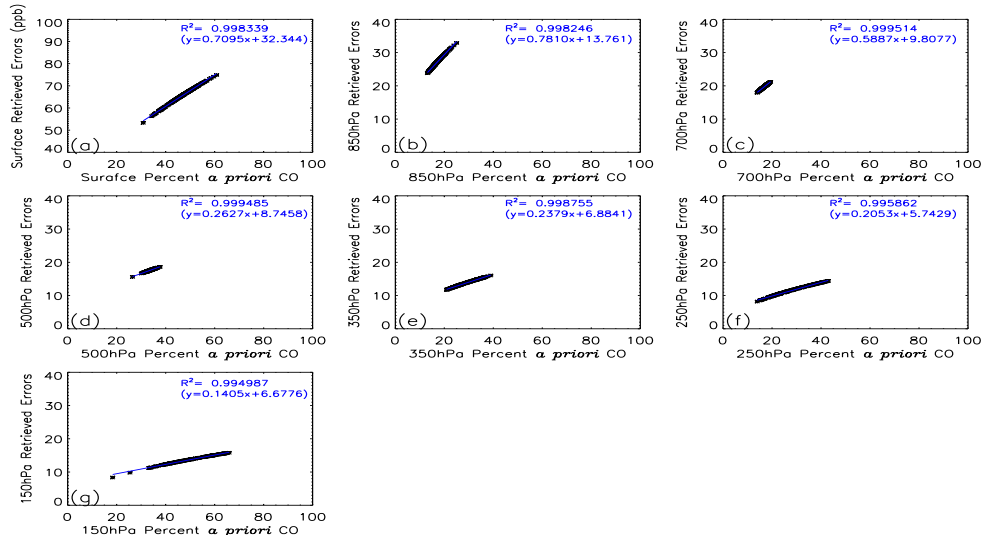


Figure 3.6: MOPITT L2V3 retrieved errors versus percent a priori CO mixing ratio, over Bihar box, for May 2007.

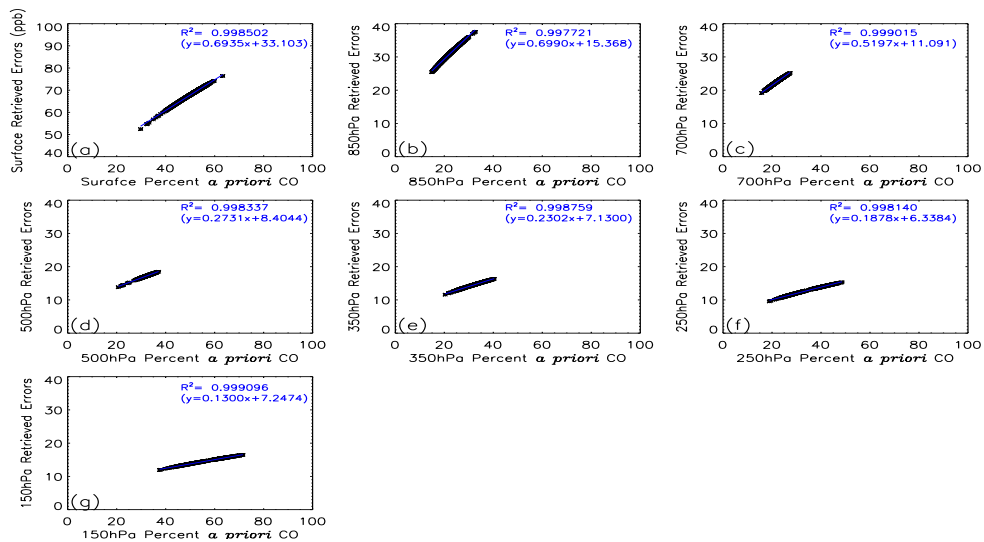
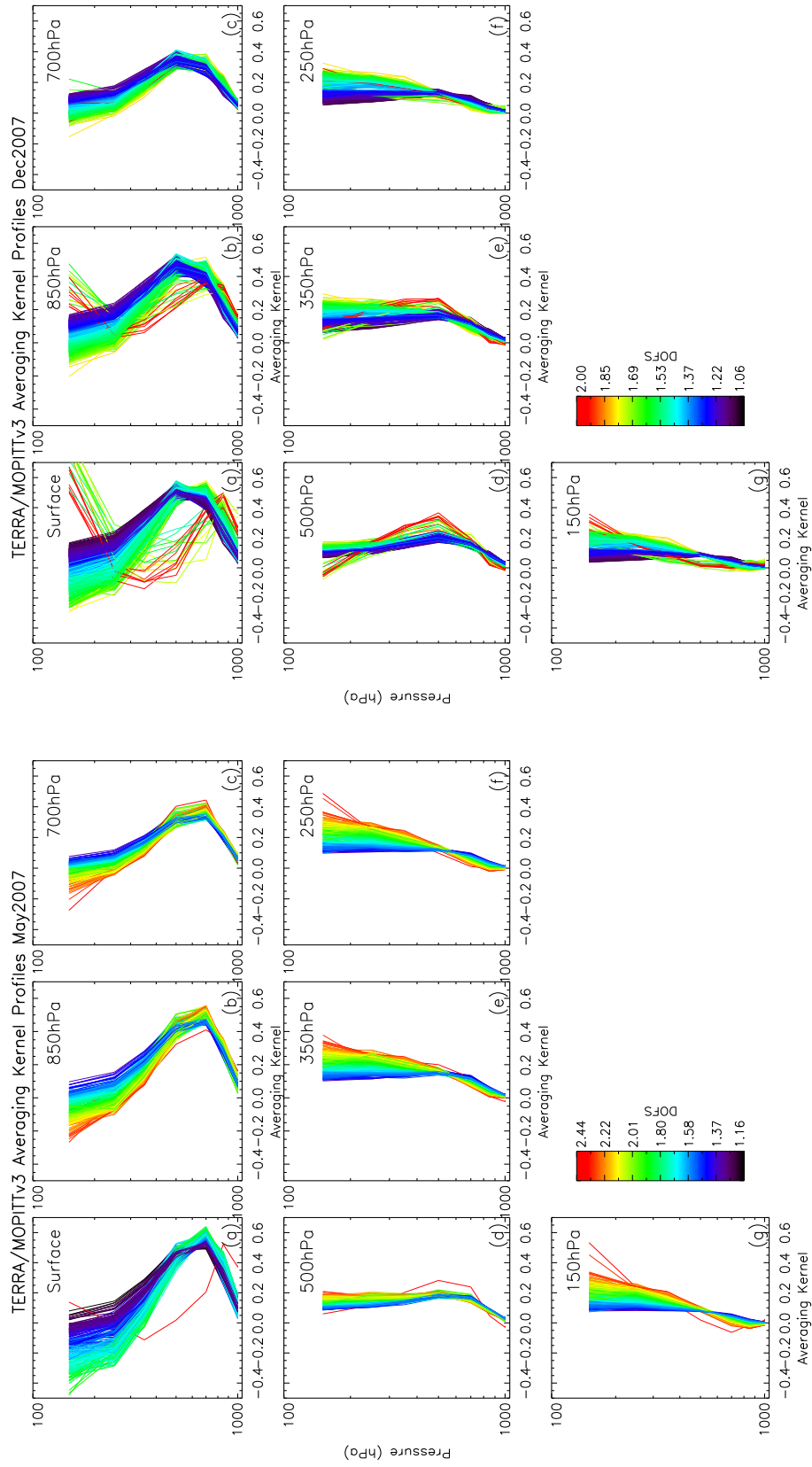


Figure 3.7: Same as Fig. 3.6 except for December 2007.

3.3.2.3 Averaging Kernels

The retrieval averaging kernel (\mathbf{A}) [Rodgers, 2000] is fundamental to understanding the physical significance of the retrieved MOPITT CO profile. In the ideal case, \mathbf{A} would equal to identity matrix (\mathbf{I}), and any perturbation to the true state vector would produce identical changes in the retrieved state vector. Generally, however, changes to any particular element of the true atmosphere result in finite changes to all elements of the retrieved state vector. Analysis of the retrieval averaging kernels permits analysis of the vertical resolution and sensitivity of the retrieved profiles and the degree to which the a priori influences the retrieval.

As stated in chapter 2, the MOPITT averaging kernels exhibit considerable variability both geographically and temporally. Deeter et al. [2003], illustrated the variation of the averaging kernel for the MOPITT operational CO retrievals between day and night for the Pacific Ocean, Canada, and Western Australia. Figure 3.8 (a) and (b) shows all MOPITT L2V3 averaging kernel profiles as a function of DOFS, over Bihar box, for May and December 2007 respectively. The case study region chosen is one where MOPITT retrievals show significantly high DOFS values during the day as a result of greatest thermal contrast during the day (Fig. 3.2a) and likely elevated boundary layer CO concentrations. The averaging kernel variability in the upper troposphere during May and December is similar suggesting that it is not likely produced by changes in atmospheric or surface properties. The uncertainties for the Level 1 radiances, which vary from pixel to pixel, possibly produced variability in the averaging kernels [Deeter et al., 2003]. It is clearly evident that the averaging kernels in the lower layer for greatest DOFS values are weighted much more to the lower layer whereas upper layer averaging kernels for greatest DOFS values are weighted more to the upper layers of the atmosphere.



(a) May

(b) December

Figure 3.8: (a) MOPITT retrieved Averaging Kernel profiles as a function of DOFS, over Bihar region, for May 2007; (b) Same as (a) except for December 2007.

Furthermore, the averaging kernel profiles can be grouped for similar values of DOFS, e.g. for 850 hPa averaging kernels in May 2007, the averaging kernel profiles can be grouped for DOFS values greater than 1.6 and DOFS values ranging from 1.0 to 1.6. This grouping is not necessarily similar for other regions and times of the year. Interestingly, few surface averaging kernel profiles for high DOFS values with enhanced sensitivity to the surface can be identified. The filtering by DOFS values range eliminates unexpected variability in the set of averaging kernels and it is useful to select ‘typical’ representative averaging kernel for given atmospheric and surface properties for the time of year.

3.3.2.4 Degrees of Freedom for a Signal

Degrees of freedom for a signal describes the number of independent pieces of information available in the retrieved vertical profile [Rodgers, 2000]. For the retrieved profiles with DOFS less than 1.0, the a priori profile dominates at most retrieval levels. As DOFS increases, retrievals are less constrained by the a priori, and relatively sensitive to the true CO profile.

Figure 3.9 (a) and (b) shows MOPITT 0.5 degree gridded daytime degrees of freedom for a signal, over India, for May and December 2007 respectively. The magnitude of the DOFS is significantly lower over Indian region during winter month compared to summer month due to low thermal contrast during winter (Fig. 3.2a). The white patches indicate regions of no data where cloud contamination are removed from retrieval algorithm or possibly pixel contaminated by dense fog. Figure 3.9 (c) and (d) shows histograms for DOFS values, over Bihar box, for May and December 2007 respectively. The dash dotted lines show selected DOFS peak values which have been used to select ‘typical’ averaging kernels for MOPITT L2V3 simulation. For Bihar region, the MOPITT L2V3 retrieved daytime and nighttime DOFS histograms show two distinct distributions hereafter referred as Lower DOFS Distribution (LDD) and Higher DOFS Distribution (HDD) and the corresponding peaks of the distribution are referred to as LDD_{peak} and HDD_{peak} respectively. In general, daytime measurements have greatest DOFS values than nighttime measurements. It is also evident that DOFS have strong spatial and temporal variability, mostly depending upon the thermal contrast between the lower atmosphere and underlying surface. The lower

DOFS values in winter than summer month suggesting reduced sensitivity of MOPITT measurements to tropospheric column, in particular to the boundary layer, during the winter month.

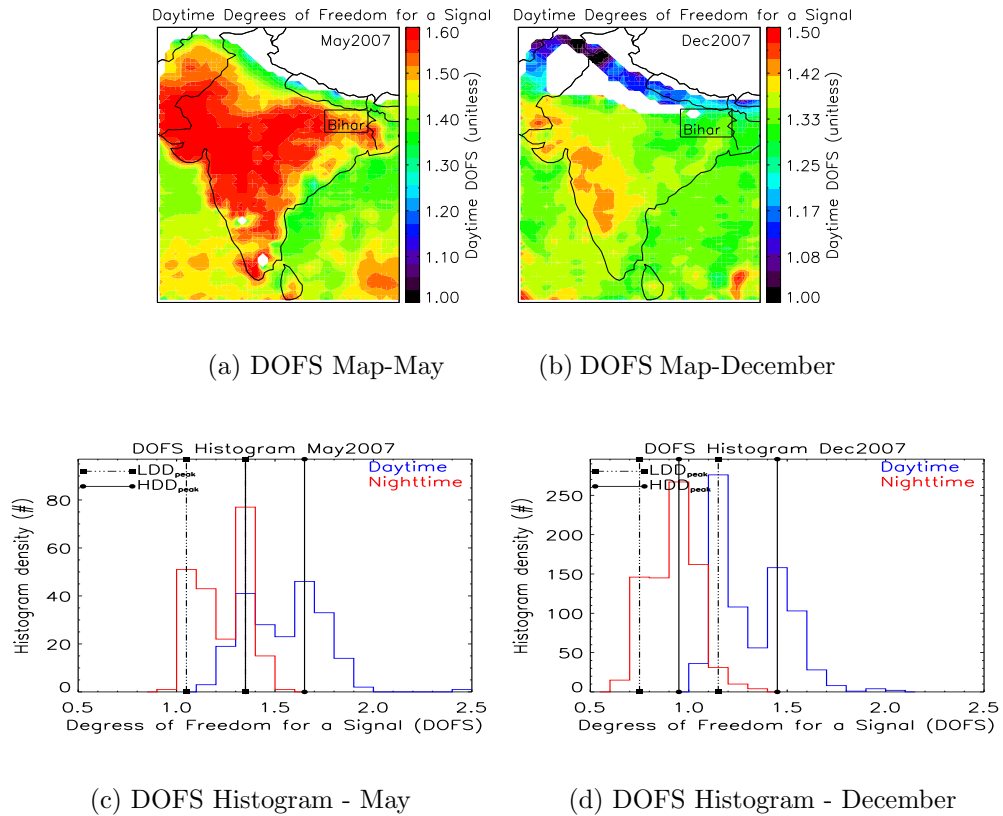
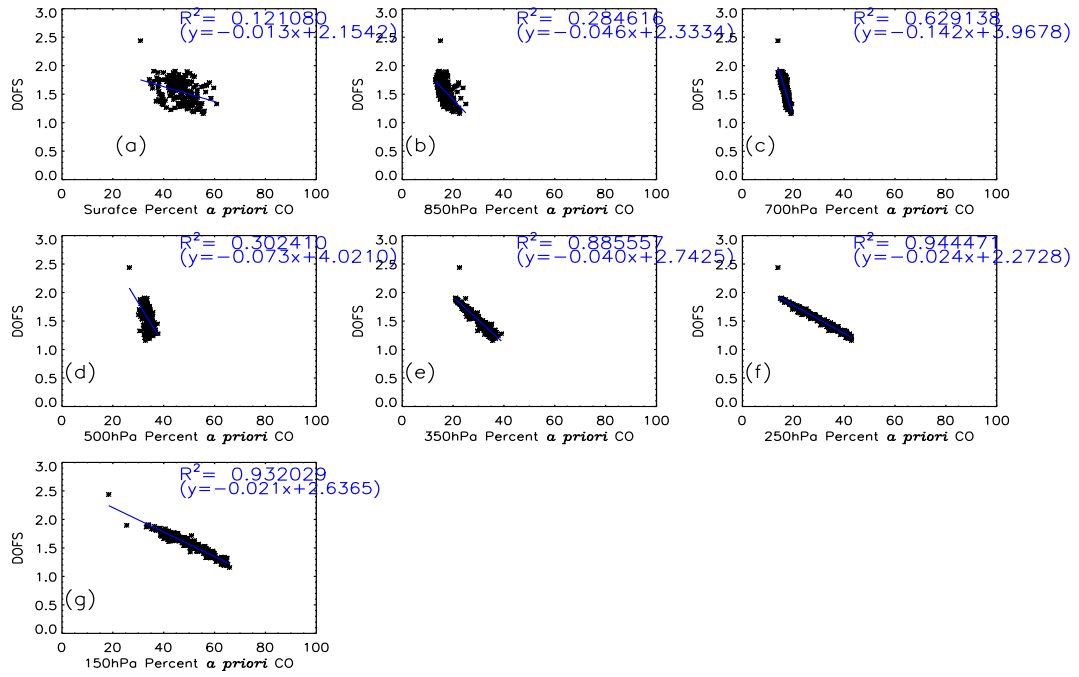


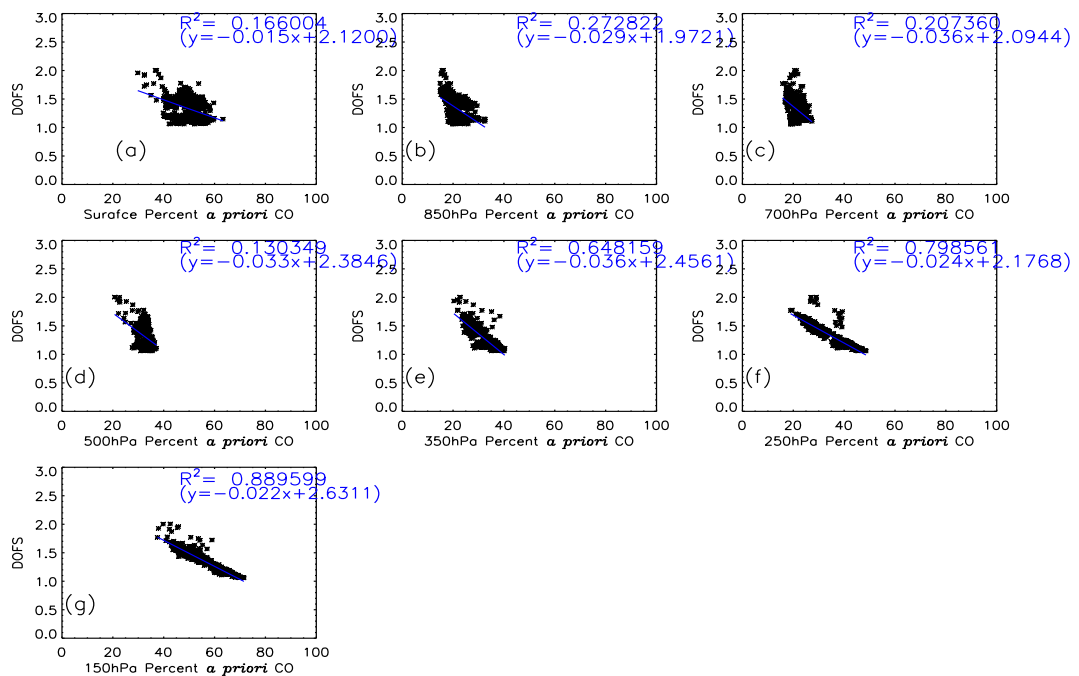
Figure 3.9: (a) MOPITT L2V3 0.5 degree gridded daytime DOFS, over India, for May 2007; (b) same as (a) except for December 2007; (c) Histogram for daytime and nighttime DOFS, over Bihar box, for May 2007; (d) same as (c) except for December 2007.

Figure 3.10 shows correlation between MOPITT retrieved DOFS and percent a priori CO mixing ratio. As stated earlier, percent a priori CO mixing ratio is a useful parameter to understand the uncertainty of the retrieved CO (at each retrieval level) as a percentage of a priori variability. The strong correlation between DOFS and percent a priori CO mixing ratio suggests one can use percent a priori rather than DOFS which for L2V3 has to be calculated since AK's are not provided in L2V3 product and it is time consuming process. As documented earlier, in general so far, only those profiles having percent a priori less than 50% in the retrievals are considered. However, one can see varying correlation between DOFS and percent a

priori CO mixing ratios retrieved on each corresponding retrieval level. It is clearly evident that DOFS are linearly correlated with percent a priori CO mixing ratio retrieved at 350 hPa retrieval. We, thus, define a percent a priori CO mixing ratio 'threshold value' which is indicative of high DOFS and can be used to define the HDD distribution. A more detailed calculation for the threshold value is discussed in chapter 5. It has to be noted that the correlation reduced significantly, over Bihar, during winter month although the shapes are similar at 350 hPa.



(a) May



(b) December

Figure 3.10: (a) MOPITT L2V3 DOFS versus percent a priori CO mixing ratio at 7 retrieval levels, over Bihar region, for May 2007; (b) Same as (a) except for December 2007.

3.3.3 Selection Criteria for a ‘Typical’ Averaging Kernel

As shown in the previous section, generally, the DOFS histogram has two distinct peaks for daytime and nighttime measurements. It is shown, in this section, that selecting a ‘typical’ averaging kernel for chosen DOFS distributions helps, in turn, to examine maximum available information content for MOPITT retrieved CO profile

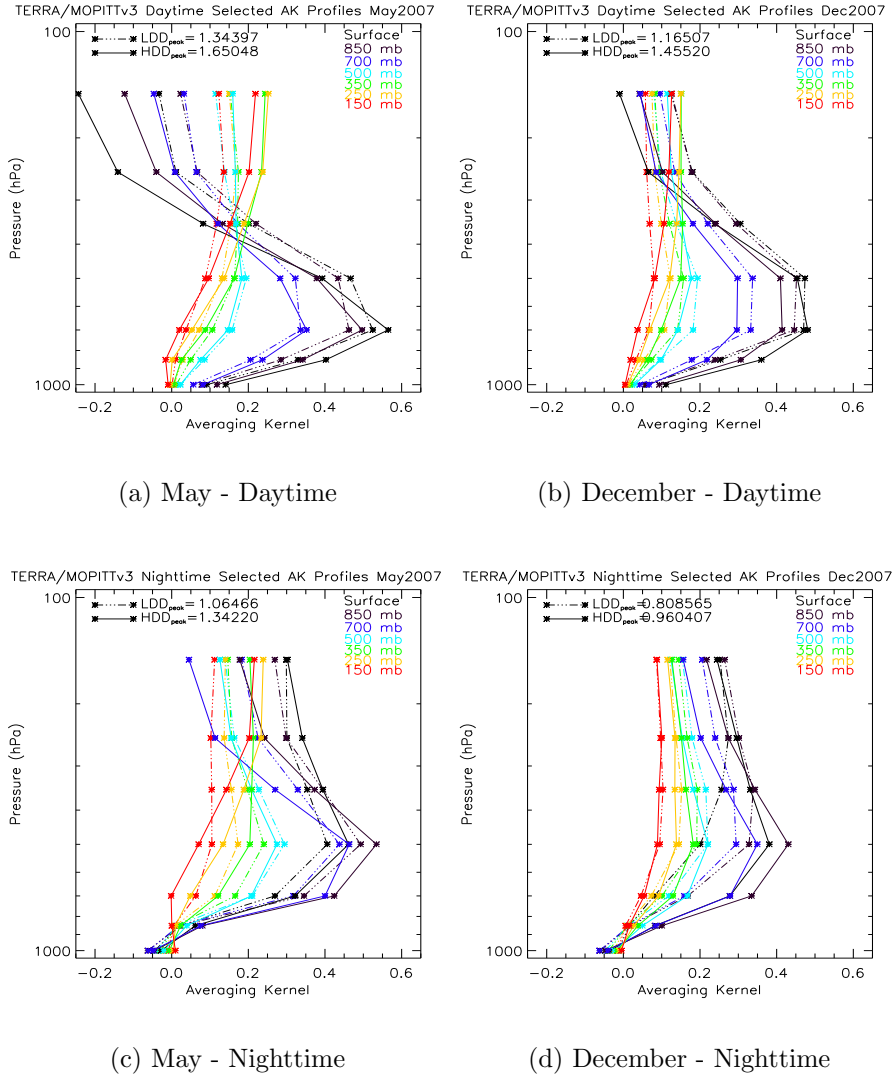


Figure 3.11: (a) MOPITT L2V3 Selected daytime ‘typical’ AK profile, over Bihar box, for May 2007; (b) Same as (a) except for December 2007; (c) Selected nighttime ‘typical’ AK profile, over Bihar box, for May 2007; (d) Same as (c) except for December 2007.

Figure 3.11 shows selected averaging kernel for DOFS peak values in fig. 3.9 (c and d) for daytime and nighttime measurements. For example, the averaging kernel

identified as surface shows how changes to the true CO mixing ratio at any levels in the true atmosphere would theoretically contribute to a change in the retrieved value at the surface. Averaging kernels for each level in the retrieved profile do not necessarily peak at the corresponding pressure level of the true profile. Thus, for the selected averaging kernel profile, the surface-level AK is in fact mainly sensitive to CO between surface and 500 hPa, rather than at the surface level. Averaging kernels for successively higher (lower pressure) retrieved levels do, systematically shift towards higher levels. Thus the averaging kernel for 250 hPa indicates highest sensitivity between 150 and 350 hPa. The averaging kernels, clearly, are rather broad and exhibit a significant degree of overlap. Mathematically, this indicates that the retrieval at the seven levels that form the retrieval grid for this specific selected case are not generally independent. This is possibly due to the fact that the number of levels in the retrieved profile exceeds the number of CO-sensitive signals used in the retrievals [Deeter et al., 2003]. In general, the averaging kernels for the surface and 850 hPa retrieved levels are finite and non-zero, although small, with respect to changes in CO near the surface for daytime measurements Fig. (3.11). At night, the averaging kernels for the lower levels are shifted upwards in the vertical and become more or less similar in shape to the upper level kernels for the nighttime measurements. There is very little or no sensitivity to surface CO. It should be noted that the nighttime DOFS are close to 1.0, suggesting that the nighttime averaging kernels are close to having only a partial column content. In fact, the averaging kernels for the lower retrieval levels (surface, 850 hPa, and 700 hPa) at night are more sensitive to upper tropospheric CO than the averaging kernels for the higher retrievals levels (150, 250 and 350 hPa) during daytime. For example, the surface averaging kernel at night shows great sensitivity to upper tropospheric CO than 350 hPa averaging kernel at night. The strong differences suggest that comparisons of day and night retrievals for the same geographical location could provide vertical discrimination of persistent features in CO in the troposphere.

3.4 Examination of Day-Night Differences in MOPITT L2V3 CO Data

Since the MOPITT data exhibit different vertical resolution and sensitivity between daytime and nighttime measurements, in particular over land, the difference in sensitivity between daytime and nighttime data indicates that when subtracting the nighttime measurements from the daytime one, the output should show more sensitivity to the lower troposphere. This is because the averaging kernels for the lower retrieval levels exhibit a considerable variation in sensitivity during daytime especially over locations which have large diurnal surface temperature changes. The shifting of the lower averaging kernels away from the surface during the nighttime may hold the key to examining vertical differentiation of CO in the troposphere. This hypothesis is now examined further.

3.4.1 Day-Night Difference CO Maps

This chapter focuses on Indian region. The high population density and recently accelerated industrial activity imply strong sources of CO in this region. Several studies over Indian subcontinents have been carried out in recent years with emphasis on the distribution and evolution of CO and other gas species in the lower troposphere [e.g., Kar et al., 2008; Roy et al., 2008]. In addition, few aerosol studies over India have also been carried out in recent years with emphasis on the Indo Gangetic (IG) basin [e.g., Singh et al., 2004; Jethva et al., 2005; Tripathi et al., 2006; Nair et al., 2007]. The lower-tropospheric and total column MOPITT retrievals along with measurements of tropospheric NO₂ from the SCIAMACHY instrument have been used to mark out possible enhanced surface sources of CO concentrations.

In this section, the spatial structure in the distribution of CO in lower tropospheric MOPITT retrieval level has been studied by examining day-night differences. The MOPITT retrieved CO total column and day-night column differences have also been examined to assess their consistency with our a priori knowledge of the CO sources together with SCIAMACHY NO₂ total column density. Because, in contrast to CO, NO₂ is a short-lived species and its distribution is more indicative of local surface pollution sources [Richter et al., 2005]. Moreover, SCIAMACHY measurements are

sensitive to NO_2 in the boundary layer and can clearly localise emissions to individual cities [Buchwitz et al., 2007]. It is shown here that the lower tropospheric MOPITT retrievals do indeed capture some of the surface source information over this region.

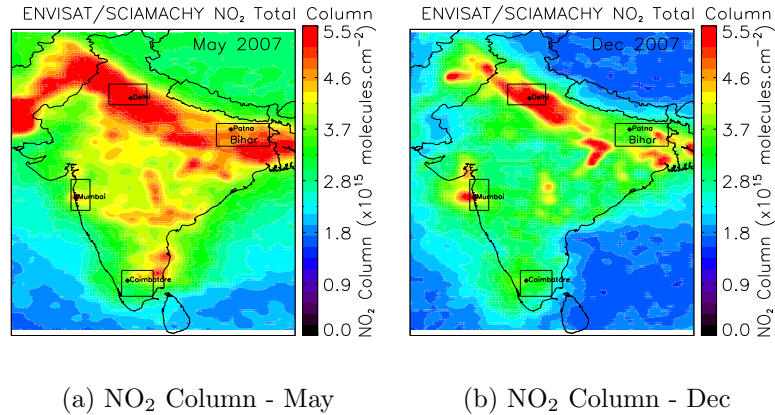
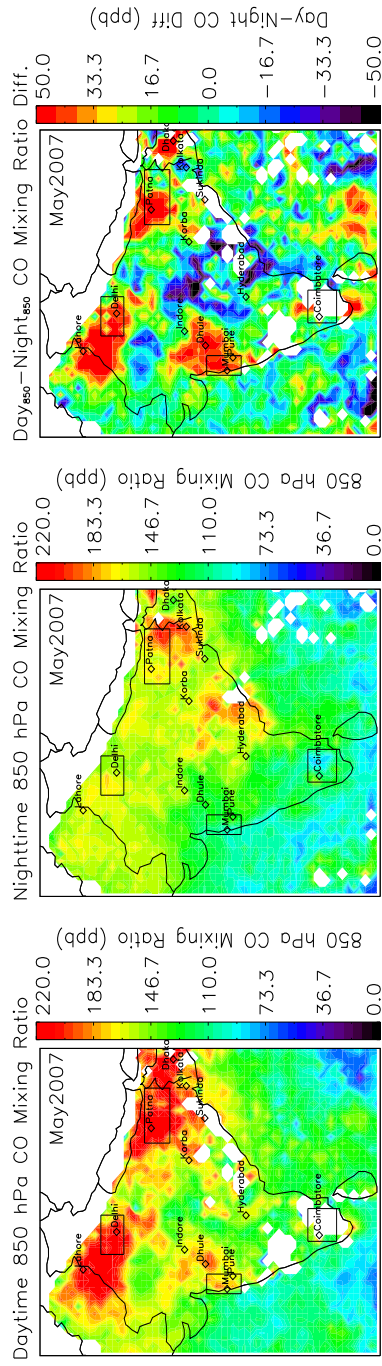


Figure 3.12: (a) SCIAMACHY 0.5 degree gridded NO_2 total column, over India, for May 2007; (b) Same as (a) except for December 2007.

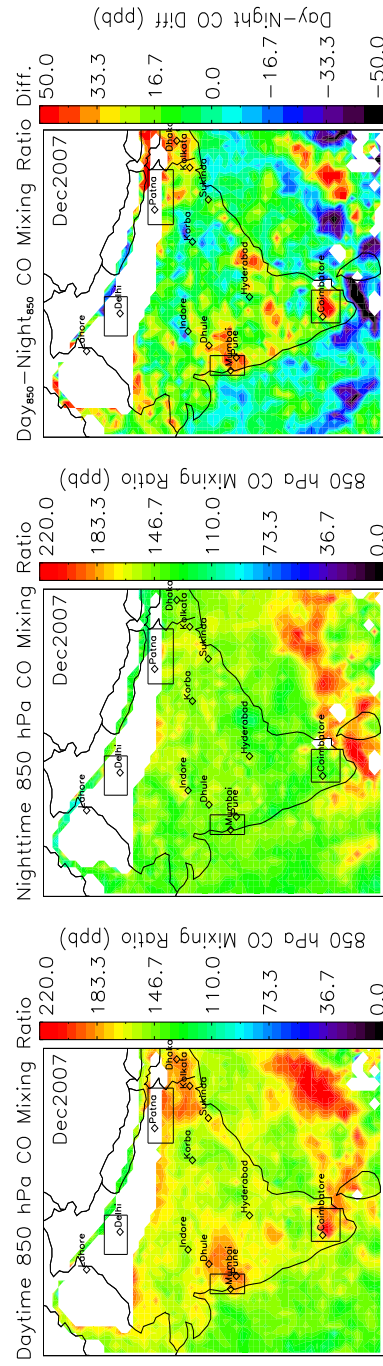
Figure 3.12 shows the tropospheric columns of NO_2 retrieved from SCIAMACHY during (a) May 2007 and (b) December 2007 respectively. Figure 3.13 shows MOPITT CO mixing ratios retrieved at 850 hPa level for (a, d) daytime measurements, (b, e) nighttime measurements, and (c, f) day-night differences in the month of May and December respectively. In the month of May and December, relatively enhanced CO retrievals at 850 hPa can be seen along the IG basin. Although emissions are at a much lower level in December as compared to the month of May. Note that there are no MOPITT L2V3 data over much of the IG basin for December except over eastern states of IG basin. This has been observed in the MOPITT data consistently for all years for the months of November-January. The reason for this is not completely understood but could be related to the intense haze and foggy conditions that develop each winter over this area [Tripathi et al., 2006; Gautam et al., 2007] that might be affecting the CO retrievals, although thick fog layers should also affect NO_2 retrievals. In December, enhanced CO retrievals at 850 hPa can be seen not only over IG basin but also other part of India. This could be, in part, trapped CO pollution in the shallow boundary layer, near surface winds over this area in winter prevent venting of the boundary layer pollution to higher altitudes.



(a) Day CO - May

(b) Night CO - May

(c) Day-Night diff - May



(d) Day CO - Dec

(e) Night CO - Dec

(f) Day-Night diff - Dec

Figure 3.13: (a) MOPITT L2V3 0.5 degree gridded daytime 850 hPa CO mixing ratios for May 2007; (b) MOPITT L2V3 0.5 degree gridded nighttime 850 hPa CO mixing ratios for May 2007; (c) MOPITT L2V3 0.5 degree gridded 850 hPa day-night CO mixing ratio differences for May 2007; (d) Same as (a) except for December 2007; (e) Same as (b) except for December 2007; (f) Same as (c) except for December 2007.

The elevated surface CO concentrations over key source regions such as the Indo Gangetic basin, Mumbai city, Southern tip of India (Coimbatore) can be seen in day-night differences (Fig. 3.13(c,f)). The greatest lower level CO concentrations over Bay of Bengal likely to be transported from eastern part of India. During the month of December the wind pattern is usually westerly-south westerly over eastern Indian and West Bengal region. These westerly-south westerly winds can help in transporting the pollutants within boundary layer from the areas where emissions are higher toward the remote locations. The study by Beig and Ali [2006] have shown that there is a steep gradient in the tracer concentrations over the IG basin as compared to other parts of India. Interestingly, signatures of enhanced CO (or large positive day-night differences) and NO₂ are matching quite well. Note the strong thick plume of CO located North-east of Mumbai and Pune to that of the isolated NO₂ plume over Mumbai city. It should be noted that the individual plumes from cities cannot be distinguished clearly in this color scale. There are also similar but somewhat extended plumes of CO around other cities like Delhi and Lahore. We do not expect one to one correspondence with NO₂ because of differences in the sources and their lifetimes [Buchwitz et al., 2007]. However, it is reasonably clear that both daytime retrievals and day-night differences show features which could be related to enhancements of CO in the lowermost layer of the atmosphere. Figure 3.14 shows the tropospheric columns of CO retrieved from MOPITT during (a,b,c) May 2007 and (d,e,f) December 2007. Similar to lower tropospheric MOPITT retrieval level day-night difference CO mixing ratio, we find considerable utility to day-night difference columns. Our day-night difference means providing thus more confidence in demonstrating lowermost atmospheric enhancements.

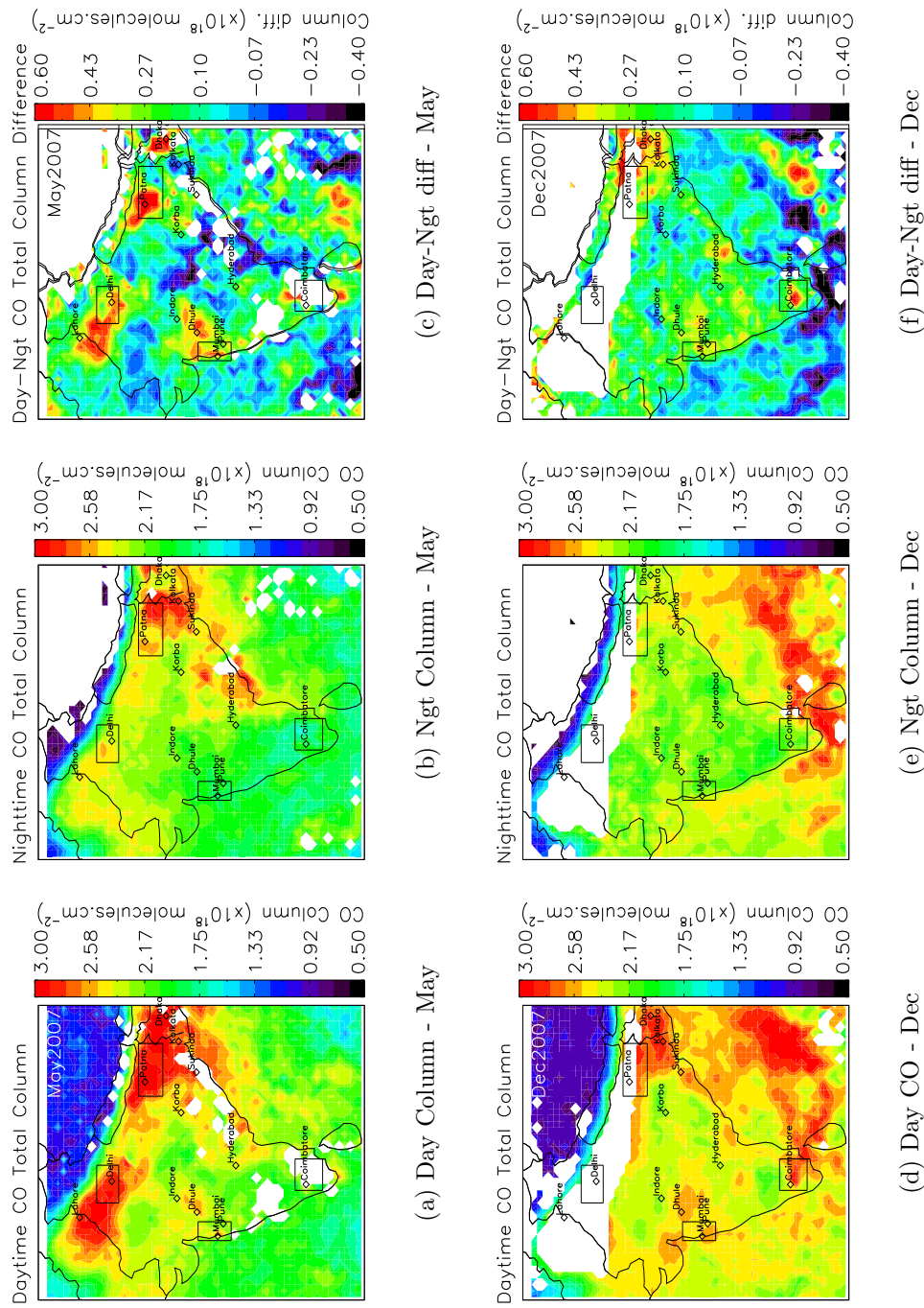


Figure 3.14: (a) MOPITT L2V3 0.5 degree gridded daytime CO total column for May 2007; (b) MOPITT L2V3 0.5 degree gridded nighttime CO total column for May 2007; (c) MOPITT L2V3 0.5 degree gridded day-night CO total column differences for May 2007; (d) Same as (a) except for December 2007; (e) Same as (b) except for December 2007; (f) Same as (c) except for December 2007.

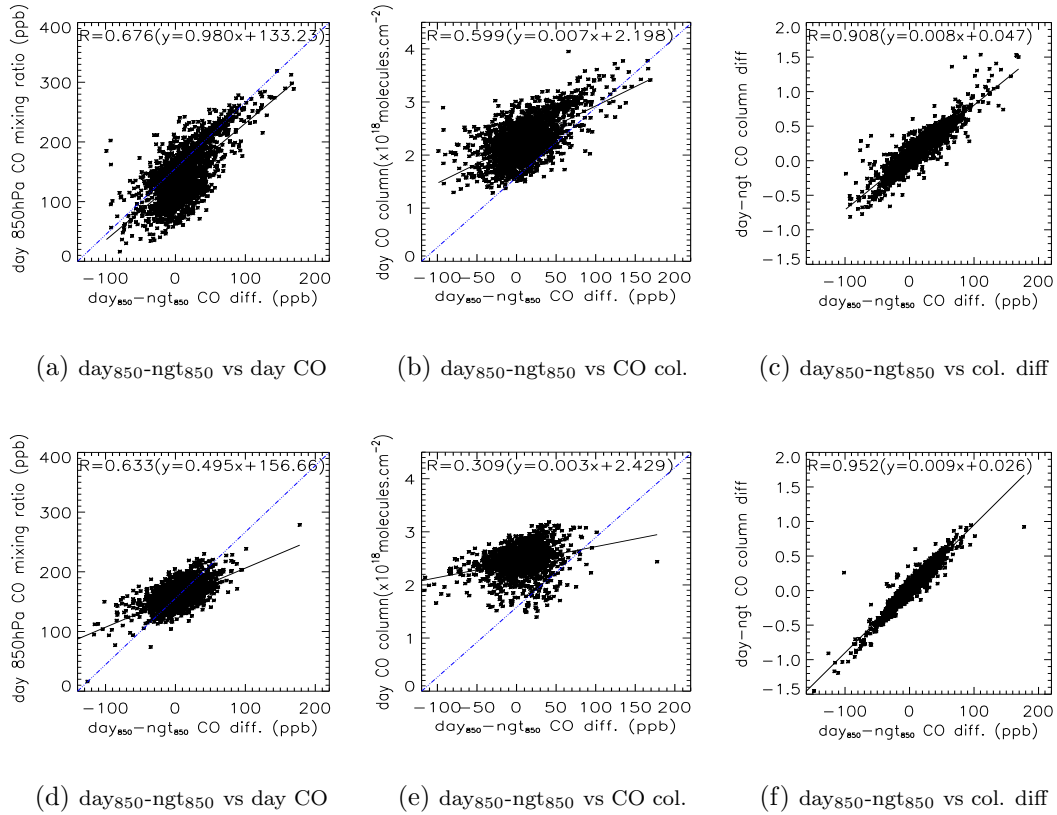


Figure 3.15: Correlation results, over India, in the month of (a-c) May and (d-f) December.

The correlation results are shown in Fig. 3.15 to improve our knowledge of CO in the lowermost layer of the troposphere. A very good correlation between the retrieved CO at 850 hPa and day₈₅₀-night₈₅₀ differences can be seen, suggesting that this differences likely to provide useful information on CO in the lowermost atmosphere. Similarly a very good correlation between day₈₅₀-night₈₅₀ and day-night CO column difference suggesting considerable utility to day-night difference columns in this region.

For India, our analysis thus confirms the pollution detected over the extremes of the IG basin [e.g., Kar et al., 2008]. We also find reasonably extensive CO pollution loading in the west coast and Southern tip of India. Small enhancements in NO₂ are also observed in these regions supporting this analysis. Nonetheless, it is reasonably clear that both daytime retrievals and day-night differences show features which could be related to enhancements of CO in the lowermost layer of the atmosphere. Therefore, in the following section, four boxes are selected for more robust testing.

3.4.2 L2V3 Profile Simulation - A Case Study of Bihar

The robust methodology developed here is based on a initial study by Richards, N. A. D. [2004]. It involves simulations of day-night differences through test of isolated layer enhancements in CO profiles. Kar et al. [2008] showed that MOPITT daytime CO at 850 hPa can capture the so-called "Bihar pollution pool" in December which is similar to earlier observation of high aerosol optical depths over the eastern states of Bihar and west Bengal in winter from the data obtained by the MISR instrument onboard Terra satellite [Di Girolamo et al., 2004]. These features were also simulated by GEOS-Chem model which supported the MOPITT results [Kar et al., 2008]. Other studies [e.g., Roy et al., 2008; Ghude et al., 2008] have also found high CO concentrations over IG basin as compared to other parts of India. The strong subsidence and light winds over this region in winter accumulates and limit CO pollution close to the source locations. Hence, the analysis here concentrate first on the Bihar region shown by rectangular box in Fig. 3.12 over the eastern state, Bihar, in the latitude range from 24.0°N to 26.4°N and longitude range from 84.0°E to 88.2°E.

3.4.2.1 Mean L2V3 CO Profile

For Bihar region, there exist two sets of LDD and HDD for range of DOFS values in the month of May and December of 2007. In section 3.3.2.4, it was shown that there exist an LDD and HDD distribution for each of daytime and nighttime conditions. In this section, mean daytime and mean nighttime profiles have been calculated for each distribution and the results are shown in Fig. 3.16 for May and December. The differences between day and night mean profiles, we also shown four combinations are produced since there are two sets of distribution for daytime/nighttime conditions.

The daytime retrieved mean profile has fairly similar features in CO for both the LDD and HDD in the month of May, whereas the nighttime retrieved CO profile for HDD has significant enhancements in the lower layer and upper layer of the troposphere. Whereas, in the month of December, the nighttime CO profile has greatest enhancements throughout the troposphere for HDD as compared to LDD. The daytime CO profile at HDD also has little enhancements in the lower layer. The day-night difference CO profiles for combination of selected LDD and HDD can

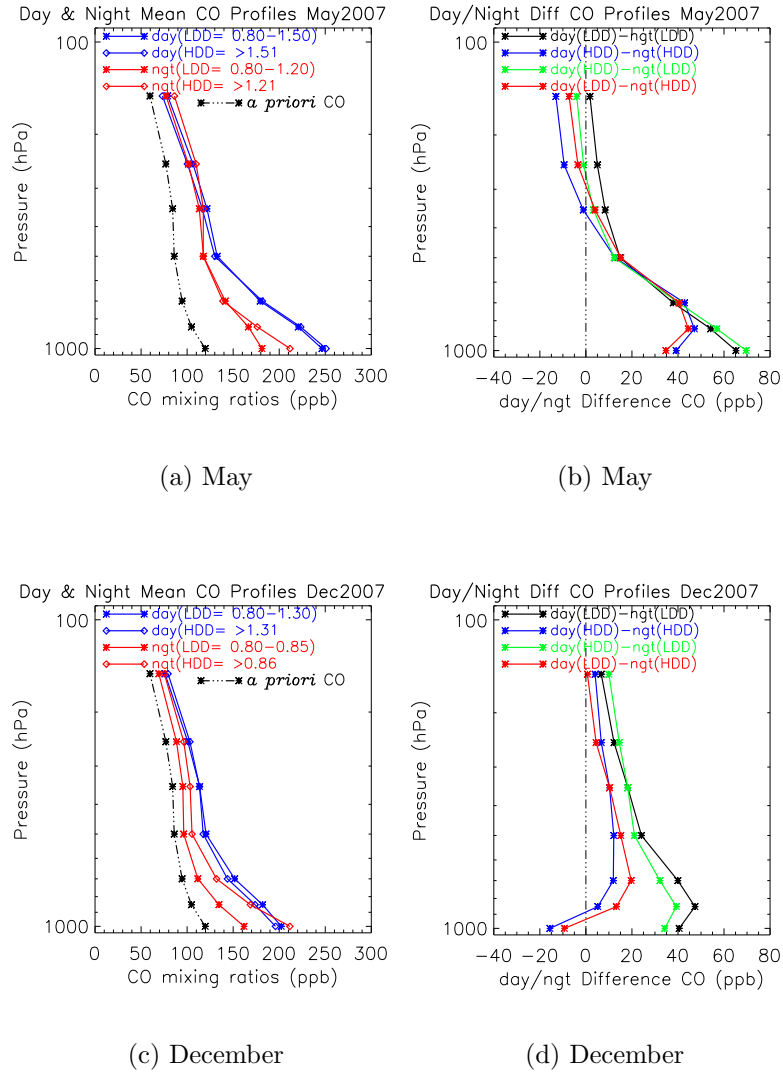


Figure 3.16: (a) MOPITT L2V3 retrieved mean daytime and nighttime CO profiles, over Bihar box, for May 2007; (b) Mean day-night difference CO profile, over Bihar box, for combination of LDD and HDD; (c) Same as (a) except for December 2007; (d) Same as (c) except for December 2007.

be, generally, separated into two sets of combinations (Fig. 3.16(b) and (d)). The combination of daytime and nighttime HDD does indeed show highest positive day-night differences in the lower layer. For the month of May, day(HDD)-ngt(LDD) and day(HDD)-ngt(HDD) have larger positive differences peaking at surface level, whereas in December a slightly lower enhancements seen, with a peak at 850 hPa pressure level. Separating retrieved CO profiles for combination of LDD and HDD

and utilizing different sets of combination gives some confidence that enhancement in the retrieved day-night CO profiles are present despite averaging kernel variability.

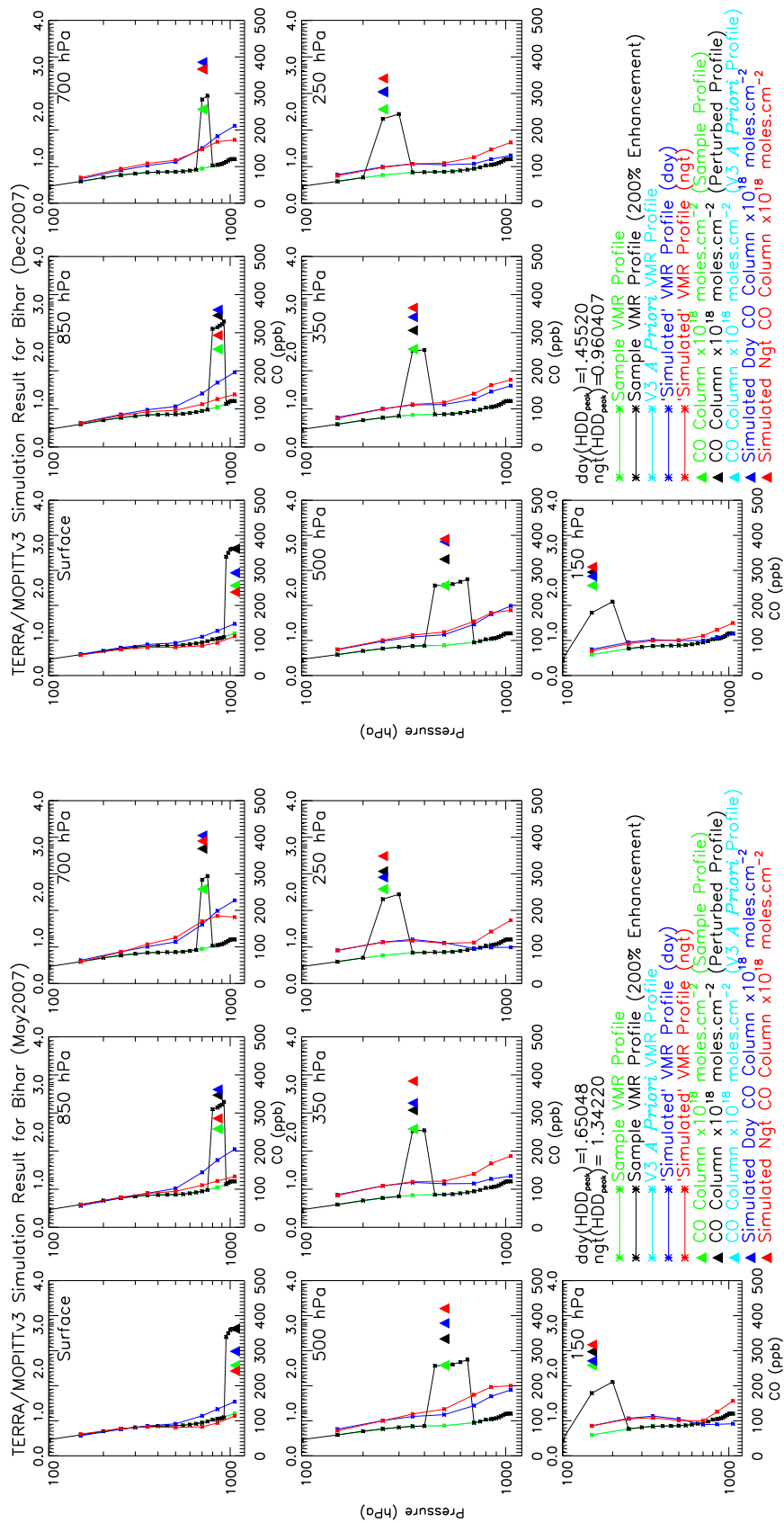
3.4.2.2 L2V3 Simulation

The MOPITT CO averaging kernels vary considerable, particularly from day to night and one can generally distinguish between the lower and upper troposphere. For this analysis, a selected ‘typical’ averaging kernel is chosen to be the best representative kernel for given surface and atmospheric properties. In this section, we examine the ability of the MOPITT instrument to make CO profile measurements using selected ‘typical’ averaging kernel for chosen case study region (i.e. Bihar) and later performed for other Indian regions. A standard analysis is developed here for simulating MOPITT CO profile to better understand MOPITT sensitivity to the lower troposphere. First, the MOPITT L2V3 a priori CO profile is taken as the sample profile for this analysis. An enhancement of 200 % was then applied to this profile in a layer stretching from surface (1100 hPa) to 920 hPa. This layer was then moved successively upwards through the profile in 7 steps to form 7 test profiles each with CO enhancements peaking at a particular MOPITT retrieval pressure level. The selected ‘typical’ averaging kernel of interest was then applied to each of these profiles using the method described in chapter 2, section 2.4.4.1. These simulations were performed for selected ‘typical’ averaging kernel at LDD_{peak} and HDD_{peak} for the month of May and December. Note that the simulation results performed for HDD_{peak} are presented and discussed here for the month of May and December.

For every MOPITT L2V3 retrieved CO profile, the Level 2 product also includes the corresponding CO total column. This quantity represents the integrated retrieved CO profile from the surface to the top of the atmosphere, and is expressed in units of molecules.cm⁻². However, in this analysis, we have calculated total column values for given CO profile. In order to calculate the total column, layers must be defined corresponding to each of the retrieved levels. Using number density at given temperature and pressure, the total column value can be calculated easily using simple linear equation. Mathematically, the CO total column C (a scalar) and retrieved profile x_{rtv} (a vector) are related by the pressure difference (Δp) through the linear relation

$$C = (x_{rtv} \times 10^{-3}) \cdot (\rho_n \times 10^{-6}) \cdot ABS(\Delta p \times 10^5) \quad (3.1)$$

Where ρ_n is the number density at given temperature and pressure, Δp is the difference in the pressure levels in km and ABS means absolute. The temperature and pressure profiles are used from ECMWF fields to calculate number density. There is, however, a persistent bias because of the implicit assumption that the CO volume mixing ratio at the highest retrieved level (150 hPa) extends up to the top of the atmosphere [Deeter et al., 2003]. Within the actual retrieval algorithm, the shape of the assumed CO profile at these levels is based on output from a chemistry model and decreases monotonically with increasing altitude. Thus, the 'effective' Δp value for this layer is substantially less than 200 hPa. Moreover, Deeter et al. [2003] found that the total column bias for L2V3 retrievals can be virtually eliminated by setting Δp to 159 hPa. It should be noted that this empirical correction is specific to L2V3 retrievals. Nevertheless, the relation for C (Eq. 3.1) produces total column values which agree with values in the Level 2 product within several percent and this level of accuracy should be quite considerable.



(a) May

(b) December

Figure 3.17: (a) MOPITT L2V3 'simulated' daytime and nighttime CO profiles for HDD_{peak} over Bihar, for May 2007; (b) Same as (a) except for December 2007. The green, black, cyan, blue, and red line indicates the considered sample CO profile, perturbed CO profile, a priori CO profile, 'simulated' day CO profile, and 'simulated' night CO profile. The green, black, cyan, blue, and red triangles show calculated total column values for corresponding CO VMR profiles (shown on upper horizontal scale).

Figure 3.17 (a, b) shows the simulation results for MOPITT L2V3 a priori profile considered as a sample profile and then applying selected ‘typical’ averaging kernel to the perturbed sample profile for the month of May and December respectively. The coloured triangles indicates the calculated total column values for each corresponding CO profile shown by individual coloured lines. Over Bihar region, a 200% enhancement in the surface level CO has similar significant enhancement for lower 3 retrieval pressure levels for the daytime measurements during May and December (Fig. 3.17b, top left panel). An enhancement of 200% between 775 hPa and 650 hPa which covers the 700 hPa MOPITT retrieval pressure level shows an enhancement at all retrieval levels with greatest effect evident in the lowest 3 retrieval levels. The enhancements during daytime and nighttime are similar except at surface retrieval level in the month of May whereas enhancements are further reduced for lowest 3 retrieval levels in the month of December. This is because the averaging kernel at 700 hPa likely to have equal sensitivity between day and night in the month of May, which is not the case in the month of December.

This suggesting that the MOPITT L2V3 measurements has greatest sensitivity at 700 hPa retrieval level and little sensitivity to the lower 2 retrieval levels during daytime measurements whereas MOPITT has no significant sensitivity to the lower 2 retrieval levels during nighttime measurements, which further most dependant on the surface and atmospheric properties (e.g. thermal contrast and CO profile). The effect of an enhancement at 500 hPa on the retrieved profile is likely to produce equally enhanced (or higher nighttime) CO profile throughout the troposphere as the averaging kernels for all retrieval levels have at least some sensitivity to this level. A 200% enhancement between 200 hPa and 300 hPa, which covers the 250 hPa MOPITT retrieval level shows an enhancement in the mid-upper troposphere retrieval level during daytime, where enhancements are greatest for mid-upper tropospheric retrieval levels. This is because the averaging kernel for the lower level have negative values above this altitude, indicating that increasing the CO in the upper troposphere will lead to a decrease in the retrieved concentration in the lower troposphere. In contrast, nighttime profiles show much less sensitivity to surface and 850 hpa perturbations. Indeed the biggest effects on the surface retrieval level arises from perturbations applied to the upper troposphere. For this region, thus, the MOPITT instrument is likely to have greatest sensitivity to the 700 hPa retrieval pressure

level and one can possibly differentiated between upper and lower tropospheric CO enhancements, with varying sensitivity between day and night measurements.

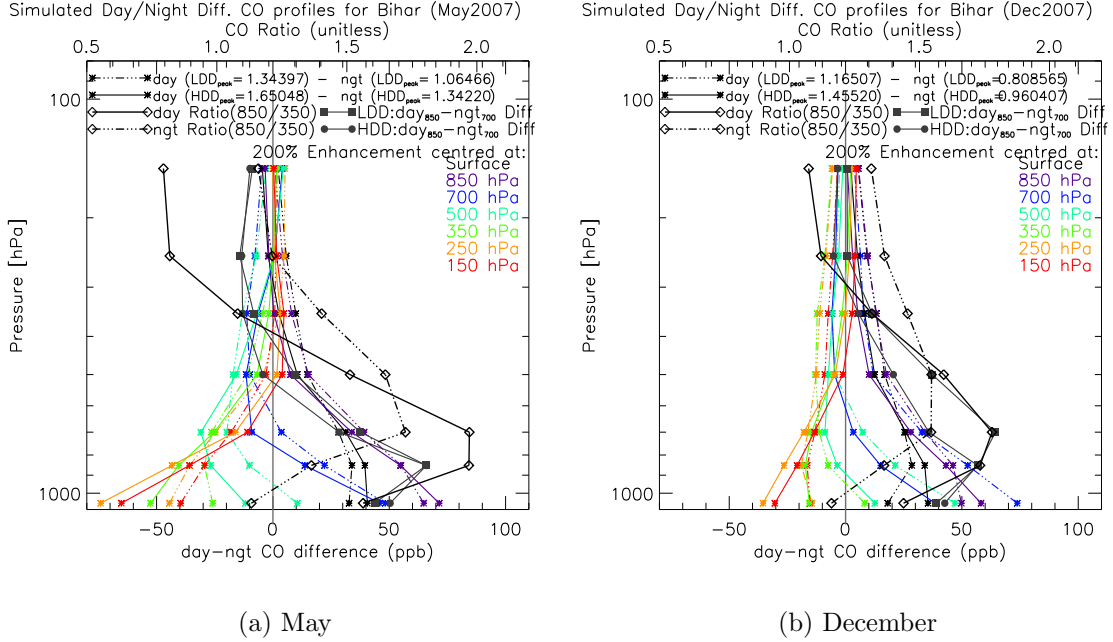


Figure 3.18: MOPITT L2V3 ‘simulated’ day-night difference CO profiles for LDD_{peak} and HDD_{peak}, over Bihar, for May 2007; (b) Same as (a) except for December 2007. The diamond solid and dash-dotted lines indicates day and night CO ratio (850/350) term respectively. The ratio scale shown as top x-axis. The dark grey coloured lines represents day₈₅₀-night₇₀₀ CO difference profiles for LDD_{peak} and HDD_{peak}. Note that the key result is depicted in Fig. 3.19.

Figure 3.18 (a, b) illustrates MOPITT L2V3 ‘simulated’ day-night difference CO profiles, over Bihar region, in the month of May and December respectively. All levels are shown. The key result is depicted in Fig. 3.19 for 850 hPa and 700 hPa (a, b). The objective in this analysis is to look at (a) positive day-night differences and (b) layer rather than smaller day-night values.

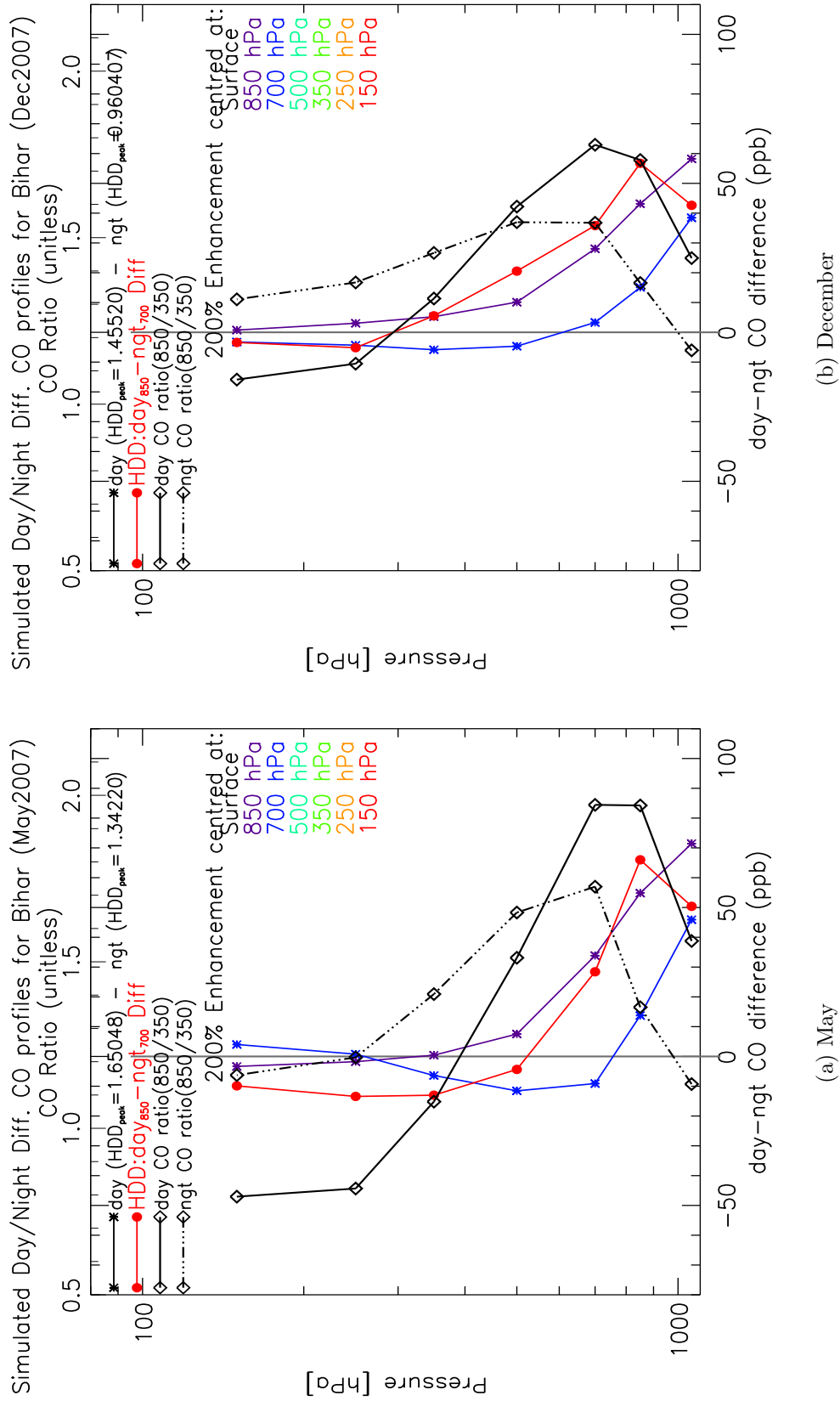


Figure 3.19: Key result from Fig. 3.18.

From Fig. 3.19, it is clearly seen that MOPITT indeed has greatest sensitivity to the 700 hPa retrieval level in this region, demonstrating 700 hPa day-night positive CO differences weighted to lower 2 retrieval levels in the month of May and 3 retrieval levels in the month of December. The 850 hPa day-night CO differences, however, are greatest at the surface but the positive CO differences are weighted to lower 5 retrieval levels. The additional diagnostic $\text{day}_{850}\text{-ngt}_{700}$ CO difference has largest positive CO differences at 850 hPa retrieval level, however, the CO differences are weighted to lower 3 retrieval levels in the month of May and 5 retrieval levels in the month of December. In addition, the ratio of the CO at 850 hPa to 350 hPa ($850/350$) used as an index for surface (lower layer) enhancements, which indeed contain shape information for MOPITT retrieved CO profile, CO ratio peaking at lower retrieval levels. The day CO ratio has a value close to 2 in the lower troposphere while night CO has a value close to 2 in the middle-upper troposphere, suggesting that CO ratio is useful term to differentiate CO in the layers. It should also be noted that [Deeter et al., 2004] reveal that the information content of MOPITT retrievals is objectively quantified through the calculation of the DOFS, which indicates the number of independent pieces of information in the retrieved profile. This means that DOFS values larger than 1 (indicating some amount of profile shape information) are common in tropical and mid-latitudes scenes. However, our analysis for this region show that selecting ‘typical’ averaging kernel for HDD_{peak} value by examining DOFS distribution, it is possible to gain maximum possible shape information of the retrieved CO profile. Nevertheless, we have also shown earlier that one can use threshold percent a priori CO mixing ratio value at 350 hPa to select retrieved data rather than DOFS, which has to be calculated and it is time consuming process.

Figure 3.20 shows MOPITT L2V3 calculated total column values for sample CO profile with 200% enhancements at each MOPITT retrieval pressure level forming 7 perturbed profiles. The total column values are calculated using Eq. 3.1. The a priori CO profile and sample CO profile have same total column value in all cases. It can clearly be seen that day-night columns differences have positive values for lower 3 retrieval pressure levels. Similar features can be seen in the month of December. These findings are consistent with our earlier results and thus, the robust methodology adopted here is more convincing.

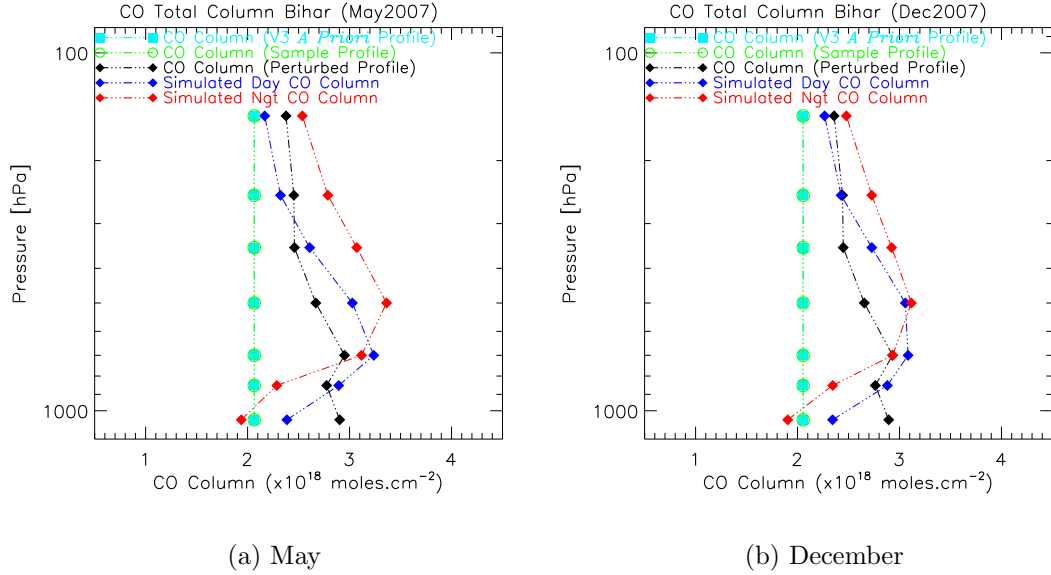


Figure 3.20: MOPITT L2V3 calculated total column values for i) a priori CO profile (cyan), ii) 7 individual sample profiles (green), iii) 7 individual perturbed sample profile (black), and iv) 7 individual simulated day (blue) and night (red) CO profiles, over Bihar, for May 2007; (b) Same as (a) except for December 2007. Note that these are not considered as profiles. For proper understanding the total column values plotted at corresponding perturbed retrieval level (layer) for each CO vmr profile.

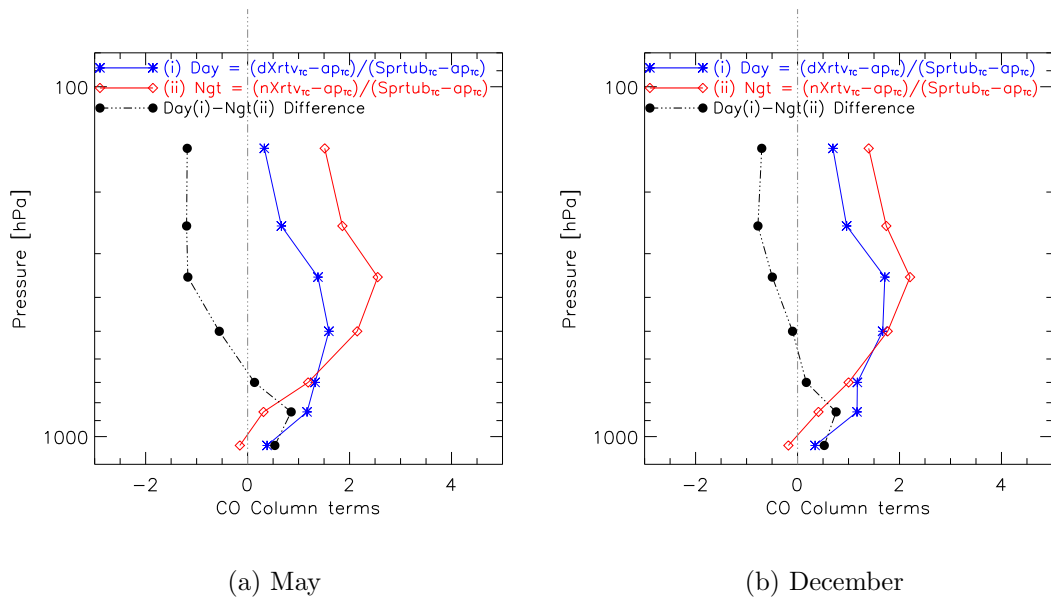


Figure 3.21: MOPITT L2V3 calculated total column tests for day and night simulated profiles in the month of (a) May and (b) December. Note that these are not considered as profiles and are in arbitrary unit.

We performed similar more tests for improved understanding (e.g. refer to Fig. 3.21). The day and night quantities indeed illustrate a persistent profile shape information available in the retrieved CO profile and their differences tend to give positive total column value for the enhancements in the lower layer of the troposphere. The positive differences for lower 2 retrieval levels in the month of May and for lower 3 retrieval level in the month of December.

3.4.2.3 TOMCAT Model CO Profile Simulation

The robust methodology described in the section 3.2 is partly adopted here. Early simulation results provide some level of confidence in our methodology. It is, therefore, possible to apply the knowledge obtained from examining MOPITT day-night difference simulation using MOPITT data alone to the examination of TOMCAT CO profile for selected L2V3 ‘typical’ averaging kernels. This section gives a brief overview on TOMCAT model, followed by discussion of simulation results.

The TOMCAT model was first described and used by Chipperfield et al. [1993] for studies of the polar stratosphere. It is, further, developed for tropospheric chemistry studies by the inclusion, for example, of convection [Stockwell and Chipperfield, 1999], wet and dry deposition [Giannakopoulos et al., 1999], lightning [Stockwell and Chipperfield, 1999], detailed gas-phase chemistry [Law et al., 1998], and tropospheric chemistry scheme [Arnold et al., 2005]. The TOMCAT/SLIMCAT [Chipperfield, 2006] is a three-dimensional (3D) off-line chemical transport model, which uses winds and temperature from meteorological analyses (e.g. from the UK Met Office or ECMWF) to specify the atmospheric transport and temperatures and calculates the abundances of chemical species (e.g. CO) in the troposphere and stratosphere. The TOMCAT model has been used to constrain CO emissions from regional to global scale [e.g., Hamilton et al., 2008; Shindell et al., 2006].

Figure 3.22 shows selected TOMCAT model CO profiles, over Bihar region, in the month of May and December of 2004. The profiles were taken on the 7th of May 2004 and 19th of December 2004, located at 26.51°N latitude and 75.93°E longitude, and 23.72°N latitude and 78.74°E longitude respectively. These CO profiles are used as a sample profile for MOPITT L2V3 simulation. Note that no enhancements are applied to these profiles, in practice therefore we will have only one modeled test profile instead of 7 test profiles as in the case of MOPITT L2V3 a priori CO profile

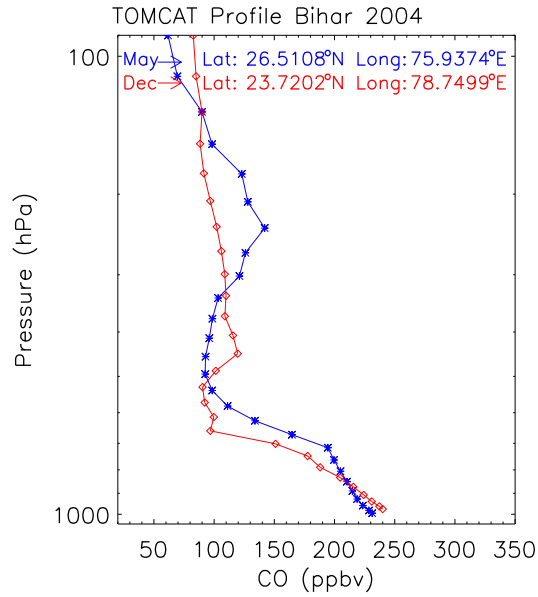


Figure 3.22: Selected TOMCAT model CO profiles, over Bihar box, for May 2004 (blue) and December 2004 (red).

simulation. The selected ‘typical’ averaging kernel of interest was then applied to these profiles. The exercise is performed for HDD_{peak} for the month of May and December are presented and discussed here.

Figure 3.23(a) show simulated CO profiles using MOPITT L2V3 selected ‘typical’ averaging kernel separately for daytime and nighttime observations, over Bihar region, in the month of May. The simulation has been performed for daytime and nighttime HDD_{peak} values. The CO total column concentrations are calculated using methodology described in section 3.4.2.2. Figure 3.24 illustrates calculated day-night difference CO profiles. It is obvious that these results are similar to our earlier findings (refer to Fig. 3.19).

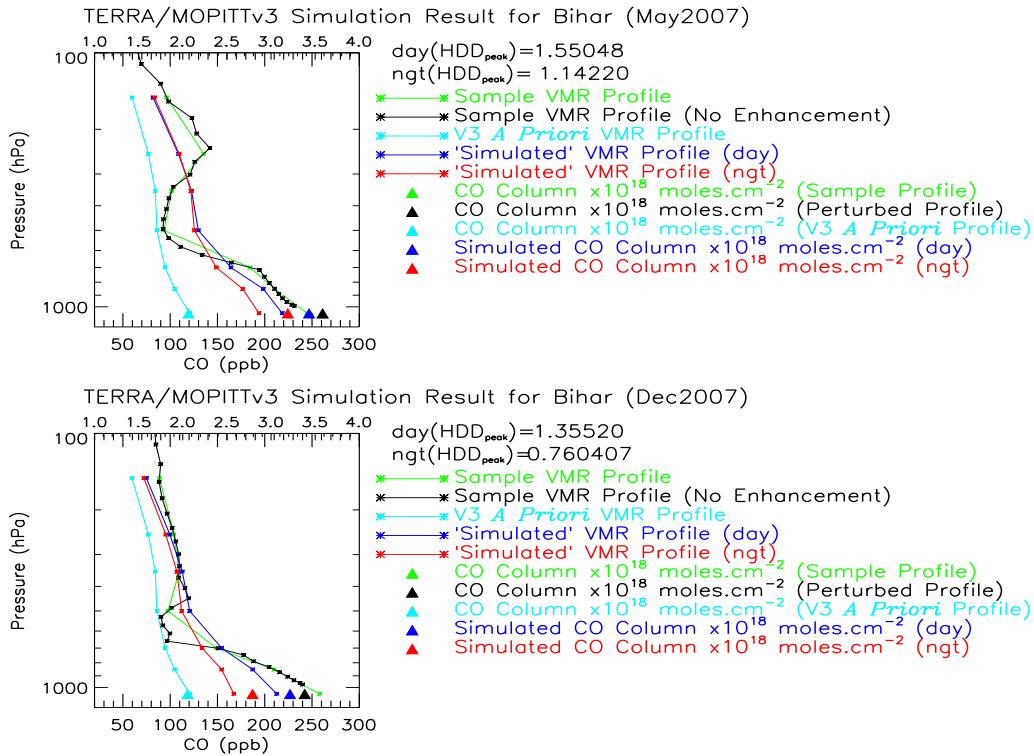
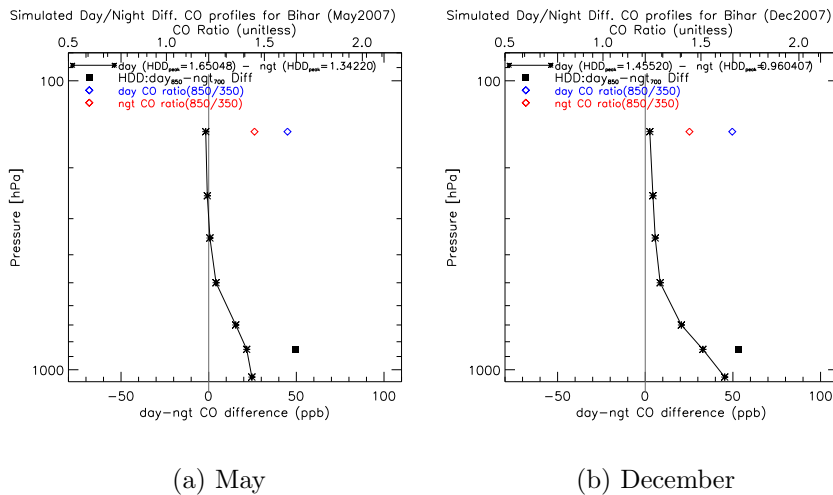


Figure 3.23: ‘Simulated’ daytime and nighttime CO profiles for TOMCAT model selected base CO profile, over Bihar, for May (top panel) and December (bottom panel) 2007.



(a) May

(b) December

Figure 3.24: (a) MOPITT L2V3 ‘simulated’ day-night difference CO profile for HDD_{peak} , over Bihar for TOMCAT, for May 2007; (b) Same as (a) except for December 2007.

3.4.3 L2V3 Profile Simulation - A Case Study of Delhi

The Delhi box is selected as a second case study region to simulate MOPITT L2V3 day-night differences and further perform MOPITT L2V3 simulation in conjunction with TOMCAT model selected CO profile in this region. The region is shown by a rectangular box in Fig. 3.12 over Delhi, in the latitude range from 28.0°N to 30.0°N and longitude range from 75.5°E to 78.5°E.

3.4.3.1 Mean L2V3 CO Profile

For Delhi region, MOPITT L2V3 retrieved daytime and nighttime DOFS histogram has two distinct distribution (refer to Appendix-I Fig. 7.1). The retrieved mean daytime and nighttime CO profiles and corresponding day-night difference CO profiles for combination of LDD and HDD in the month of May and December 2007 are shown in Fig. 3.25. From Fig. 3.25(a) it is obvious that the mean daytime and nighttime CO profiles, in general, have similar features in CO for both LDD and HDD, except showing significant enhancements in the lowermost layer and upper troposphere for HDD. The day-night CO difference profiles for combination of LDD and HDD can be separated into two sets of combinations similar to that of observed for Bihar region earlier, suggesting utility of day(HDD)-ngt(LDD) and day(HDD)-ngt(HDD) in differentiating CO into layers. In the month of December, the retrieved mean nighttime CO profile for HDD show large enhancements at lower 3 retrieval levels but the LDD show negative differences. The two sets of LDD and HDD combinations can be grouped. However, the two sets has reduced day-night CO differences for lowermost 3 retrieval levels, suggesting reduced sensitivity in the month of December as compared to the month of May in this region.

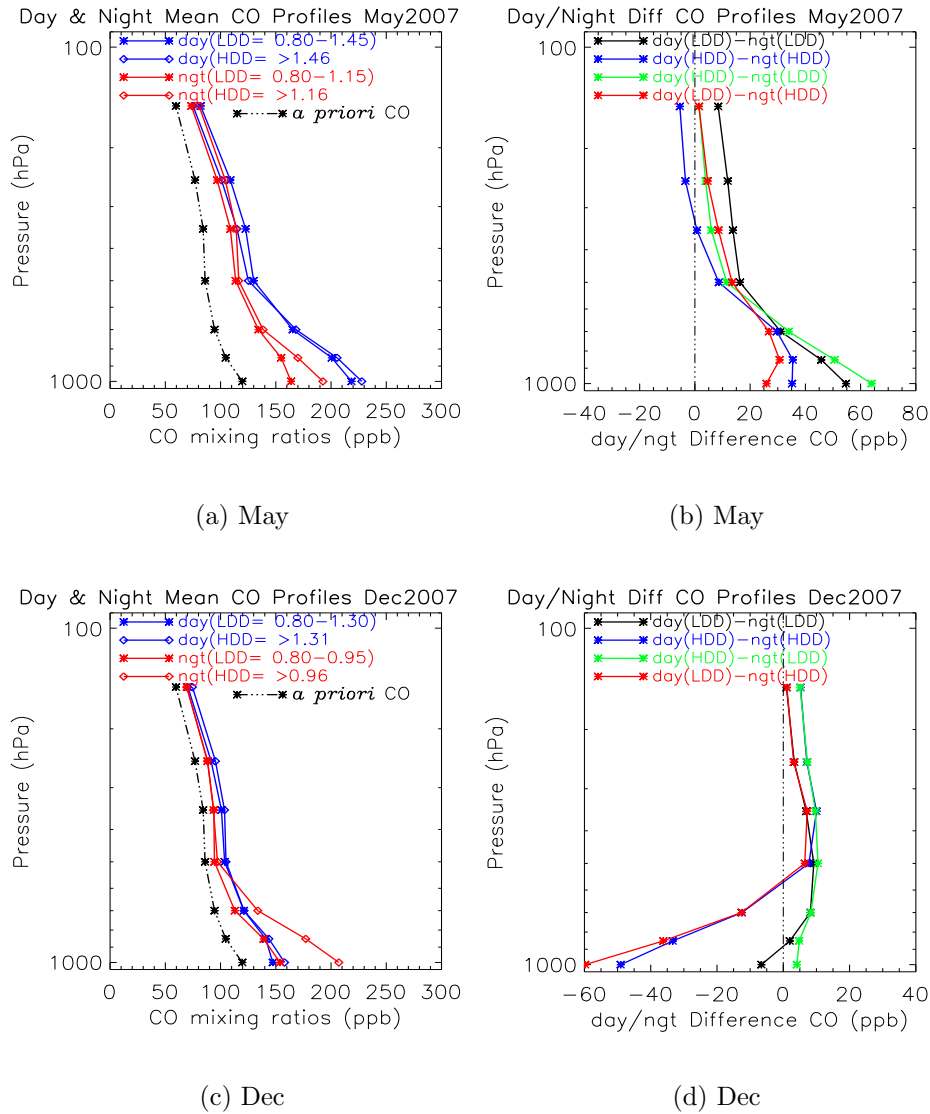


Figure 3.25: (a) MOPITT L2V3 retrieved mean daytime and nighttime CO profiles, over Delhi box, for May 2007; (b) Mean day-night difference CO profile, over Delhi box, for combination of LDD and HDD; (c) Same as (a) except for December 2007; (d) Same as (b) except for December 2007.

3.4.3.2 L2V3 Simulation

Similar to Bihar region, we examine day-night differences using L2V3 a priori profile simulation and selected ‘typical’ averaging kernels over Delhi box in the month of May and December 2007. The methodology discussed earlier in section 3.2 and 3.4.2.2 used to simulate day and night profiles and total column values. Note that the simulation results performed for HDD_{peak} are presented and discussed here for

the months of May and December.

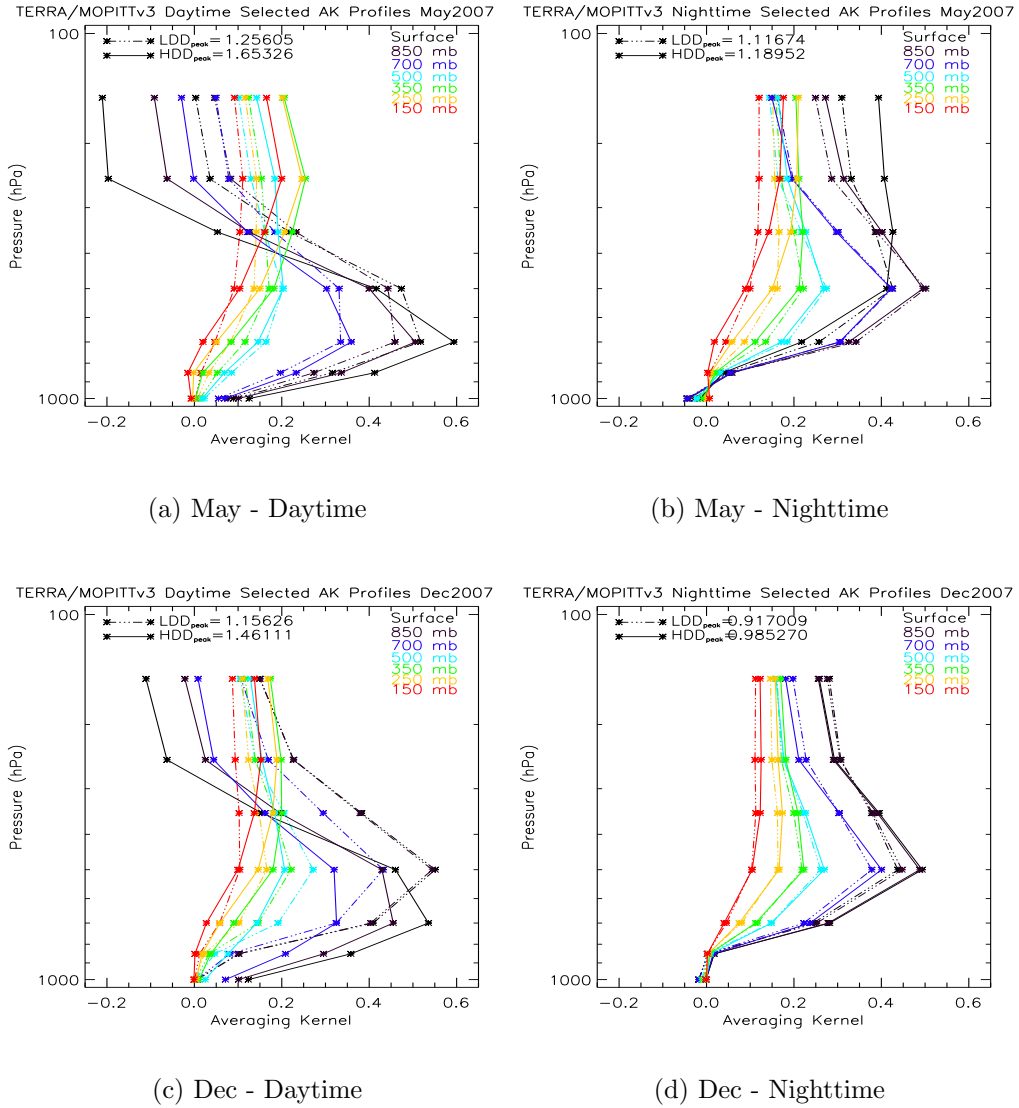
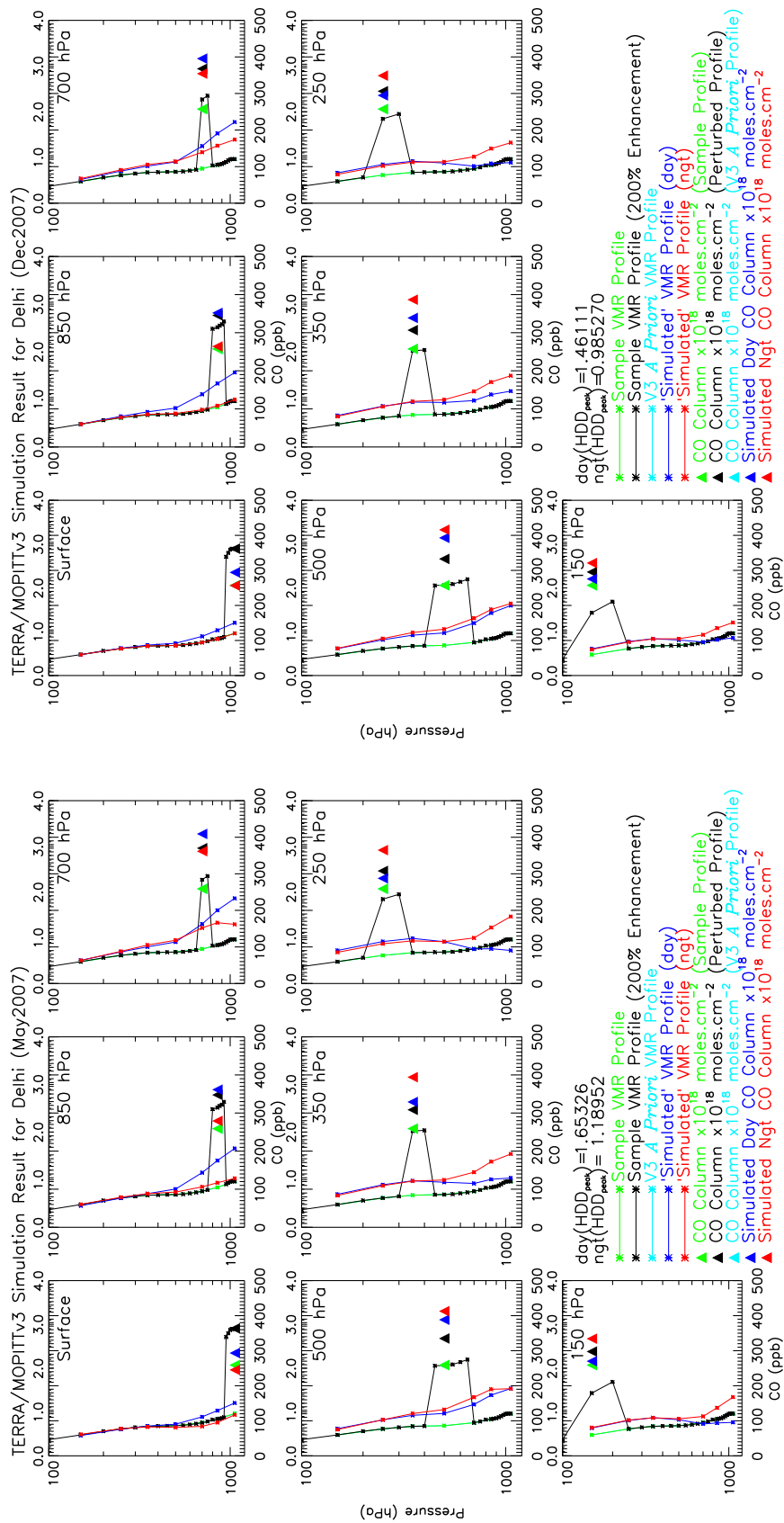


Figure 3.26: (a) MOPITT L2V3 Selected daytime ‘typical’ AK profile, over Delhi box, for May 2007; (b) Selected nighttime ‘typical’ AK profile, over Delhi box, for May 2007; (c) Same as (a) except for December 2007; (d) Same as (b) except for December 2007.

Figure 3.26 show selected ‘typical’ averaging kernels for LDD_{peak} and HDD_{peak} values for daytime and nighttime measurements. These ‘typical’ averaging kernels have very little differences compared to selected ‘typical’ averaging kernels for Bihar region in the month of May and December. It is, because, the surface and atmospheric properties are likely to be same in these regions with having similar thermal contrast and boundary layer height (refer to Fig. 3.2).



(a) May

(b) Dec

Figure 3-27: (a) MOPITT L2V3 'simulated' daytime and nighttime CO profiles for HDD_{peak} over Delhi, for May 2007; (b) Same as (a) except for December 2007. The green (black, cyan, blue, and red) line indicates the considered sample CO profile (perturbed CO profile, a priori CO profile, 'simulated' day CO profile, and 'simulated' night CO profile). The green (black, cyan, blue, and red) triangles show calculated total column values for considered sample profile (perturbed sample profile, a priori profile, 'simulated' daytime profile, and 'simulated' nighttime profile).

Figure 3.27 shows simulation results for MOPITT L2V3 a priori profile considered as a sample profile and then applying selected ‘typical’ averaging kernels, over Delhi box, to the perturbed profile for the month of May and December. It should be first noted that the ‘simulated’ daytime and nighttime CO profiles in this region are comparable to that ‘simulated’ daytime and nighttime CO profiles in Bihar region (refer to Fig. 3.17) with less significant differences as expected. Because, selected ‘typical’ averaging kernels have more or less similar features in these regions. Similarly the calculated total column values for ‘simulated’ daytime and nighttime CO profiles are fairly matching. However, the MOPITT sensitivity over this region likely to slightly reduced for the nighttime measurements as compared to Bihar region. For example, an enhancement of 200% between 775 hPa and 650 hPa which covers the 700 hPa MOPITT retrieval pressure level shows an enhancement at all retrieval levels with greatest effect evident in the lowest 3 retrieval levels. The enhancements during daytime and nighttime are similar except at lower two retrieval levels in this region whereas the enhancements during daytime and nighttime are similar except surface retrieval levels in Bihar region (refer to Fig. 3.17) in the month of May and December.

Figure 3.28 (a, b) illustrates MOPITT L2V3 ‘simulated’ day-night difference CO profiles, over Delhi region, in the month of May and December respectively. The key result is depicted in Fig. 3.29 (a, b). First, it is most obvious that the key result from Fig. 3.29 in this region has similar features as compared to that of key result from Fig. 3.19 for Bihar region, demonstrating 700 hPa day-night positive CO differences weighted to lowermost layer of the troposphere. It is, thus, providing supporting evidence to MOPITT greatest sensitivity to the 700 hPa retrieval level for both regions. Although, the MOPITT sensitivity likely to vary considerable between these two regions. For example, 700 hPa day-night positive CO differences weighted to lower 3 retrieval levels in the month of May and 4 retrieval levels in the month of December in this region whereas 700 hPa day-night positive CO differences weighted to lower 2 retrieval levels in the month of May and 3 retrieval levels in the month of December for Bihar region (refer to Fig. 3.19). This means that MOPITT shows greatest sensitivity to the lowermost layer (approx. 0- 2.5 km) over Bihar region whereas the MOPITT has little reduced sensitivity over Delhi region showing positive day-night differences for approximately 0-4 km layer. Similar differences for these two regions can be observed for day₈₅₀-ngt₇₀₀ diagnostic. It has also to be noted

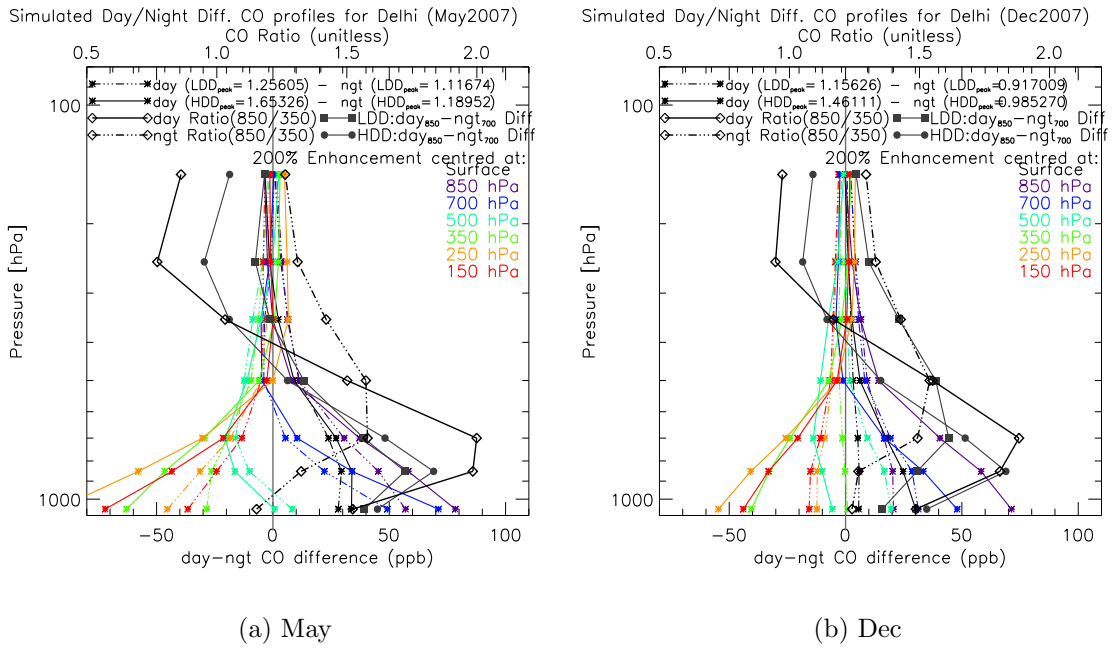


Figure 3.28: MOPITT L2V3 ‘simulated’ day-night difference CO profiles for LDD_{peak} and HDD_{peak} , over Delhi, for May 2007; (b) Same as (a) except for December 2007. The diamond solid and dash-dotted lines indicates day and night CO ratio (850/350) term respectively. The ratio scale shown as top x-axis. The dark grey coloured lines represents $day_{850}-night_{700}$ CO difference profiles for LDD_{peak} and HDD_{peak} . Note that the key result is depicted in Fig. 3.29.

that the day CO ratio peaks in the lowermost layer and night CO ratio peak in the middle troposphere as of Bihar region, suggesting utility to differentiating CO into the layers.

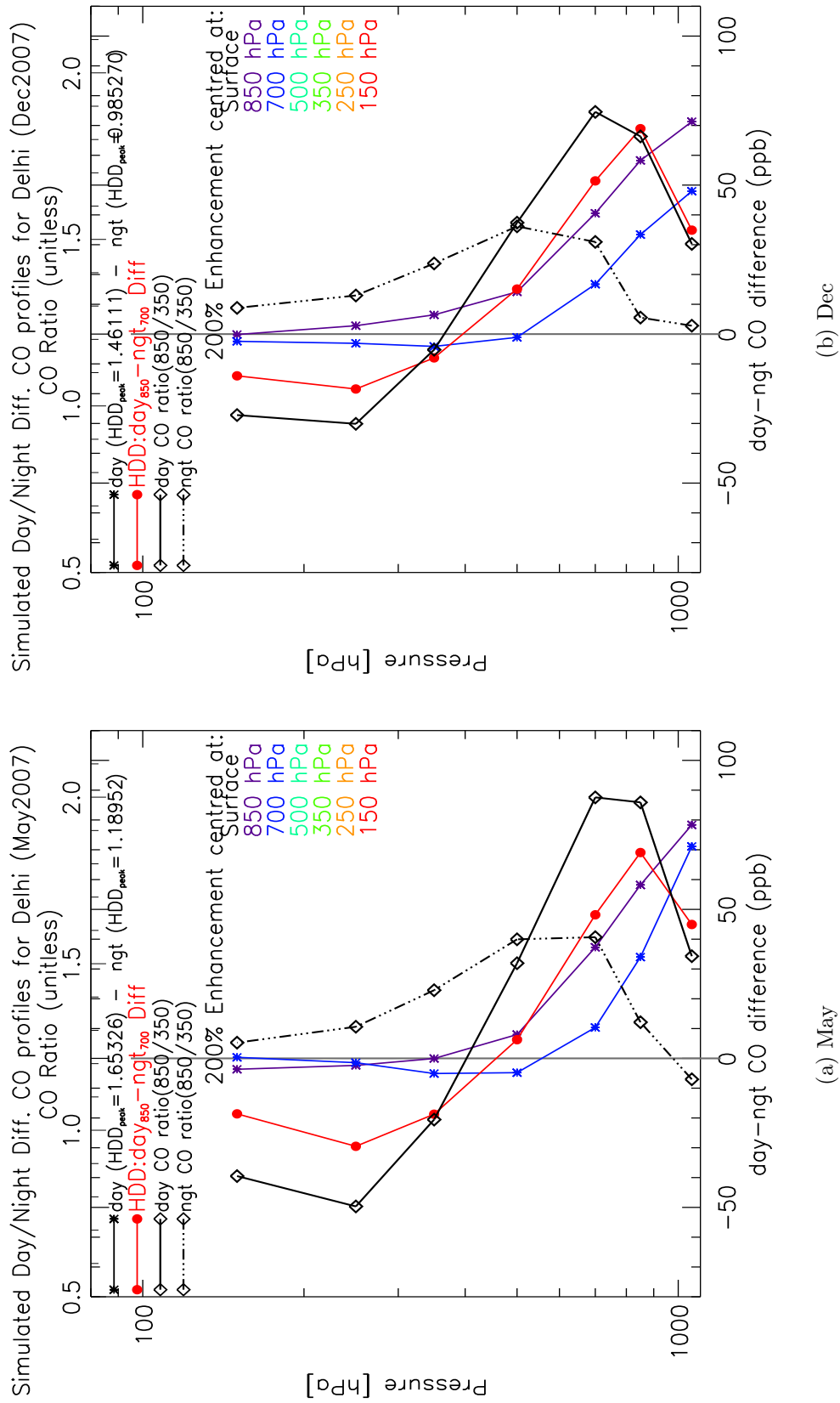


Figure 3.29: (a) Key result from Fig. 3.28 for May 2007; (b) Same as (a) except for December 2007.

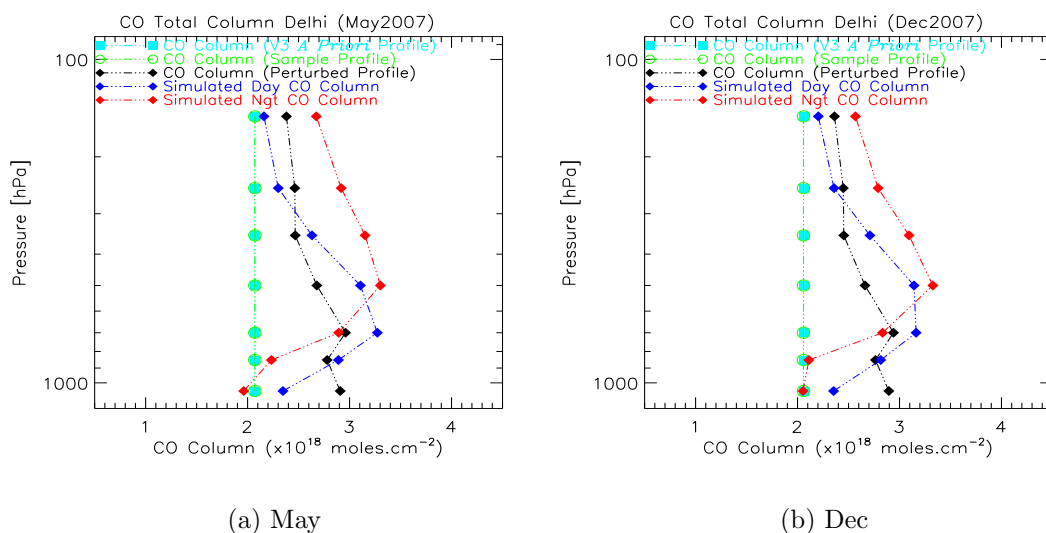


Figure 3.30: (a) MOPITT L2V3 calculated total column values for May 2007; i) a priori CO profile (cyan), ii) 7 individual sample profiles (green), iii) 7 individual perturbed sample profile (black), and iv) 7 individual simulated day (blue) and night (red) CO profiles, over Delhi, for May 2007; (b) Same as (a) except for December 2007. Note that these are not considered as profiles. For proper understanding the total column values plotted at corresponding perturbed retrieval level (layer) for each CO vmr profile.

Figure 3.30 gives MOPITT L2V3 calculated total column values using Eq. 3.1 for each profile used in MOPITT L2V3 simulation and ‘simulated’ CO profiles. It is apparent that the total column values calculated for this region are very much comparable to the total column values for Bihar region. It can be seen that the daytime calculated CO total column values are higher than the perturbed profile calculated column values for lower-middle troposphere except for surface retrieval level whereas the nighttime calculated values are much higher than the perturbed profile column values for middle-upper troposphere. Similar features can be seen for Bihar region (refer to Fig. 3.20). This is strongly suggesting that MOPITT is able to differentiate CO in the troposphere into two broad layers.

Figure 3.31 illustrate a similar test performed for Bihar region and it is indeed in agreement as well. These tests likely to enhance our ability to understand differentiation of CO into vertical layers for MOPITT retrieved CO data. In the next section we performed MOPITT L2V3 simulation in conjunction with TOMCAT model CO profile.

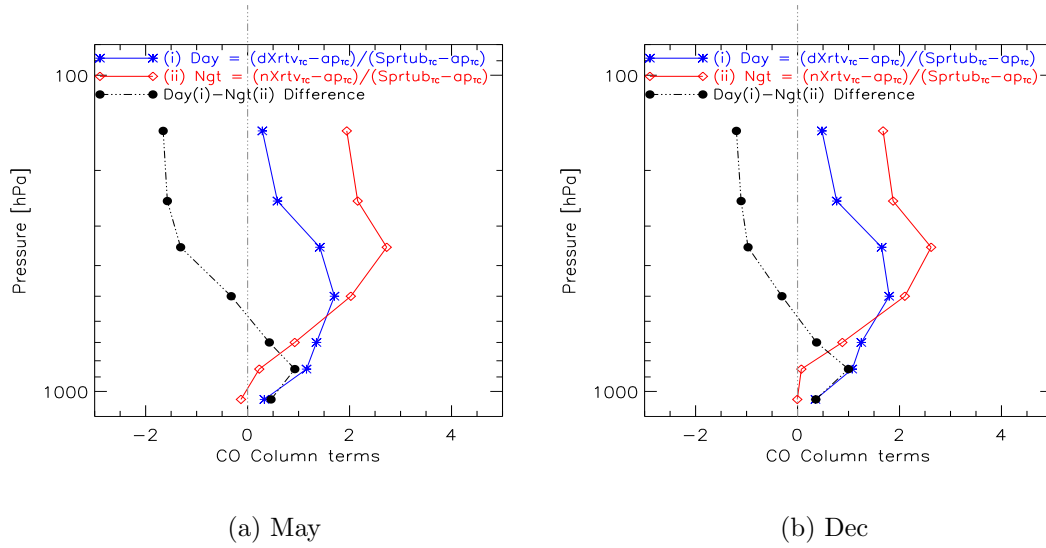


Figure 3.31: MOPITT L2V3 calculated total column tests for day and night simulated profiles in the month of (a) May and (b) December.

3.4.3.3 TOMCAT Model CO Profile Simulation

Similar MOPITT L2V3 simulations for the TOMCAT model CO profile has been performed in this region as in case of Bihar region to improve our knowledge about CO in the troposphere over India subcontinent region and to test our methodology. A profile over Delhi box was selected to represent a case where our analysis suggests the location of a CO source region in the month of May and December. The profiles were taken on the 5th of May 2004 and 12th of December 2004, located at 28.51°N latitude and 77.56°E longitude.

Figure 3.32 shows selected TOMCAT CO profiles, over the Delhi box, used as a sample profile for MOPITT L2V3 simulation. Similar simulations were performed as in the case of the Bihar region (refer to Section 3.4.2.3). Simulation results are presented in Fig. 3.33 for May and December of 2007. The ‘simulated’ daytime and nighttime CO profiles have similar features in this region as in case of Bihar region. The ‘simulated’ daytime CO profile has slightly less enhancements in the lowermost troposphere. The reason is that the chosen TOMCAT CO profile indeed has less enhancements in the boundary layer as compared to the CO profiles over Bihar region. Moreover, in the month of May, CO profile is quite flat within the planetary boundary layer. Simulated CO total column values are quite comparable.

Figure 3.34 illustrates the ‘simulated’ day-night difference CO profile for chosen

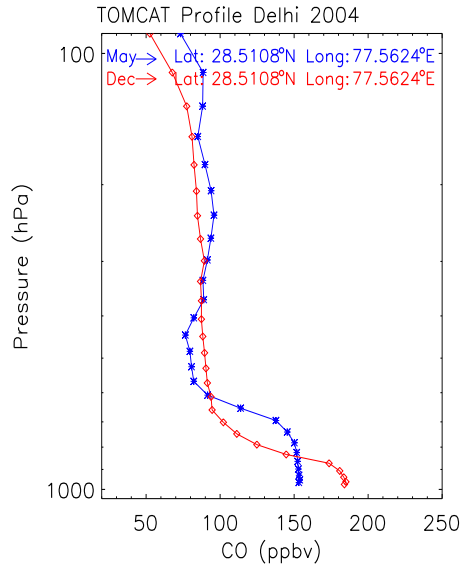


Figure 3.32: Selected TOMCAT model CO profiles, over Delhi box, for May 2004 (blue) and December 2004 (red) for the given latitude and longitude co-ordinate.

TOMCAT CO profile over Delhi box in the month of May and December. It is apparent that the results are quite similar to our earlier findings, suggesting that the MOPITT sensitivity to the CO in the lowermost layer is likely to be dependent on the amount of CO in the boundary layer together with thermal contrast condition and boundary layer height.

For the Delhi region, our analysis confirms the extensive CO pollution over this region, enhancements in NO_2 also observed in this region supporting this analysis. A robust methodology used in this examination further provide evidence to MOPITT sensitivity to near surface CO concentrations in this region and thus we believe that MOPITT has significant sensitivity to the CO in the boundary layer in this region.

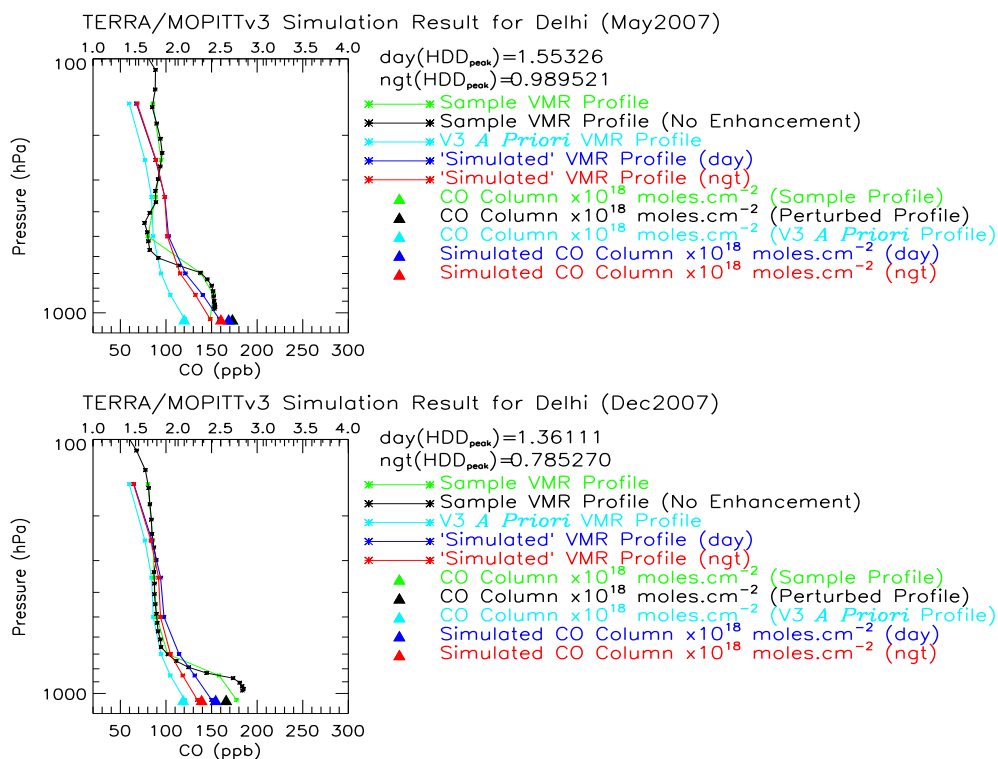


Figure 3.33: (a) ‘Simulated’ daytime and nighttime CO profiles for TOMCAT model selected base CO profile, over Delhi, for May (top panel) 2007; (b) Same as (a) except for December (bottom panel) 2007.

3.4.4 L2V3 Profile Simulation - A Case Study of Mumbai

We now apply our knowledge to simulate day-night differences over western part of India i.e. Mumbai region. The region is shown by rectangular box in Fig. 3.12 over Mumbai, in the latitude range from 17.8°N to 20.8°N and longitude range from 72.5°E to 74.5°E. Similar analysis test performed as in case of Bihar and Delhi region and the simulation results discussed here to further examine ability of MOPITT instrument to make observations of CO.

3.4.4.1 Mean L2V3 CO Profile

For Mumbai region, MOPITT L2V3 retrieved daytime and nighttime DOFS histogram has two distinct distributions (refer to Appendix-I Fig. 7.1) as observed for Bihar and Delhi regions. The mean averaged CO profiles for both daytime and nighttime measurements for LDD and HDD in the month of May and December of 2007 are shown in Fig. 3.35. Persistent features in CO over this region similar to earlier

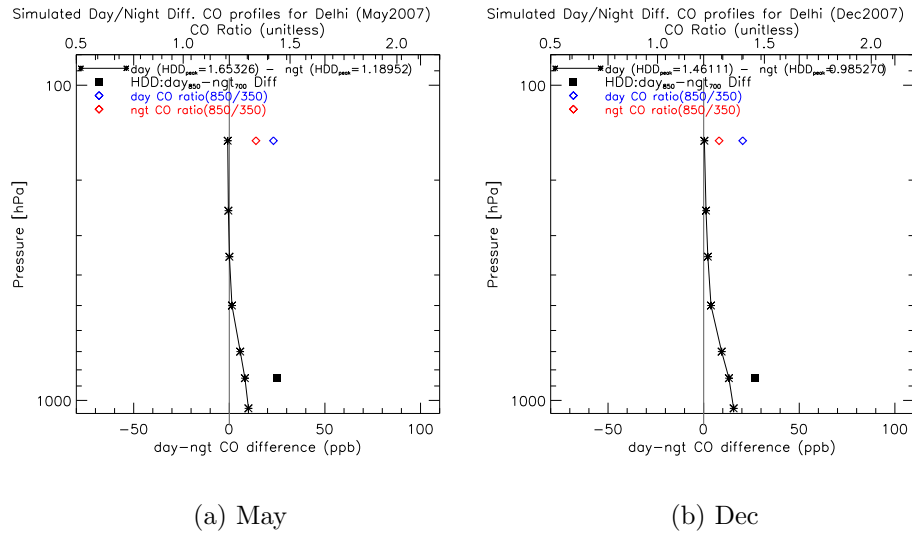


Figure 3.34: (a) MOPITT L2V3 ‘simulated’ day-night difference CO profile for HDD_{peak} , over Delhi, for May 2007; (b) Same as (a) except for December 2007.

findings can be seen in the month of December. However, in the month of May, the sets of combination of LDD and HDD can not be separated clearly in particular in the lowermost layer of the troposphere. This could be because the DOFS distribution does not have sharp peaks and tend to cover a wide range of DOFS values.

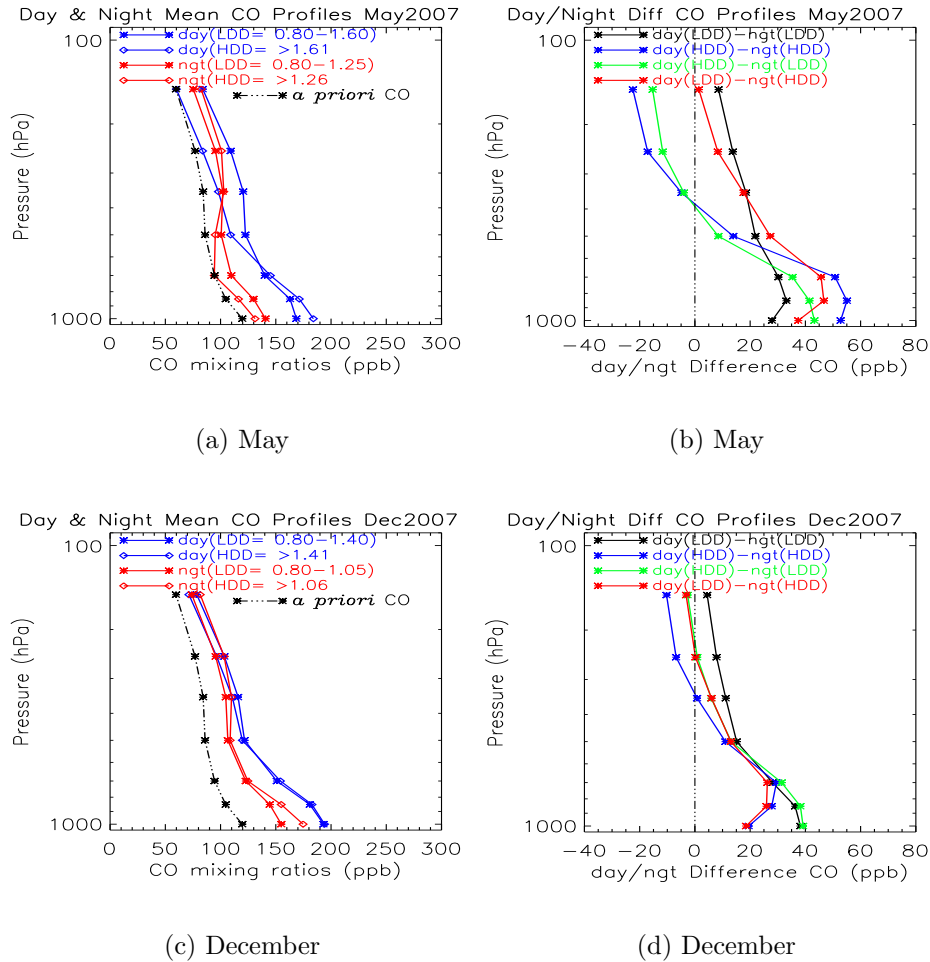


Figure 3.35: (a) MOPITT L2V3 retrieved mean daytime and nighttime CO profiles, over Mumbai box, for May 2007; (b) Mean day-night difference CO profile, over Mumbai box, for combination of LDD and HDD; (c) Same as (a) except for December 2007; (d) Same as (b) except for December 2007.

3.4.4.2 L2V3 Simulation

For Mumbai region, similar MOPITT L2V3 simulations are performed using L2V3 a priori profile and selected ‘typical’ averaging kernels over Mumbai region in the month of May and December 2007. Figure 3.36 shows selected ‘typical’ averaging kernels over Mumbai region in the month of May and December.

Figure 3.37 show simulation results obtained by applying selected ‘typical’ averaging kernels, in this region, to the perturbed sample profile at each retrieval pressure level. Over Mumbai region, a 200 % enhancement at surface retrieval level has significant enhancement for lower 3 retrieval levels in ‘simulated’ daytime CO profile

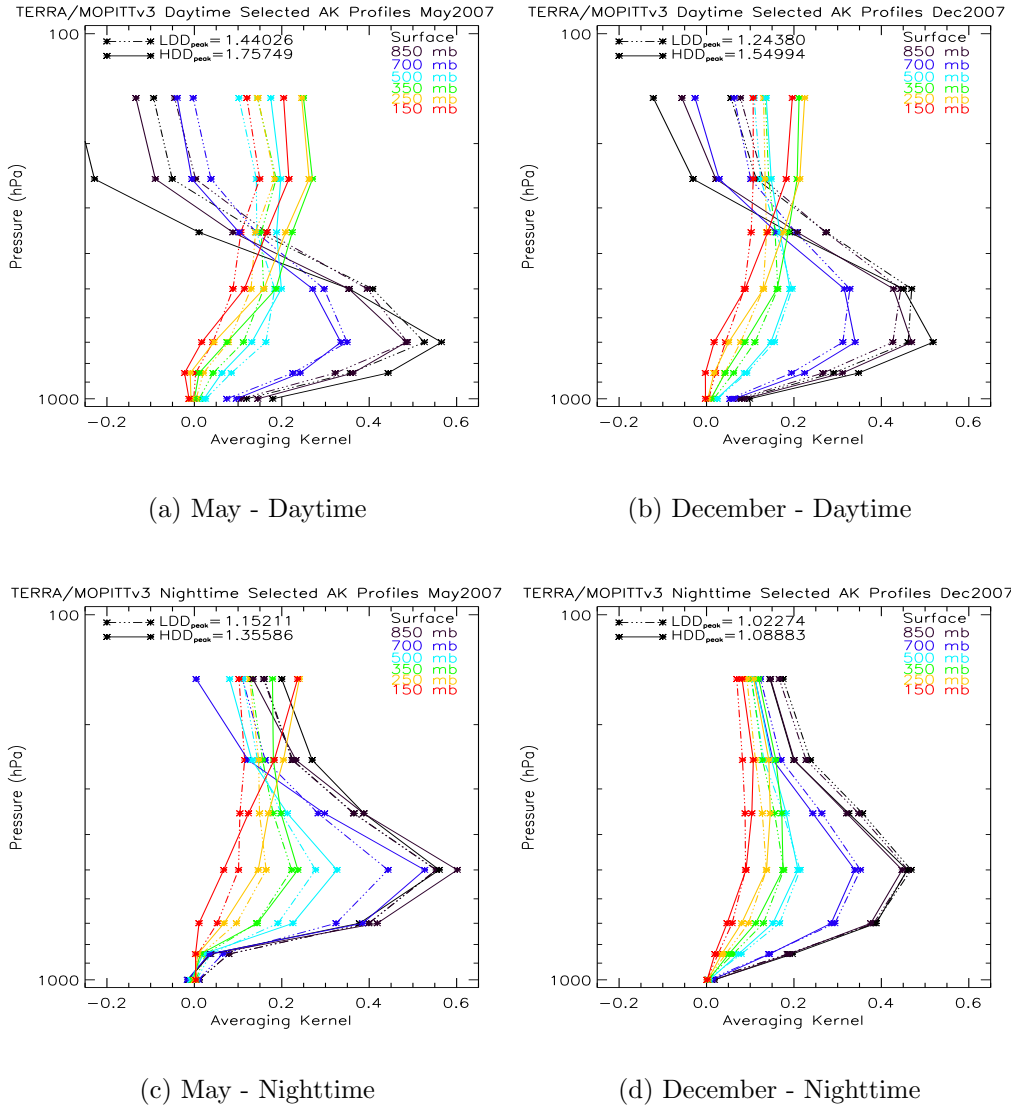
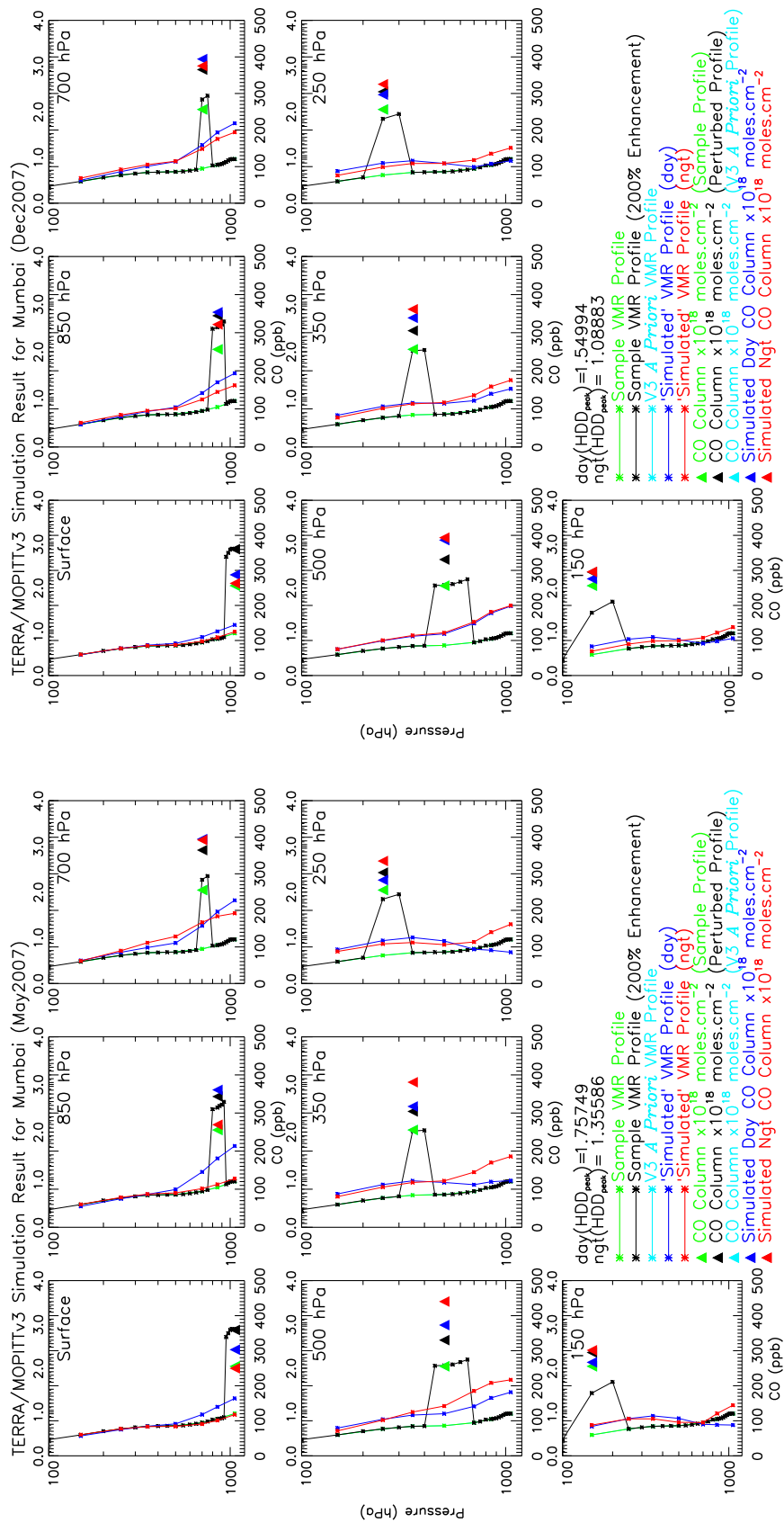


Figure 3.36: (a) MOPITT L2V3 Selected daytime ‘typical’ AK profile, over Mumbai box, for May 2007; (b) Same as (a) except for December 2007; (c) Selected nighttime ‘typical’ AK profile, over Mumbai box, for May 2007; (d) Same as (c) except for December 2007.

whereas there are almost no enhancement in ‘simulated’ nighttime CO profile. This is analogous to earlier findings for Bihar (Fig. 3.17) and Delhi region (Fig. 3.27) with less significant differences in ‘simulated’ CO profiles as expected.



(a) May

(b) December

Figure 3-37: (a) MOPITT L2V3 ‘simulated’ daytime and nighttime CO profiles for HDD_{peak} over Mumbai, for May 2007; (b) Same as (a) except for December 2007. The green (black, cyan, blue, and red) line indicates the considered sample CO profile (perturbed CO profile, a priori CO profile, ‘simulated’ day CO profile, and ‘simulated’ night CO profile). The green (black, cyan, blue, and red) triangles show calculated total column values for considered sample profile (perturbed sample profile, a priori profile, ‘simulated’ daytime profile, and ‘simulated’ nighttime profile).

In contrast to Bihar and Delhi region, an enhancement of 200% between 775 hPa and 650 hPa which covers the 700 hPa MOPITT retrieval pressure level shows enhancements during daytime and nighttime which are similar in this region except that at the enhancements during nighttime in the month of December are at lower 3 retrieval levels. This can be seen by looking at calculated total column value for nighttime ‘simulated’ CO profile in the month of May 2007. Secondly, an enhancement of 200% between 200 hPa and top of the atmosphere, which covers the 150 hPa MOPITT L2V3 retrieval level shows significant enhancements in the daytime ‘simulated’ CO profile in the middle-upper troposphere in the month of December, which is not the case for Bihar and Delhi region during this time of year. In general, simulation results in this region are fairly similar to earlier findings and thus building up confidence in our simulation methodology.

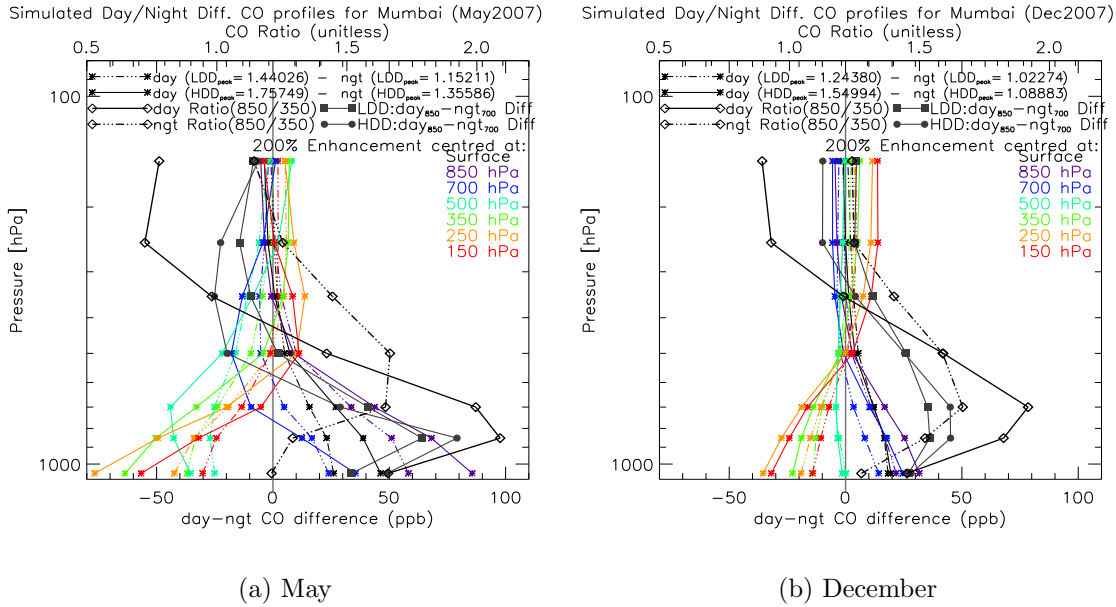


Figure 3.38: MOPITT L2V3 ‘simulated’ day-night difference CO profiles for LDD_{peak} and HDD_{peak} , over Mumbai, for May 2007; (b) Same as (a) except for December 2007. The diamond symbol solid and dash-dotted lines indicates day and night CO ratio (850/350) term respectively. The ratio indicated by top x-axis. The dark grey coloured lines represents day₈₅₀-night₇₀₀ CO difference profiles for LDD_{peak} and HDD_{peak} . Note that the key result is depicted in Fig. 3.39.

Figure 3.38 (a, b) illustrates MOPITT L2V3 ‘simulated’ day-night difference CO profiles, over Mumbai region, in the month of May and December respectively. The key result is depicted in Fig. 3.39 (a, b).

It is clearly obvious from Fig. 3.39 that MOPITT has superior sensitivity to the 700 hPa retrieval pressure level in this region similar to Bihar and Delhi region from Indian subcontinent. The result demonstrating 700 hPa day-night positive CO differences weighted to lower 2 retrieval levels in the month of May and to lower 4 retrieval levels in the month of December. It should be noted that MOPITT sensitivity to the lower layer in the month May for 3 regions discussed so far has similar features and equal sensitivity whereas there are significant differences in the MOPITT sensitivity to the lower layer during December month for these regions. It is not possible to explain what causing for this variability but it could be possibly due to varying surface and atmospheric properties and further Delhi and Bihar regions are affected by dense foggy and haze condition during winter months (November-January) whereas Mumbai region is not likely affected by dense fog and haze. Moreover, in the month of May, the CO ratio and $\text{day}_{850}\text{-ngt}_{700}$ differences have sharp peak in the lower layer in this region as compared to broad peak for Bihar and Delhi region.

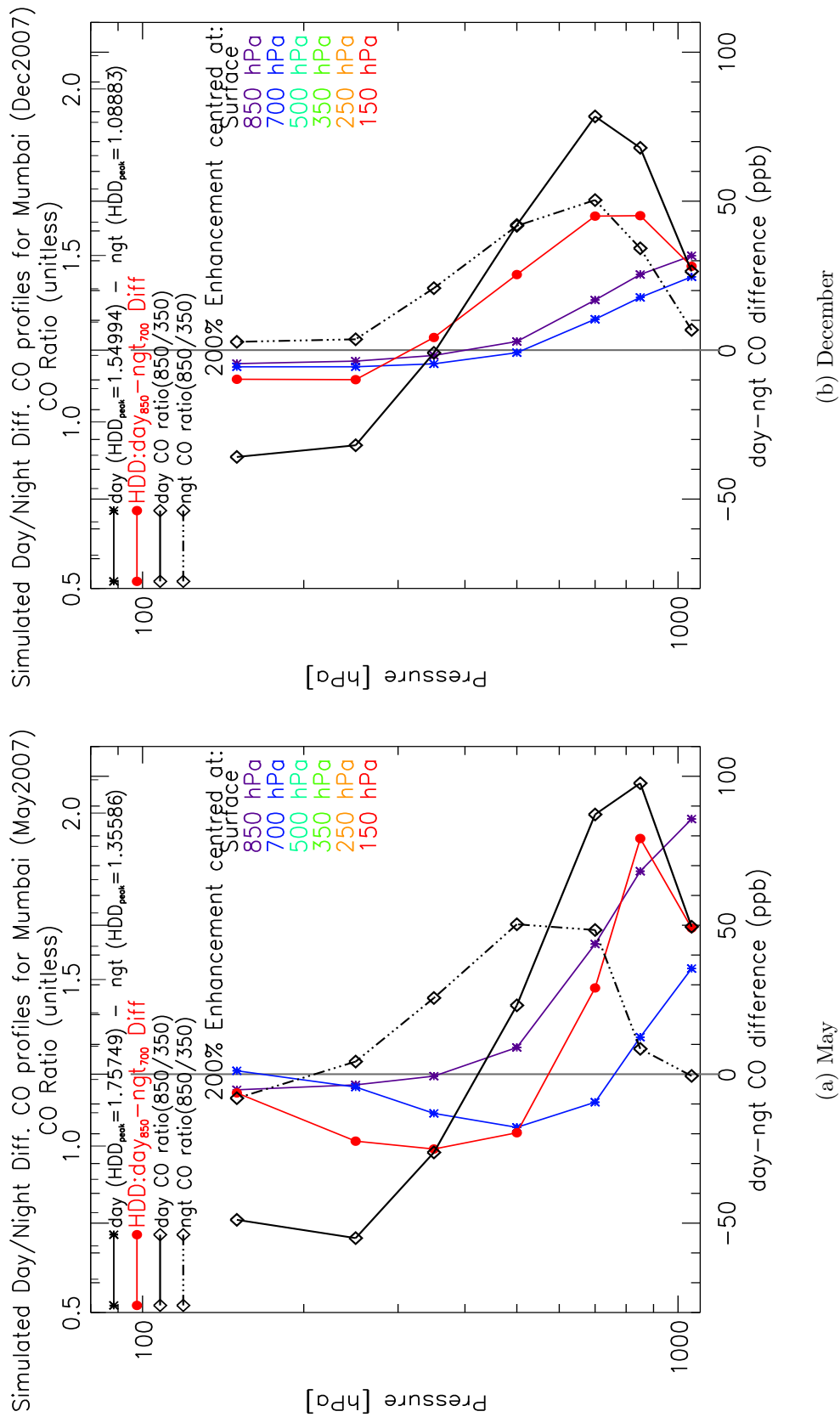


Figure 3.39: Key result from Fig. 3.38.

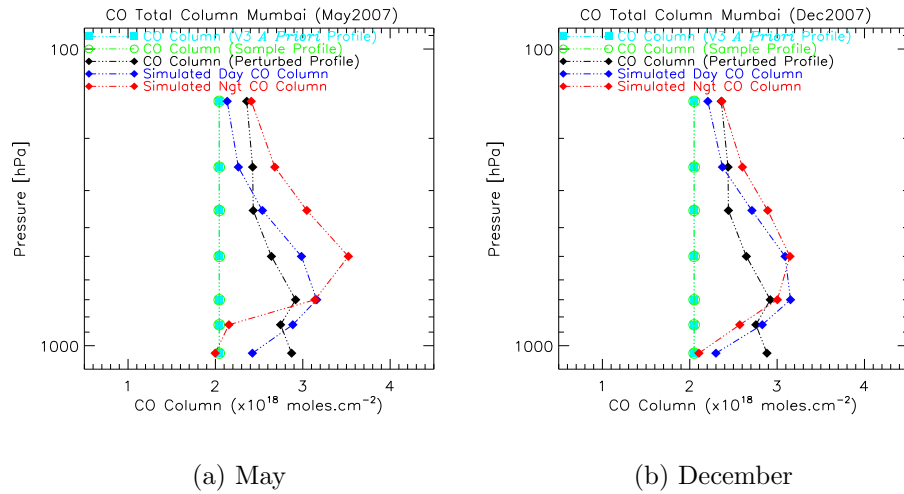


Figure 3.40: MOPITT L2V3 calculated total column values for i) a priori CO profile (cyan), ii) 7 individual sample profiles (green), iii) 7 individual perturbed sample profile (black), and iv) 7 individual simulated day (blue) and night (red) CO profiles, over Mumbai, for May 2007; (b) Same as (a) except for December 2007. Note that these are not considered as profiles. For proper understanding the total column values plotted at corresponding perturbed retrieval level (layer) for corresponding perturbed or simulated profile.

Figure 3.40 shows calculated total column values for corresponding each CO profile in the month of May and December. Similar, slightly reduced, values obtained in the month of December. In general, these results are consistent with the earlier findings. Additional total column tests also show more or less similar results (Fig. 3.41), particularly showing that MOPITT has great sensitivity to the CO in the boundary layer during both winter and summer depending mostly on thermal contrast conditions and boundary layer height.

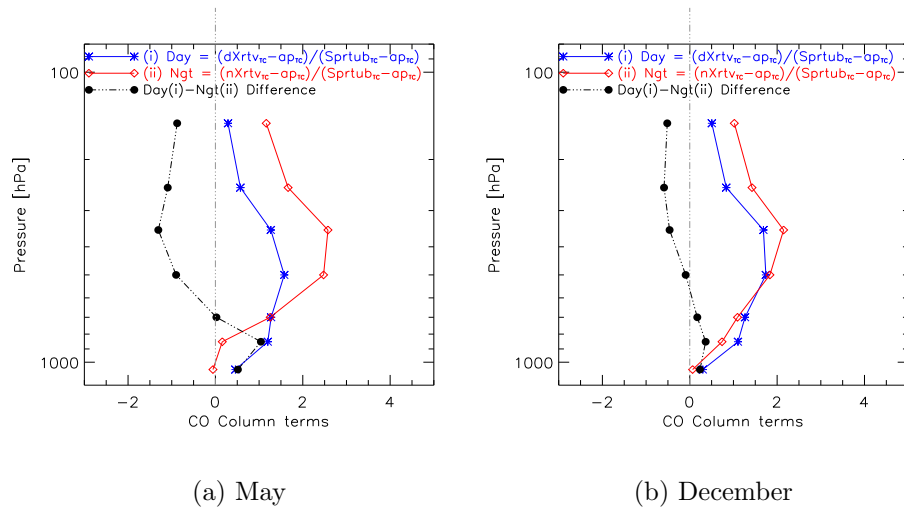


Figure 3.41: MOPITT L2V3 calculated total column tests for day and night simulated profiles in the month of (a) May and (b) December.

3.4.4.3 TOMCAT Model CO Profile Simulation

In this section, MOPITT L2V3 simulation for chosen TOMCAT model CO profile, in this region, has been performed similar to earlier case studies to support our methodology and precise understanding about CO in the troposphere. A profile over Mumbai box was selected to represent a case where our analysis suggesting the location of elevated CO source region in the month of May and December. The profiles were taken on the 3rd of May 2004 and 22nd of December 2004, located at 18.09°N latitude and 73.93°E longitude.

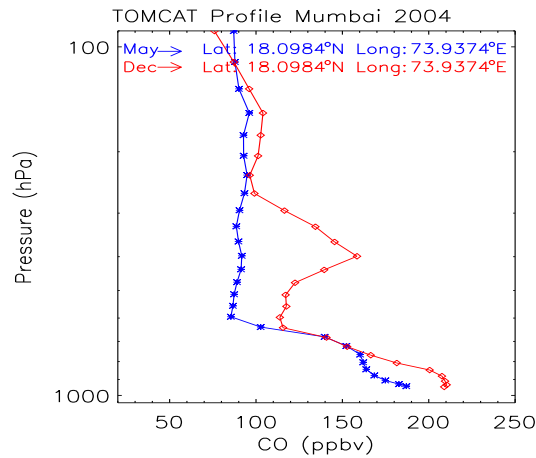
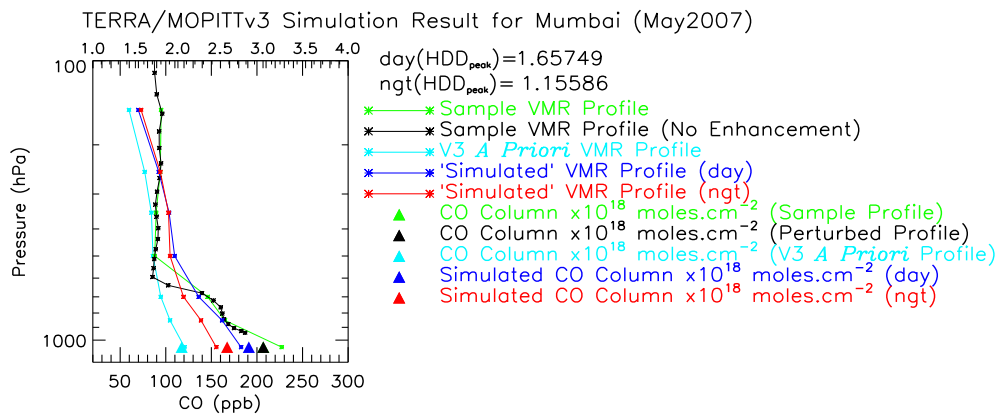
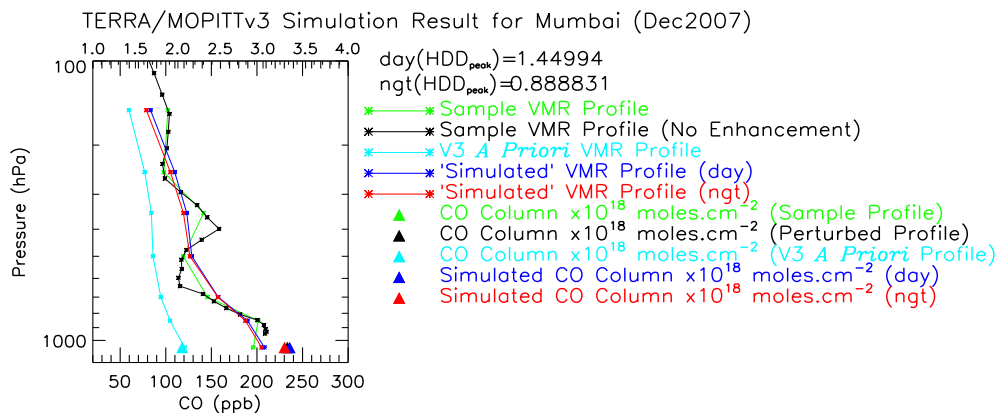


Figure 3.42: Selected TOMCAT model CO profiles, over Mumbai box, for May 2004 (blue) and December 2004 (red) for the given latitude and longitude co-ordinate.

Figure 3.42 show selected TOMCAT model CO profiles, over Mumbai region, in the month of May and December for given latitude and longitudes shown on plot. These profiles are used as a sample profile with no enhancement applied to it for MOPITT L2V3 simulation. The selected ‘typical’ averaging kernels, in this region, are then applied to these profiles to simulate daytime and nighttime CO profiles and examine day-night CO differences for HDD_{peak} . This will be more realistic case study simulation as compared to a priori simulation to correctly assess the MOPITT sensitivity to the lowermost layer of the troposphere, in particularity in this region.



(a) May



(b) Dec

Figure 3.43: (a) ‘Simulated’ daytime and nighttime CO profiles for TOMCAT model selected base CO profile, over Mumbai, for May 2007; (b) Same as (a) except for December 2007.

The simulation results are illustrated in Fig. 3.43 for the month of May and

December 2007. It is obvious that daytime ‘simulated’ CO profile has significant enhancement for lower 4 retrieval pressure levels in the month of May compared to nighttime ‘simulated’ CO profile and there are almost similar enhancements in both the daytime and nighttime ‘simulated’ CO profiles in the month of December. This, in turn, possibly suggesting that enormous amount of CO in the lowermost layer and a layer above it offers indistinguishable sensitivity to the tropospheric column for the MOPITT daytime and nighttime observations. These result does indeed provide useful profile shape information in the MOPITT retrieved CO profile.

Figure 3.44 illustrates ‘simulated’ day-night difference CO profile for assumed TOMCAT model CO profile in this simulation. It is obvious that these results are similar to earlier findings except for the month of December. It is clearly evident that day-night differences are positive, though not significant compared to May month, for the lowermost layer and upper troposphere, depicting apparent vertical differentiation of CO in the troposphere and usefulness of this methodology to better resolve CO into layers. This strongly leads to conclusion that MOPITT indeed has greatest sensitivity, plausibly, to enhanced layers of CO.

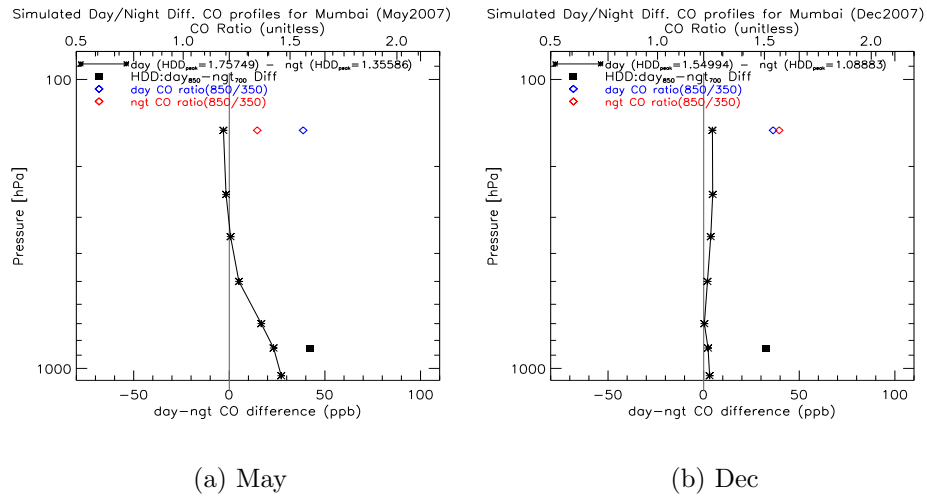


Figure 3.44: (a) MOPITT L2V3 ‘simulated’ day-night difference CO profile for HDD_{peak} , over Mumbai, for May 2007; (b) Same as (a) except for December 2007.

3.4.5 L2V3 Profile Simulation - A Case Study of Coimbatore

As pointed earlier, we find more extensive CO pollution loading in the Southern tip of India (i.e. Coimbatore), small enhancements in NO_2 are observed in this region supporting our day-night difference analysis. To develop superior understanding in our day-night difference analysis and robust methodology to examine MOPITT sensitivity to CO in the layers, in particular for Indian region, we perform simulation for this region as well. Coimbatore region spans in the latitude range from 10.5°N to 13.0°N and longitude range from 76.0°E to 78.5°E .

3.4.5.1 Mean L2V3 CO Profile

For Coimbatore region, MOPITT L2V3 retrieved daytime and nighttime DOFS histogram has two distinct distributions (refer to Appendix-I Fig. 7.1). Note that for the nighttime data, DOFS distribution has two close sharp peaks which are not clearly visible in this style plot. The retrieved mean daytime and nighttime mean CO profiles, over Coimbatore region, for May and December months are shown in Fig. 3.45. The retrieved mean CO profiles for LDD and HDD have similar features as observed for case study region (i.e. Bihar) in the month of May. It should be noted that the $\text{day}_{HDD}\text{-ngt}_{HDD}$ and $\text{day}_{HDD}\text{-ngt}_{LDD}$ sets have less enhancements in the lowermost layer except at surface compared to other two sets of LDD and HDD combination.

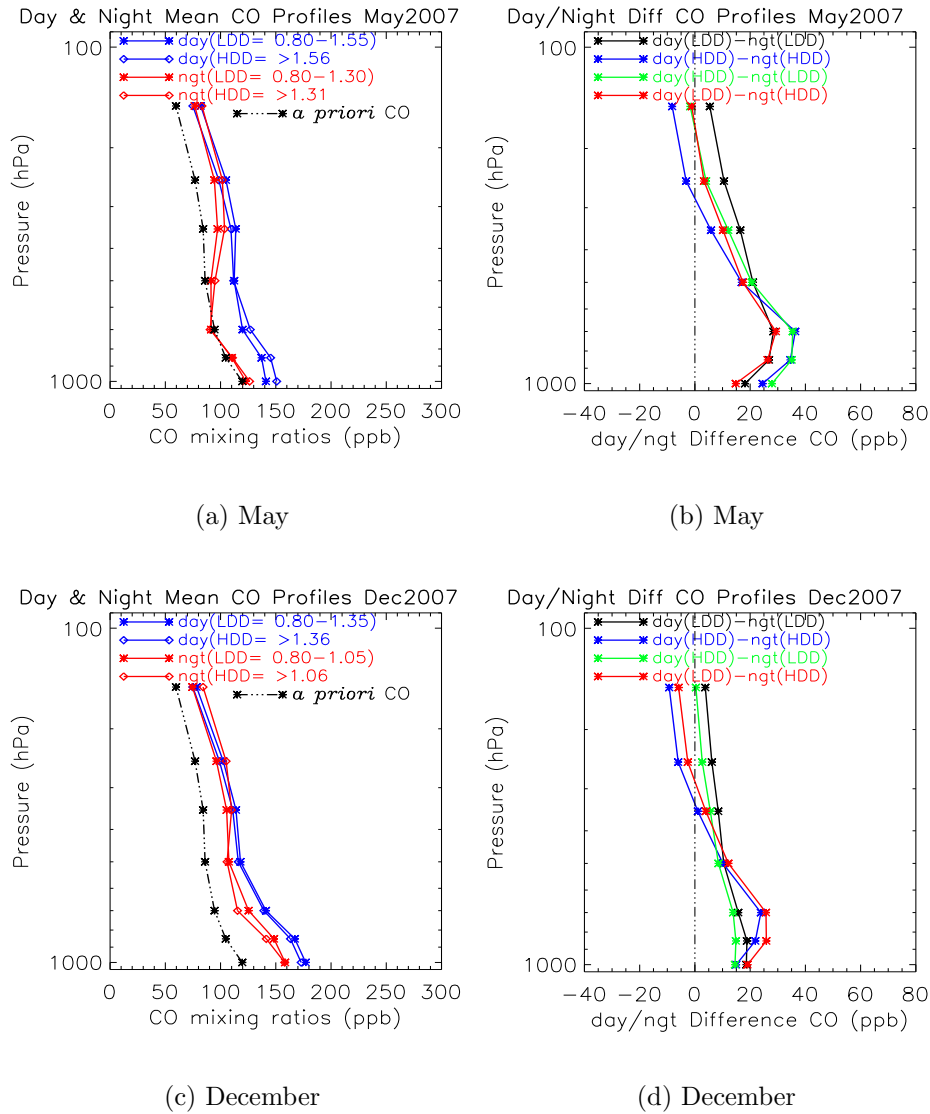


Figure 3.45: (a) MOPITT L2V3 retrieved mean daytime and nighttime CO profiles, over Coimbatore box, for May 2007; (b) Mean day-night difference CO profile, over Coimbatore box, for combination of LDD and HDD; (c) Same as (a) except for December 2007; (d) Same as (b) except for December 2007.

3.4.5.2 L2V3 Simulation

The MOPITT L2V3 CO ‘typical’ averaging kernels selected for in this region are shown in Fig. 3.46. First, the MOPITT L2V3 a priori CO profile taken as sample profile and then an enhancement of 200% was applied at each retrieval pressure level to simulate daytime and nighttime CO profiles using selected ‘typical’ averaging kernels.

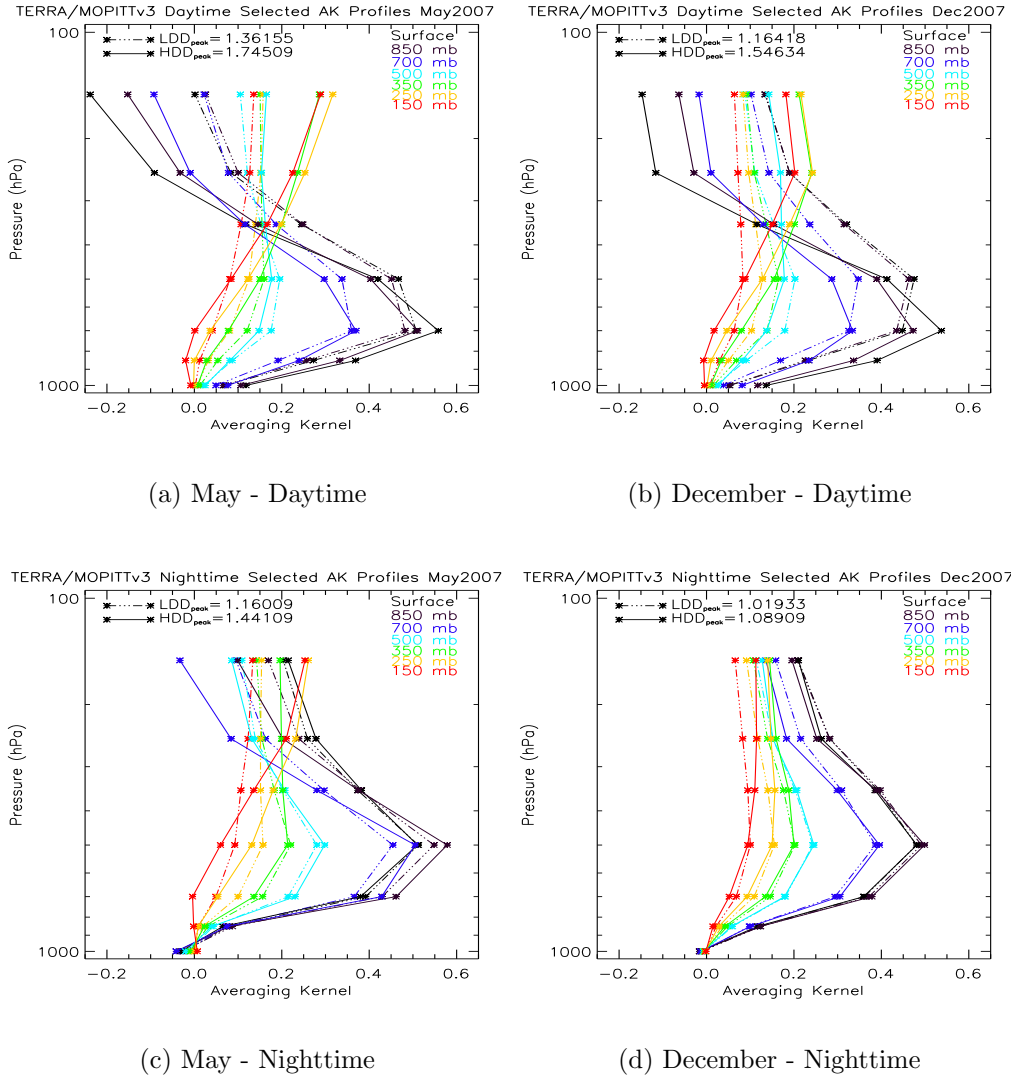
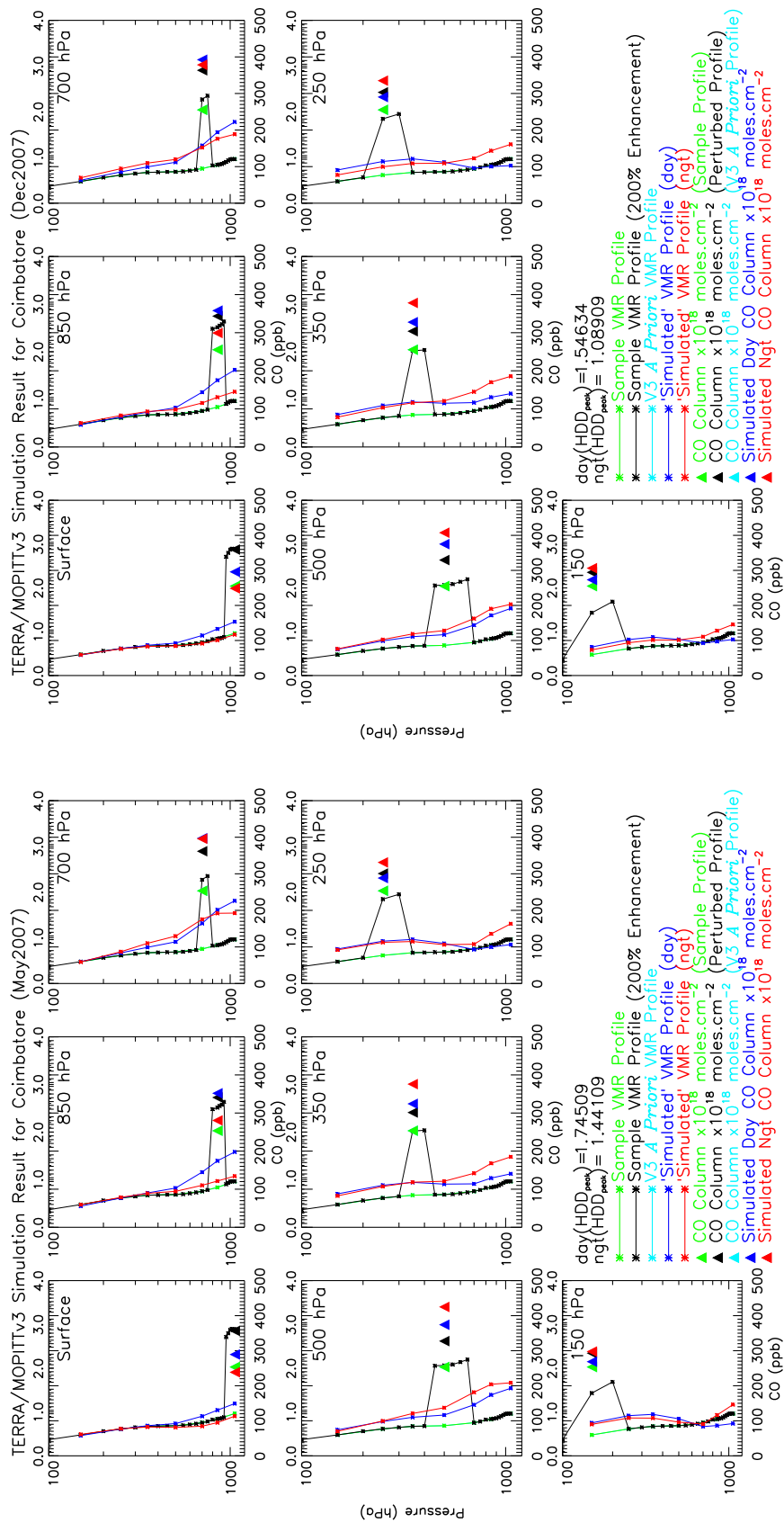


Figure 3.46: (a) MOPITT L2V3 Selected daytime ‘typical’ AK profile, over Coimbatore box, for May 2007; (b) Same as (a) except for December 2007; (c) Selected nighttime ‘typical’ AK profile, over Coimbatore box, for May 2007; (d) Same as (c) except for December 2007.

The simulation results are shown in Fig. 3.47. The coloured triangles indicates the calculated total column values for each CO profile used in this simulation and also for ‘simulated’ daytime and nighttime CO profiles. The simulation results are very similar to as observed in Bihar region as expected. For this region, the MOPITT is able to make observations with greatest sensitivity at 700 hPa retrieval level and one can possibly differentiate CO into layers. From this analysis and earlier findings, we believe that our simulation methodology works well for Indian region.



(a) May

(b) December

Figure 3.47: (a) MOPITT L2V3 ‘simulated’ daytime and nighttime CO profiles for HDD_{peak} over Coimbatore, for May 2007; (b) Same as (a) except for December 2007. The green (black, cyan, blue, and red) line indicates the considered sample CO profile (perturbed CO profile, a priori CO profile, ‘simulated’ day CO profile, and ‘simulated’ night CO profile). The green (black, cyan, blue, and red) triangles show calculated total column values for considered sample profile (perturbed sample profile, a priori profile, ‘simulated’ daytime profile, and ‘simulated’ nighttime profile).

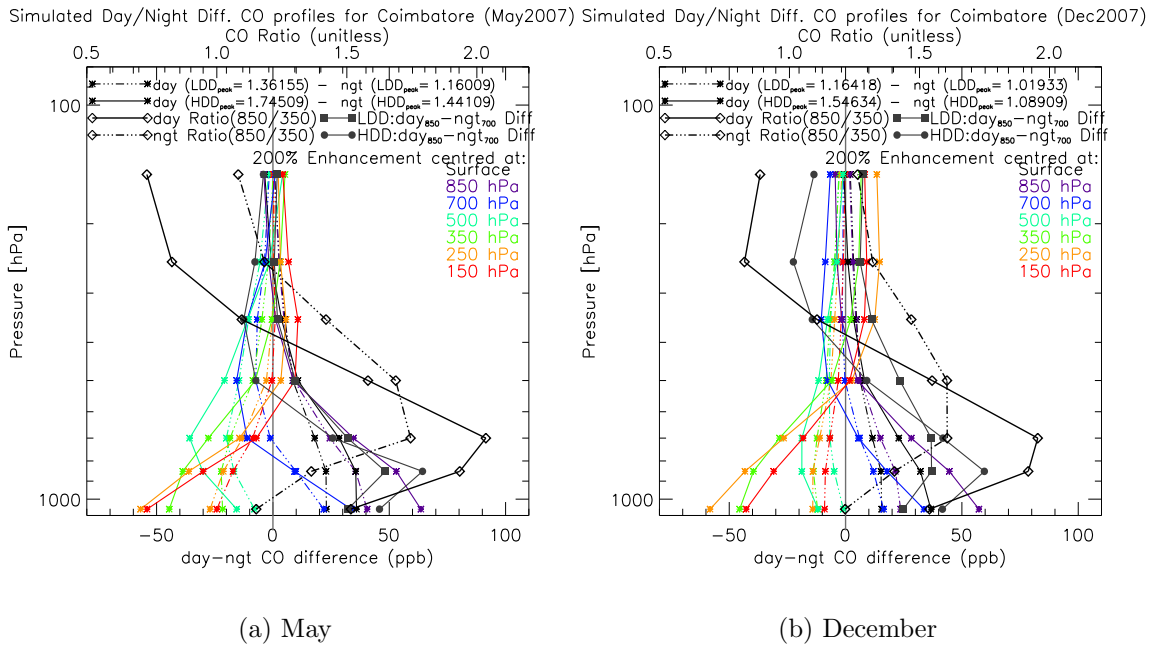


Figure 3.48: MOPITT L2V3 ‘simulated’ day-night difference CO profiles for LDD_{peak} and HDD_{peak} , over Coimbatore, for May 2007; (b) Same as (a) except for December 2007. The diamond symbol solid and dash-dotted lines indicates day and night CO ratio (850/350) term respectively. The ratio indicated by top x-axis. The dark grey coloured lines represents $day_{850}-night_{700}$ CO difference profiles for LDD_{peak} and HDD_{peak} . Note that the key result is depicted in Fig. 3.49.

Figure 3.48 (a, b) illustrates MOPITT L2V3 ‘simulated’ day-night difference CO profiles, over Coimbatore region, in the month of May and December 2007 respectively. The key result is depicted in Fig. 3.49

From Fig. 3.49, it is clearly evident that MOPITT has enhanced sensitivity to 700 hPa retrieval pressure level in this region as observed for case study region earlier (i.e. Bihar). The ‘simulated’ features in daytime and nighttime CO profiles in this region are very much similar to the case study region except that the CO ratio has sharp peak at 700 hPa retrieval level. It should be noted that the daytime and nighttime HDD_{peak} value in this region is slightly larger compared to the other Indian regions. One can, therefore, expect more sensitivity for MOPITT to CO observation in this region, which has good thermal contrast and high boundary layer height.

Simulated Day/Night Diff. CO profiles for Coimbatore (May2007) Simulated Day/Night Diff. CO profiles for Coimbatore (Dec2007)

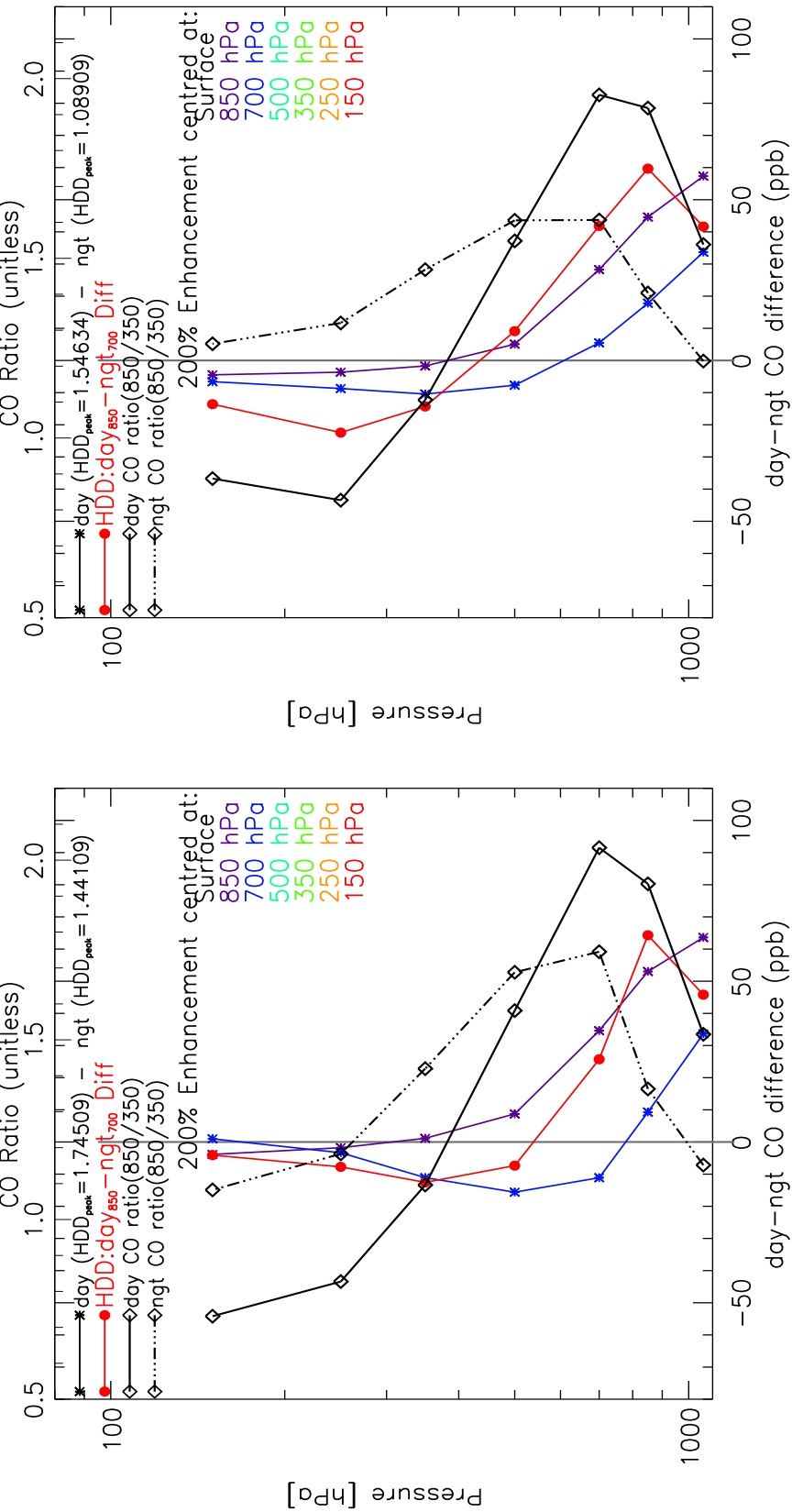


Figure 3.49: Key result from Fig. 3.48.

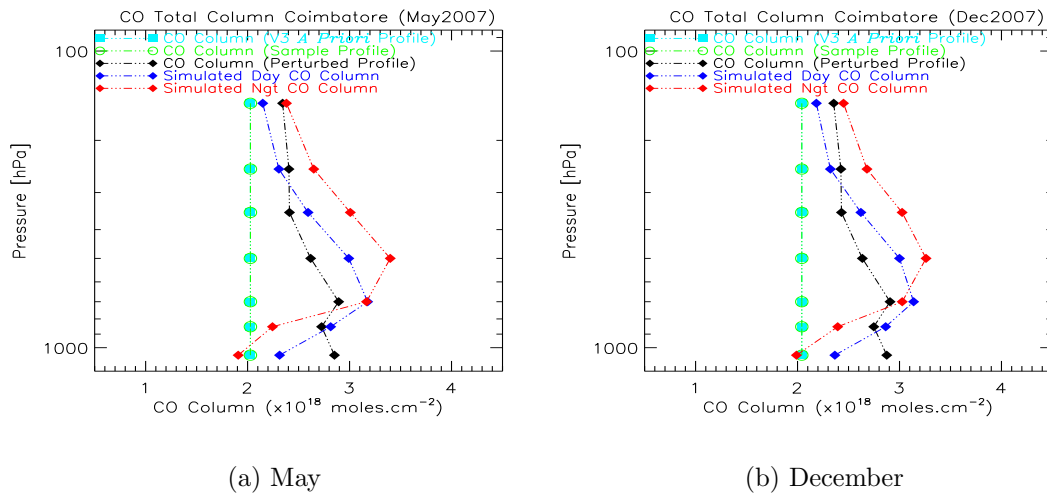


Figure 3.50: MOPITT L2V3 calculated total column values for i) a priori CO profile (cyan), ii) 7 individual sample profiles (green), iii) 7 individual perturbed sample profile (black), and iv) 7 individual simulated day (blue) and night (red) CO profiles, over Coimbatore, for May 2007; (b) Same as (a) except for December 2007.

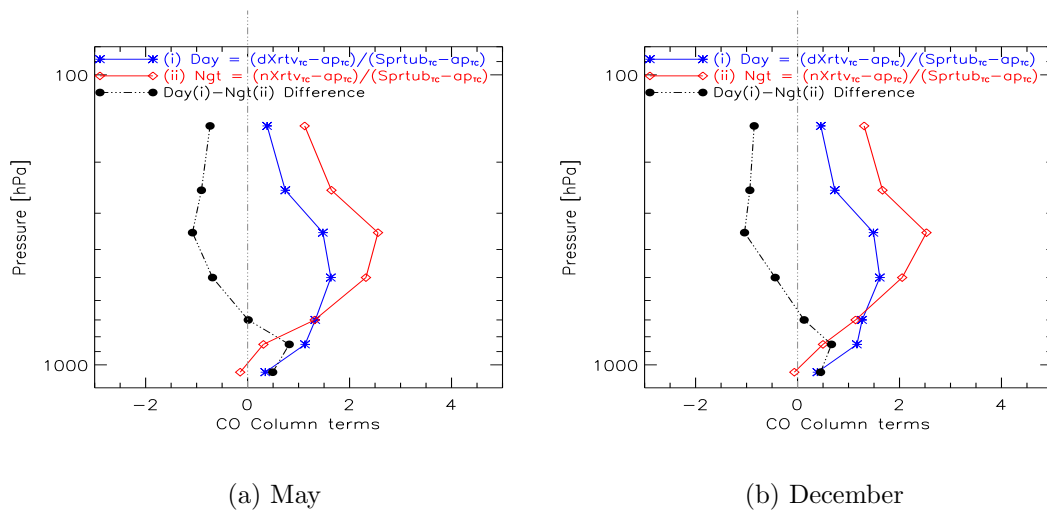


Figure 3.51: MOPITT L2V3 calculated total column tests for day and night simulated profiles in the month of (a) May and (b) December. Note that these are not considered as profiles and are in arbitrary unit.

Figure 3.50 and 3.51 illustrates total column tests performed in this region for May and December of 2007. These findings are very much consistent with our earlier results for other Indian regions with less significant differences.

3.4.5.3 TOMCAT Model CO Profile Simulation

For Coimbatore region, we have performed similar MOPITT L2V3 simulations for chosen TOMCAT model CO profile in this region as in case of other Indian regions. So far, our methodology seems to be working very well and it is expected to work other parts of world. A profile over Coimbatore region was selected to represent a case where our analysis suggesting the location of a CO source region in the month of May and December. The profiles were taken on the 10th of May 2004 and 21st of December 2004, located at 12.55°N latitude and 77.74°E longitude and at 11.26°N latitude and 76.93°E longitude.

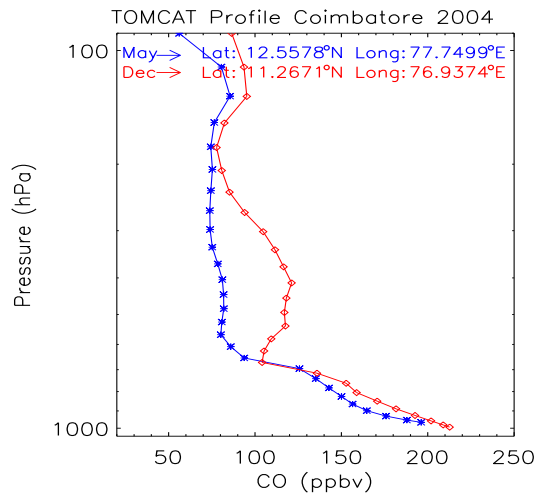
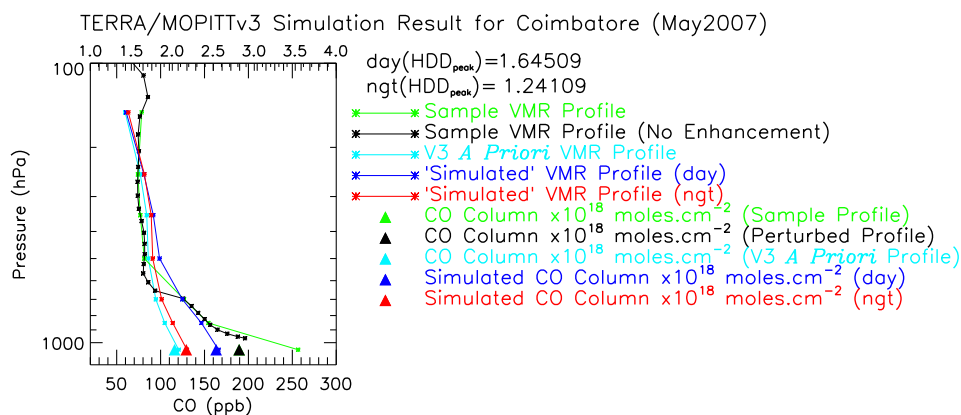


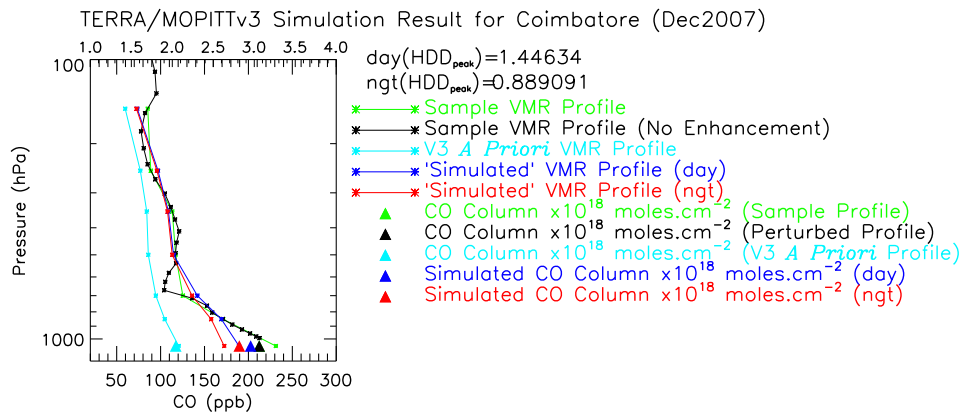
Figure 3.52: Show selected TOMCAT model CO profiles, over Coimbatore box, for May 2004 (blue) and December 2004 (red) for the given latitude and longitude coordinate.

Figure 3.52 show selected TOMCAT model CO profiles, over Coimbatore region, in the month of May and December of 2004. These profiles have then used as a sample profile with no enhancements applied to it to simulate daytime and nighttime CO profiles using selected ‘typical’ averaging kernels in this region for the month of May and December respectively. The simulations are performed for LDD_{peak} and HDD_{peak} and presented here only for HDD_{peak} . The simulation results are shown in Fig. 3.53.

As expected, these findings are consistent with our earlier analysis. These results does indeed convincing and provide useful profile shape information content in the MOPITT retrieved CO profile. Figure 3.54 illustrates ‘simulated’ day-night



(a) May



(b) December

Figure 3.53: ((a)MOPITT L2V3 'Simulated' daytime and nighttime CO profiles for TOMCAT model selected base CO profile, over Coimbatore, for May 2007; (b) Same as (a) except for December 2007.

difference CO profile in this region. It is again obvious that this results is consistent with preceding findings. In general, our findings for Indian region strongly suggests that the MOPITT has greatest sensitivity to CO in the boundary layer having large boundary layer height in this region.

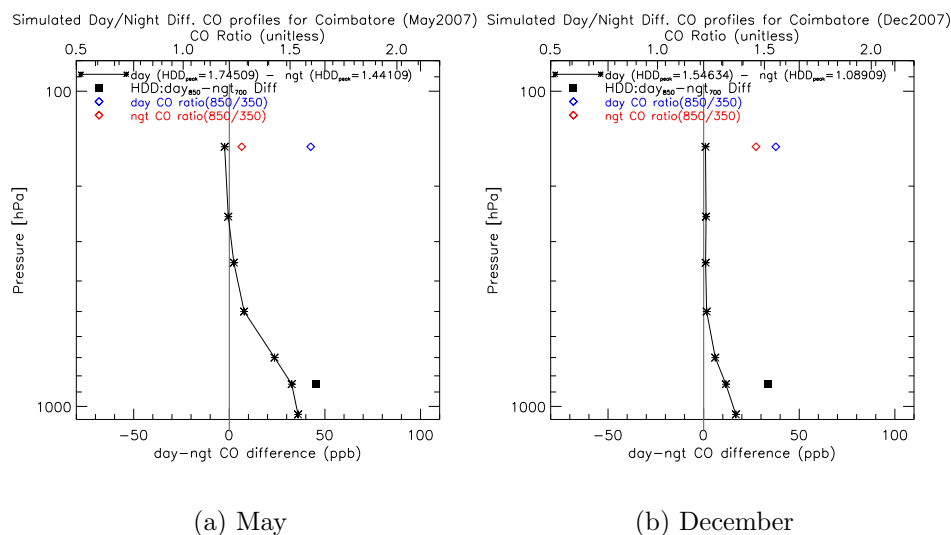


Figure 3.54: (a) MOPITT L2V3 ‘simulated’ day-night difference CO profile for HDD_{peak} , over Coimbatore, for May 2007; (b) Same as (a) except for December 2007.

We now have proficiency in our methodology to assess MOPITT sensitivity to the lower troposphere, particularly for Indian region. In fact, this methodology is adopted in chapter 4 to perform comparison between MOPITT L2V3 and L2V4 data for selected Indian regions together with several other regions across the world. Our prior analysis and simulation studies have shown that day-night difference could give a more sensitive indicator to the monthly averaged component of lower atmosphere enhancements. Further, our simulation studies have shown that 700 hPa day-night difference is clearly superior, for chosen boxes over Indian region, to $day_{850}-ngt_{700}$ and (850/350) CO ratio in demonstrating lowermost tropospheric enhancements. It would be interesting to look at spatial structure of CO distribution at 700 hPa retrieval pressure level together with day-night differences at this level. The results are presented and discussed in the following section.

3.5 CO Over Indian Subcontinent

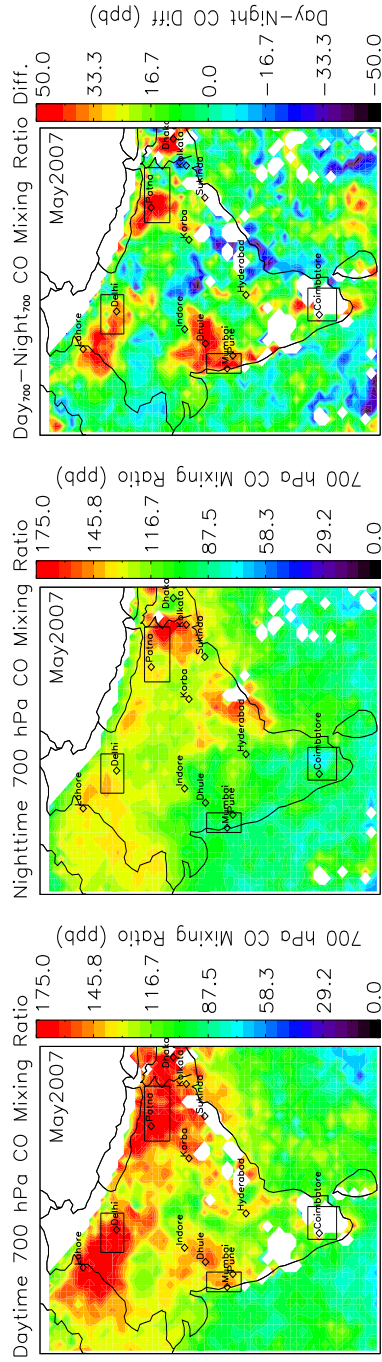
Here, we show that the daytime and nighttime MOPITT retrieved CO data at 700 hPa retrieval level can provide foremost information on surface sources of atmospheric CO over the Indian subcontinent. From our simulation studies, we find that MOPITT has great sensitivity to 700 hPa level, as one can demonstrated by looking at ‘simulated’ day-night differences. Our selected ‘typical’ averaging kernels indeed indicate that the MOPITT retrievals are sensitive to CO in the lowermost layer of the troposphere. Furthermore, these simulation results are consistent for all chosen boxes over Indian region, demonstrating that the MOPITT L2V3 retrievals do have sensitivity to the CO in the boundary layer. Similarly, we also find considerable utility to additional diagnostics used e.g. CO ratio, total column calculation and ‘simulated’ day-night column differences. The CO ratio quantity is the ratio of retrieved CO at 850 hPa to 350 hPa retrieval level. Using this knowledge, we believe that MOPITT retrievals day-night CO differences at 700 hPa retrieval could provide truthful information on surface sources of CO, in particularly for Indian region.

3.5.1 Spatial Distribution of CO

It is shown in this section that the MOPITT retrievals day-night CO differences at 700 hPa retrieval level do indeed capture widespread surface source information on CO. Figure 3.55 (a, b, c) shows the daytime and nighttime distribution of MOPITT CO mixing ratios at 700 hPa as well as the resultant day-night differences over India for May respectively. The data drop outs in the CO distribution over the southern India are due to clouds contaminated pixel which are not considered in the L2V3 retrieval algorithm. Despite these data drop outs, strong spatial gradients can be seen in the CO distribution. In particular, there are several areas of localised enhancements in the daytime 700 hPa CO map which are in fair agreement with the daytime 850 hPa CO map (refer to 3.13(a)). It should be noted day-night difference 700 hPa CO indeed confirming likely surface sources of CO in this region, which can be related to large point sources e.g. megacity or industrial sectors. Figure 3.55 (d, e, f) shows the daytime and nighttime distribution of MOPITT CO mixing ratios at 700 hPa and the resultant day-night differences over India for December respectively. The data drop outs in the CO distribution over Indo-Gangetic basin the southern India are

due to the intense haze and foggy conditions that develop each winter over this area [Tripathi et al., 2006; Gautam et al., 2007] that might be affecting the CO retrievals. Regardless of low thermal contrast conditions during winter months, using MOPITT retrievals 700 hPa day-night difference map, it is still possible to mark out localised enhancements over Indian region which can not be possible using daytime data alone. Our analysis, thus, strongly suggests utility to 700 hPa day-night differences to mark out surface sources of atmospheric CO.

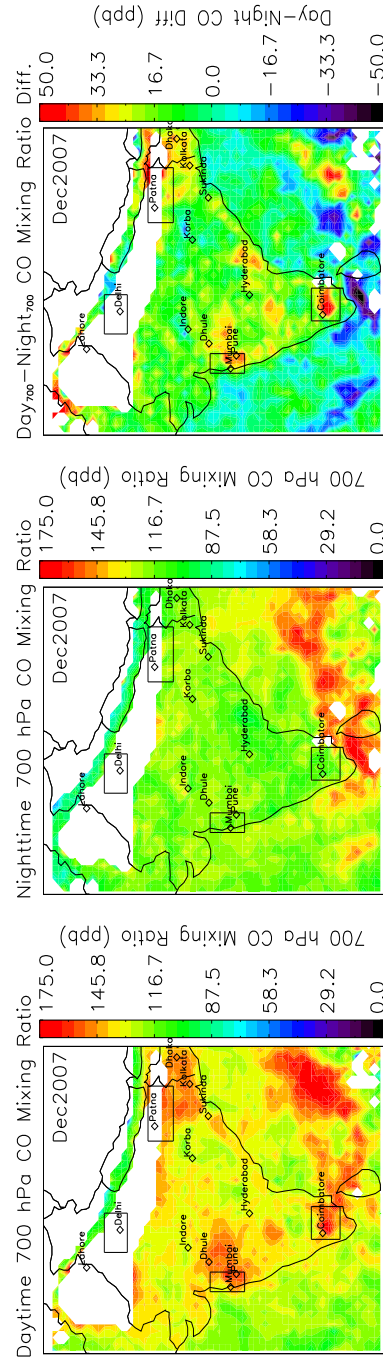
Recent studies by Deeter et al. [2004] and Kar et al. [2004] have used ratio of CO mixing ratio at 350 and 850 hPa levels (i.e. 350/850) as an useful index for convection. Whereas, the reverse ratio of CO mixing ratio at 850 and 350 hPa levels (i.e. 850/350) is likely to provide useful information about CO in the lower tropospheric layer (0–3 km). This ratio indeed sharpen features captured by 850 hPa day-night difference CO and day-night CO columns data. Additional diagnostic such as the difference between day 850 hPa and night 700 hpa (i.e. $\text{day}_{850}\text{-night}_{700}$) CO mixing ratios could be used and one can see that it is indeed convincing to mark out strong elevated near surface CO concentrations in Fig. 3.56. As demonstrated from MOPITT retrieved averaging kernels, the MOPITT measurements has no or very little sensitivity to 850 hPa during nighttime measurements and it is mostly dependent thermal contrast between the lower atmosphere and underlying surface. Whereas, the MOPITT has great sensitivity at 700 hPa retrieval level for nighttime measurements, thus $\text{day}_{850}\text{-night}_{700}$ would probably offer best picture of persistent CO in the planetary boundary layer. Our $\text{day}_{850}\text{-night}_{700}$ is likely to be superior in this region to 850/350 ratio in demonstrating lowermost CO enhancements.



(a) Day CO - May

(b) Night CO - May

(c) Day-Night diff - May



(d) Day CO - Dec

(e) Night CO - Dec

(f) Day-Night diff - Dec

Figure 3.55: (a) MOPITT L2V3 0.5 degree gridded daytime 700 hPa CO mixing ratios, over India, for May 2007; (b) MOPITT L2V3 0.5 degree gridded nighttime 700 hPa CO mixing ratios, over India, for May 2007; (c) MOPITT L2V3 0.5 degree gridded 700 hPa day-night CO mixing ratio differences, over India, for May 2007; (d) Same as (a) except for December 2007; (e) Same as (b) except for December 2007; (f) Same as (c) except for December 2007.

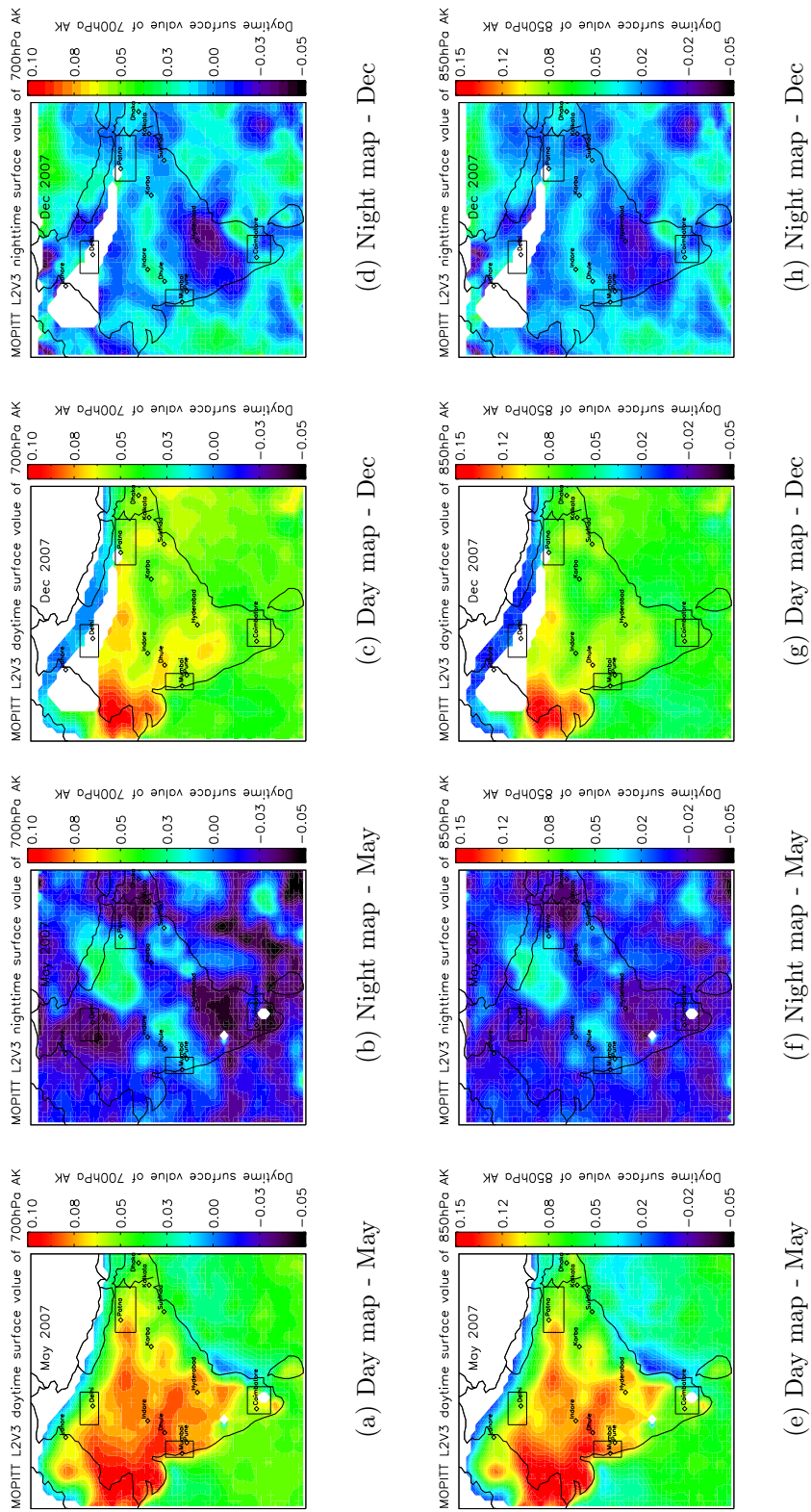


Figure 3.57: Top panel: show spatial distribution of the (a) daytime and (b) nighttime surface value of the MOPITT L2V3 700 hPa averaging kernel for May 2007; (c) and (d) same as (a) and (b) respec. except for December 2007. Bottom panel: (e) and (f) same as (a) and (b) respec. except for surface value of the 850 hPa averaging kernel; (g) and (h) same as (c) and (d) respec. except for surface value of the 850 hPa averaging kernel.

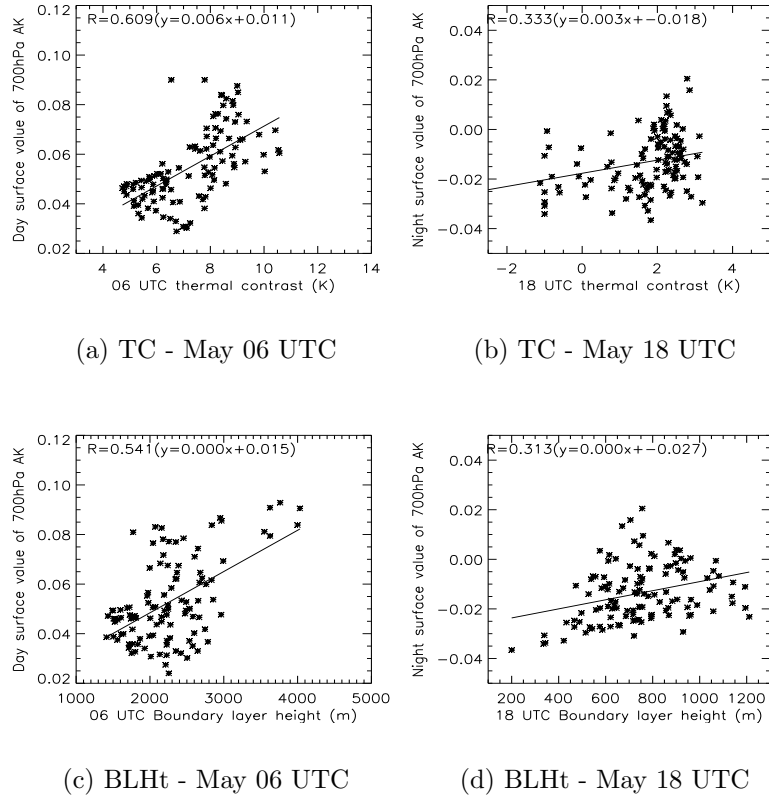


Figure 3.58: (a) and (b) show correlation plots between the thermal contrast and surface value of 700 hPa averaging kernels in May 2007 for 06 UTC and 18 UTC respectively; (c) and (d) show correlation plots between the boundary layer height and surface value of 700 hPa averaging kernels in May 2007 for 06 UTC and 18 UTC respectively. Note TC refer to thermal contrast and BLHt refer to boundary layer height.

Figure 3.58 shows scatter plot for the thermal contrast and boundary layer height with surface value of 700 hPa averaging kernels in May 2007. It clearly shows the superior correlation of daytime surface value of 700 hPa averaging kernel with thermal contrast than the boundary layer height. Since the surface value of 700 hPa and 850 hPa averaging kernels show similar variations, one can expect same correlation of surface value of 850 hPa averaging kernel with thermal contrast in daytime.

3.5.2 Correlation Results

Here, we perform correlation between the daytime and nighttime MOPITT L2V3 retrievals together with day-night differences in CO mixing ratios and total column

amounts. Figure 3.59 and 3.60 show correlation results, over Indian subcontinent, for May and December respectively. It has to be noted that the correlation results are significantly better in respect to earlier results. For example, the correlation between 850 hPa daytime CO data and 850 hPa day-night difference CO data has correlation coefficient 0.67 (refer to Fig. 3.15) whereas the correlation between 700 hPa daytime CO data and 700 hPa day-night difference CO data has correlation coefficient of 0.85. Similarly, for total column data, one can see utility to day-night CO total column differences. These results indeed present evidence that MOPITT retrievals have utility to day-night difference analysis in this region, providing useful information on surface emissions of CO.

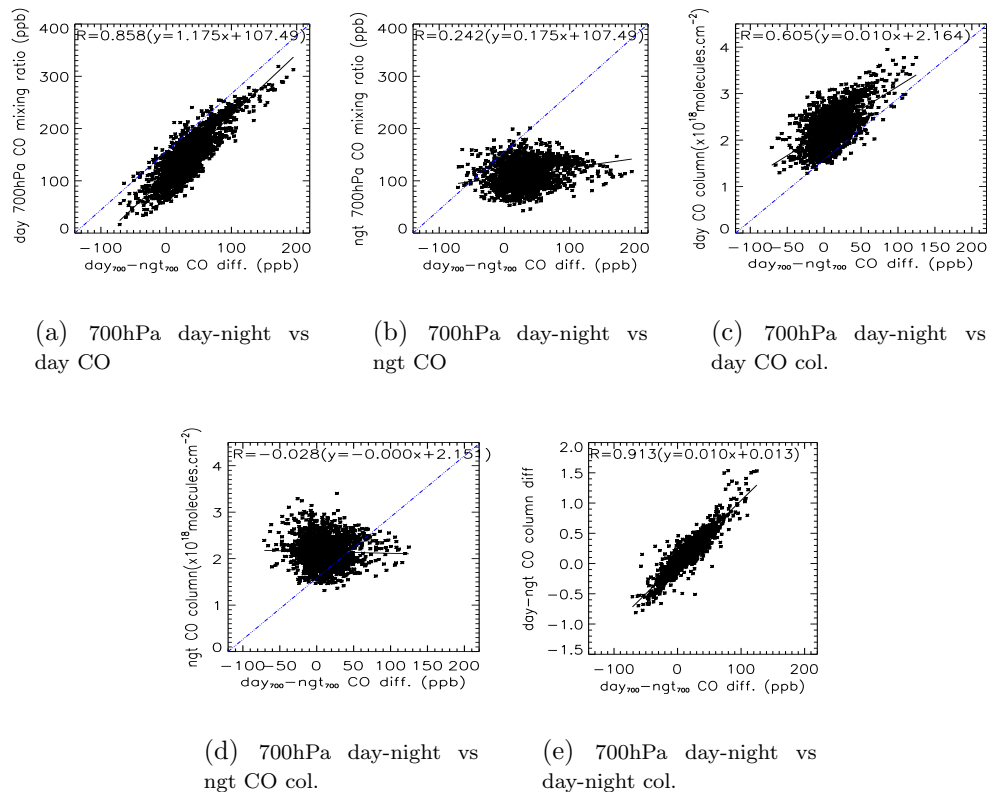


Figure 3.59: Correlation results, over India, in the month of May 2007.

MOPITT L2V3 data is retrieved on 7 vertical pressure levels although these are highly correlated. Thus, one can expect a good correlation between the retrieved CO on individual retrieval levels. However, for example 850 hPa and 350 hPa levels are selected to calculate CO ratio(850/350) because their averaging kernels are usually distinctly different, as observed in Fig. 3.11, and because their ratio provides a simple

index for the overall shape of the retrieved profile. Likewise, the term $\text{day}_{850}\text{-ngt}_{700}$ CO difference is probably the best utility to understand MOPITT sensitivity to the lower troposphere including planetary boundary layer. Figure 3.61 shows correlation between the $\text{day}_{850}\text{-ngt}_{700}$ differences and CO ratio term for May and December.

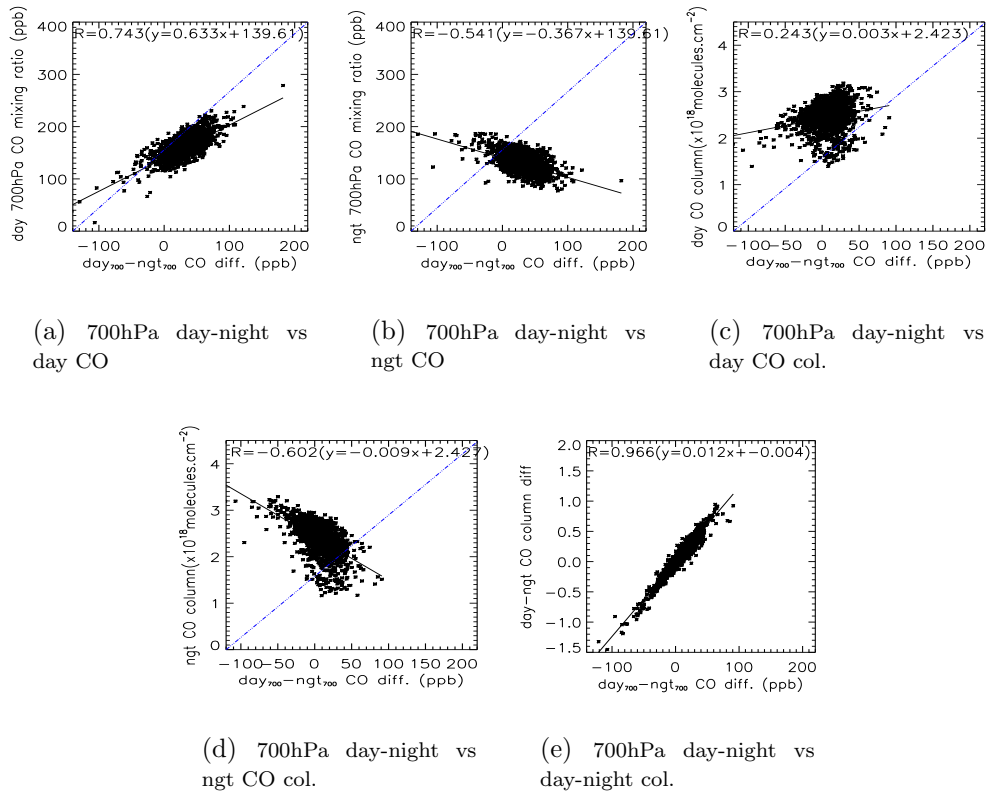


Figure 3.60: Correlation results, over India, in the month of Dec 2007.

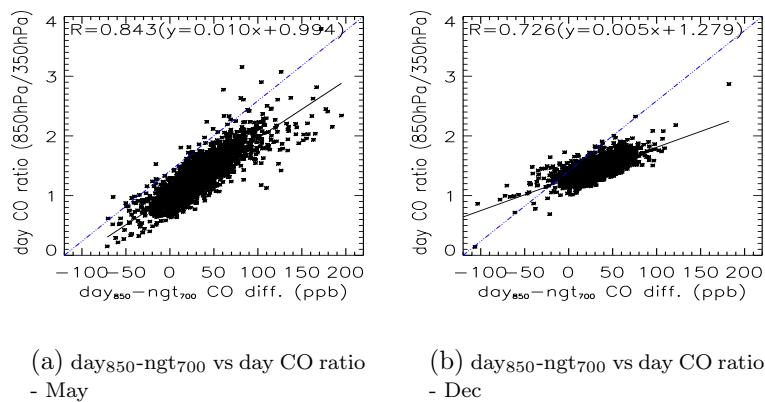


Figure 3.61: Correlation results, over India, in the month of May 2007.

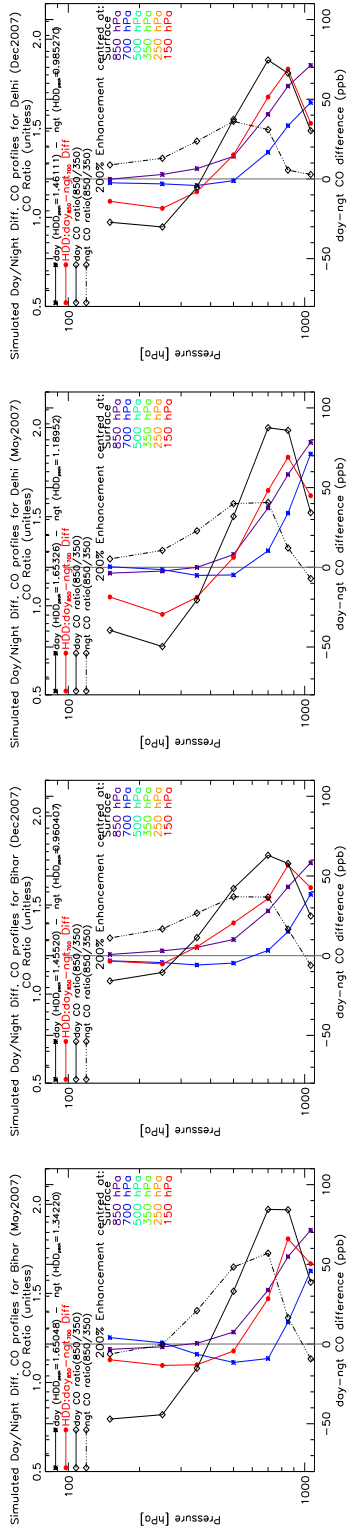
For India, our analysis thus confirms the pollution detected over the extremes of the IG basin [e.g., Kar et al., 2008]. We also find reasonably extensive CO pollution loading in the west coast and Southern tip of India, small enhancements in NO₂ are also observed in these regions supporting this analysis. In general, MOPITT retrievals are nominally most sensitive to the mid and upper troposphere although our data analysis and simulation studies indeed confirms that the sensitivity to the lower troposphere is also present in the MOPITT retrievals. Our robust methodology works well for Indian region and provides useful information about CO in the lowermost layer of the troposphere in this region. To develop foremost understanding, we further use our methodology to perform MOPITT L2V4 simulations and compare with MOPITT L2V3 simulations for Indian subcontinent.

3.6 Evaluation of a Robust Methodology

In this thesis, a robust methodology is developed to detect places where MOPITT would have largest sensitivity to the lowermost layer, and hence could detect elevated boundary layer CO pollution (e.g. urban centres or megacities). However, this methodology could be, in part, in error as it involves numerous parameters, such as CO concentration, surface-atmosphere thermal contrast, atmospheric temperature and surface emissivity and the relationship between them. The possible error sources in day-night difference are illustrated below,

- The estimated random error for the MOPITT L2V3 retrieval is about 10% standard deviation, with regional biases of a few parts per billion (ppb) [Emmons et al., 2004]. The random error on daytime retrievals in a monthly grid box will decrease because of averaging a large no of profiles. There will also be an increased uncertainty on the daytime value related to changing CO in this time in the vertical profile above the city (or region of interest) due to transport of CO from elsewhere which is further dependent on the magnitude and direction of wind. The same effects can be observed for the nighttime. Thus, by subtracting nighttime data from the daytime one possibly eliminate a considerable amount of random error part on day-night quantity and also the mean transport component. There will however be a residual error due to variations in sampling of transport between daytime and nighttime monthly averages.

- Improving the accuracy of MOPITT simulations will require better characterization of systematic errors in the observations. Although there is evidence of some systematic errors in the MOPITT retrievals [Emmons et al., 2009], there is not much discussion for systematic error in literature. The low sensitivity of the MOPITT instrument to the lowermost layer of the atmosphere combined with the presence of systematic errors in the retrievals could produce error in the day-night difference.
- There is also a sampling error potentially due to the number of days for which CO is sampled at the location in a month. This is difficult to estimate because it depends on the sampling times and the variability of CO in the lower atmosphere. Because of the variable nature of the transport and sampling terms, there are highly dependent on the location and so a generalised total error cannot be computed.
- The robust methodology developed here illustrates a way to select ‘typical’ averaging kernel for given set of atmospheric and surface properties rather than averaging of the averaging kernels. An attempt to examine whether selecting ‘typical’ averaging kernel produces error in day-night difference has been undertaken. A simulation methodology discussed earlier in this thesis is used to simulate day-night difference profiles using L2V3 a priori profile and mean averaging kernel profile (mean calculated by averaging all averaging kernel profiles without filtering for DOFS) and compared with simulations performed using ‘typical’ averaging kernel as shown in Fig. 3.62. For example, from Fig. 3.62(c), the simulated day-night differences using mean averaging kernel are +80 ppbv whereas the simulated day-night differences using ‘typical’ averaging kernel are +70 ppbv. This means that using mean averaging kernel possibly increases surface (lowermost layer) sensitivity but also increases the upper troposphere sensitivity and further would have more error on this quantity due to upper tropospheric errors due to changing CO over time. For the Indian subcontinent, the estimated error on this quantity could be about 10-20 % (one standard deviation). Note that this error is estimated as average of two simulated day-night differences.

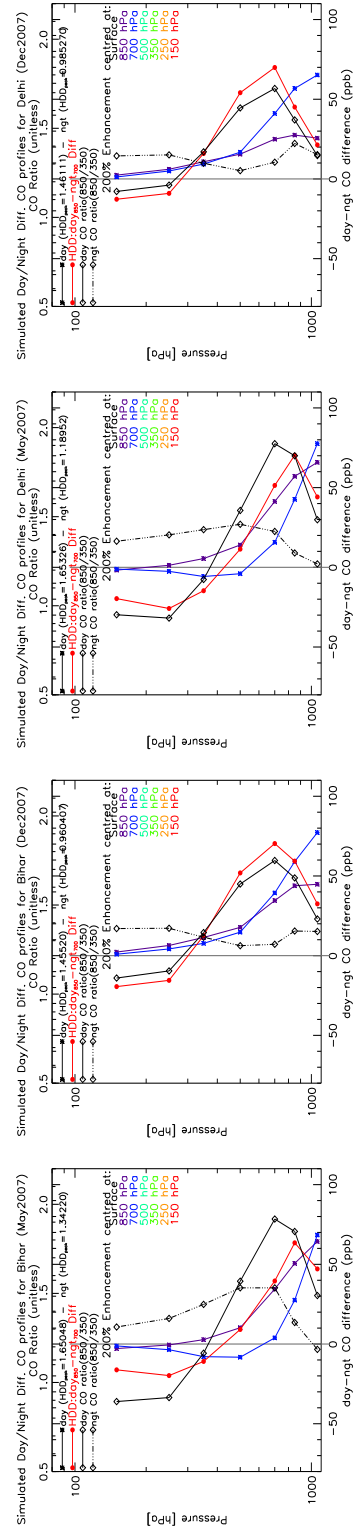


(a) Bihar - May

(b) Bihar - Dec

(c) Delhi - May

(d) Delhi - Dec



(e) Bihar - May

(f) Bihar - Dec

(g) Delhi - May

(h) Delhi - Dec

Figure 3.62: Top panel (a-d): MOPITT L2V3 ‘simulated’ using mean averaging kernel key day-night difference CO profiles for HDDpeak, over Bihar and Delhi, for May and December 2007; Bottom panel (e-h): Same as top panel except for ‘simulated’ using selected ‘typical’ averaging kernel.

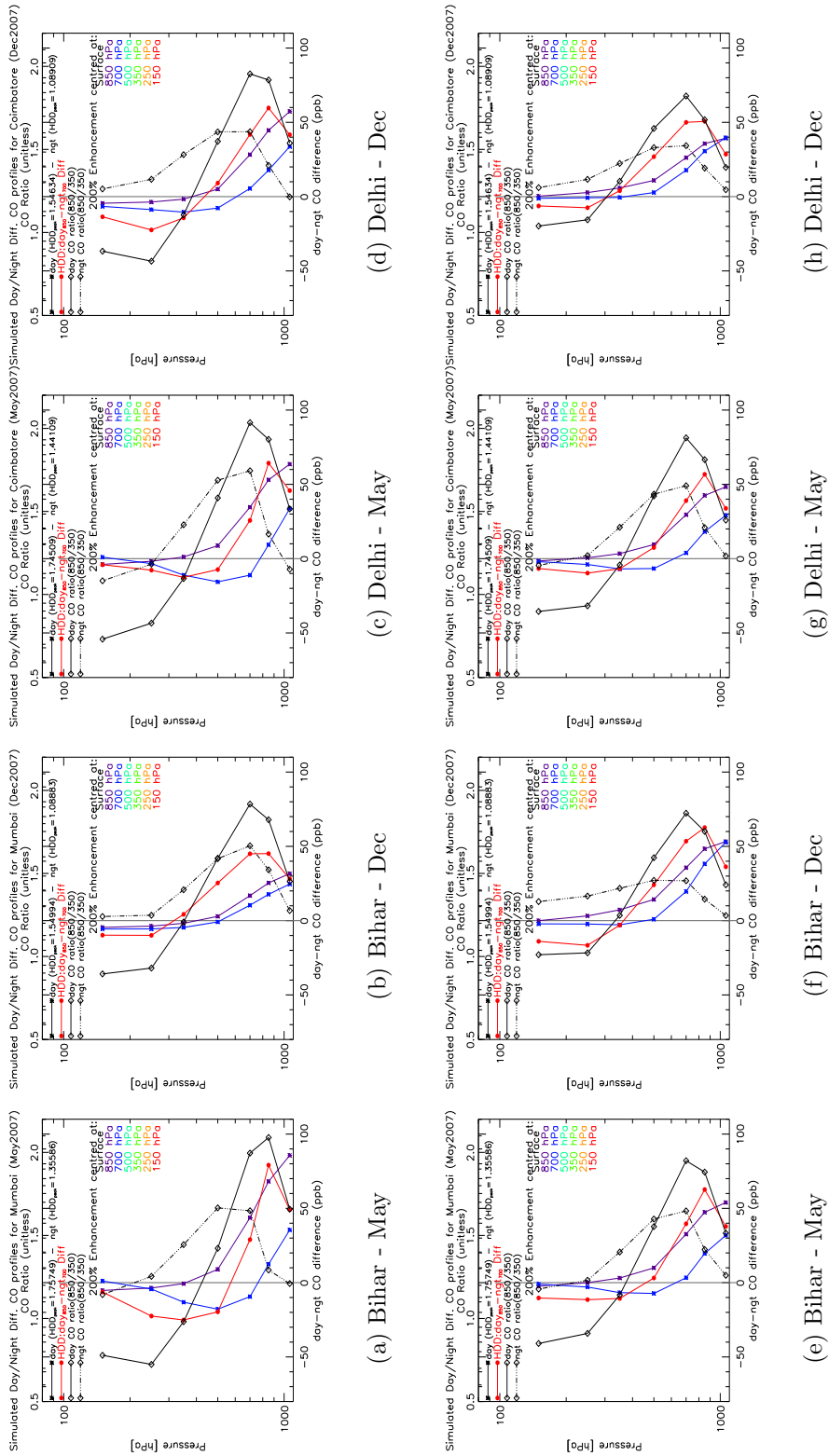


Figure 3.63: Top panel (a-d): MOPITT L2V3 ‘simulated’ using mean averaging kernel key day-night difference CO profiles for HDDpeak, over Mumbai and Coimbatore, for May and December 2007; Bottom panel (e-h): Same as top panel except for ‘simulated’ using selected ‘typical’ averaging kernel.

3.7 Summary of Chapter 3

The MOPITT sensitivity to CO in the lowermost layer of the troposphere varies widely as the result of variability in thermal contrast conditions and boundary layer height and in particular from day to night. This effect is clearly evident in the MOPITT retrieval averaging kernels. The thermal contrast condition plays a key role in determining whether or not MOPITT has sensitivity to the lower troposphere, and this parameter can vary greatly with location, time of the day and season of the year. Our analysis challenge the common conception that satellite instruments based on thermal-infrared observations are generally insensitive to the near-surface troposphere depends strongly on thermal contrast conditions.

A robust methodology developed to ‘simulate’ day-night difference CO profiles to better constrain CO in the lowermost layer of the troposphere. Simulations were performed using MOPITT L2V3 selected ‘typical’ averaging kernels to examine the ability of the instrument to identify CO enhancements with limited vertical extent. The simulation methodology works well for Indian subcontinent region, providing evidence that MOPITT instrument indeed is able to resolve CO into layer and one can obtain measurements of vertical structure of CO. For selected boxes over Indian subcontinent, it is shown that MOPITT retrievals have significant sensitivity to CO in the lowermost layer of the atmosphere. MOPITT retrieved averaging kernels have large variability, particularly in the upper troposphere over a given region which has fairly uniform underlying surface properties (land vs ocean, surface temperature) and atmospheric properties (CO, temperature profile). Over land, daytime thermal contrast conditions appear to often produce significant sensitivity to lower tropospheric CO. In particular over the Indian subcontinent, the ‘simulated’ day-night CO differences can effectively delineate the strong surface source regions in summer as well as in winter.

MOPITT L2V3 retrieval averaging kernels vary considerably, particularly from day to night and over land. Further, the DOFS analysis shows greater sensitivity to lower atmosphere in daytime than of nighttime observations as expected, with greater DOFS in daytime. It is clearly evident that DOFS is well correlated to upper-troposphere (i.e. 350 hPa) percent a priori CO mixing ratios as expected. The percent a priori CO mixing ratio is a useful parameter to understand uncertainty of

the retrieved CO (at each retrieval level) as a percentage of a priori variability. The strong correlation between DOFS and percent a priori CO mixing ratio suggests one can use percent a priori instead DOFS which has to be calculated for each retrieved profile in L2V3 and it is time consuming process. The daytime and nighttime DOFS exhibits a bi-modal DOFS for all selected Indian regions. A similar distribution can be seen in thermal contrast.

It is also shown that day-night could give a more sensitive indicator to the monthly averaged component of lower atmosphere enhancements, at the price of a loss of data and assumptions on variations of CO on monthly timescales. This finding is consistent with [Richards, N. A. D., 2004] thesis. An analysis demonstrate for the first time that 700 hPa day-night differences gives a closer differentiation of lowermost CO than other measures for MOPITT data. It can further shown that 700 hPa day-night difference is clearly superior to (850/350) CO ratio in demonstrating lowermost atmosphere enhancement. Similarly for columns, a considerable utility to day-night columns difference which further provide confidence in adopted robust methodology. For Indian subcontinent, this analysis confirms the pollution pools at the extremes of the Indo-Gangetic basin ("Bihar Pollution Pool" reported by [Kar et al., 2008]). A more extensive CO pollution loading in the west coast and southern tip of India are also observed. Small enhancements in NO₂ are also observed in these regions supporting this analysis.

It should be noted that since MOPITT instrument takes about 3 days to give global coverage, daytime and nighttime measurements over a particular location may be separated by a period of days. It is therefore possible to apply our methodology on a monthly mean basis from local (e.g. megacity) to global scale.

Chapter 4

MOPITT CO Profile Information Content: Comparison Between L2V3 and L2V4 Retrievals

4.1 Introduction

It has been emphasised already that L2V3 data have been the main MOPITT product analysed in this thesis but that L2V4 data were released recently in April 2009. Nonetheless it is useful to consider L2V4 data in relation to L2V3 data and in particular w. r. t. the findings in chapter 3. Hence in this chapter, MOPITT L2V4 simulations and TOMCAT profiles are studied in a manner similar to chapter 3. Significant aspects are the different pressure grid for the state vector, the varying a priori and explicit averaging kernel in the data file.

In this chapter, we first perform MOPITT L2V4 simulations using L2V4 a priori CO mixing ratio profile as a sample profile by applying perturbation at each retrieval level. Similarly, TOMCAT model CO profile simulations have been also carried out here. Then, we compare MOPITT L2V4 simulation to our earlier MOPITT L2V3 simulations in order to better constrain vertical structure and persistent features of CO in the troposphere. It should be noted that there are significant differences in between these two MOPITT retrieved datasets. The MOPITT L2V4 operational product has been released recently in early April, 2009 and it benefit from significant advances in radiative transfer modeling, state vector representation, and a priori

statistics. The features and appropriate analysis methods used in L2V4 product to retrieve CO from MOPITT thermal IR radiances discussed in detail by Deeter [2009]. Section 4.2.1 of this chapter demonstrates a quick review of L2V3 product and silent features of L2V4 product.

4.2 MOPITT Level 2 Products

For each MOPITT observation, the Level 2 data file includes (i) primary MOPITT CO products (including both a volume mixing ratio (VMR) profile and a corresponding CO total column value), (ii) retrieved surface temperature and emissivity, a priori information (which is constant for L2V3 and can vary geographically and temporally for L2V4), and a variety of different diagnostics (e.g. 'DOFS' for L2V4, 'Retrieval averaging kernel' for L2V4, 'Percent a priori CO mixing ratio' for L2V3).

4.2.1 Review of L2V3 Product

The MOPITT L2V3 product was described in chapter 2. The main characteristics of this product includes:

- Retrievals algorithm based on nonlinear optimal estimation principles [Rodgers, 2000] to combine measurements with statistical background information a priori profile).
- Retrievals expressed as profiles of CO VMR values on fixed 7-level pressure grid and corresponding total column value.
- Retrievals based on the same and constant global CO VMR a priori profile and covariance matrix.
- Retrievals based on subset of MOPITT thermal-IR radiances, though Deeter et al. [2009] recently reported the first retrieval results of CO exclusively using NIR radiances in the 2.3 μm CO overtone band observed by MOPITT.
- Operational radiative transfer model (MOPFAS) based on pre-launch estimates and laboratory measurements of instrument parameters and training set mainly composed of low-to-moderate CO concentrations.

4.2.2 Features of L2V4 Product

The retrieval algorithm for L2V4 product incorporates a variety of features to enhance its scientific value, however, it should be treated carefully. Because CO variability in the L2V4 product is modelled in terms of a log-normal distribution, in contrast to the L2V3 product [Deeter et al., 2007], random errors in the VMR retrievals due to instrument noise will also follow a log-normal distribution. The retrieval algorithm used to generate the L2V4 product benefits from significant advances in radiative transfer modelling, state vector representation, and a priori statistics, however, radiance basis set, ancillary data and cloud detection algorithm are unchanged from their L2V3 counterparts. The significant changes in the L2V4 product with respect to both scientific content and diagnostics are detailed in [Deeter, 2009] and some of them includes;

- For L2V4 product, both the PMC and LMC models have been updated for consistency with the actual cell pressure (P) and temperature (T) values observed during the mission. Specifically, for Phase II observations, the LMC P and T time-means are calculated over 2006 as it represents the approximate midpoint of the Phase II period.
- The L2V4 state vector represent the CO profiles as a set of $\log(\text{VMR})$ values whereas the L2V3 state vector represented the CO vertical profile as a set of VMR values.
- The L2V4 state vector expresses the CO profile on a ten-level pressure grid (surface level followed by nine uniformly-spaced levels from 900 to 100 hPa) instead of the seven-level grid used for L2V3.
- The L2V4 product for both Phase I and Phase II are respectively based on the same radiance sets employed for the L2V3 product; these L2V4 products have been validated separately.
- The a priori profile vary geographically and temporally. In contrast, the L2V4 a priori covariance matrix describes variability of $\log(\text{VMR})$.
- Unlike L2V3, however, L2V4 surface emissivity a priori values are based on an analysis of gridded MOPITT radiances and corresponding MODIS surface

temperature [Ho et al., 2005]. The assumed surface emissivity a priori variance for L2V4 is 0.0025, corresponding to an uncertainty of 0.05.

- For L2V4 processing, the updated algorithm for water vapour is applied to the entire record of MOPITT observations. This new scheme exploits the NCEP/NCAR Reanalysis long-term monthly-mean water vapour product.
- The MOPFAS training set has been expanded in order to permit retrievals involving especially high CO values, which are not considered for L2V3 retrievals. Specifically, the original training set composed of 58 profiles used in L2V3 has been expanded to 116 atmospheres. The added atmospheres were formed by scaling all of the original training set profiles by a factor of two.
- In general, retrieval convergence in the L2V4 product is higher than in the L2V3 product. For L2V3, failed retrievals commonly followed one of two paths, characterised by regions of exceptionally low and high CO values. In L2V4, these convergence problems are substantially reduced through (i) the use of $\log(\text{VMR})$ in the retrieval state vector, which prevent negative VMR values, and (ii) an expanded training set for MOPFAS, allowing retrievals with higher values than in L2V3 (up to a factor of two).
- The cloud detection module ("MOPCLD") for L2V4 is unchanged from L2V3.
- In L2V4, corresponding to each ten level retrieved profile, a ten-by-ten retrieval averaging kernel is provided with the product. Note that L2V4 averaging kernel describes the sensitivity of retrieved $\log(\text{VMR})$ to actual $\log(\text{VMR})$, and are thus not exactly equivalent to L2V3 VMR-based averaging kernels.
- In L2V4 product, new diagnostics e.g. "Degrees of Freedom for Signal", "Water Vapour Climatology Content", and "Retrieval Iterations" are provided.
- MOPITT L2V4 CO retrievals should first be converted to $\log(\text{VMR})$ values, when one intends to perform comparison between retrieval profile and in-situ measured.

Figure 4.1 show the difference in MOPITT L2V3 and L2V4 retrieved daily number of profiles on global scale for the year 2007. It is obvious that the number of

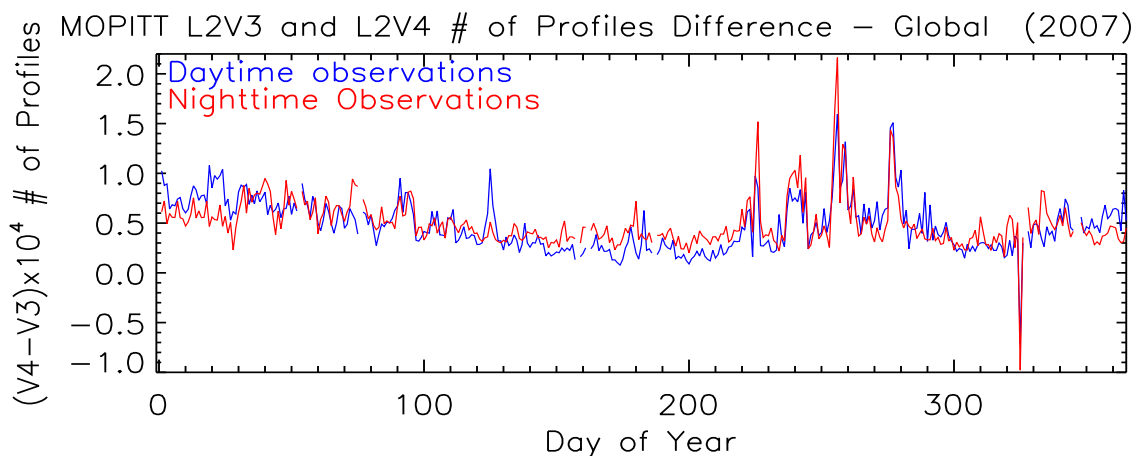


Figure 4.1: Difference in the MOPITT L2V3 and L2V4 retrieved number of profiles on global scale for the year 2007.

profiles retrieved for L2V4 are higher of the order of 3 than L2V3 retrieved profiles. This is because, in the L2V3 retrieval product, some MOPITT retrievals failed systematically. Subsequent analysis by Deeter [2009] demonstrated that such retrievals were sometimes failing because they fell outside the bounds of the original MOPFAS training set which is prohibited. Application of MOPFAS to profiles with VMRs outside of the envelope defined by the training set profiles produces unreliable radiances and is therefore prohibited within MOPFAS. Retrieval simulations and limited case studies both indicate that this approach yields reliable retrievals of high CO profiles without degrading retrieval quality for low and moderate CO concentrations [Deeter, 2009].

4.3 L2V4 Product Diagnostics

4.3.1 L2V4 A Priori CO

In L2V4, both the CO profile and the surface emissivity were added. For CO results from the global chemical transport model MOZART-4 (Model of Ozone And Related Chemical Tracers, version 4) were used to create a monthly mean climatology for use as the a priori. MOZART-4 simulates 100 chemical species with relatively detailed hydrocarbon chemistry [Apel et al., 2009]. The simulation used for this climatology was for 1997-2004, with a horizontal resolution of T42 (2.8×2.8 deg) and 28 vertical

levels, driven by meteorology from NCEP/NCAR reanalyses. The anthropogenic emissions were constant over the simulation, but biomass burning emissions were based on satellite fire counts for each month from the Global Fire Emissions Database (GFED-v2) [Van der Werf et al., 2006]. The climatology was created by making monthly means over the 8 years of simulation, retaining the horizontal resolution and interpolating in the vertical to the MOPITT Forward Model 35 levels. For each retrieval, the climatology for the same month as the observation is spatially interpolated to the location of the observation. Thus, L2V4 a priori profiles vary geographically and temporally for each retrieval.

In the L2V3 retrieval algorithm, where the retrieval state vector represented CO in terms of VMR, the CO a priori covariance matrix quantified VMR variability. In contrast, the L2V4 a priori covariance matrix describes variability of $\log(\text{VMR})$. Thus, because

$$\partial(\ln(\text{VMR})) = \partial(\text{VMR})/\text{VMR} \quad (4.1)$$

$\log(\text{VMR})$ variances and covariances describe fractional VMR variability rather than absolute VMR variability.

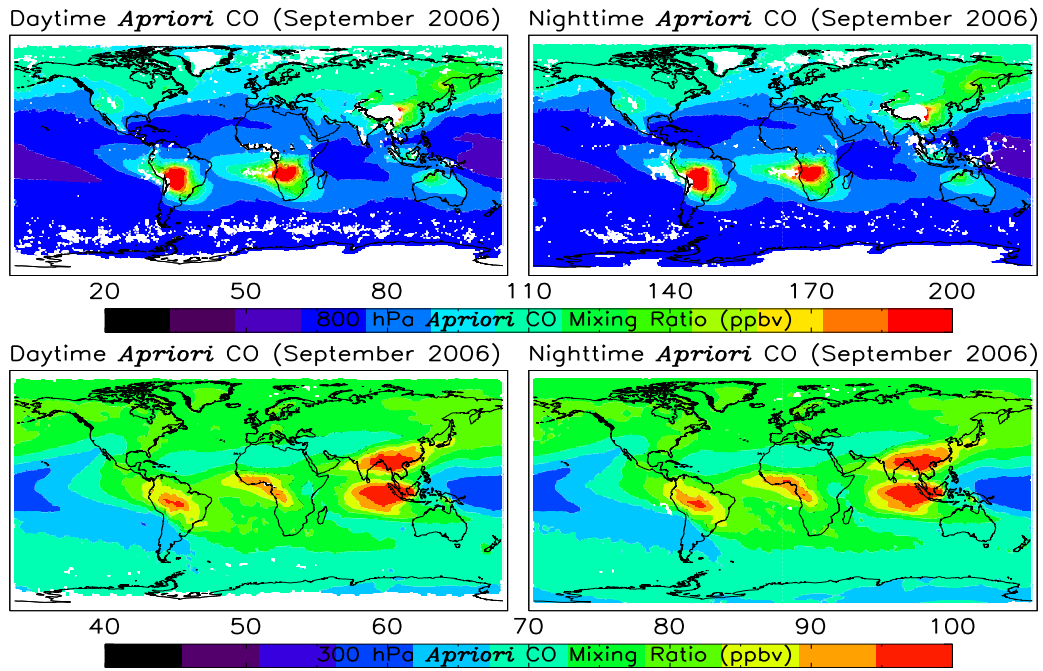
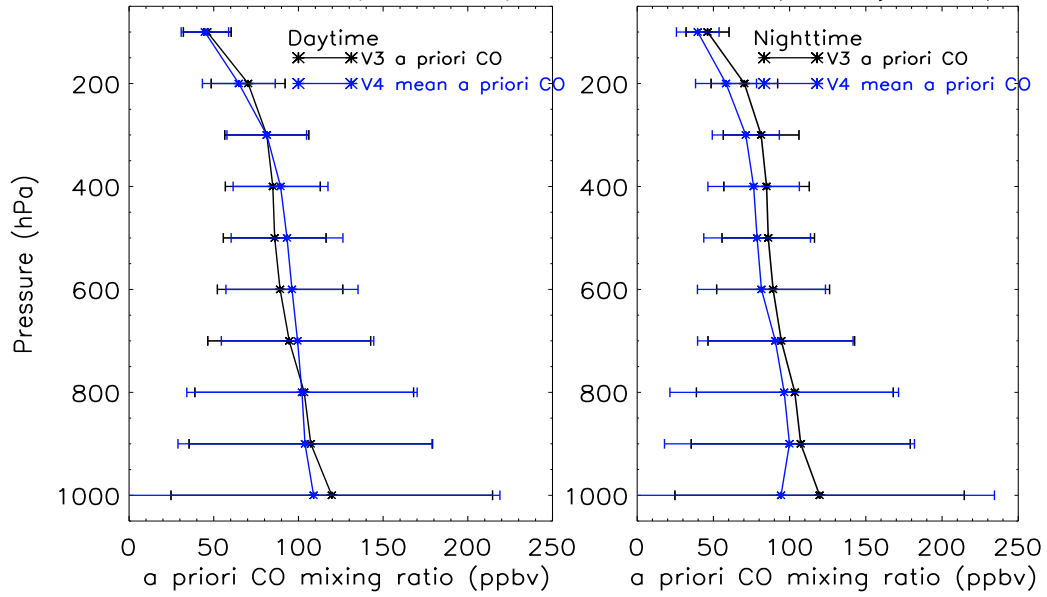


Figure 4.2: (a) MOPITT L2V4 retrieved 800 hPa 0.5 deg. gridded a priori CO mixing ratios during daytime and nighttime for September 2006; (b) Same as (a) except for 300 hPa level.

Figure 4.2 shows the spatial distribution of 800 hPa and 300 hPa a priori CO mixing ratios constrained by the MOPITT L2V4 retrievals. As shown by [Deeter et al., 2007], analysis of in-situ datasets for geographically diverse locations demonstrates that fractional VMR variability is more consistent (i.e., varies less from site to site) than absolute VMR variability. It is also clearly evident from Fig. 4.2 that the regions which are typically unpolluted (on average) exhibit small a priori CO VMR values than CO source regions which exhibit large mean a priori CO VMR values. Thus, although $\log(\text{VMR})$ variability statistics are not well established for all geographic regions and seasons, the results of [Deeter et al., 2007] support the use of a single 'global' a priori covariance matrix for L2V4 CO retrievals, which are based on a $\log(\text{VMR})$ state vector.

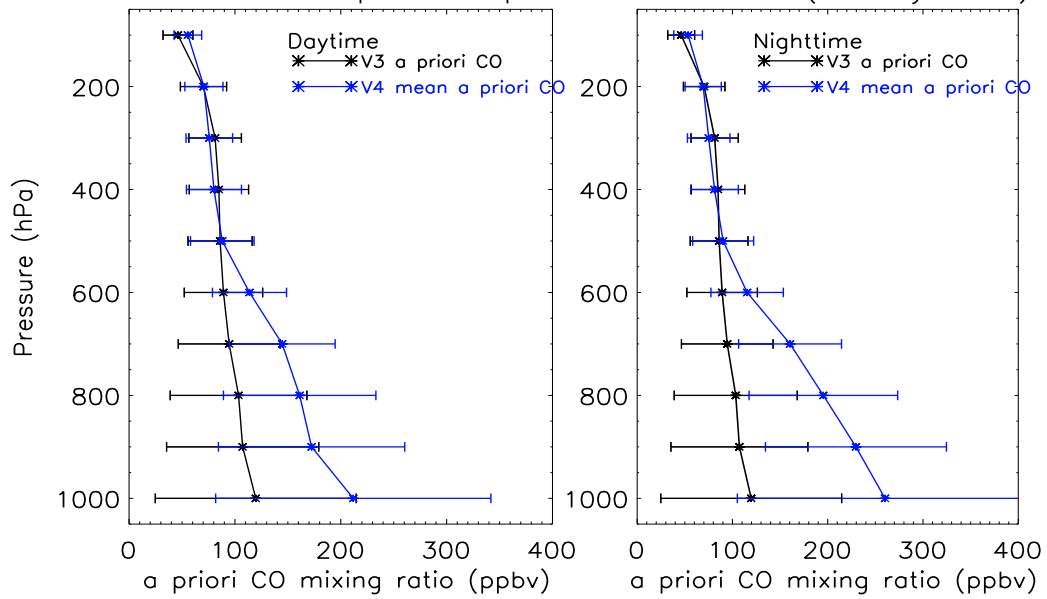
From Fig. 4.3 (b), it is clear that L2V4 retrieved a priori CO VMR profiles, over IG basin, have larger values in lower tropospheric levels compared to L2V3 where CO in the atmosphere is likely to be enhanced. However, L2V4 retrieved global mean a priori CO VMR profile is very much comparable to L2V3 single global a priori profile. These differences are attributed to failed L2V3 retrievals for exceptionally low and high CO values. Hence the observation of enhanced CO in L2V4 data and differences between L2V3 and L2V4 CO retrievals has to be interpreted carefully.

MOPITT V3 & V4 a priori CO profiles – Global (01 May 2006)



(a) Global

MOPITT V3 & V4 a priori CO profiles – IG Basin (01 May 2006)



(b) IG Basin

Figure 4.3: MOPITT L2V4 a priori CO mixing ratio profiles as a function of DOFS, for global case (left panel), and IG basin (right panel) on 01 May 2006.

4.3.2 L2V4 Retrieval Averaging Kernels

Figure 4.4 shows example averaging kernels for MOPITT L2V4 retrievals conducted at day and night over the (a) Libya desert and (b) South Atlantic Ocean. It is obvious that MOPITT operational L2V4 kernels are similar to L2V3 and the averaging kernels for each level in the retrieved profile do not necessarily peak at the corresponding pressure level of the true profile. It can be seen that MOPITT L2V4 retrievals are generally more sensitive to CO in the middle and upper troposphere over water surfaces than in the lower troposphere (Fig. 4.4b); this is a consequence of the relatively weak thermal contrast over water surface. It can also be seen that the kernels for individual levels in the retrieved profile are often more similar between day and night than was the case for L2V3. Nonetheless day retrievals over land have higher sensitivities apparent at the surface level than was the case for L2V3. For example, the strong similarity of the averaging kernels for 800 hPa and 600 hPa levels indicate a high correlation for the retrieved values at these levels.

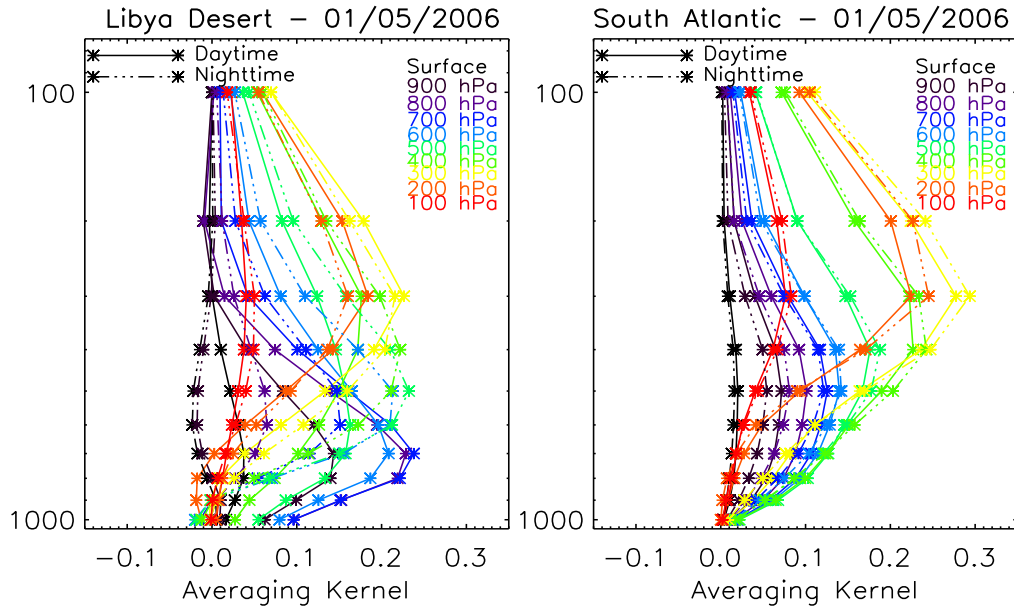


Figure 4.4: MOPITT L2V4 mean averaging kernels obtained by averaging all daytime and nighttime averaging kernels separately on 01 May 2006. (a) in the box defined by $20^{\circ}N$, $30^{\circ}N$, $10^{\circ}E$, and $25^{\circ}E$ (over Libyan desert) and (b) in the box defined by $15^{\circ}S$, $30^{\circ}S$, $5^{\circ}W$, and $20^{\circ}W$ (over South Atlantic).

It should be noted that L2V4 averaging kernels describe the sensitivity of retrieved $\log(\text{VMR})$ to actual $\log(\text{VMR})$, and are thus not exactly equivalent to L2V3 VMR-based averaging kernels. It is also important to note that employing a retrieval grid with uniform grid spacing (in pressure) substantially simplifies the physical interpretation of the retrieval averaging kernels, whereas L2V3 averaging kernel was based on non-uniform grids.

4.3.3 L2V4 Degrees Of Freedom for a Signal

Figure 4.5 shows 1.0 deg. gridded MOPITT L2V4 retrieved DOFS map separately for daytime and nighttime measurements for September, 2006. The data drop out in Fig. 4.5 correspond to regions of persistent cloudiness; since cloud-contaminated observations are discarded for L2V4 operational product similar to L2V3 retrievals. Daytime DOFS values tend to be higher than nighttime values because (i) higher daytime surface temperatures (especially over land) tend to improve the thermal contrast between the surface and lower atmosphere, and (ii) solar radiation at $4.7 \mu\text{m}$ contributes a non-negligible component to the daytime observed radiances and therefore affects the radiance weighting functions. In general, the L2V4 DOFS values are slightly higher than the L2V3 retrieved values by a few %. Therefore the main effect is the different retrieval sensitivity and different a priori content.

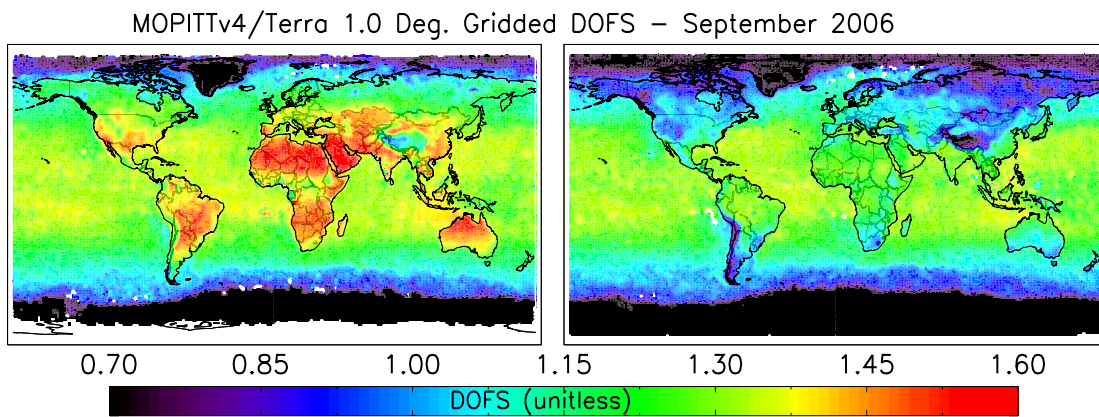


Figure 4.5: Degrees Of Freedom for Signal for September, 2006 for (a) daytime and (b) Nighttime MOPITT L2V4 data .

4.4 Methodology

The methodology illustrated in chapter 3 is used here for MOPITT L2V4 simulation for comparison to L2V3. First MOPITT L2V4 a priori CO profile taken as sample profile and enhancements have been applied to this profile to simulate day and night CO profiles by applying selected ‘typical’ averaging kernels to examine day-night differences. Similar approach is used here to decide DOFS ranges and to select a ‘typical’ averaging kernel representative for given atmospheric and surface properties for the same latitude-longitude location as for L2V3. Using two retrieval products one can possibly easily interpret if it is possible for MOPITT instrument to detect plumes or layers of enhanced CO, which have limited vertical extent. It is also important to understand the key differences in ‘simulated’ CO profiles between L2V3 and L2V4 as it will help to understand what is possibly causing these differences. In this chapter we perform L2V3 and L2V4 simulation comparison for Indian subcontinent region and results are discussed. We have also tested our methodology for other parts of world and the results are presented in Appendix-I.

4.5 Examination of Day-Night Differences : MOPITT L2V3 Vs L2V4

Since there are significant differences between MOPITT retrievals of L2V3 and L2V4, it is first crucial to understand the key differences between these and then apply our knowledge to examine MOPITT sensitivity to the CO in the lower troposphere. Some of the key differences are summarised in section 4.2. In case of L2V4, the retrieval averaging kernels for the lower retrieval levels exhibit a considerable variation in sensitivity during daytime especially over land. The shifting of the lower averaging kernels away from the surface during nighttime, similar of L2V3 CO averaging kernels, may hold the key to examine vertical differentiation of CO in the troposphere.

4.5.1 Day-Night Difference CO Maps

Here the focus is on Indian subcontinent region as for chapter 3. It should be pointed out that our analysis for L2V3 show that MOPITT indeed has greatest sensitivity to

700 hPa retrieval level. Figure 4.6 (top panel) shows the MOPITT L2V3 CO mixing ratios and day-night CO distribution retrieved at 700 hPa level for the month of May, and December 2007. The corresponding MOPITT L2V4 CO mixing ratios and day-night CO differences distribution maps are shown (bottom panel). The evolution of the CO distribution in the lower troposphere as seen in MOPITT L2V3 retrievals is quite similar to the MOPITT L2V4 distribution with the plume over eastern states of Bihar and West Bengal, a maximum in December, plume over Delhi and north-west of it and elevated surface CO concentrations over western and southern part of country (i.e Mumbai and Coimbatore). Similarly, elevated plumes from key regions can be identified in day-night difference CO map for both the L2V3 and L2V4 retrieved data with less significant differences.

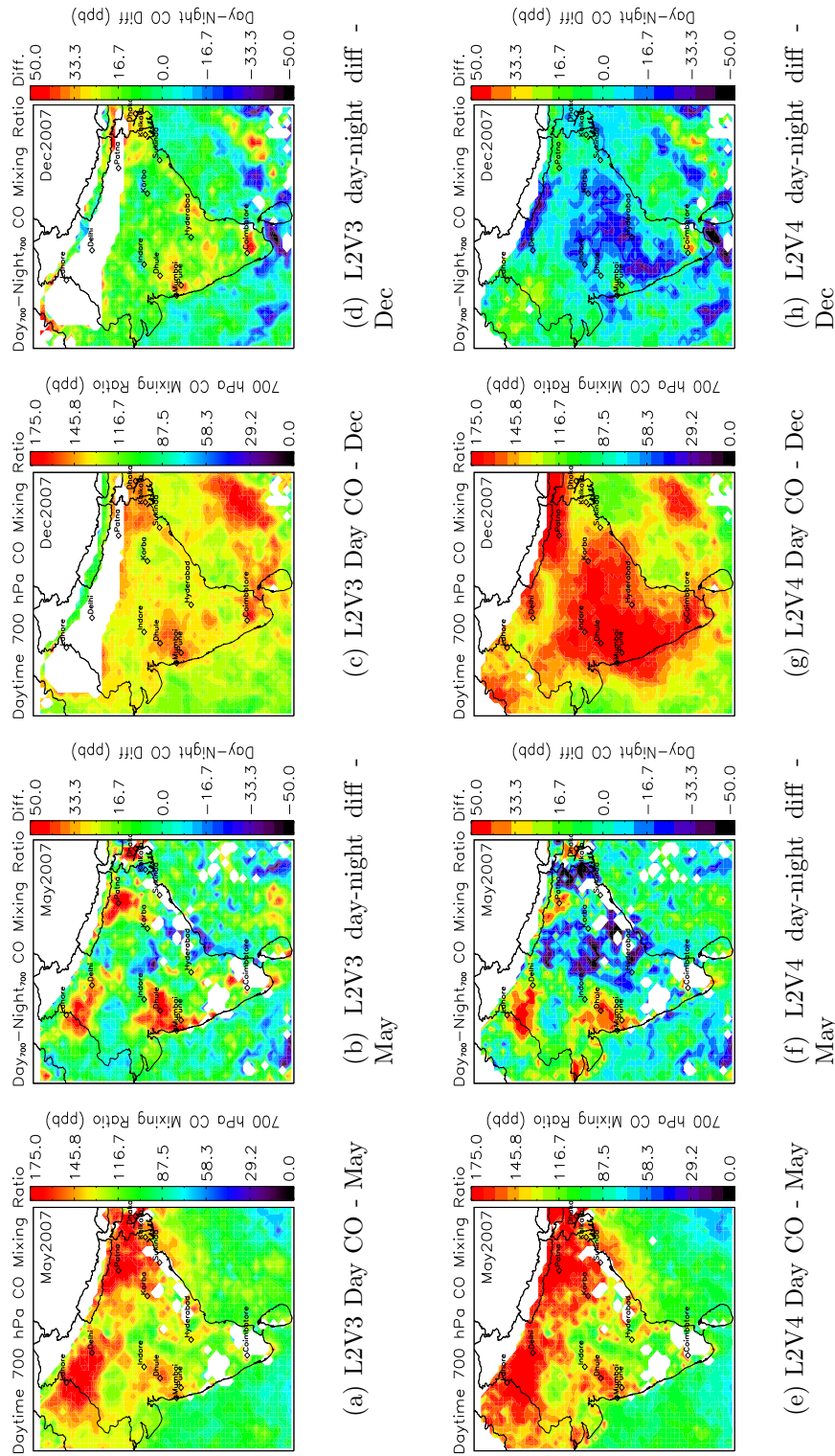


Figure 4.6: (a) MOPITT L2V3 0.5 deg. gridded 700 hPa daytime CO mixing ratios, over India, for May 2007; (b) MOPITT L2V3 0.5 deg. gridded 700 hPa day-night difference CO mixing ratios, over India, for May 2007; (c) Same as (a) except for December 2007; (d) Same as (b) except for December 2007; (e) Same as (a) except for L2V4; (f) Same as (b) except for L2V4; (g) Same as (c) except for L2V4; (h) Same as (d) except for L2V4.

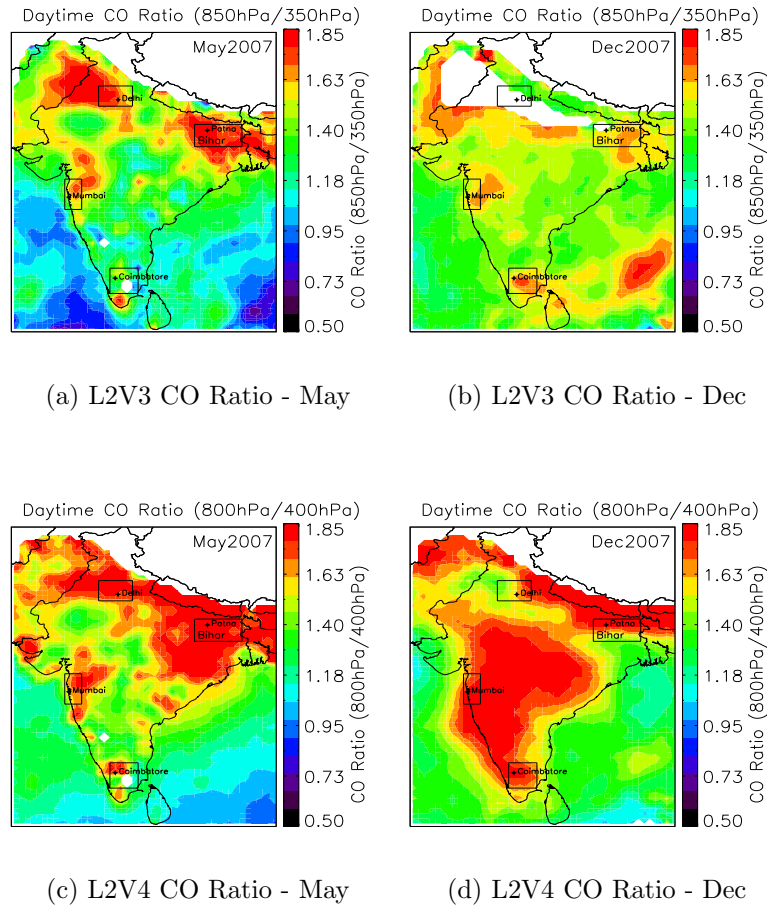
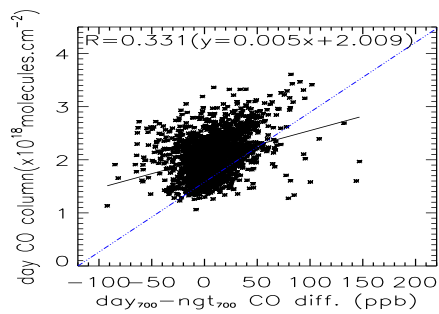
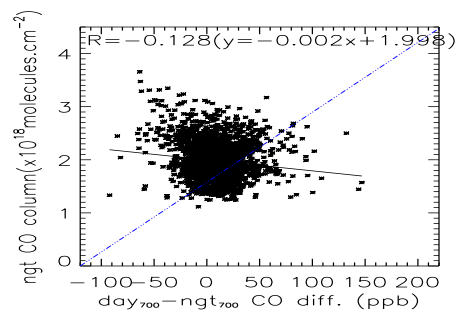


Figure 4.7: (a) MOPITT L2V3 0.5 deg. gridded (850hPa/350hPa) daytime CO mixing ratios, over India, for May 2007; (b) Same as (a) except for December 2007; (c) MOPITT L2V4 0.5 deg. gridded (800hPa/400hPa) daytime CO mixing ratios, over India, for May 2007; (d) Same as (c) except for December 2007.

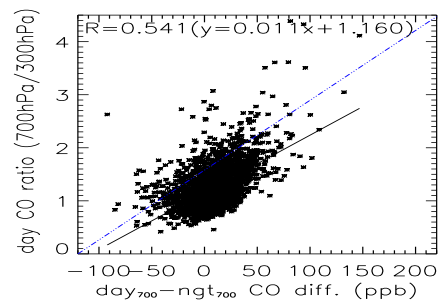
Figure 4.7 shows the spatial structure in the distribution of CO ratio for MOPITT L2V3 (850hPa/350hPa) and L2V4 (800hPa/400hPa) retrievals for May, and December 2007 respectively. It is shown earlier that the CO ratio quantity indeed has significance to differentiate CO into vertical layers and provides an useful index on information of surface source of CO. Figure 4.8 shows considered correlation results for MOPITT L2V4 as in Fig. 3.59 for MOPITT L2V3 retrievals. This analysis further useful to support our findings.



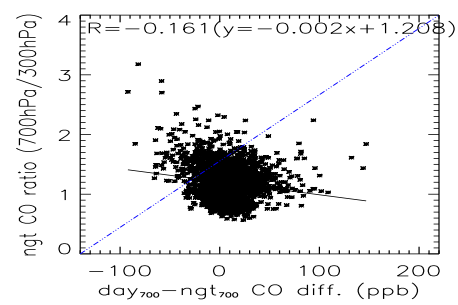
(a) 700hPa day-night vs day CO



(b) 700hPa day-night vs ngt CO

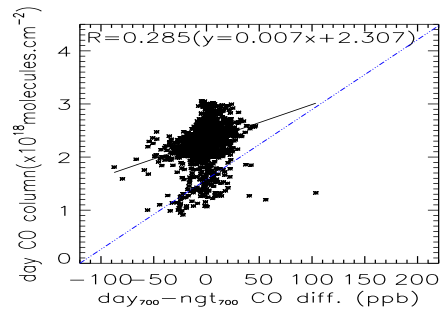


(c) 700hPa day-night vs day ratio

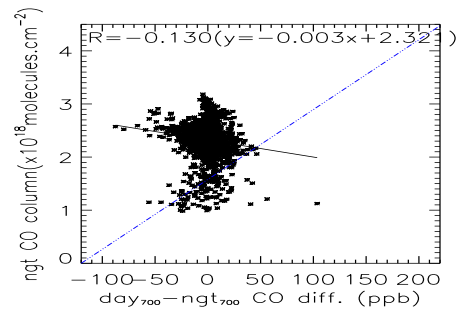


(d) 700hPa day-night vs ngt ratio

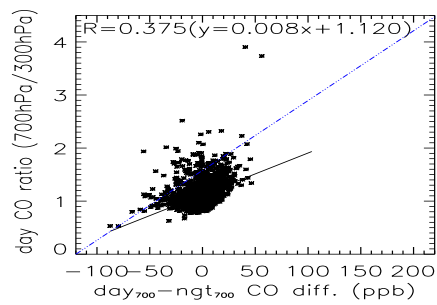
Figure 4.8: Correlation results, over India, in the month of May 2007.



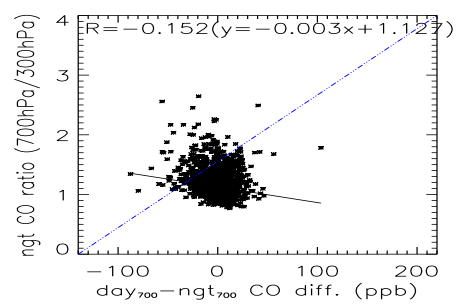
(a) 700hPa day-night vs day CO



(b) 700hPa day-night vs ngt CO



(c) 700hPa day-night vs day ratio



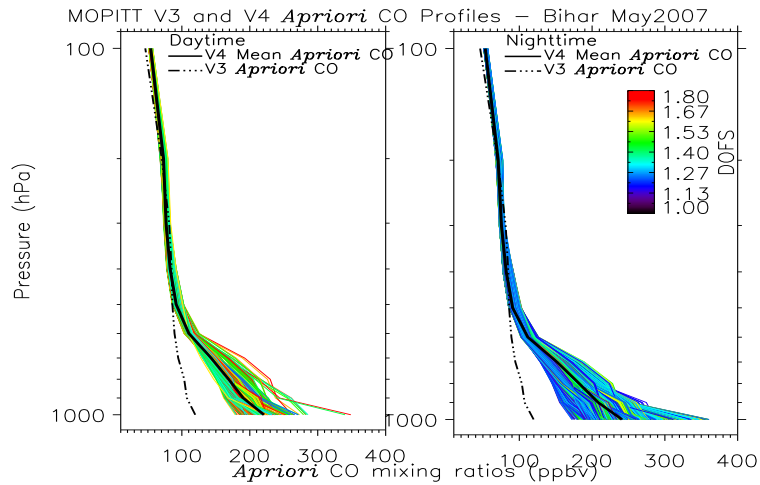
(d) 700hPa day-night vs ngt ratio

Figure 4.9: Correlation results, over India, in the month of December 2007.

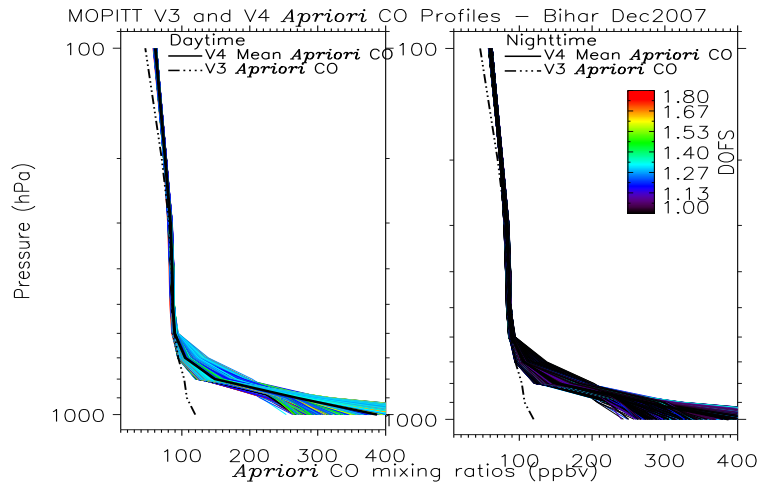
4.5.2 A Case Study of Bihar

4.5.2.1 L2V3 and L2V4 Simulations

The robustly used methodology in chapter 3 is adopted here to perform MOPITT L2V4 a priori CO profile simulations. We have shown that this methodology works well for MOPITT L2V3 retrievals for Indian subcontinent to measure layer enhancements of CO in the troposphere having good thermal contrast conditions.



(a) L2V3 and L2V4 a priori CO - May



(b) L2V3 and L2V4 a priori CO - Dec

Figure 4.10: (a) MOPITT L2V3 and L2V4 a priori CO mixing ratio profile(s), over Bihar region, in the month of May 2007; (b) Same as (a) except for December 2007.

Figure 4.10 shows MOPITT L2V3 and L2V4 retrievals a priori CO mixing ratio profiles, over Bihar region, in the month of May and December. It can be seen that there are significant differences between L2V3 and L2V4 a priori CO profiles at the lower 4 retrieval pressure levels. The a priori CO profile in both cases have similar features in the mid-upper troposphere. The data were averaged together to produce a sample profile for the simulation study.

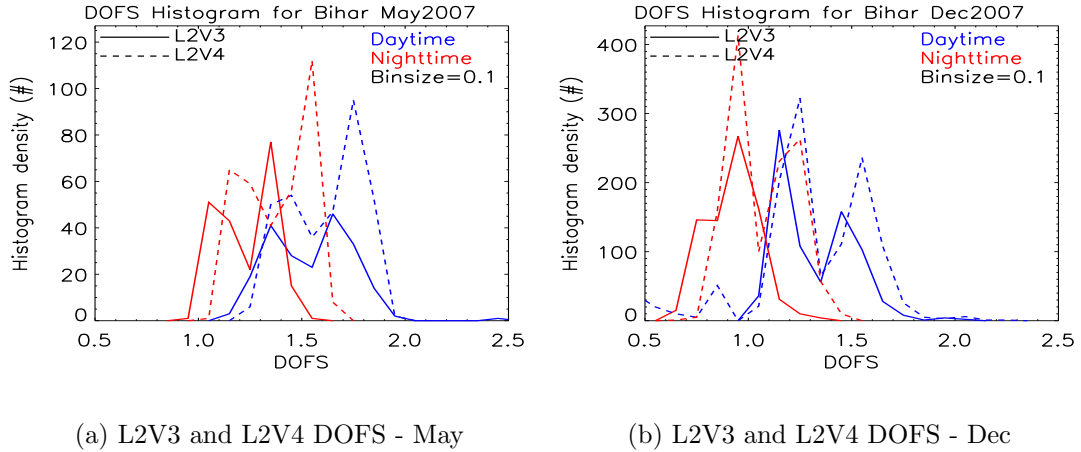
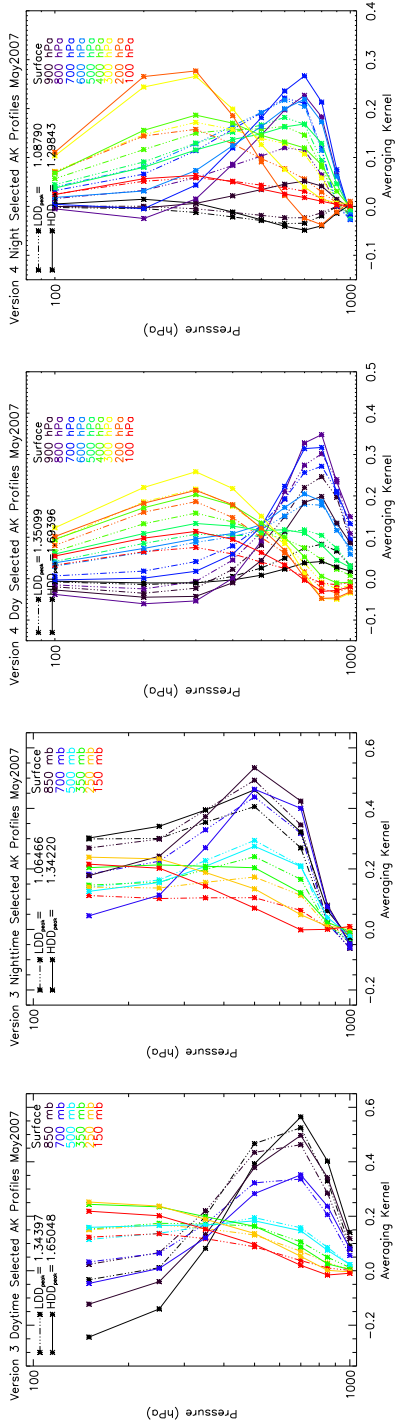
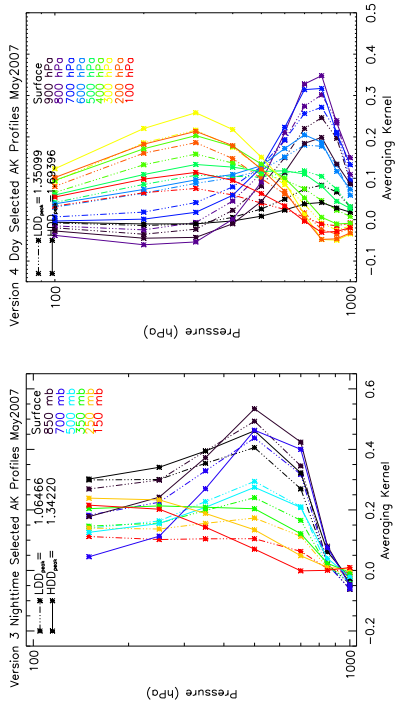


Figure 4.11: (a) MOPITT L2V3 and L2V4 DOFS histogram plot, over Bihar region, in the month of May 2007; (b) Same as (a) except for December 2007.

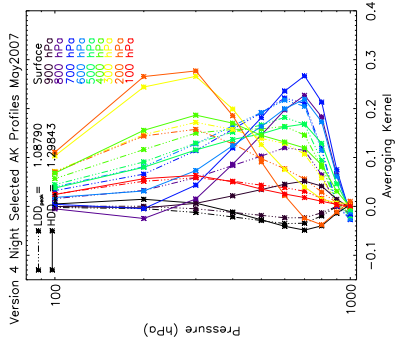
Figure 4.11 (a, b) shows MOPITT L2V3 and L2V4 daytime and nighttime histogram plots for DOFS, over Bihar region, for May, and December of 2007. The L2V4 DOFS histogram is shown by dashed line. For Bihar region, both the L2V3 and L2V4 daytime and nighttime DOFS has two distinct distributions. It is clearly evident that L2V4 DOFS are superior to L2V3 DOFS for both the daytime and nighttime measurements. It is also obvious that daytime measurements have greatest DOFS values than the nighttime measurements in both the L2V3 and L2V4 retrievals. It should be noted that the DOFS distribution is slightly shifted to lower DOFS value (to the left) in winter month, suggesting reduced sensitivity of MOPITT to the tropospheric CO column, particularly to the boundary layer.



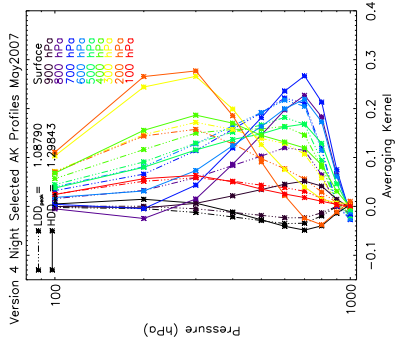
(a) L2V3 - Day AK



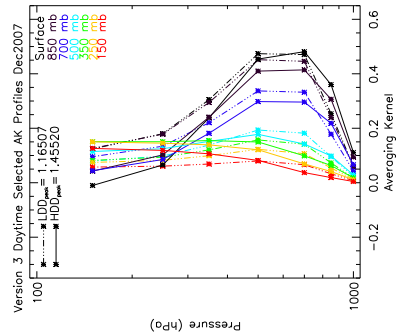
(b) L2V3 - Night AK



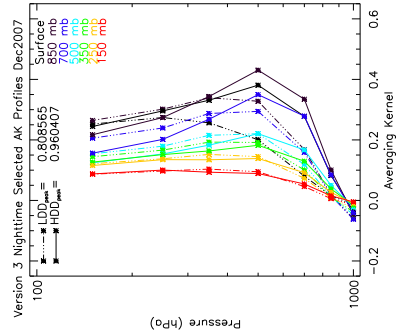
(c) L2V4 - Day AK



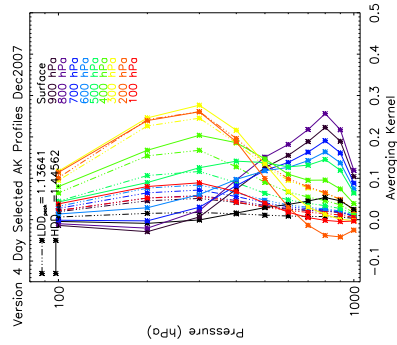
(d) L2V4 - Night AK



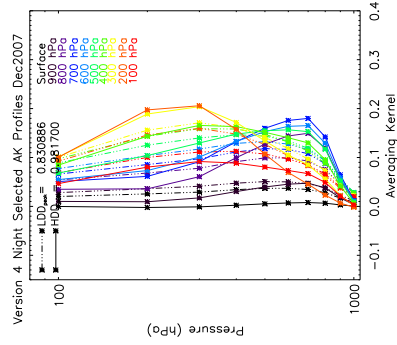
(e) L2V3 - Day AK



(f) L2V3 - Night AK



(g) L2V4 - Day AK



(h) L2V4 - Night AK

Figure 4.12: (a) MOPITT L2V3 selected daytime 'typical' averaging kernel, over Bihar region, in the month of May 2007; (b) Same as (a) except for nighttime; (c) MOPITT L2V4 selected daytime 'typical' averaging kernel, over Bihar region, in the month of May 2007; (d) Same as (c) except for nighttime; (e-f) Same as (a-d) except for December 2007.

Figure 4.12 shows daytime and nighttime MOPITT L2V3 and L2V4 CO retrievals selected ‘typical’ averaging kernels, over Bihar region, for May (top panel) and December (bottom panel). It should be noted that L2V4 averaging kernels describe the sensitivity of retrieved $\log(\text{VMR})$ to actual $\log(\text{VMR})$, and are thus not exactly equivalent to L2V3 VMR-based averaging kernels. Moreover, the L2V4 state vector expresses the CO profile on a ten-level pressure grid instead of the seven-level grid used for L2V3. The L2V3 lower level averaging kernels have finite values in the upper troposphere (some sensitivity to the upper troposphere) while the L2V4 lower level averaging kernels have negative value or close to zero showing no sensitivity to the upper troposphere.

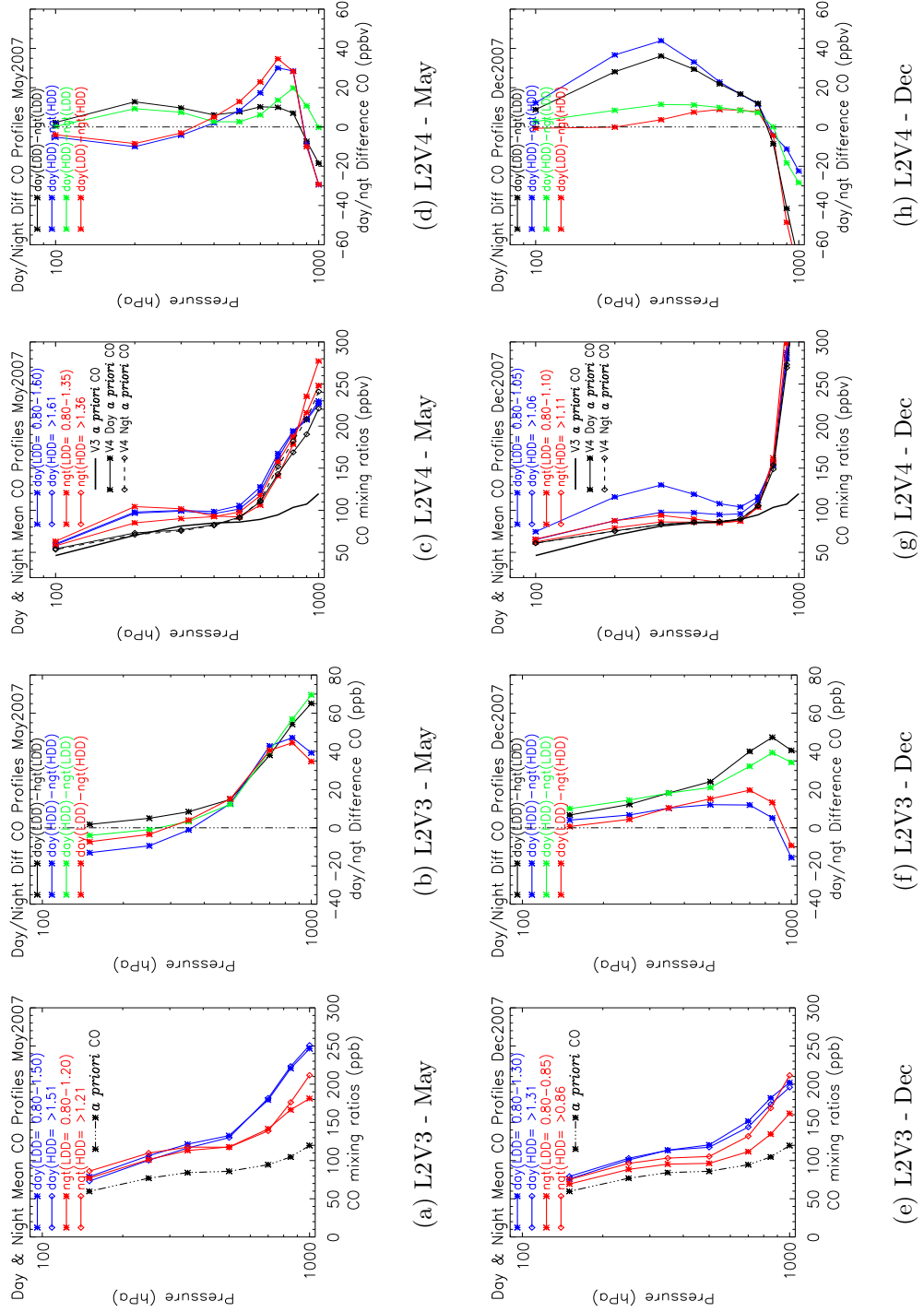
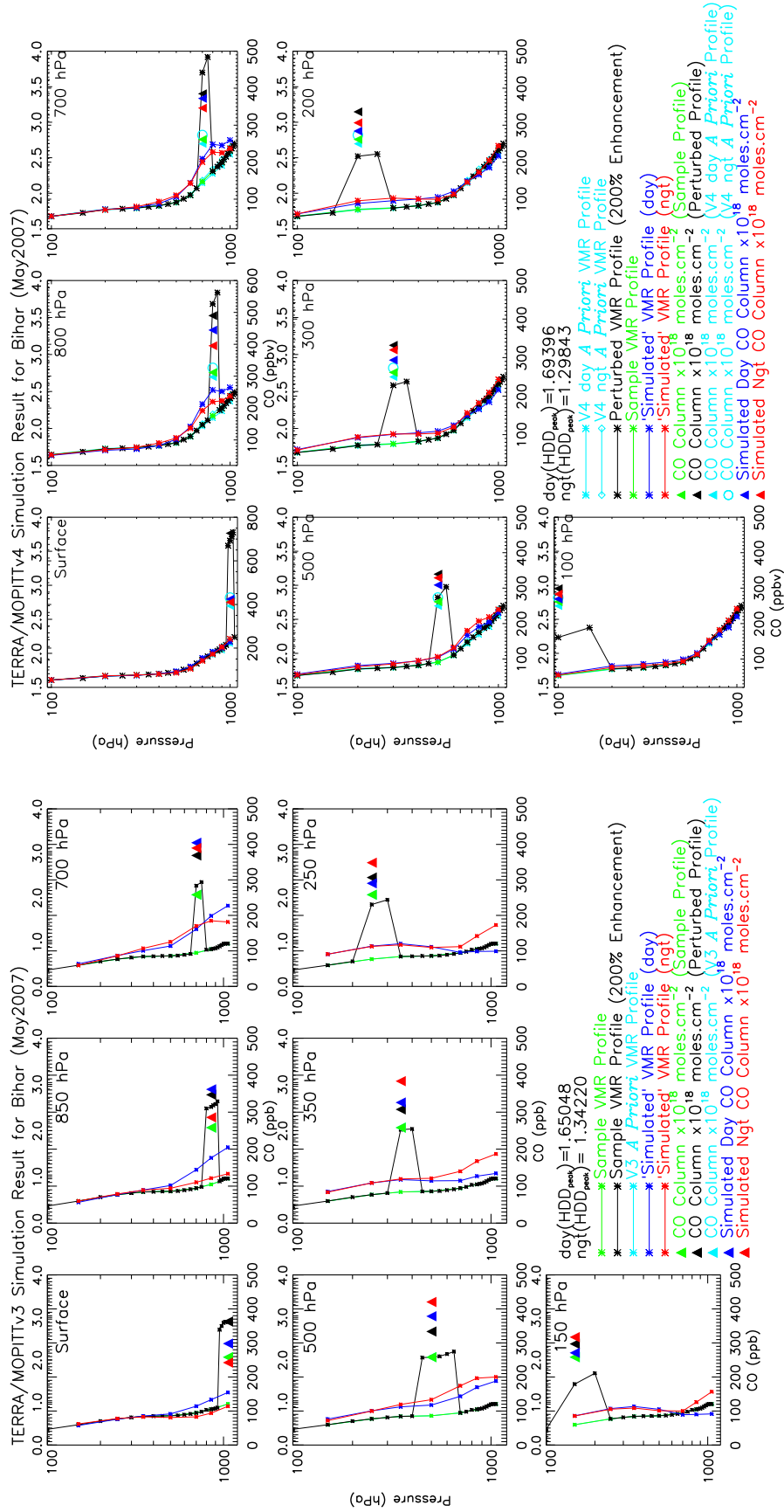


Figure 4.13: (a) MOPITT L2V3 retrieved mean daytime and nighttime CO profiles, over Bihar box, for May 2007; (b) Mean day-night difference CO profiles, over Bihar box, for combination of LDD and HDD; (c) Same as (a) except for MOPITT L2V4; (d) Same as (b) except for MOPITT L2V4; (e) Same as (a) except for December 2007; (f) Same as (b) except for December 2007; (g) Same as (c) except for December 2007; (h) Same as (d) except for December 2007;

For Bihar region, there exists two sets of LDD and HDD for a range of DOFS values in the month of May and December. Figure 4.13 shows MOPITT L2V3 and L2V4 retrieved daytime and nighttime mean CO profiles calculated for both the LDD and HDD and their resultant day-night difference CO profiles in the month of May (top panel) and December (bottom panel).

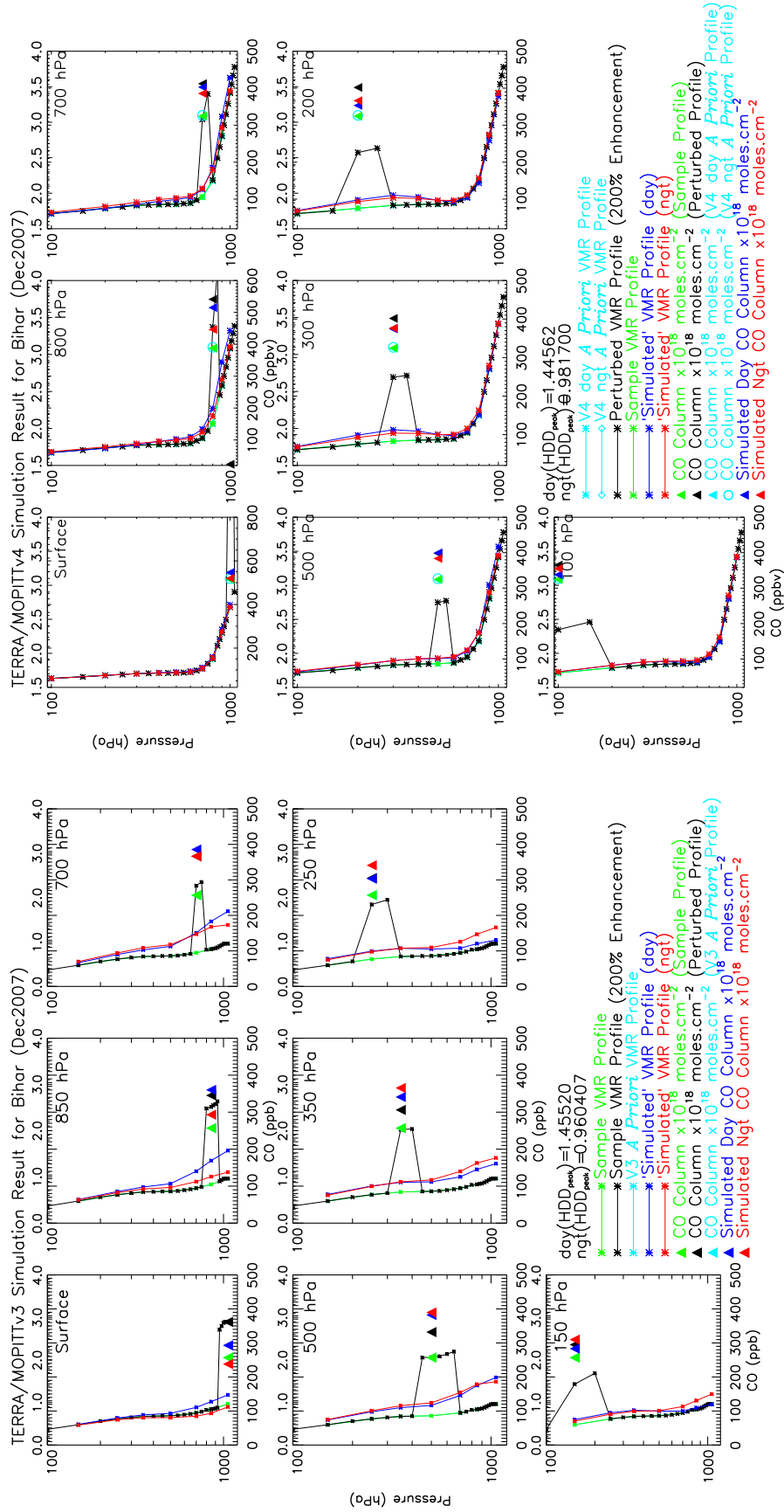
For L2V3, the daytime retrieved mean profile has fairly similar features in CO for both the LDD and HDD in the month of May, whereas the nighttime retrieved CO profile for HDD has significant enhancements in the lower layer of the troposphere. Whereas for L2V4, the daytime and nighttime retrieved mean CO profiles have similar features as seen in the a priori CO profile, except little enhancements in the upper troposphere in the month of May. The corresponding day-night difference CO profiles, for L2V3 and L2V4, for combination of selected LDD and HDD can be separated into two equivalent groups (Fig. 4.13(b, d)). These are day(HDD)-ngt(LDD) and day(HDD)-ngt(HDD). There are significant differences between L2V3 and L2V4 retrieved day-night difference profiles, particularly at lower retrieval levels. For L2V4, day-night difference profiles have enhancements in the upper troposphere and a layer from 800 to 400 hPa but show negative day-night differences for lower 2 retrieval levels. The potential reason for this is apparent from the next plots.



(a) L2V3 - May

(b) L2V4 - May

Figure 4.14: (a) MOPITT L2V3 ‘simulated’ daytime and nighttime CO profiles for HDD_{peak} over Bihar, for May 2007; (b) Same as (a) except for MOPITT L2V4. The green, black, cyan, blue, and red line indicates the considered sample CO profile, perturbed CO profile, a priori CO profile, ‘simulated’ day CO profile, and ‘simulated’ night CO profile. The green, black, cyan, blue, and red triangles show calculated total column values for corresponding CO VMR profiles.



(a) L2V3 - Dec

(b) L2V4 - Dec

Figure 4.15: (a) MOPITT L2V3 'simulated' daytime and nighttime CO profiles for HDD_{peak} over Bihar, for December 2007; (b) Same as (a) except for MOPITT L2V4. The green, black, cyan, blue, and red line indicates the considered sample CO profile, perturbed CO profile, a priori CO profile, 'simulated' day CO profile, and 'simulated' night CO profile. The green, black, cyan, blue, and red triangles show calculated total column values for corresponding CO VMR profiles.

Figure 4.14 and 4.15 shows simulation results for L2V3 and L2V4 in the month of May and December respectively. For these simulation, the methodology briefly described in section 3.2 is used for L2V3. For MOPITT L2V4 simulations, mean averaged (day and night) a priori CO profile was calculated and taken as a sample profile. An enhancement of 200% was then applied to this profile in a layer stretching from surface (1100 hPa) to 950hPa. This layer was then moved successively upwards with uniform grid spacing (in pressure) through the profile in 10 steps to form 10 test profiles. In Fig. 4.14 and 4.15 the simulation results for L2V4 are shown only for corresponding retrieval pressure levels to L2V3. The selected ‘typical’ L2V4 averaging kernel was then applied to these profiles to simulate day and night CO profiles. The simulation in both the cases were performed for HDD_{peak} . The coloured triangles indicates the calculated total column values for each corresponding profiles shown by individual coloured line for both the L2V3 and L2V4.

Over Bihar region, a 200% enhancement in the surface level CO is barely captured in the retrieved MOPITT L2V4 profile, however significant enhancement for lower 3 retrieval levels for daytime measurements can be seen of L2V3 (refer to Fig. 4.14(b and a) top right corner plot). An enhancement of 200% for the 700 hPa MOPITT L2V3 retrieval pressure level shows an enhancement at all retrieval levels with greatest effect evident in the lowest 3 retrieval levels for both the daytime and nighttime retrieved profiles in the month of May. However, an enhancement of 200% between 750 hPa and 650 hPa which covers the 700 hPa MOPITT L2V4 retrieval pressure level show an enhancement at lower 6 retrieval levels except at surface level. Note that enhancements at 800 hPa are highest in case of L2V4 while enhancements are highest at surface level for L2V3 for the perturbation at 700 hPa retrieval level. Surprisingly, VMRs for L2V4 do not show as strong differences from a priori as were found for L2V3. For L2V4 upper troposphere influences on the lower retrieval level is smaller compared to as found for L2V3. The ‘simulated’ total column values for L2V3 and L2V4 are matching very well for enhancements at all retrieval pressure levels. Similar simulation results can be seen in the month of December (refer Fig. 4.15) except that the enhancements are reduced significantly.

Figure 4.16 shows MOPITT L2V3 and L2V4 ‘simulated’ day-night difference CO profiles for HDD_{peak} , over Bihar, in the month of May. It is clearly seen from L2V3 simulation results that this factor has greatest sensitivity to 700 hPa retrieval level,

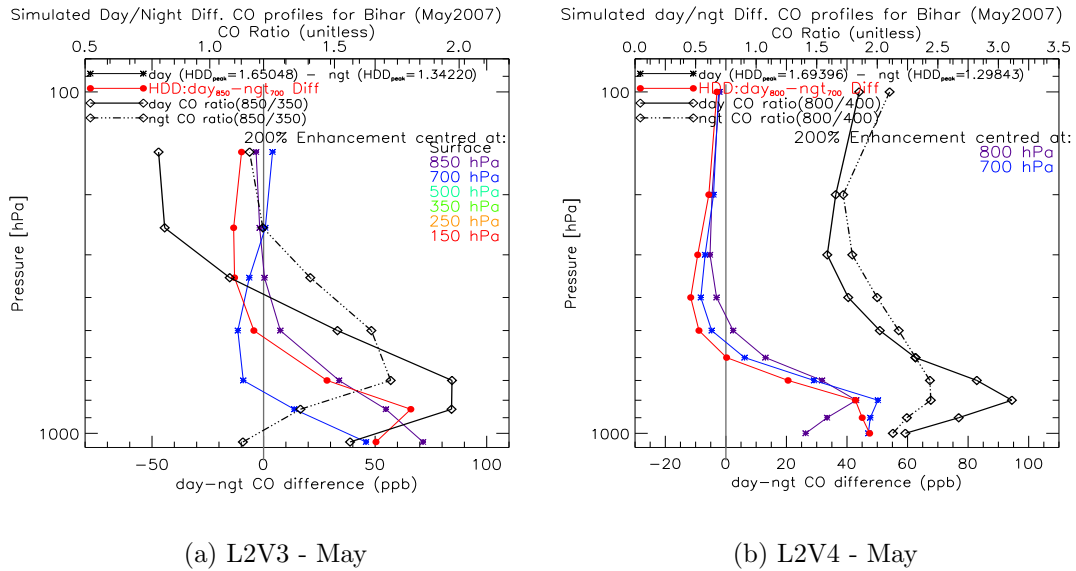


Figure 4.16: (a) MOPITT L2V3 ‘simulated’ key day-night difference CO profiles for HDD_{peak} , over Bihar, for May 2007; (b) Same as (a) except for MOPITT L2V4. The diamond solid and dash-dotted lines indicates day and night CO ratio (L2V3: 850hPa/350hPa and L2V4: 800hPa/400hPa) terms respectively. The ratio scale shown as top x-axis. The red coloured line represents $day_{850}-night_{700}$ (for L2V3) and $day_{800}-night_{700}$ (for L2V4) CO difference profiles for HDD_{peak} .

demonstrating 700 hPa day-night positive CO differences weighted to lower 2 retrieval levels in this region. Whilst, simulation shows that L2V4 have greatest sensitivity to 800 hPa, demonstrating $day_{800}-night_{700}$ positive differences weighted to lower 4 retrieval levels. Here we demonstrate for the first time that $day_{800}-night_{700}$ gives a closer differentiation of lowermost CO. Note that for L2V4 we have a priori CO profile for daytime and nighttime measurements separately which vary spatially and temporally. While L2V3 retrievals based on the same and constant global CO a priori profile. We, thus, have subtracted day and night a priori from ‘simulated’ day and night CO in case of L2V4 simulations to reflect a priori influence on the L2V4 ‘simulated’ profiles. Since the surface emissivity and CO profiles are retrieved simultaneously, the CO retrievals consequently will have a greater dependence on the a priori CO. The ratio of the CO at 800 hPa to 400 hPa (800/400) for L2V4 used, for the first time, as an index for lowermost layer enhancements, which indeed contain shape information for the MOPITT retrieved CO profile, CO peaking at 800 hPa provide more evidence for the MOPITT sensitivity to this level.

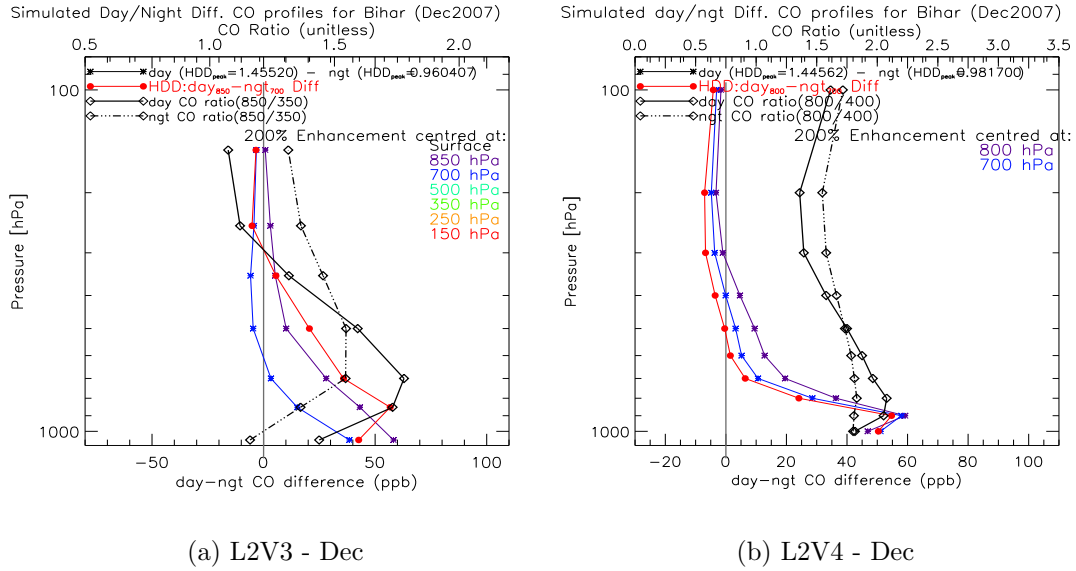


Figure 4.17: (a) MOPITT L2V3 ‘simulated’ key day-night difference CO profiles for HDD_{peak} , over Bihar, for December 2007; (b) Same as (a) except for MOPITT L2V4. The diamond solid and dash-dotted lines indicates day and night CO ratio (L2V3:850hPa/350hPa and L2V4: 800hPa/400hPa) terms respectively. The ratio scale shown as top x-axis. The red coloured line represents $day_{850}-night_{700}$ (for L2V3) and $day_{800}-night_{700}$ (for L2V4) CO difference profiles for HDD_{peak} .

Figure 4.17 shows MOPITT L2V3 and L2V4 ‘simulated’ day-night difference CO profiles for HDD_{peak} , over Bihar, in the month of December. Similar simulation results can be seen as in Fig. 4.16 for L2V3 and L2V4 except that the sensitivity weighted to slightly broad lowermost layer and MOPITT likely to have reduced sensitivity during this time, possibly due to low thermal contrast conditions.

Figure 4.18 shows MOPITT L2V3 and L2V4 calculated total column values for sample CO profile and a profile with 200% enhancements at each retrieval level forming 7 and 10 perturbed profiles respectively. The total column values are calculated using Eq. 3.1. The a priori CO profile and sample CO profile has same total column value in all cases. It can be seen that MOPITT show greatest sensitivity for daytime measurements at 700 hPa for L2V3 retrievals and at 800 hPa for L2V4 retrievals. This could be possibly due to that fact that L2V4 retrieval grid based on uniform grid spacing (in pressure) while L2V3 retrieval grid based on non uniform grid spacing (in pressure) i.e. layer are not uniformly thick. These findings are consistent with our early results.

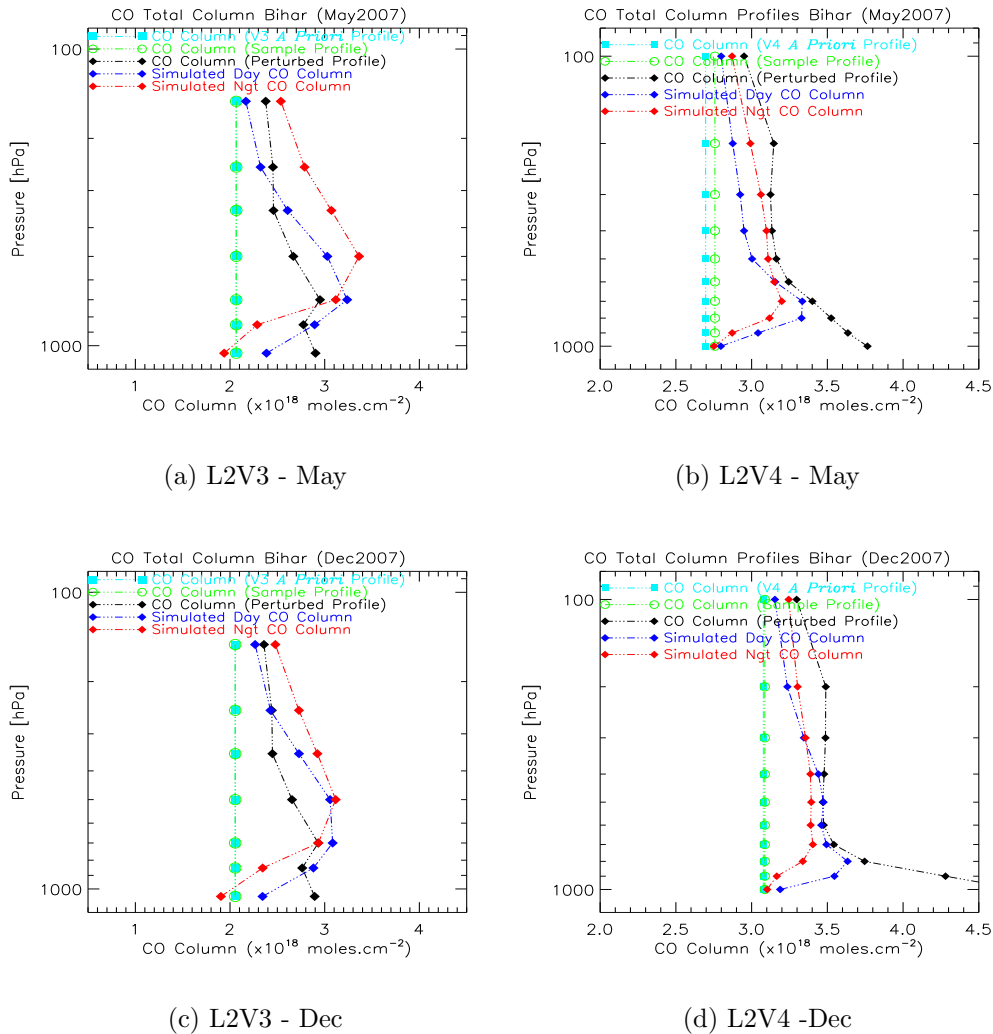


Figure 4.18: MOPITT L2V3 and L2V4 retrieval calculated total column values for i) a priori CO profile (cyan), ii) 7 individual sample profiles (green), iii) 7 individual perturbed sample profile (black), and iv) 7 individual simulated day (blue) and night (red) CO profiles, over Bihar, for May (top panel) and December (bottom panel) 2007; Note that these are not considered as profiles. For proper understanding the total column values plotted at corresponding perturbed retrieval level (layer) for each CO VMR profile.

4.5.2.2 TOMCAT Model CO Profile Simulation

We now perform MOPITT L2V3 and L2V4 simulation comparison for selected TOMCAT model CO profile as a sample profile (with no enhancements applied to it) and then by applying selected ‘typical’ averaging kernels for L2V3 and L2V4 respectively in this region. A brief overview of TOMCAT model has been given in Chapter 3.

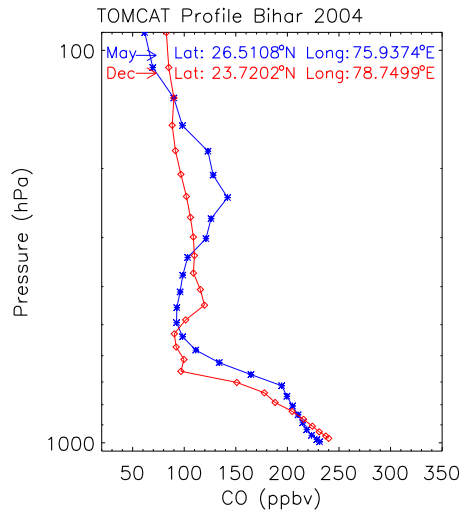
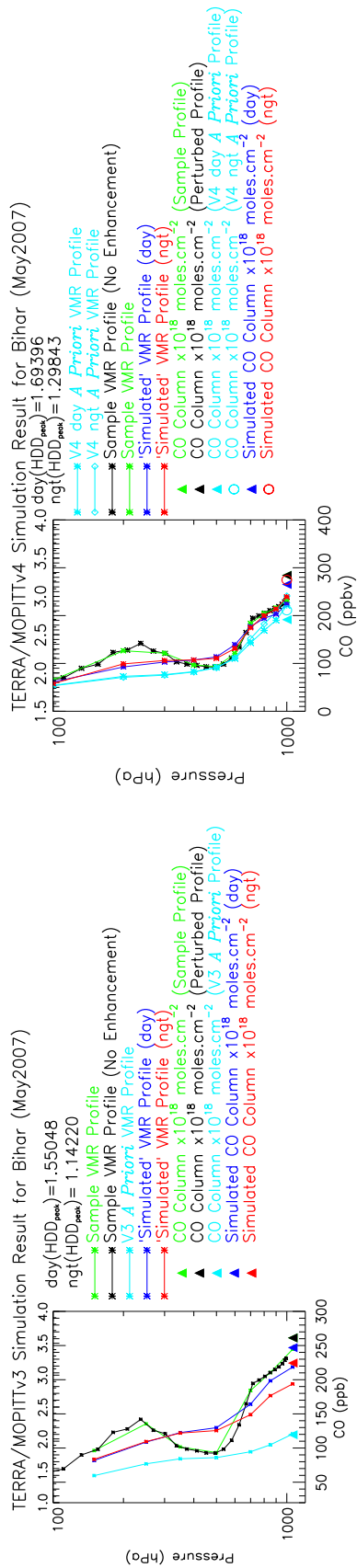
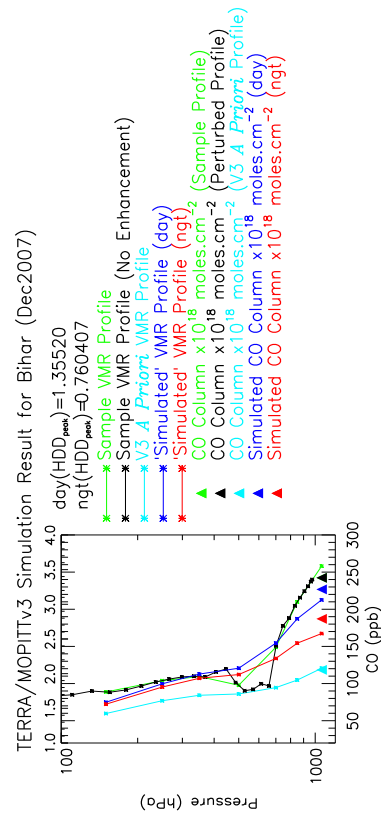


Figure 4.19: Selected TOMCAT model CO profiles, over Bihar box, for May 2004 (blue) and December 2004 (red).

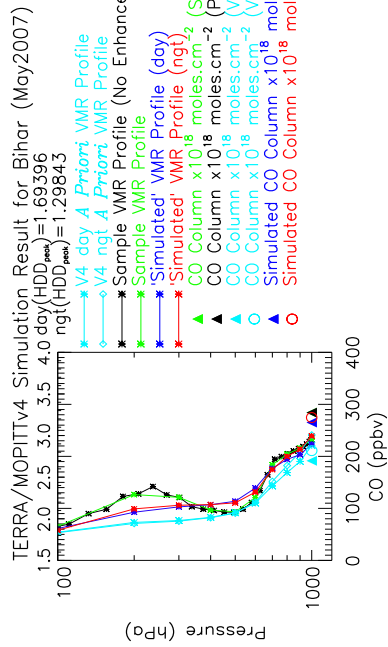
Figure 4.19 show selected TOMCAT model CO profiles, over Bihar region, in the month of May and December of 2004. The profiles were taken on the 7th of May 2004 and 19th of December 2004, located at 26.51°N latitude and 75.93°E longitude, and 23.72°N latitude and 78.74°E longitude respectively. These CO profiles are used as a sample profile for MOPITT L2V3 and L2V4 simulations. The selected ‘typical’ averaging kernel of interest was applied to these profiles using the method described in chapter 2, section 2.3.4.1. The simulation results performed for HDD_{peak} for the month of May and December are presented and discussed here.



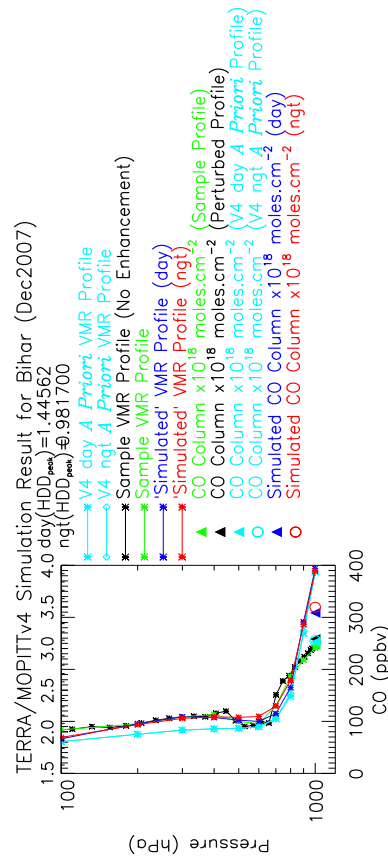
(a) L2V3 - May



(c) L2V3 - Dec



(b) L2V4 - May



(d) L2V4 - Dec

Figure 4-20: (a)MOPITT L2V3 ‘Simulated’ daytime and nighttime CO profiles for TOMCAT model selected base CO profile, over Bihar, for May 2007; (b) Same as (a) except for MOPITT L2V4; (c) Same as (a) except for December 2007; (d) Same as (a) except for MOPITT L2V4 and for December 2007.

Figure 4.20(a) and (c) show simulated CO profiles using MOPITT L2V3 selected ‘typical’ averaging kernel, over Bihar region, in the month of May and December respectively. Figure 4.20(b) and (d) show simulated CO profiles using MOPITT L2V4 selected ‘typical’ averaging kernel, over Bihar region, in the month of May and December respectively. For L2V3, daytime ‘simulated’ CO profile has greatest enhancements at lower 3 retrieval pressure levels where L2V4 ‘simulated’ daytime CO has less significant enhancements compared to nighttime ‘simulated’ CO profiles for lower 3 retrieval levels. This could be attributed to likely a priori influence on retrieved CO profile. Similar features can be seen in the month of December, suggesting that L2V4 ‘simulated’ daytime and nighttime CO profiles are weighted more by daytime and nighttime a priori profiles respectively. This needs further a priori influence analysis to effectively understand profile shape information in the MOPITT L2V4 retrieved CO profile.

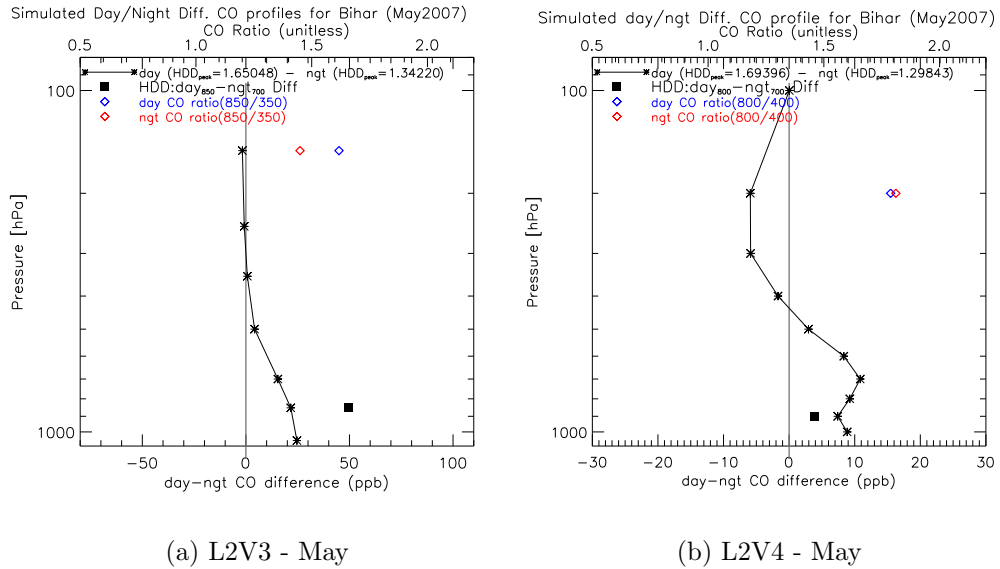


Figure 4.21: (a) MOPITT L2V3 ‘simulated’ day-night difference CO profile for HDD_{peak} , over Bihar, for May 2007; (b) Same as (a) except for MOPITT L2V4.

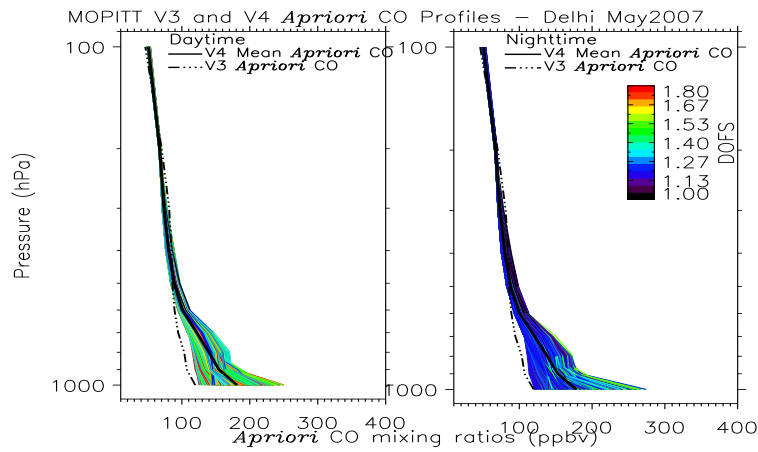
Figure 4.21 illustrates (a) L2V3 and (b) L2V4 ‘simulated’ day-night difference CO profiles for assumed more realistic TOMCAT model CO profile. For L2V3, the day-night positive differences can be seen for lower 4 retrieval levels peaking at surface retrieval level. For L2V4, however, day-night positive differences likely to provide layer enhancements at surface and a layer above it. Thus, our analysis confirms that

the MOPITT instrument indeed has significant sensitivity to the CO, in general, to the boundary layer having good thermal contrast between the lower atmosphere and underlying surface. Finally, it is worth noting that we have tested our L2V4 simulations for daytime and nighttime a priori CO VMR profiles taken as a sample profile separately, however it is reasonable to choose same and one a priori CO profile as a sample profile for our simulations (for similar atmospheric conditions).

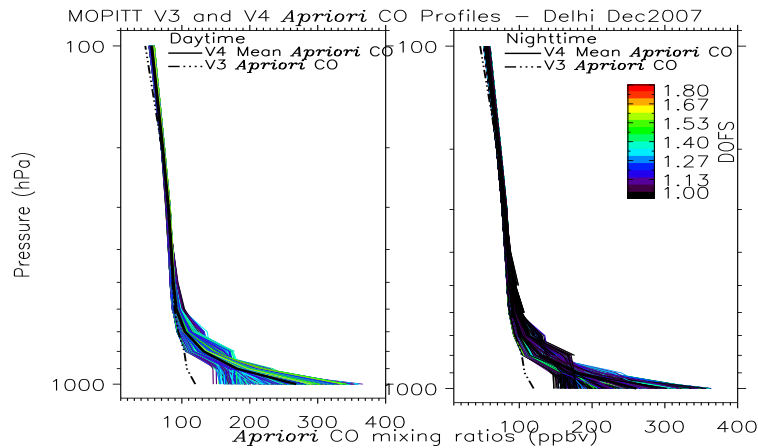
4.5.3 A Case Study of Delhi

4.5.3.1 L2V3 and L2V4 Simulations

Here, similar simulation study carried out as for Bihar region. Our earlier finding focus MOPITT L2V3 simulation for this region indeed show that MOPITT has greatest sensitivity to the lowermost layer of the troposphere. In this section, we perform comparison between MOPITT L2V3 and L2V4 retrieval simulation to better understand MOPITT sensitivity to CO in the boundary layer.



(a) L2V3 and L2V4 a priori CO - May



(b) L2V3 and L2V4 a priori CO - Dec

Figure 4.22: (a) MOPITT L2V3 and L2V4 retrievals a priori CO mixing ratio profile(s), over Delhi region, in the month of May 2007; (b) Same as (a) except for December 2007.

Figure 4.22 shows MOPITT L2V3 and L2V4 retrievals a priori CO mixing ratio profiles, over Delhi region, in the month of May and December. It can be seen that there are significant differences between L2V3 and L2V4 a priori CO profiles at lower 4 retrieval pressure levels. The a priori CO profile in both the case has similar features in the mid-upper troposphere. The averaged (day and night) a priori profile taken as a sample profile for MOPITT L2V4 simulations in this region.

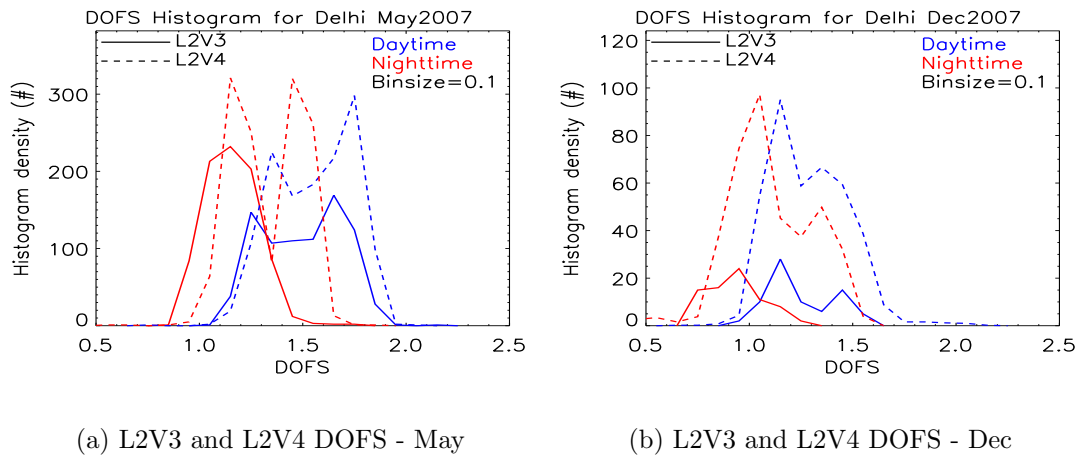
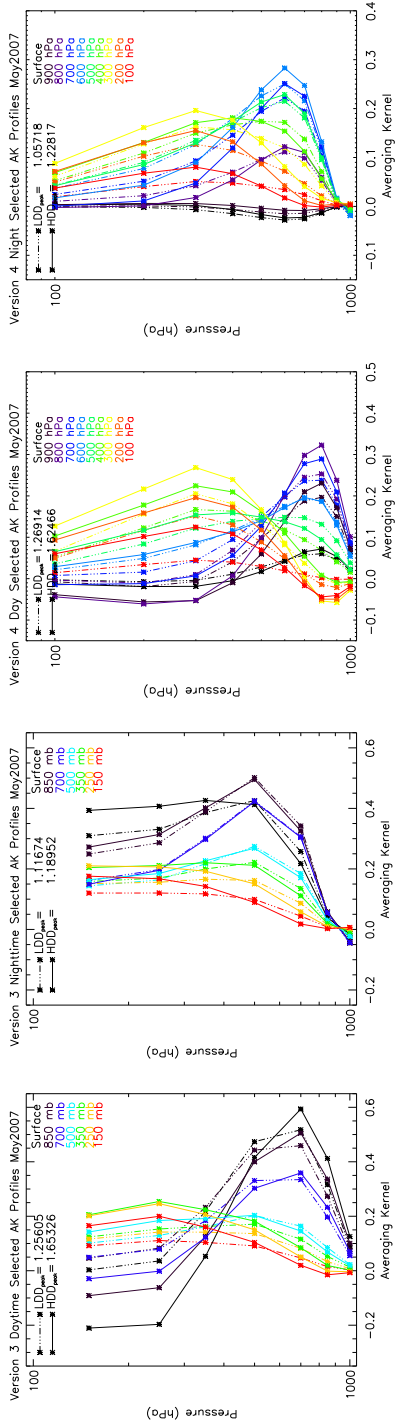


Figure 4.23: (a) MOPITT L2V3 and L2V4 DOFS histogram plot, over Delhi region, in the month of May 2007; (b) Same as (a) except for December 2007.

Figure 4.23 (a and b) shows MOPITT L2V3 and L2V4 daytime and nighttime histogram plot for DOFS, over Delhi region, for May and December 2007 respectively. It is clearly evident that L2V4 DOFS are superior to L2V3 DOFS for both the daytime and nighttime measurements as expected. It is also obvious that daytime measurements has greatest DOFS values than the nighttime measurements in both the L2V3 and L2V4 retrievals.

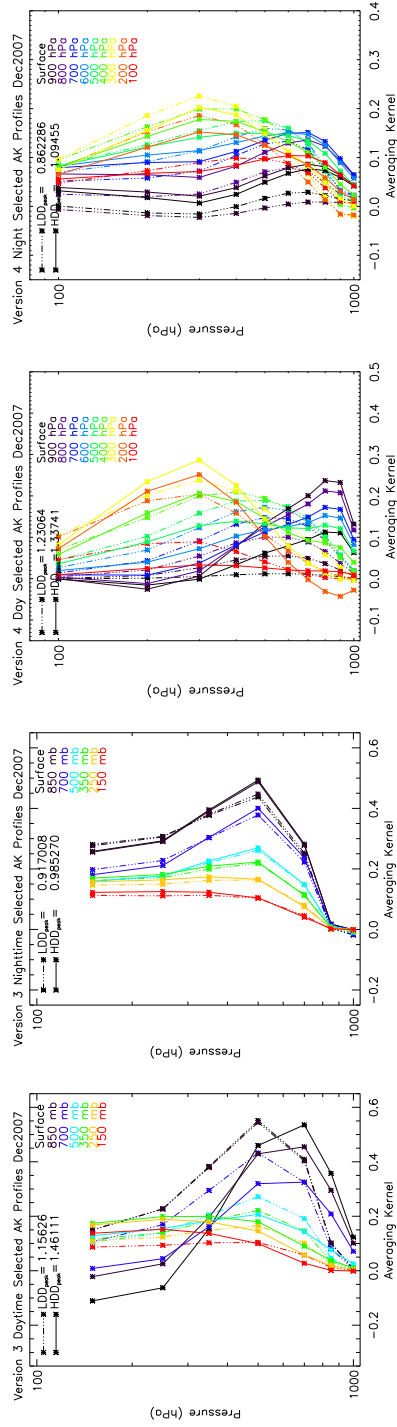


(a) L2V3 - Day AK

(b) L2V3 - Night AK

(c) L2V4 - Day AK

(d) L2V4 - Night AK



(e) L2V3 - Day AK

(f) L2V3 - Night AK

(g) L2V4 - Day AK

(h) L2V4 - Night AK

Figure 4.24: (a) MOPITT L2V3 selected daytime 'typical' averaging kernel, over Delhi region, in the month of May 2007; (b) Same as (a) except for nighttime; (c) MOPITT L2V4 selected daytime 'typical' averaging kernel, over Delhi region, in the month of May 2007; (d) Same as (c) except for nighttime; (e-f) Same as (a-d) except for December 2007.

The daytime and nighttime selected ‘typical’ averaging kernels for MOPITT L2V3 and L2V4 retrievals, over Delhi region, in the month of May (top panel) and December (bottom panel) are shown in Fig. 4.24. The nighttime MOPITT L2V3 retrievals averaging kernels in the month of May and December have similar features except for surface level averaging kernel. Due to the warm surface temperature during the day in the month of May as compared to December, the MOPITT L2V3 retrieval averaging kernels for the lower retrieval levels have peaks closer to the surface, peaking at 700 hPa retrieval pressure level. A much steeper vertical gradient in the atmospheric temperature profile are expected during summer months which probably lead to distinction between the lower and upper level averaging kernels. Similar features observed in MOPITT L2V4 CO averaging kernels except that L2V4 retrieval 800 hPa averaging peaking at corresponding level. Interestingly, the clear distinction between lower and upper level averaging kernels is clearly evident in this region.

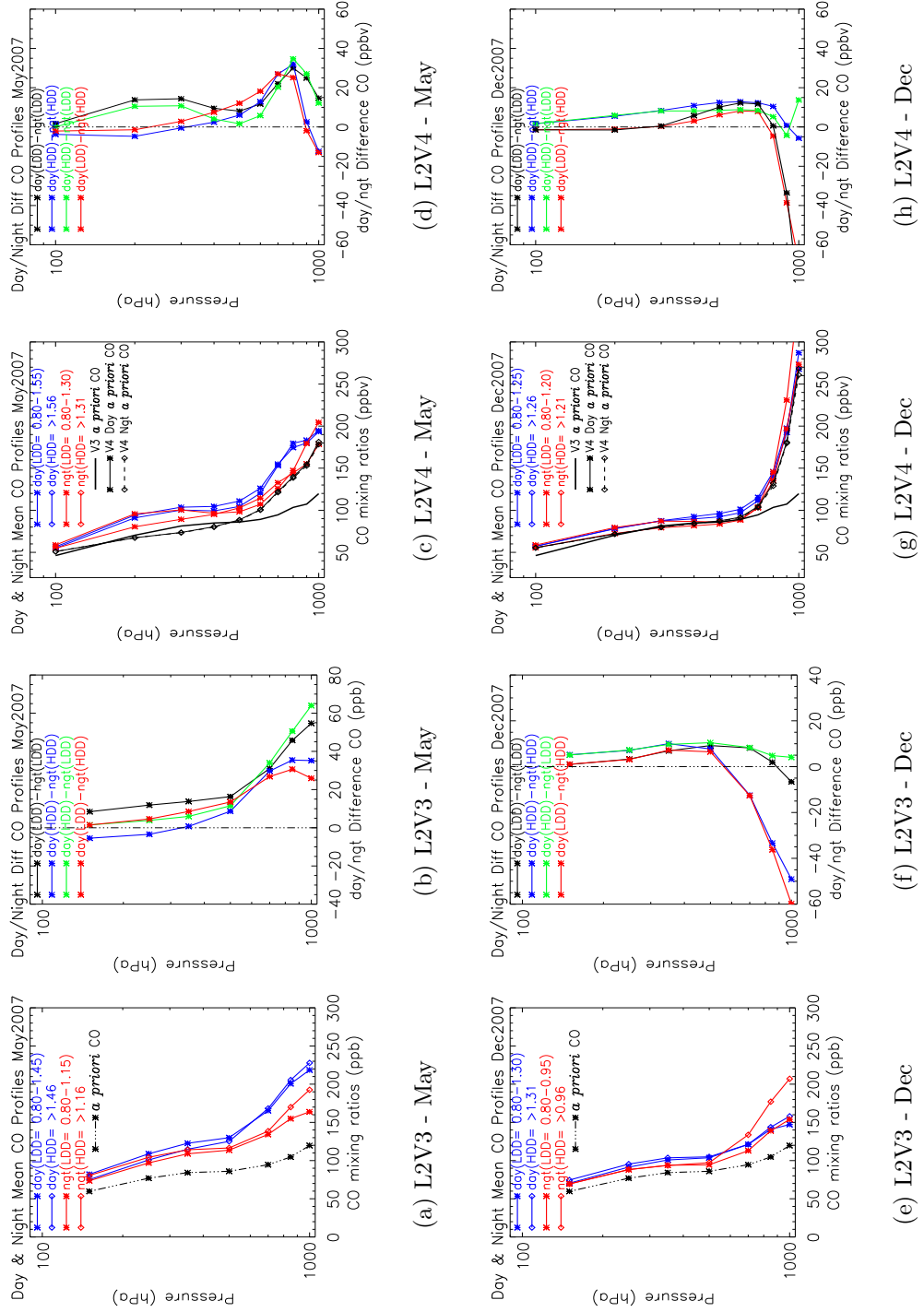
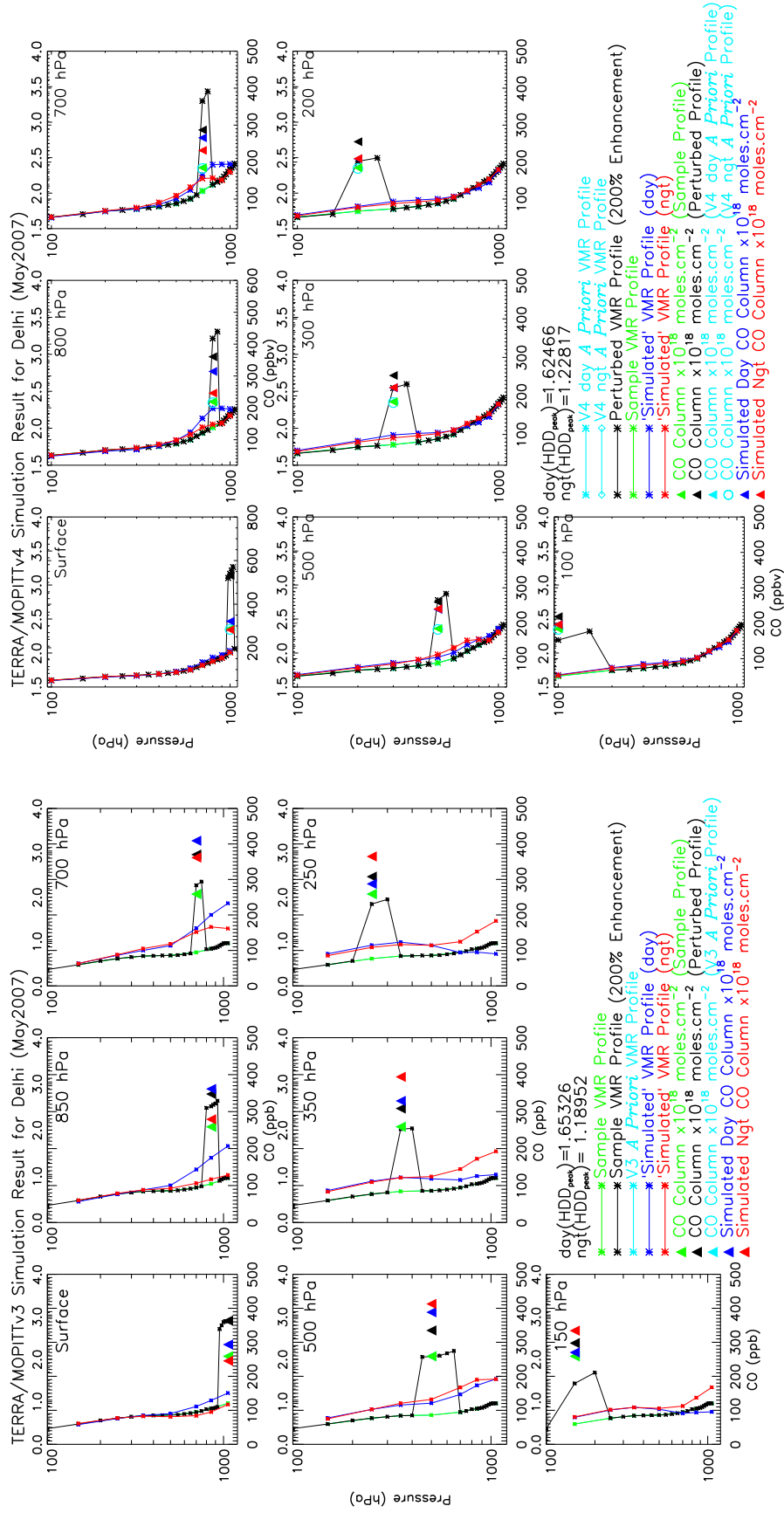


Figure 4.25: (a) MOPITT L2V3 retrieved mean daytime and nighttime CO profiles, over Delhi box, for May 2007; (b) Mean day-night difference CO profiles, over Delhi box, for combination of LDD and HDD; (c) Same as (a) except for MOPITT L2V4; (d) Same as (b) except for MOPITT L2V4; (e) Same as (a) except for December 2007; (f) Same as (b) except for December 2007; (g) Same as (c) except for December 2007; (h) Same as (d) except for December 2007;

Figure 4.25 shows MOPITT L2V3 and L2V4 retrieved daytime and nighttime mean CO profiles calculated for both the LDD and HDD and their resultant day-night difference CO profiles in the month of May (top panel) and December (bottom panel). It is obvious that retrieved day-night CO difference profiles have similar features as in case of Bihar region showing combination of selected LDD and HDD can be separated into two equivalent groups. For L2V3, the retrieved CO profile for HDD has significant enhancements in the lowermost layer for night data while very small enhancements in the lowermost layer for day data. It should be noted that there are significant differences in the retrieved day-night difference CO profiles for L2V3 and L2V4 retrievals. For L2V3, day(HDD)-ngt(LDD) and day(HDD)-ngt(HDD) difference profiles have highest positive differences at surface. For L2V4, these two difference profiles indeed have highest positive differences peaking at two retrieval levels, i.e. 800 hPa and 200 hPa. In the month of December, whereas both the L2V3 and L2V4 difference profiles have more or less similar features showing differences close to zero at surface and flat profile throughout the troposphere. No significant enhancements in the middle-upper troposphere are observed.

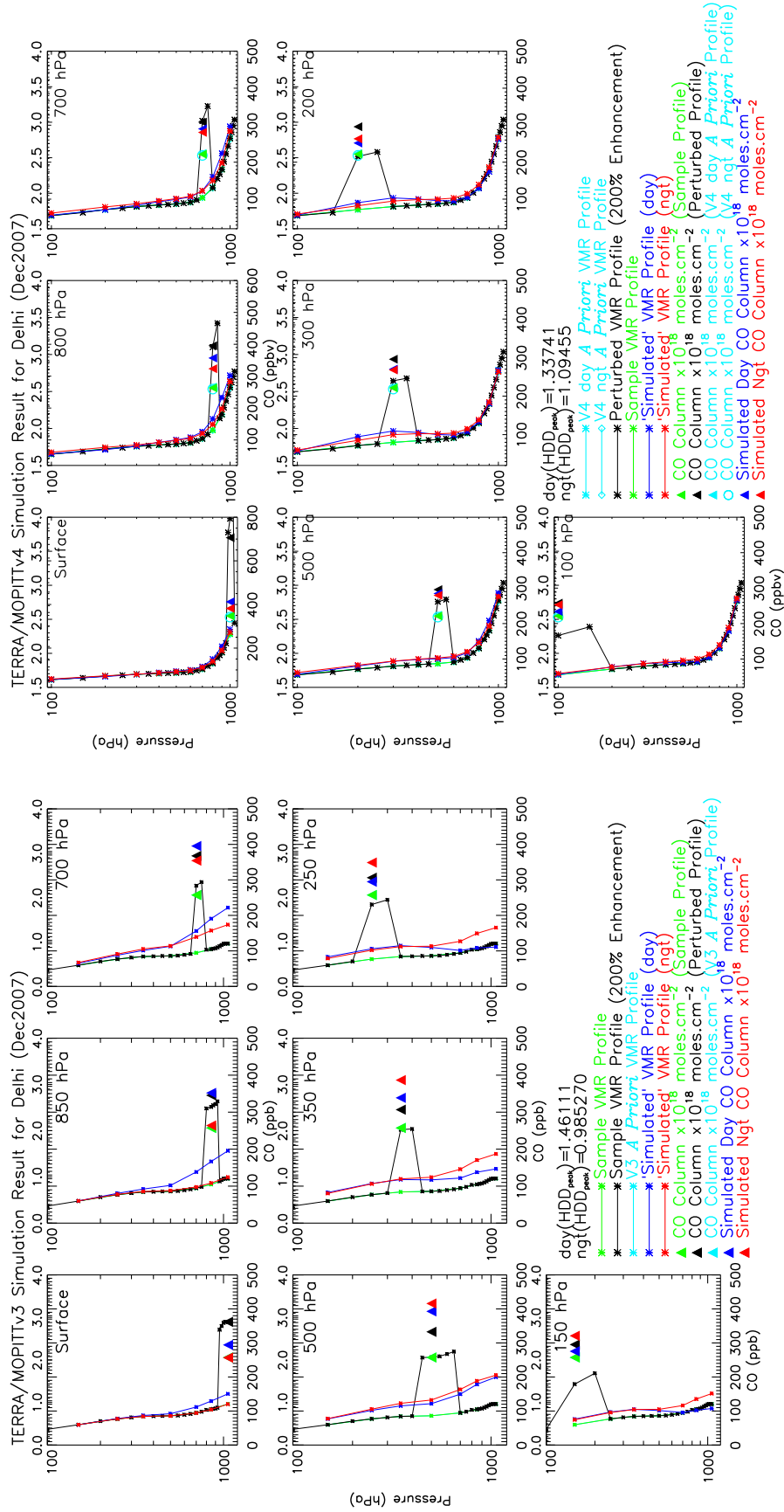
Figure 4.26 and 4.27 shows simulation results for L2V3 and L2V4, in this region, for May and December respectively. In general similar simulation results observed in this region as compared to Bihar region with less significant differences in the ‘simulated’ daytime and nighttime CO profiles. The total columns for sample and simulated profiles are shown by coloured triangles.



(a) L2V3 - May

(b) L2V4 - May

Figure 4.26: (a) MOPITT L2V3 'simulated' daytime and nighttime CO profiles for HDD_{peak} over Delhi, for May 2007; (b) Same as (a) except for MOPITT L2V4. The green, black, cyan, blue, and red line indicates the considered sample CO profile, perturbed CO profile, a priori CO profile, 'simulated' day CO profile, and 'simulated' night CO profile. The green, black, cyan, blue, and red triangles show calculated total column values for corresponding CO VMR profiles.



(a) L2V3 - Dec

(b) L2V4 - Dec

Figure 4.27: (a) MOPITT L2V3 ‘simulated’ daytime and nighttime CO profiles for HDD_{peak}, over Delhi, for December 2007; (b) Same as (a) except for MOPITT L2V4. The green, black, cyan, blue, and red line indicates the considered sample CO profile, perturbed CO profile, a priori CO profile, ‘simulated’ day CO profile, and ‘simulated’ night CO profile. The green, black, cyan, blue, and red triangles show calculated total column values for corresponding CO VMR profiles.

Over Delhi region, a 200% enhancement in the surface level CO barely captured in the retrieved MOPITT L2V4 profile. For L2V3, however, small enhancements can be seen for lower 3 retrieval levels for daytime measurements (refer to Fig. 4.26(b and a) top right corner plot). An enhancement of 200% between 775 hPa and 650 hPa which covers the 700 hPa MOPITT L2V3 retrieval pressure level show an enhancement at all retrieval levels with greatest effect evident in the lowest 3 retrieval levels for both the daytime and nighttime retrieved profiles in the month of May. However, an enhancement of 200% between 750 hPa and 650 hPa which covers the 700 hPa MOPITT L2V4 retrieval pressure level show an enhancement at lower 2 equivalent retrieval levels compared to L2V3. For nighttime measurements, L2V3 retrieval simulation indeed show enhancements for lower 3 retrieval levels whereas for L2V4, no enhancements can be seen at lower 2 retrieval levels. This can be further seen by looking at ‘simulated’ total column values for these profiles. The perturbation in the upper troposphere produce significant enhancements in the ‘simulated’ nighttime profile at lower 3 retrieval levels for L2V3 whereas there are no significant enhancement for L2V4 simulations in the nighttime ‘simulated’ CO profile. Moreover similar simulation results can be seen in the month of December (refer Fig. 4.27) except that the enhancements are reduced significantly.

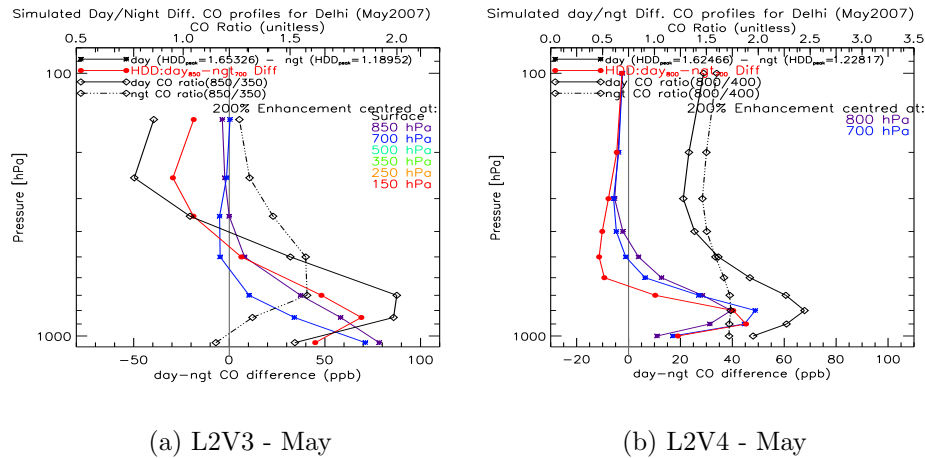


Figure 4.28: (a) MOPITT L2V3 ‘simulated’ key day-night difference CO profiles for HDD_{peak} , over Delhi, for May 2007; (b) Same as (a) except for MOPITT L2V4. The diamond solid and dash-dotted lines indicates day and night CO ratio (L2V3: 850hPa/350hPa and L2V4: 800hPa/400hPa) terms respectively. The ratio scale shown as top x-axis. The red coloured line represents $day_{850}-night_{700}$ (for L2V3) and $day_{800}-night_{700}$ (for L2V4) CO difference profiles for HDD_{peak} .

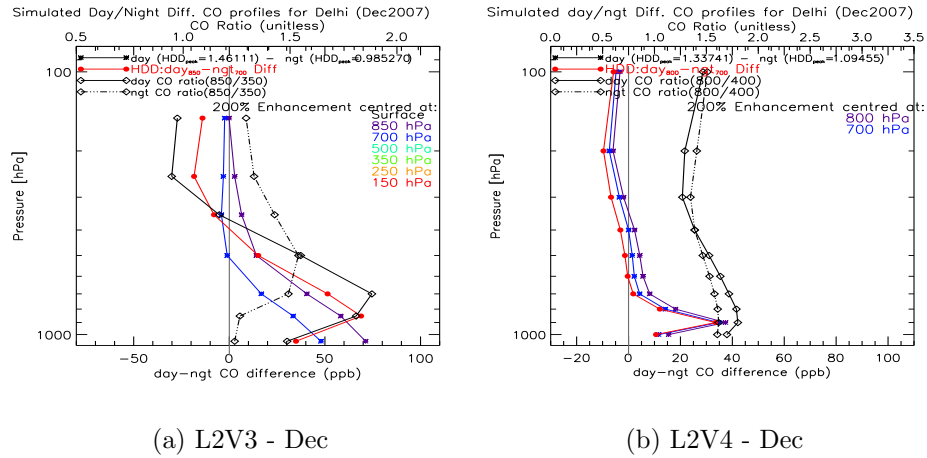
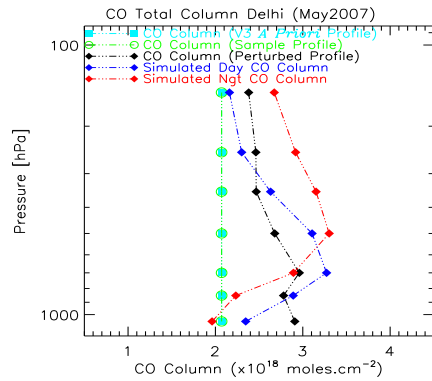


Figure 4.29: (a) MOPITT L2V3 ‘simulated’ key day-night difference CO profiles for HDD_{peak} , over Delhi, for December 2007; (b) Same as (a) except for MOPITT L2V4.

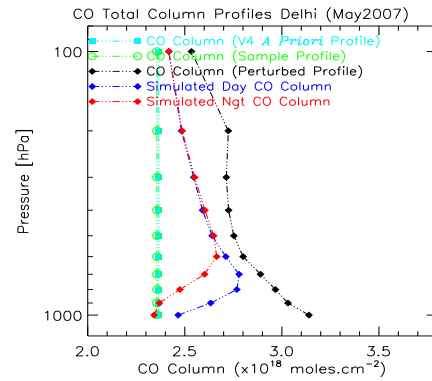
Figure 4.28 shows MOPITT L2V3 and L2V4 ‘simulated’ day-night difference CO profiles for HDD_{peak} , over Delhi, in the month of May. It is clearly seen from L2V3 simulation results that MOPITT indeed has greatest sensitivity to 700 hPa retrieval level, demonstrating 700 hPa day-night positive CO differences weighted to lower 2 retrieval levels in this region. For L2V4, $day_{800}-ngt_{700}$ difference profile has highest positive differences at surface peaking at 800 hPa and weighted to lower 4 retrieval pressure levels indeed show that MOPITT has greatest sensitivity to this level in this region. The ratio of the CO at 800 hPa to 400 hPa (800/400) for L2V4 show similar features as observed for Bihar region confirming that MOPITT has significant sensitivity to lowermost layer in this region and one can able to detect CO in layers.

Figure 4.29 shows MOPITT L2V3 and L2V4 ‘simulated’ day-night difference CO profiles for HDD_{peak} , over Delhi, in the month of December. Similar simulation results can be seen compared to month of May except that sensitivity significantly reduced further in the month of December.

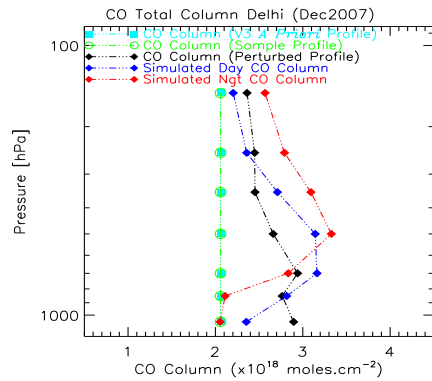
Figure 4.30 shows MOPITT L2V3 and L2V4 calculated total column values for sample CO profile with 200% enhancements at each retrieval level forming 7 and 10 perturbed profiles respectively. It can be further confirmed for this result that MOPITT has greatest sensitivity for daytime measurements at 700 hPa for L2V3 retrievals and at 800 hPa for L2V4 retrievals in this region.



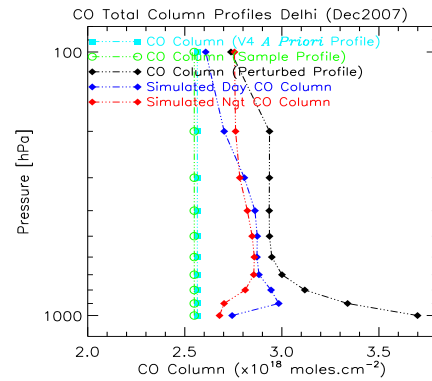
(a) L2V3 - May



(b) L2V4 - May



(c) L2V3 - Dec



(d) L2V4 -Dec

Figure 4.30: MOPITT L2V3 and L2V4 retrieval calculated total column values for i) a priori CO profile (cyan), ii) 7 individual sample profiles (green), iii) 7 individual perturbed sample profile (black), and iv) 7 individual simulated day (blue) and night (red) CO profiles, over Delhi, for May (top panel) and December (bottom panel) 2007.

4.5.3.2 TOMCAT Model CO Profile Simulation

Similar MOPITT L2V4 simulation for TOMCAT model CO profile has been performed in this region as in case of Bihar region and compared with MOPITT L2V3 simulations to improve our knowledge about CO in this region. A profile over Delhi box was selected to represent a case where our analysis suggesting the location of a CO source region in the month of May and December. The profiles were taken on the 5th of May 2004 and 12th of December 2004, located at 28.51°N latitude and 77.56°E longitude.

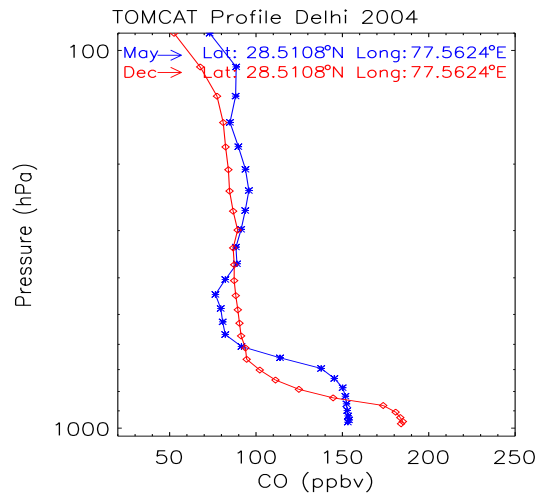
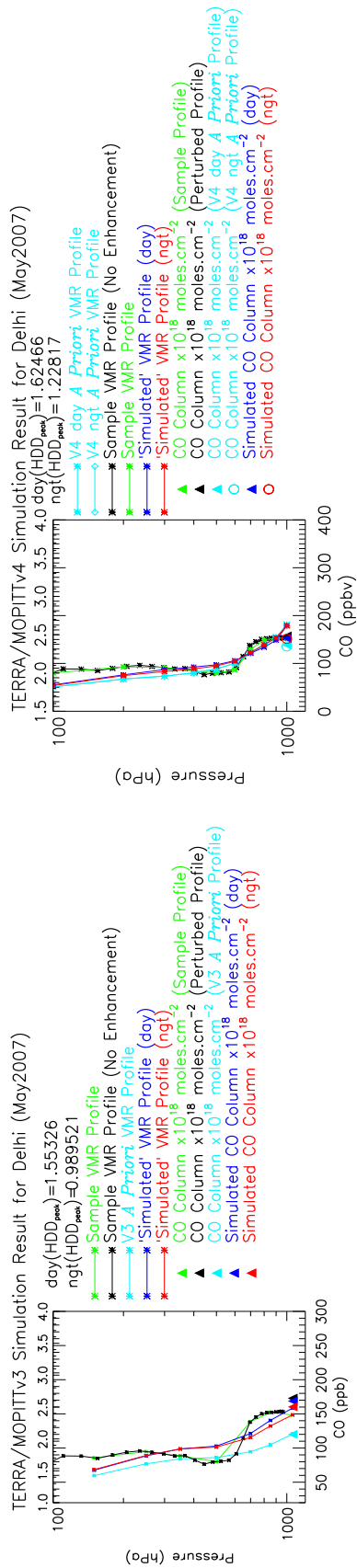
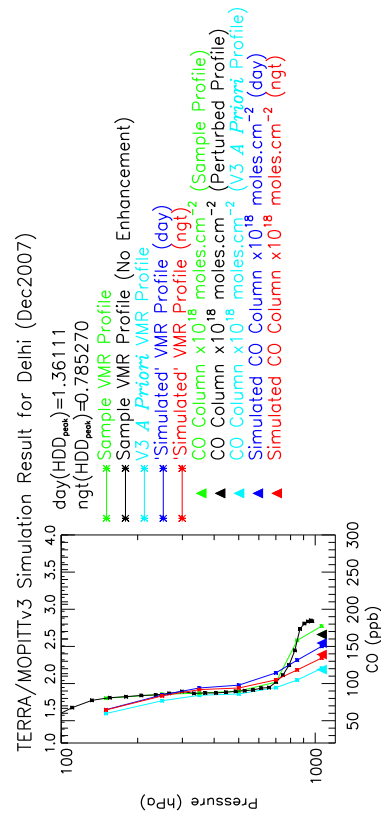


Figure 4.31: Selected TOMCAT model CO profiles, over Delhi box, for May 2004 (blue) and December 2004 (red).

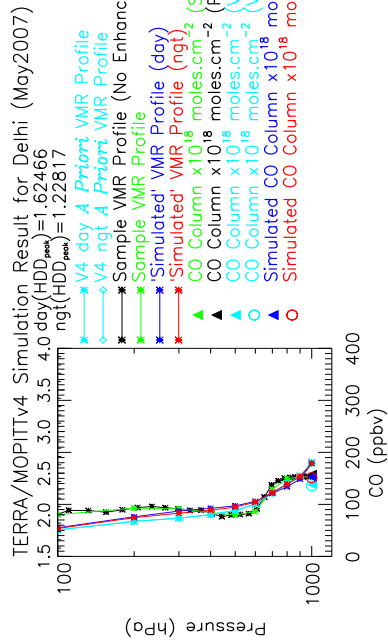
Figure 4.31 show selected TOMCAT model CO profiles, over Delhi region, in the month of May and December of 2004. These CO profiles are used as a sample profile for MOPITT L2V3 and L2V4 simulations. Note that no enhancements applied to these profiles, in practice therefore we will have only one modeled test profile instead of 7 test profiles as incase L2V3 a priori CO profile simulation and 10 test profiles as incase of L2V4 a priori CO profile simulation. The selected ‘typical’ averaging kernel of interest was then applied to these profiles.



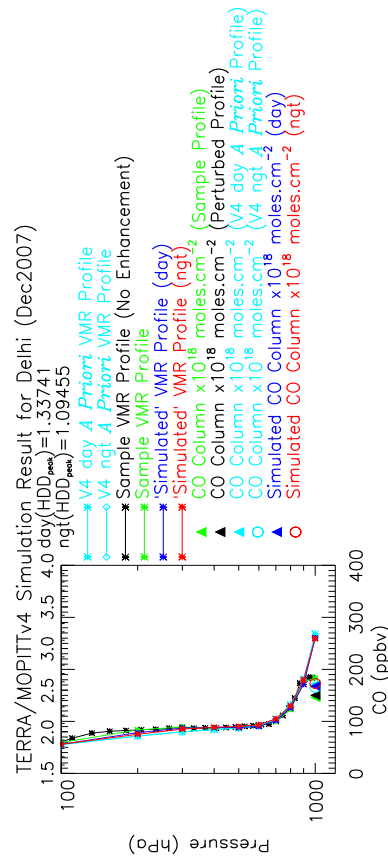
(a) L2V3 - May



(c) L2V3 - Dec



(b) L2V4 - May



(d) L2V4 - Dec

Figure 4.32: (a)MOPITT L2V3 ‘Simulated’ daytime and nighttime CO profiles for TOMCAT model selected base CO profile, over Delhi, for May 2007; (b) Same as (a) except for MOPITT L2V4; (c) Same as (a) except for December 2007; (d) Same as (a) except for MOPITT L2V4 and for December 2007.

Figure 4.32(a) and (c) show simulated CO profiles using MOPITT L2V3 selected ‘typical’ averaging kernel, over Delhi region, in the month of May and December respectively. Figure 4.32(b) and (d) show simulated CO profiles using MOPITT L2V4 selected ‘typical’ averaging kernel, over Delhi region, in the month of May and December respectively. For L2V3, daytime ‘simulated’ CO profile has significant enhancements at lower 3 retrieval levels in the month of May and lower 4 retrieval levels in the month of December. MOPITT L2V4 ‘simulated’ daytime CO has no enhancements compared to nighttime ‘simulated’ CO profile in the lower 3 retrieval levels.

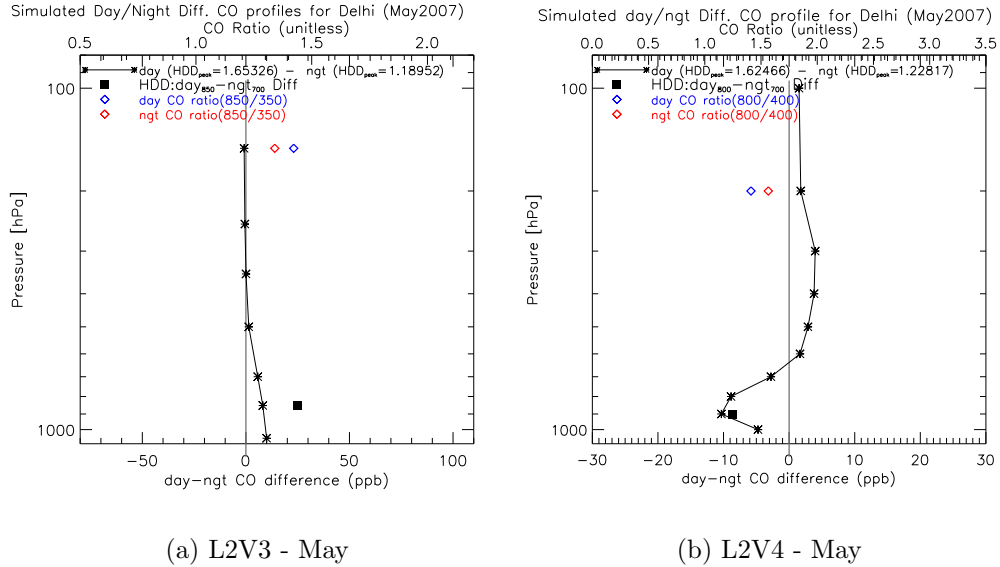


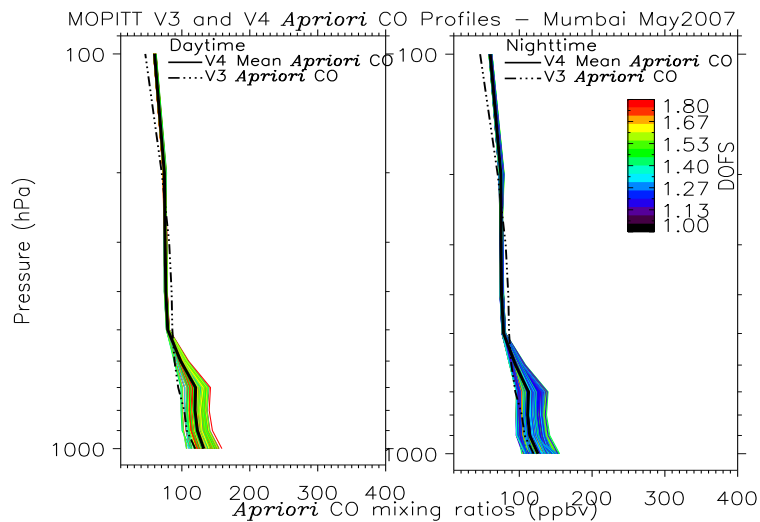
Figure 4.33: (a) MOPITT L2V3 ‘simulated’ day-night difference CO profile for HDD_{peak} , over Delhi, for May 2007; (b) Same as (a) except for MOPITT L2V4.

Figure 4.33 illustrates (a) L2V3 and (b) L2V4 ‘simulated’ day-night difference CO profiles for assumed more realistic TOMCAT model CO profile. For L2V3, the day-night positive differences can be seen for lower 4 retrieval levels peaking at surface retrieval level. For L2V4, however, day-night differences are negative for lower 4 retrieval levels, suggesting that MOPITT L2V4 likely to have less significant sensitivity to the CO in the boundary layer.

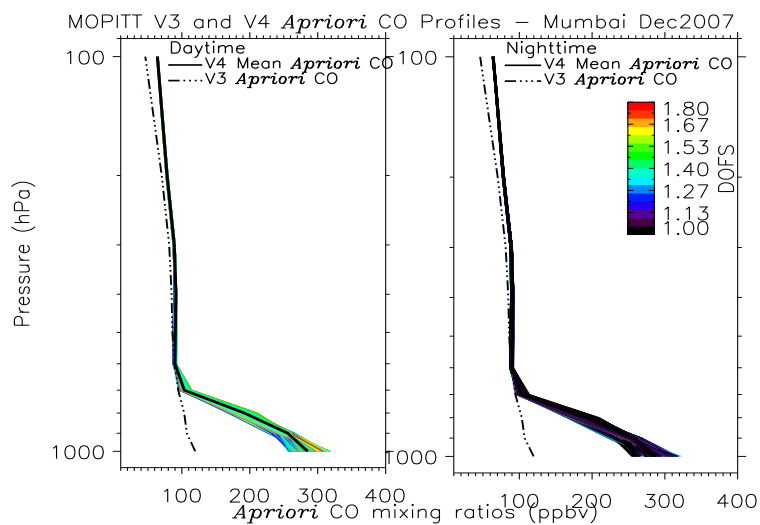
4.5.4 A Case Study of Mumbai

4.5.4.1 L2V3 and L2V4 Simulations

In this section, MOPITT L2V4 simulations performed over Mumbai region and compared with our earlier findings of MOPITT L2V3 simulation in this region.



(a) L2V3 and L2V4 a priori CO - May



(b) L2V3 and L2V4 a priori CO - Dec

Figure 4.34: (a) MOPITT L2V3 and L2V4 retrievals a priori CO mixing ratio profile(s), over Mumbai region, in the month of May 2007; (b) Same as (a) except for December 2007.

Figure 4.34 shows MOPITT L2V3 and L2V4 retrievals a priori CO mixing ratio profiles, over Mumbai region, in the month of May and December. A very different features in MOPITT L2V4 a priori CO can be seen. In the month of May, the MOPITT L2V3 and L2V4 a priori CO profiles are very much similar with only minor difference in lowermost layer. There are quite large differences in L2V3 and L2V4 a priori CO at lower 4 retrieval level in the month of December.

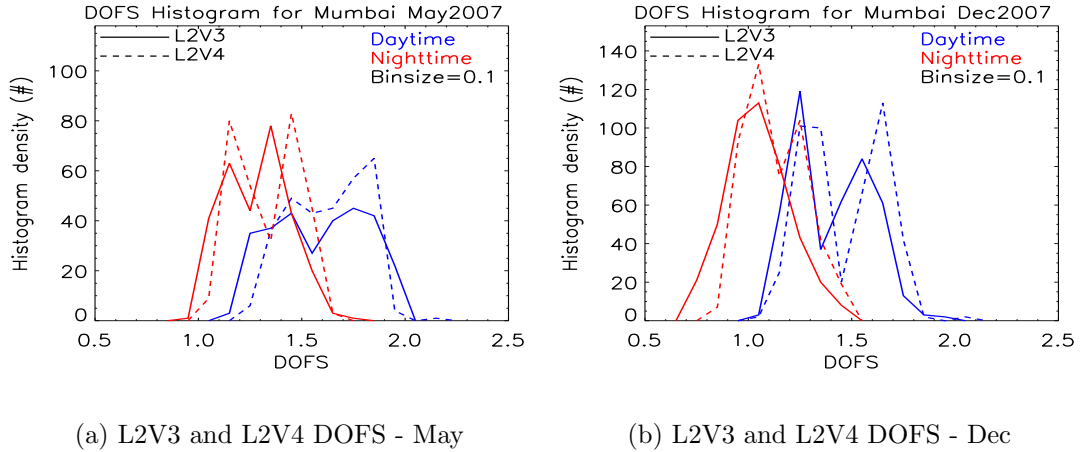
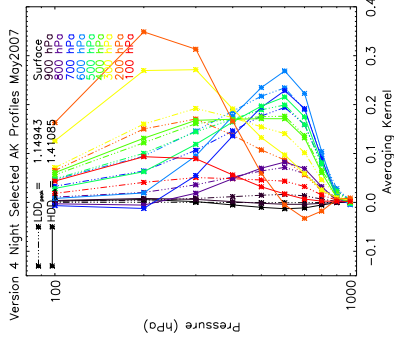
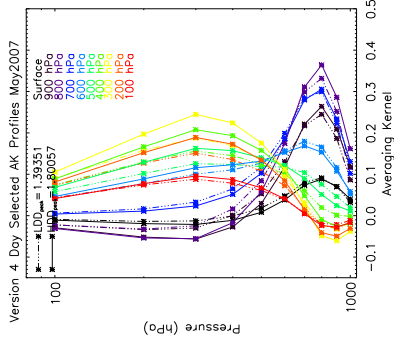


Figure 4.35: (a) MOPITT L2V3 and L2V4 DOFS histogram plot, over Mumbai region, in the month of May 2007; (b) Same as (a) except for December 2007.

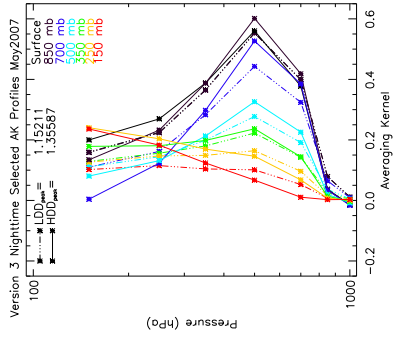
Figure 4.35 (a, b) shows MOPITT L2V3 and L2V4 daytime and nighttime histogram plot for DOFS, over Mumbai region, for May and December 2007. For Mumbai region, both the L2V3 and L2V4 daytime and nighttime DOFS has two distinct distributions except for nighttime L2V3 retrieved DOFS values. It is clearly evident that L2V4 DOFS are superior to L2V3 DOFS for both the daytime and nighttime measurements.



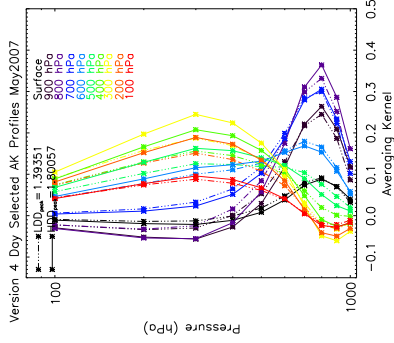
(a) L2V3 - Day AK



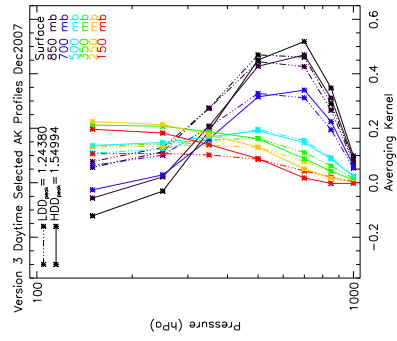
(b) L2V3 - Night AK



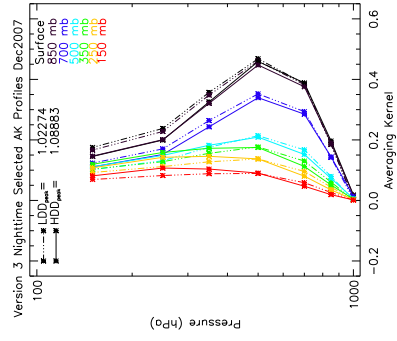
(c) L2V4 - Day AK



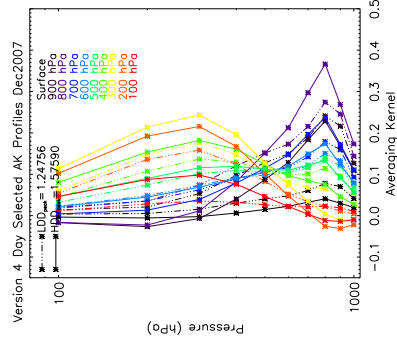
(d) L2V4 - Night AK



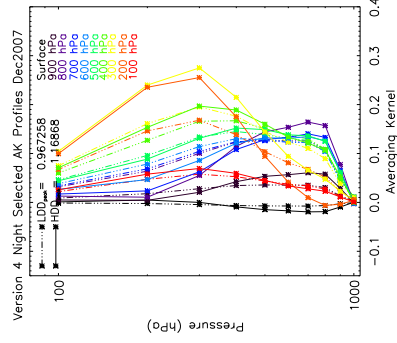
(e) L2V3 - Day AK



(f) L2V3 - Night AK



(g) L2V4 - Day AK



(h) L2V4 - Night AK

Figure 4.36: (a) MOPITT L2V3 selected daytime 'typical' averaging kernel, over Mumbai region, in the month of May 2007; (b) Same as (a) except for nighttime; (c) MOPITT L2V4 selected daytime 'typical' averaging kernel, over Mumbai region, in the month of May 2007; (d) Same as (c) except for nighttime; (e-f) Same as (a-b) except for December 2007.

Figure 4.36 shows daytime and nighttime MOPITT L2V3 and L2V4 CO retrievals selected ‘typical’ averaging kernels, over Mumbai region, for May (top panel) and December (bottom panel). It can be seen that MOPITT L2V3 retrieval CO averaging kernels for LDD and HDD in the month of December are very similar, it is due to the fact that nighttime DOFS has only one board peak for which we have selected LDD and HDD. In fact LDD_{peak} and HDD_{peak} values found to be lie closely.

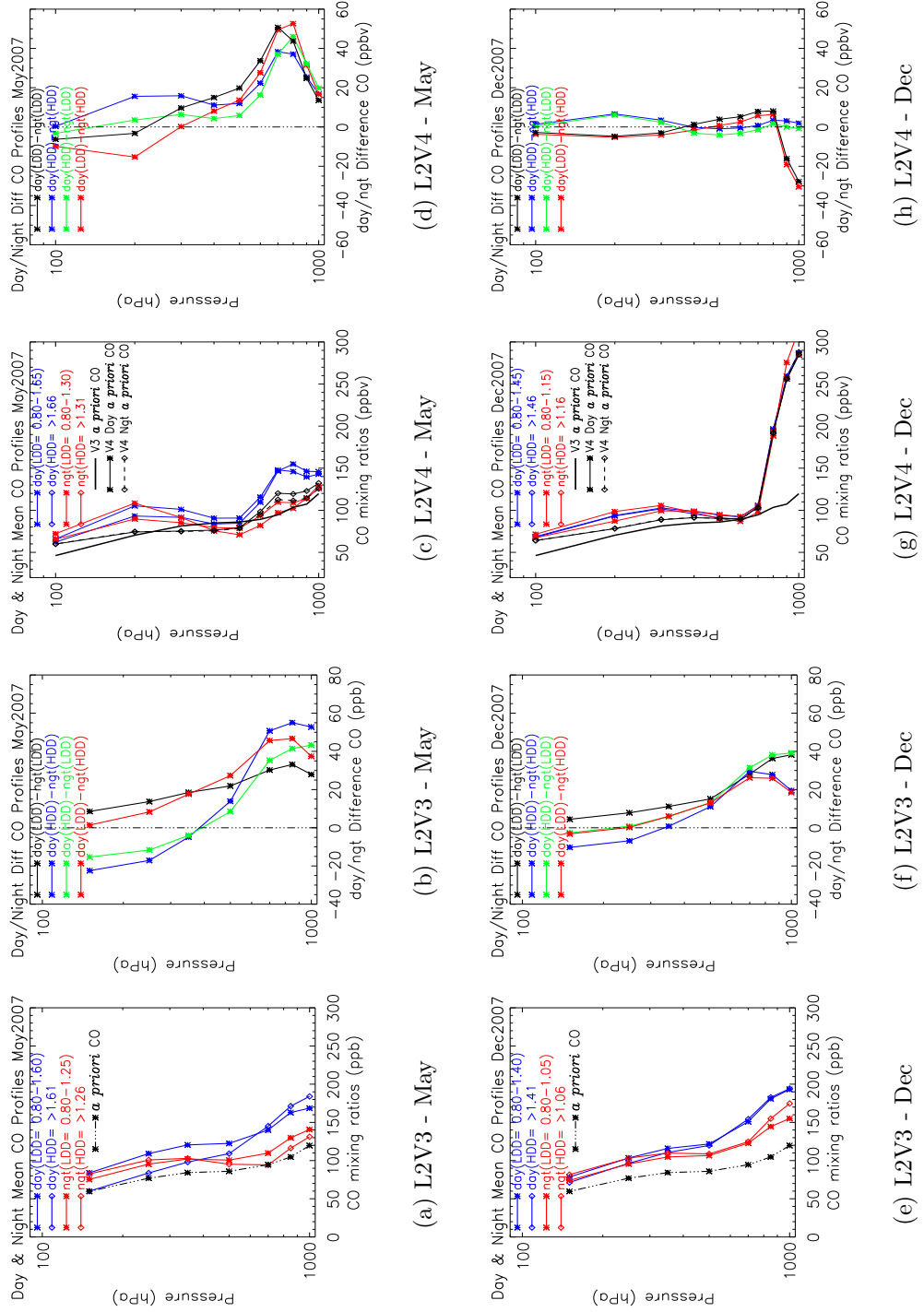
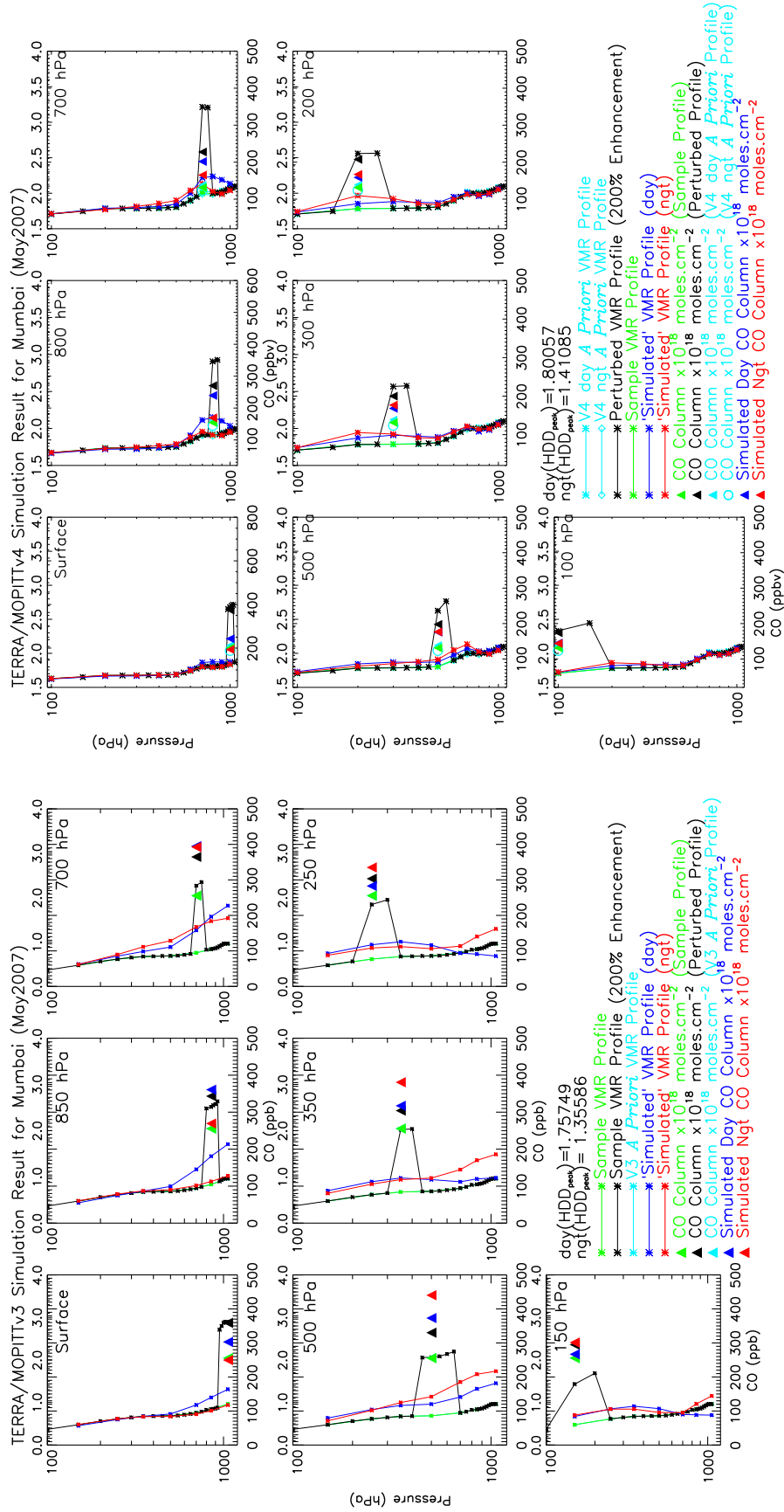


Figure 4.37: (a) MOPITT L2V3 retrieved mean daytime and nighttime CO profiles, over Mumbai box, for May 2007; (b) Mean day-night difference CO profiles, over Mumbai box, for combination of LDD and HDD; (c) Same as (a) except for MOPITT L2V4; (d) Same as (b) except for MOPITT L2V4; (e) Same as (a) except for December 2007; (f) Same as (b) except for December 2007; (g) Same as (c) except for December 2007; (h) Same as (d) except for December 2007;

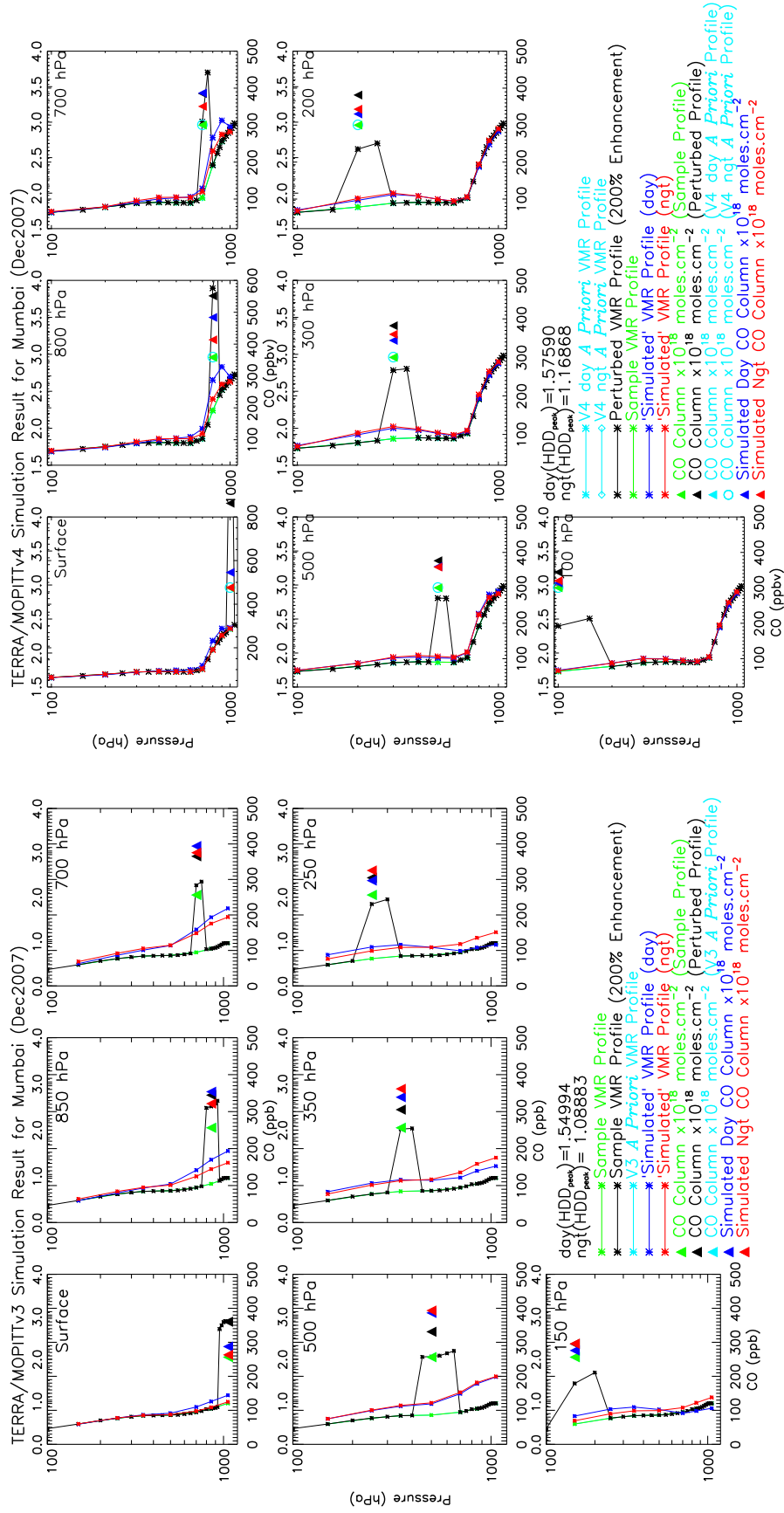
Figure 4.37 shows MOPITT L2V3 and L2V4 retrieved daytime and nighttime mean CO profiles calculated for both the LDD and HDD and their resultant day-night difference CO profiles in the month of May (top panel) and December (bottom panel). The L2V3 and L2V4 retrieved mean CO profiles in this regions have similar features as seen in earlier discussion except that in the month of May, the combination of selected LDD and HDD can not be separated into two groups as observed earlier.



(a) L2V3 - May

(b) L2V4 - May

Figure 4.38: (a) MOPITT L2V3 ‘simulated’ daytime and nighttime CO profiles for HDD_{peak} over Mumbai, for May 2007; (b) Same as (a) except for MOPITT L2V4. The green, black, cyan, blue, and red line indicates the considered sample CO profile, perturbed CO profile, a priori CO profile, ‘simulated’ day CO profile, and ‘simulated’ night CO profile. The green, black, cyan, blue, and red triangles show calculated total column values for corresponding CO VMR profiles.



(a) L2V3 - Dec

(b) L2V4 - Dec

Figure 4.39: (a) MOPITT L2V3 ‘simulated’ daytime and nighttime CO profiles for HDD_{peak} over Mumbai, for December 2007; (b) Same as (a) except for MOPITT L2V4. The green, black, cyan, blue, and red line indicates the considered sample CO profile, perturbed CO profile, a priori CO profile, ‘simulated’ day CO profile, and ‘simulated’ night CO profile. The green, black, cyan, blue, and red triangles show calculated total column values for corresponding CO VMR profiles.

Figure 4.38 and 4.39 shows simulation results for L2V3 and L2V4 in the month of May and December respectively. Similar MOPITT L2V4 simulation performed in this region as incase of Bihar region. The simulation results are shown for HDD_{peak} . In this region, comparable simulation results obtained as observed for Bihar region with less significant differences. This is also clearly evident by looking at selected ‘typical’ MOPITT CO averaging kernels which are moreorless very similar to Bihar region. It is, in turn, confirming utility to our simulation methodology to study CO in lowermost layer of the atmosphere.

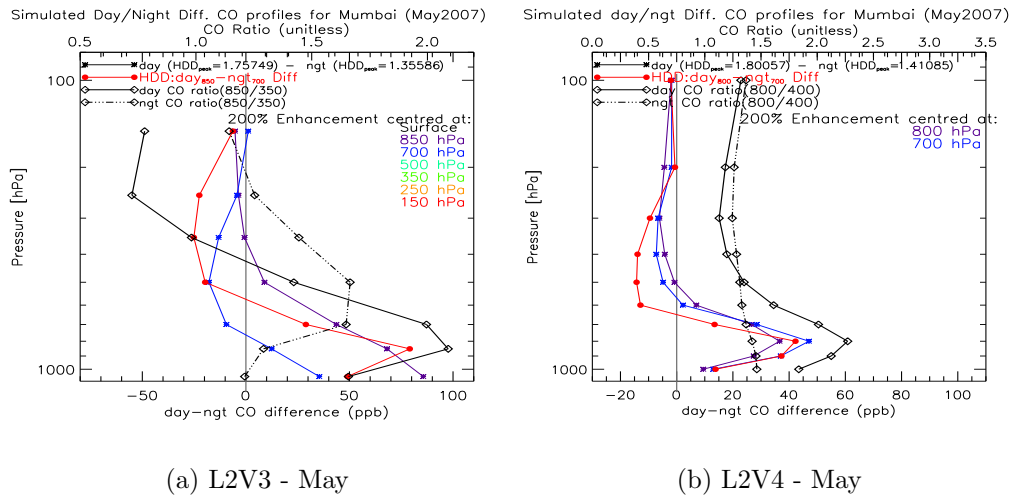


Figure 4.40: (a) MOPITT L2V3 ‘simulated’ key day-night difference CO profiles for HDD_{peak} , over Mumbai, for May 2007; (b) Same as (a) except for MOPITT L2V4. The diamond solid and dash-dotted lines indicates day and night CO ratio (L2V3: 850hPa/350hPa and L2V4: 800hPa/400hPa) terms respectively. The ratio scale shown as top x-axis. The red coloured line represents day₈₅₀-night₇₀₀ (for L2V3) and day₈₀₀-night₇₀₀ (for L2V4) CO difference profiles for HDD_{peak} .

Figure 4.40 shows MOPITT L2V3 and L2V4 ‘simulated’ day-night difference CO profiles for HDD_{peak} , over Mumbai, in the month of May. It is clearly seen from L2V3 simulation results that MOPITT indeed has greatest sensitivity to 700 hPa retrieval level, demonstrating 700 hPa day-night positive CO differences weighted to lower 2 retrieval levels in this region. Whilst, L2V4 simulation results shows that MOPITT likely to have greatest sensitivity to 800 hPa, demonstrating day₈₀₀-ngt₇₀₀ positive differences weighted to lower 4 retrieval levels which is equivalent lowermost sensitivity to L2V3. Our analysis, thus, demonstrate utility to day₈₀₀-ngt₇₀₀ for the first time to differentiate lowermost layer of CO. Additionally, the ratio of the CO

at 800 hPa to 400 hPa (800/400) provides more evidence to our findings and one can use as an index for lowermost layer enhancements.

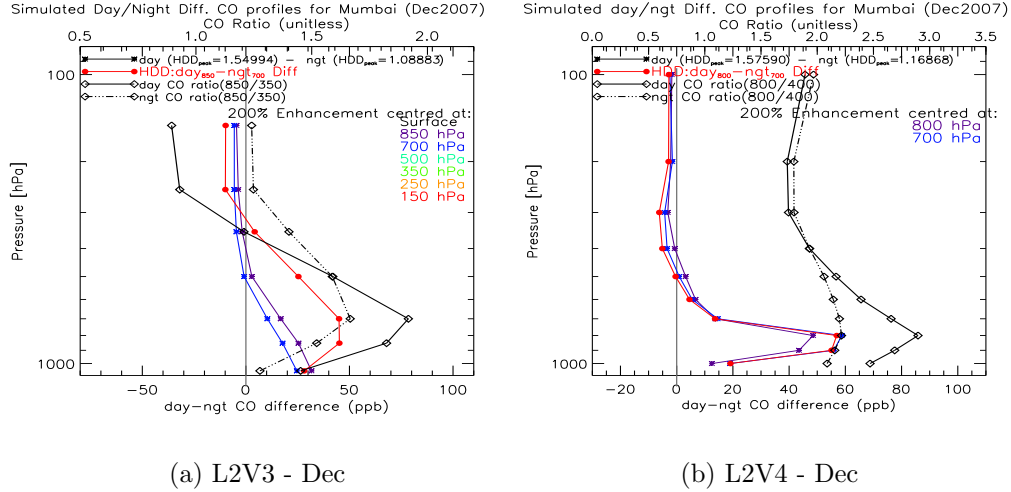
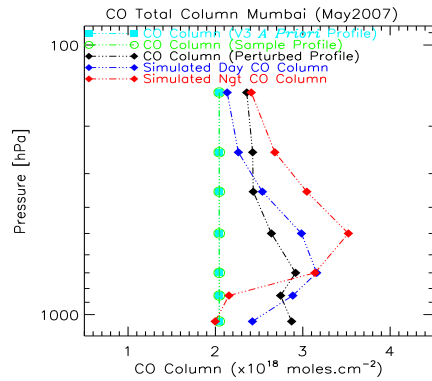


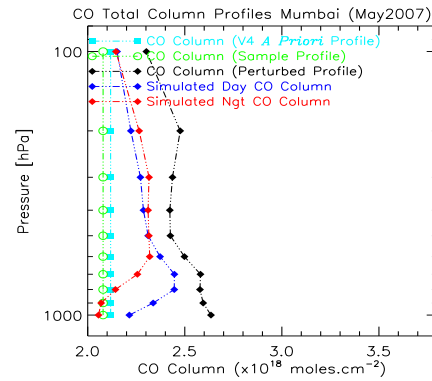
Figure 4.41: (a) MOPITT L2V3 ‘simulated’ key day-night difference CO profiles for HDD_{peak} , over Mumbai, for December 2007; (b) Same as (a) except for MOPITT L2V4. The diamond solid and dash-dotted lines indicates day and night CO ratio (L2V3:850hPa/350hPa and L2V4: 800hPa/400hPa) terms respectively. The ratio scale shown as top x-axis. The red coloured line represents $day_{850}-night_{700}$ (for L2V3) and $day_{800}-night_{700}$ (for L2V4) CO difference profiles for HDD_{peak} .

Figure 4.41 shows MOPITT L2V3 and L2V4 ‘simulated’ day-night difference CO profiles for HDD_{peak} , over Mumbai, in the month of December. Similar simulation results can be seen as in Fig. 4.40 for L2V3 and L2V4 except that the sensitivity weighted to slightly broad lowermost layer and MOPITT likely to have reduced sensitivity during this time, possibly due to low thermal contrast conditions.

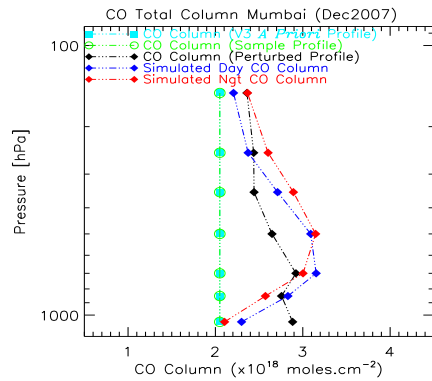
Figure 4.42 shows MOPITT L2V3 and L2V4 calculated total column values for sample CO profile with 200% enhancements at each retrieval level forming 7 and 10 perturbed profiles respectively. In general, ‘simulated’ total column values for all regions discussed in this chapter are comparable, thus providing confidence in the adopted methodology to understand MOPITT sensitivity to the lowermost layer by looking at day-night differences.



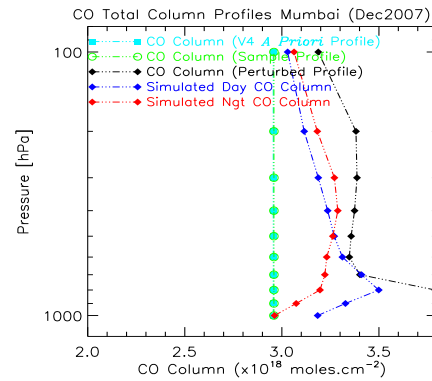
(a) L2V3 - May



(b) L2V4 - May



(c) L2V3 - Dec



(d) L2V4 -Dec

Figure 4.42: MOPITT L2V3 and L2V4 retrieval calculated total column values for i) a priori CO profile (cyan), ii) 7 individual sample profiles (green), iii) 7 individual perturbed sample profile (black), and iv) 7 individual simulated day (blue) and night (red) CO profiles, over Mumbai, for May (top panel) and December (bottom panel) 2007; Note that these are not considered as profiles. For proper understanding the total column values plotted at corresponding perturbed retrieval level (layer) for each CO VMR profile.

4.5.4.2 TOMCAT Model CO Profile Simulation

For this region, MOPITT L2V4 simulations performed for chosen TOMCAT CO profile for L2V3 simulation. A profile over Mumbai box represent a case where our analysis suggesting the location of elevated CO source region in the month of May and December. The profiles were taken on the 3rd of May 2004 and 22nd of December 2004, located at 18.09°N latitude and 73.93°E longitude.

Figure 4.43 show selected TOMCAT model CO profiles, over Mumbai region, in

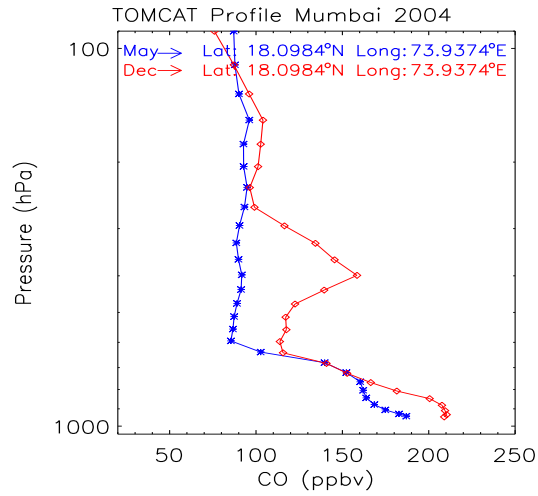
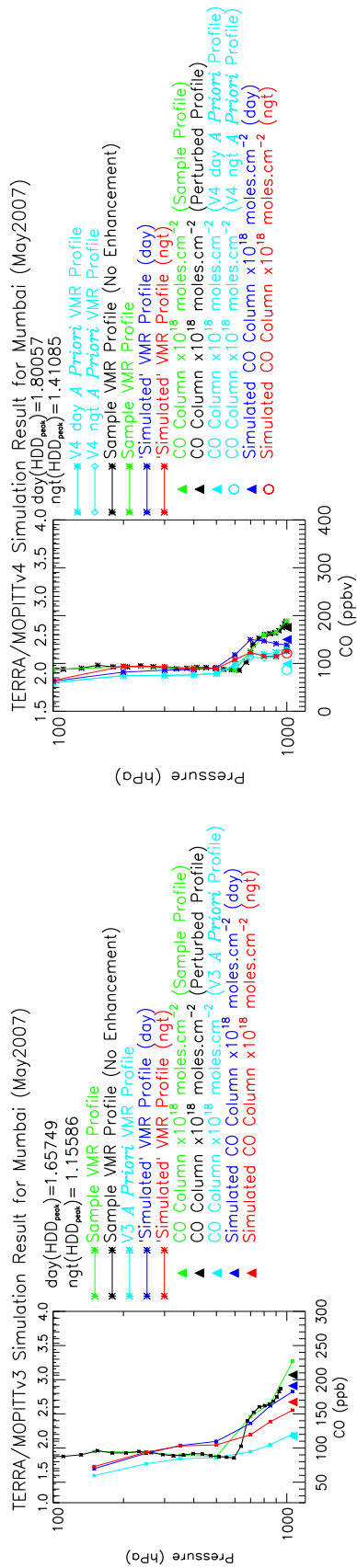
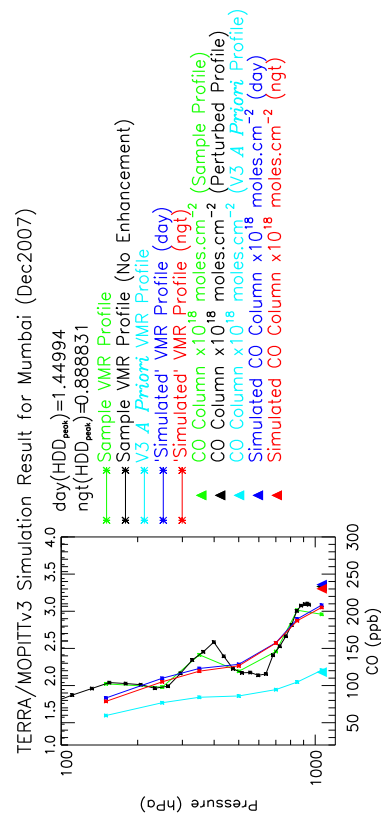


Figure 4.43: Selected TOMCAT model CO profiles, over Mumbai box, for May 2004 (blue) and December 2004 (red).

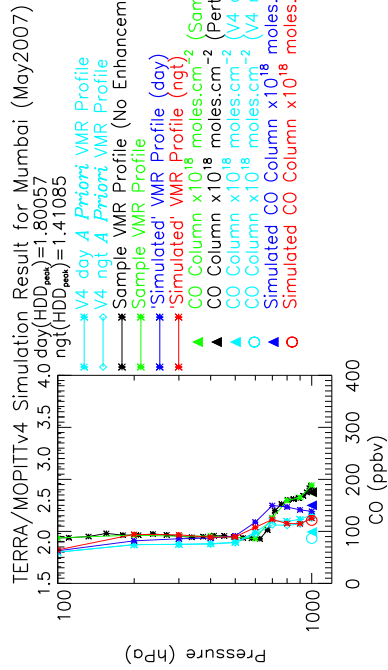
the month of May and December of 2004. These CO profiles are used as a sample profile for MOPITT L2V3 and L2V4 simulations. Note that no enhancements applied to these profiles, in practice therefore we will have only one modeled test profile instead of 7 test profiles as incase L2V3 a priori CO profile simulation and 10 test profiles as incase of L2V4 a priori CO profile simulation. The selected ‘typical’ averaging kernel of interest was then applied to these profiles.



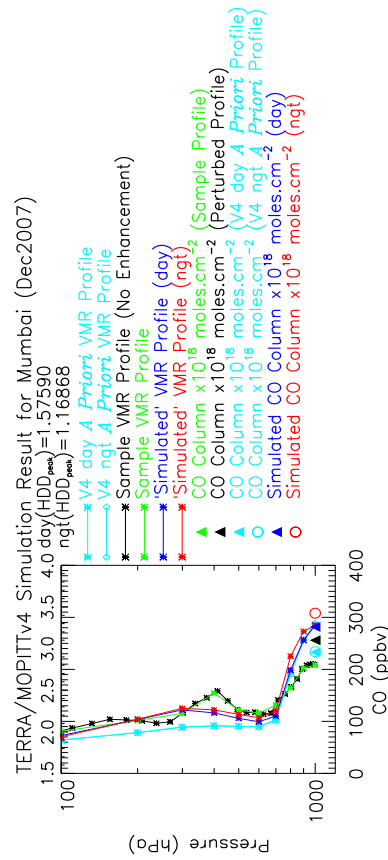
(a) L2V3 - May



(c) L2V3 - Dec



(b) L2V4 - May



(d) L2V4 - Dec

Figure 4.44: (a)MOPITT L2V3 ‘Simulated’ daytime and nighttime CO profiles for TOMCAT model selected base CO profile, over Mumbai, for May 2007; (b) Same as (a) except for MOPITT L2V4; (c) Same as (a) except for December 2007; (d) Same as (a) except for MOPITT L2V4 and for December 2007.

Figure 4.44(a) and (c) show simulated CO profiles using MOPITT L2V3 selected ‘typical’ averaging kernel, over Mumbai region, in the month of May and December respectively. Figure 4.44(b) and (d) show simulated CO profiles using MOPITT L2V4 selected ‘typical’ averaging kernel, over Mumbai region, in the month of May and December respectively. For L2V3, daytime ‘simulated’ CO profile has greatest enhancements at lower 3 retrieval pressure levels where L2V4 ‘simulated’ daytime CO has significant enhancements for lower 3 retrieval levels except at surface level. A very similar enhancements for L2V3 and L2V4 can be seen, showing less significant enhancements for ‘simulated’ nighttime CO profiles.

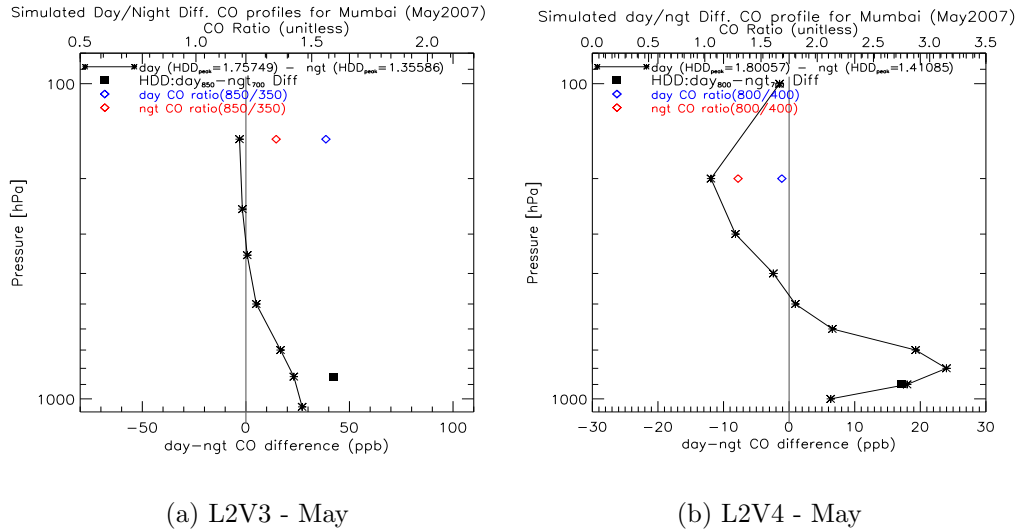


Figure 4.45: (a) MOPITT L2V3 ‘simulated’ day-night difference CO profile for HDD_{peak} , over Mumbai, for May 2007; (b) Same as (a) except for MOPITT L2V4.

Figure 4.45 illustrates (a) L2V3 and (b) L2V4 ‘simulated’ day-night difference CO profiles for chosen TOMCAT model CO profile. For L2V3, the day-night positive differences can be seen for lower 4 retrieval levels peaking at surface retrieval level. For L2V4, however, day-night positive differences can be seen for lower 5 retrieval levels, peaking at 800 hPa. Our analysis, thus, confirms that MOPITT L2V3 and L2V4 has significant differences in sensitivity to CO in the troposphere for similar surface and atmospheric properties.

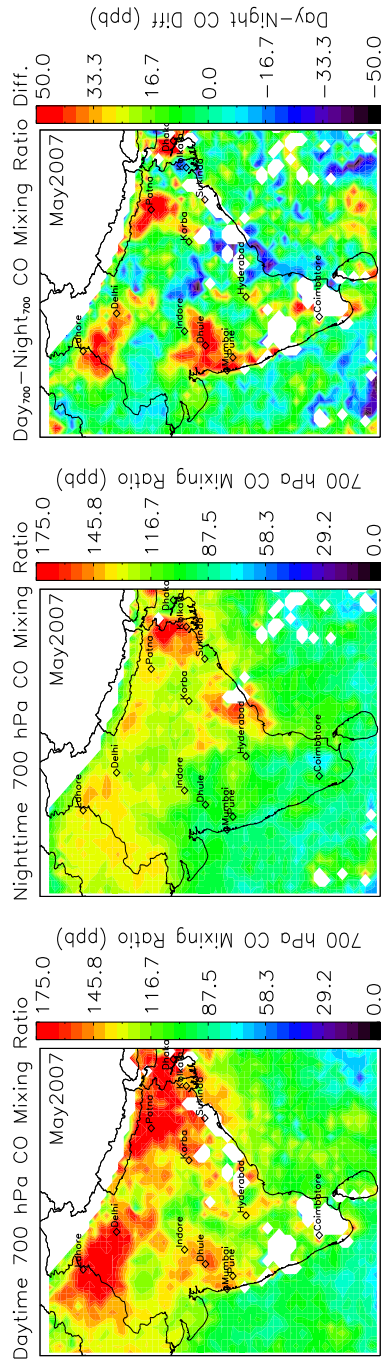
L2V4 simulation studies have shown that $day_{850}-ngt_{700}$ difference is clearly superior, for Indian subcontinent region, to 700 hPa day-night difference and (800/400)

CO ratio in demonstrating lowermost layer enhancements. While our L2V3 simulation shows 700 hPa day-night difference is useful to understand MOPITT sensitivity to CO in the boundary layer. As pointed out earlier, MOPITT L2V4 retrievals benefit from significant advances in radiative transfer modeling, state vector representation, and a priori statistics as compared to L2V3 retrievals. The significant differences can be clearly evident from our simulation studies show varying sensitivity for MOPITT to CO in the boundary layer for persistent surface and atmospheric conditions. In the next section we, therefore, look at spatial structure of L2V3 700 hPa day-night and L2V4 $\text{day}_{850}\text{-ngt}_{700}$ CO distribution.

It is now possible to apply our knowledge and test simulation methodology for other key regions of the world which are likely to have different atmospheric and surface properties such as Mexico City and Johannesburg. The former case study region is surrounded by mountains and likely to have greatest DOFS compared to Indian subcontinent region. The later case study region falls in southern latitudes and likely to have significantly less DOFS values compared to Indian subcontinent and Mexico city region. The simulations results for these key regions are presented in the Appendix-I (refer Fig. 7.10 onwards)

4.6 Spatial Distribution of CO

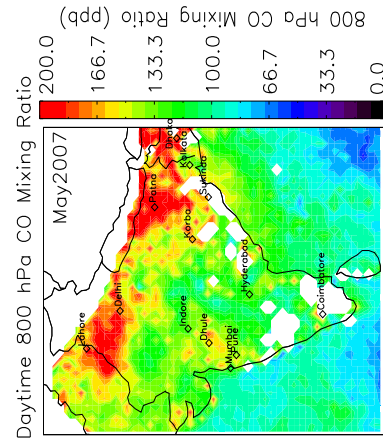
It is shown in this section that the MOPITT retrievals day-night CO differences at 700 hPa retrieval level do indeed capture widespread surface source information on CO. Note that we present this analysis for Indian subcontinent. Figure 4.46 top panel shows L2V3 day, night, and day-night distribution of MOPITT CO mixing ratios at 700 hPa in the month of May and the bottom panel show L2V4 day and night 800 hPa and $\text{day}_{800}\text{-ngt}_{700}$ differences CO mixing ratios in the month of May. From our simulations studies, it appears that MOPITT L2V3 has greatest sensitivity to CO in the boundary layer at 700 hPa whereas for L2V4 the greatest sensitivity likely to be at 800 hPa. It can also further confirmed by looking at 700 hPa day-night differences and $\text{day}_{800}\text{-ngt}_{700}$ differences for L2V3 and L2V4 retrievals respectively. The localised enhancements can be easily seen in both the cases and are matching very well, showing high positive day-night differences.



(a) L2V3 day CO - May

(b) L2V3 ngt CO - May

(c) L2V3 day-night diff - May

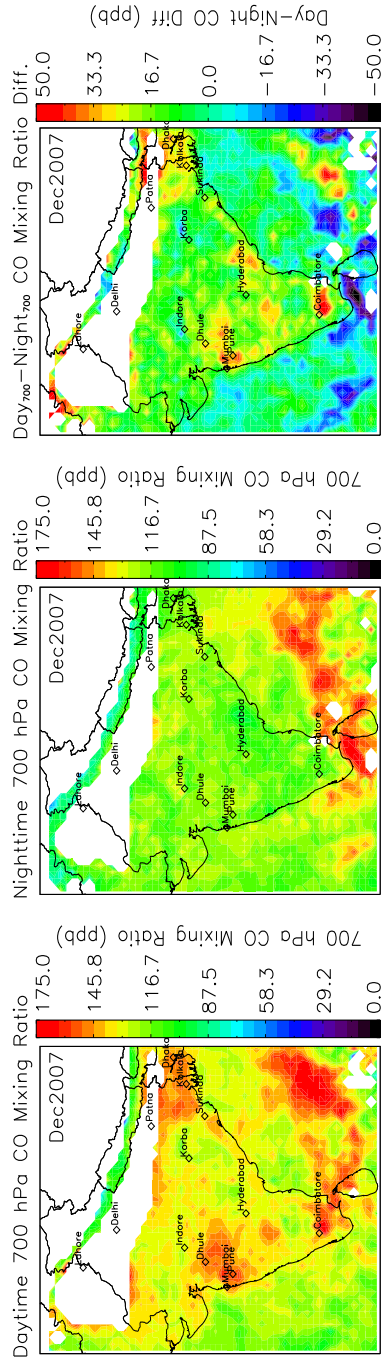


(d) L2V4 day CO - May

(e) L2V4 ngt CO - May

(f) L2V4 day-night diff - May

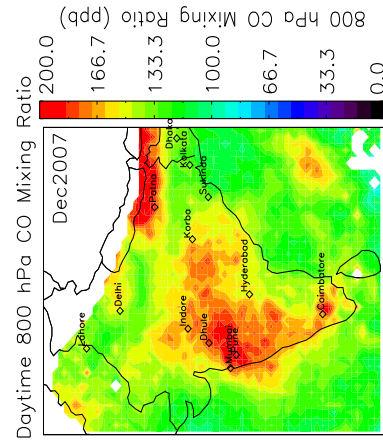
Figure 4.46: (a) MOPITT L2V3 0.5 degree gridded daytime 700 hPa CO mixing ratios, over India, for May 2007; (b) MOPITT L2V3 0.5 degree gridded nighttime 700 hPa CO mixing ratios, over India, for May 2007; (c) MOPITT L2V3 0.5 degree gridded daytime 700 hPa day-night CO mixing ratio differences, over India, for May 2007; (d) MOPITT L2V4 0.5 degree gridded daytime 800 hPa CO mixing ratios, over India, for May 2007; (e) MOPITT L2V4 0.5 degree gridded nighttime 800 hPa CO mixing ratios, over India, for May 2007; (f) MOPITT L2V4 0.5 degree gridded day_{800-ngt-700} CO mixing ratio differences, over India, for May 2007.



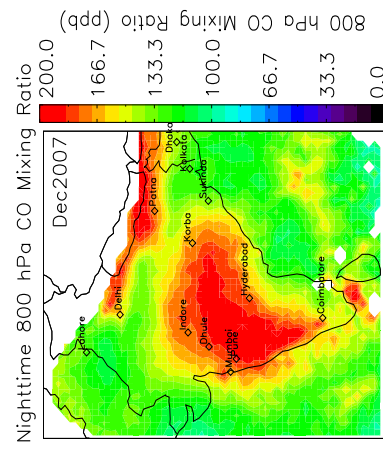
(a) L2V3 day CO - Dec

(b) L2V3 ngt CO - Dec

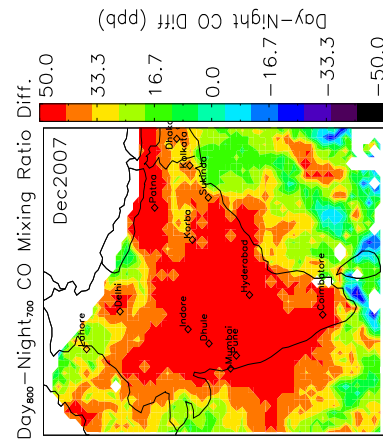
(c) L2V3 day-night diff - Dec



(d) L2V4 day CO - Dec



(e) L2V4 ngt CO - Dec



(f) L2V4 day-night diff - Dec

Figure 4.47: (a) MOPITT L2V3 0.5 degree gridded daytime 700 hPa CO mixing ratios, over India, for December 2007; (b) MOPITT L2V3 0.5 degree gridded nighttime 700 hPa CO mixing ratios, over India, for December 2007; (c) MOPITT L2V3 0.5 degree gridded 700 hPa day-night CO mixing ratio differences, over India, for December 2007; (d) MOPITT L2V4 0.5 degree gridded daytime 800 hPa CO mixing ratios, over India, for December 2007; (e) MOPITT L2V4 0.5 degree gridded nighttime 800 hPa CO mixing ratios, over India, for December 2007; (f) MOPITT L2V4 0.5 degree gridded day₈₀₀-ngt₇₀₀ CO mixing ratio differences, over India, for December 2007.

Figure 4.48 shows correlation between the daytime and nighttime MOPITT L2V3 retrievals together with day-night differences in CO mixing ratios and corresponding correlation results for L2V4 retrievals. These results indeed present evidence that MOPITT retrievals have utility to day-night difference analysis in this region, providing useful information on surface emissions of CO.

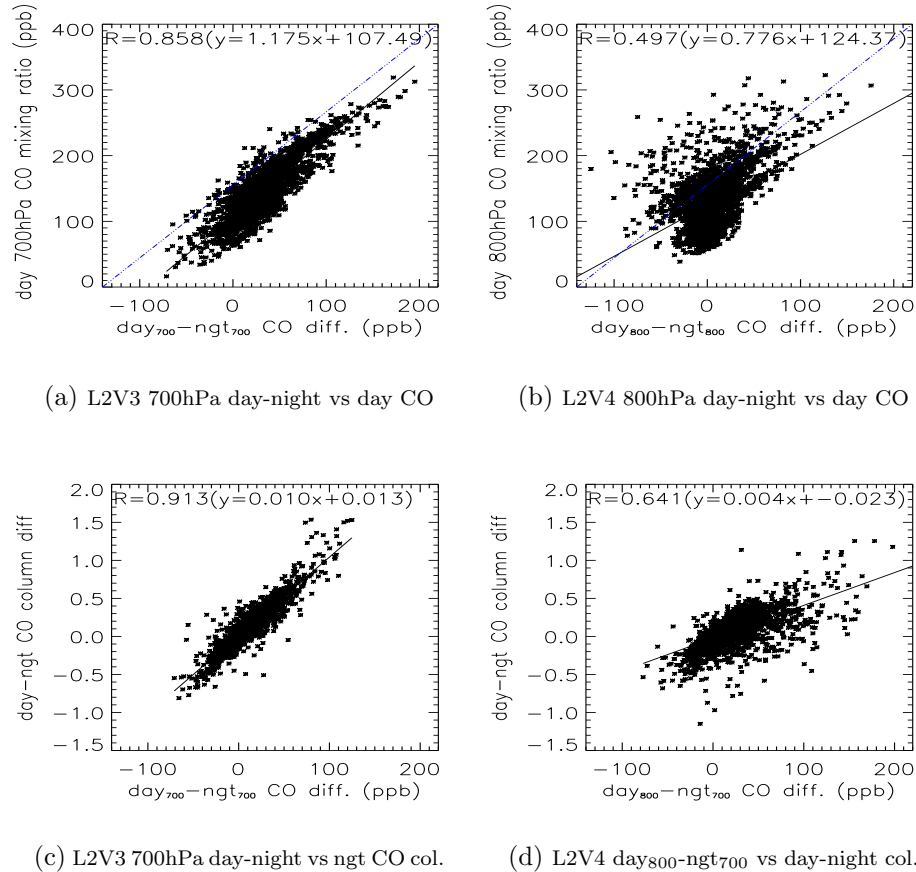
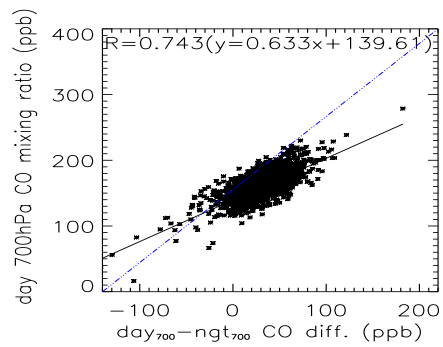
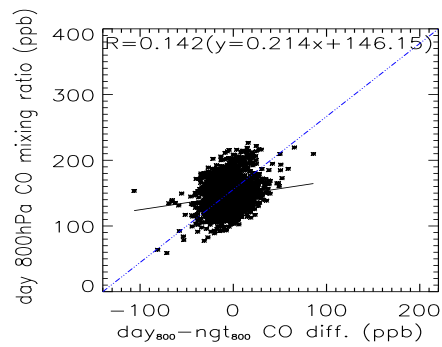


Figure 4.48: Correlation results, over India, in the month of May 2007.

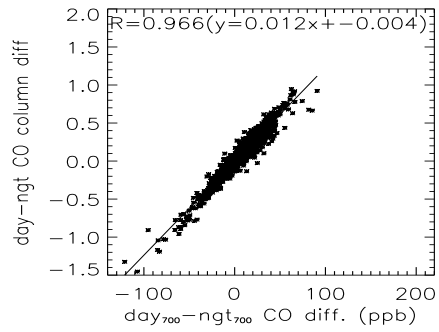
For Indian subcontinent, our simulation studies for L2V3 and L2V4 retrievals thus confirms the localised enhancements over the extremes of the IG basin, west coast and southern tip of India. Our simulation methodology works well in this region and could possible be extended to other regions of world. This analysis indeed confirms that MOPITT L2V3 retrievals show greatest sensitivity to 700 hPa while MOPITT L2V4 retrievals show greatest sensitivity to 800 hPa retrieval level. This, in turn, support that MOPITT instrument indeed has significant sensitivity to CO in the troposphere.



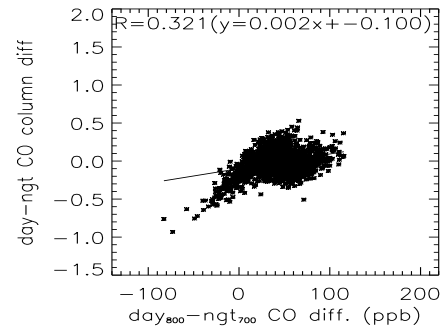
(a) L2V3 700hPa day-night vs day CO



(b) L2V4 800hPa day-night vs day CO



(c) L2V3 700hPa day-night vs ngt CO col.



(d) L2V4 days800-ngt700 vs day-night col.

Figure 4.49: Correlation results, over India, in the month of December 2007.

4.7 Summary of Chapter 4

In this chapter, we have presented two-fold evidence that MOPITT retrievals indeed have sensitivity to the boundary layer CO which mostly depends upon the thermal contrast conditions and boundary layer height. The MOPITT L2V3 and L2V4 retrievals show that it is possible to use day-night differences in retrieved CO data to detect lowermost and high altitude enhancements which indeed helpful to study transport of CO to long distances from source regions. The results also indicate that in order to determine the vertical structure of CO using MOPITT profile data, a selection methodology for ‘typical’ averaging kernel is required. The method developed in this thesis for MOPITT L2V3 and L2V4 retrievals is thought to be reasonable and appropriate for this kind of analysis. Moreover, the simulation tests for more realistic TOMCAT model CO profile further enhance our knowledge about CO and build-up confidence in this methodology.

Similar to L2V3 retrievals, the L2V4 retrievals averaging kernels also vary considerably, particularly from day to night and from land to water surfaces. However, the L2V4 retrieval averaging kernels likely to provide 2 pieces of profile shape information for the retrieved CO profile, averaging kernel peaking at 800 hPa, 500 hPa and 300 hPa retrieval level. The L2V4 retrievals also show greater sensitivity to lower atmosphere in daytime than of nighttime observations as expected, with greater DOFS in daytime. The L2V4 DOFS are always superior to L2V3 DOFS. We also find that daytime and nighttime DOFS exhibits a bi-modal DOFS for all selected Indian regions similar to L2V3 retrievals. In this case, we demonstrate that $\text{day}_{800\text{-ngt}700}$ differences gives a closer differentiation of lowermost CO, showing greatest sensitivity to 800 hpa retrieval level for the daytime measurements having large planetary boundary layer height. For Indian subcontinent, our analysis confirms the elevated lower layer CO concentrations over extremes of the Indo-Gangetic basin (i.e. Bihar), Delhi, west coast (i.e. Mumbai) and southern tip of India (i.e. Coimbatore) in the month of May and December owing to variability of the sensitivity in these regions. We also tend to find the MOPITT L2V4 a priori has significant influence of profile shape information for the retrieved CO profile. Though, it need further analysis to correctly asses a priori influence on L2V4 retrievals.

Chapter 5

Signatures of CO from Megacities

5.1 Introduction

Urban air pollution in a megacity (metropolitan area with a total population in excess of 10 million inhabitants) is a major environmental problem in the world [Fuchs et al., 1994] with consequences of air quality, climate change, and human health [Mage et al., 1996; Molina and Molina, 2004; Butler et al., 2008]. In these urban areas, air quality is becoming a major concern, and an important area of research has emerged during the last decades in order to quantify the emission sources of pollutants, to model the chemical and physical transformation that leads to the production of secondary pollutants, and to study the transport pathways for the dispersal of pollution [Clerbaux et al., 2008]. Anthropogenic emissions in developing countries are larger than those in developed countries today and will continue to increase in the future [Akimoto, 2003]. For example, recent tropospheric satellite observations have demonstrated that NO_x emissions in China have accelerated strongly since 2000 [Irie et al., 2005; Richter et al., 2005]. It should be noted that city-specific, specialised regional and global emission inventories have been developed and can be used to estimate CO (and other trace and greenhouse gaseous) emissions on city-scale. However, the study by Butler et al. [2008] reveal that despite the fact that the many common sources of data between the emissions inventories, and the similarities in their construction methodologies, there are significant differences between the emissions for individual megacities, even when the total global or regional emissions are very similar. Based on expert knowledge [Olivier and Berdowski, 2001], global emissions from fossil fuel

combustion have an uncertainty of about 50%, from biofuel combustion about 100%, from industrial processes about 50-100%, and from waste handling about 100%.

Because CO sources are highly variable in space and time and good measurements of their spatial pattern and time evolution are required especially for air pollution monitoring and forecasting applications in highly populated areas but also for regional and global chemistry. It is worth noting again that MOPITT satellite sensor offers CO measurements over extended periods of time (nearly a decade). Hence it does indeed allow the good characterisation of the impact of intense local (or urban) pollution sources on continental and global scale air quality then this would be a major step forward, for example Clerbaux et al. [2008] exploited MOPITT surface CO daytime data, by averaging them over long time periods (7 years), to trace CO pollution arising from the large cities and urban areas. Their findings reveal that there were strong enhancements, most likely associated with cities, where the most favourable situations appear e.g. i) places surrounded by mountains such as Milan, Jakarta, Teheran and Mexico City, where the CO pollution is trapped and the source is isolated to some extent from the surroundings, and ii) locations where high thermal contrast conditions are found, such as Tokyo, Moscow, San Diego, San Francisco and Johannesburg. However, their findings did not prove that all large urban centres or megacities could be identified and they still required 7 years of data to detect plumes from selected cities. Their analysis suggests that only particular urban centre could be identified through the averaging of 7 years of data.

The work presented in chapter 3 and 4 has outlined methodologies which demonstrate that there is real sensitivity to lowermost atmosphere CO where day-night retrieval differences are positive. One could exploit day-night differences and daytime CO as a guide to investigate possibility of using MOPITT observations to detect CO enhancements over large urban centres or megacities, by averaging data over a year time. Furthermore the results of chapters 3 and 4 have suggested that surface level CO retrievals are not optimal for detection of lowermost atmosphere features. Hence the analyses developed in this thesis could be a step forward in our ability to observe CO emissions at key locations across the globe and offers utility to the information available in current satellite sensors.

5.2 Methodology

A variety of effects besides instrument noise influence individual MOPITT retrieved CO profiles. Some of these effects are well understood and some are not. For MOPITT retrievals based on upwelling thermal infrared radiation, the weighting functions typically yield poor sensitivity near the surface (except in regions of strong thermal contrast and large planetary boundary layer height). Because of the potential variability of MOPITT CO data quality, it is crucial to use available information content thresholds to focus on particular subsets of the data with the highest lower atmosphere sensitivity.

In L2V3 data, two aspects of the present a priori CO mixing ratio are utilised; the variable percent a priori CO mixing ratio give the fraction of information in each retrieval that came from the a priori. First, those profiles having percent a priori CO mixing ratio less than 50% in the retrievals at corresponding retrieval pressure level are considered to ensure that the results are minimally influenced by the assumed a priori profile. Secondly, in L2V3, the other available diagnostic to filter data is DOFS, it quantifies information content; larger values of DOFS indicate smaller weighting of a priori profile information. Our analysis clearly indicate that DOFS are linearly correlated with percent a priori CO mixing ratio retrieved at 350 hPa. A strong correlation between these two suggests one can use percent a priori CO mixing ratio instead of DOFS which has to be calculated for individual profile in L2V3 and it is time consuming process. We therefore make a percent a priori CO mixing ratio threshold value by available DOFS limit values (by looking at available DOFS histogram) to ensure that the data with highest DOFS are employed. (refer to Table 5.1).

Whilst, in L2V4 retrievals percent a priori CO mixing ratio diagnostic has not been included but retrieval averaging kernels and DOFS diagnostics are provided in the L2V4 product. As stated earlier, DOFS is derived from the averaging kernel matrix, which is the optimal estimation retrieval algorithm, depends on the weighting function matrix. Radiative transfer modelling shows that the magnitude of the MOPITT weighting function varies significantly as the CO concentration changes. Thus, the DOFS diagnostic is not independent of the CO profile and must be treated while selecting retrieved profile data. Based on our DOFS histogram analysis for L2V4

Table 5.1: L2V3 and L2V4 DOFS limit and equivalent L2V3 percent a priori CO mixing ratio for selected regions.

Region	Month	DOFS limit L2V3 (L2V4)	Equivalent Percent a priori CO mixing ratio (%)
Bihar	May	1.51 (1.61)	31
	Dec	1.31 (1.06)	38
Chuquicamata	May	1.56 (1.06)	37
	Dec	1.31 (1.31)	27
Coimbatore	May	1.56 (1.56)	28
	Dec	1.36 (1.41)	31
Delhi	May	1.46 (1.56)	31
	Dec	1.31 (1.26)	25
Mexico	May	1.36 (1.51)	35
	Dec	1.31 (1.31)	28
Mumbai	May	1.61 (1.66)	30
	Dec	1.41 (1.46)	20
Moscow	May	1.41 (1.36)	35
	Dec	0.85 (0.86)	31
New York	May	1.26 (1.41)	38
	Dec	1.06 (1.16)	36
Global	May	1.51 (1.56)	30
	Dec	1.36 (1.25)	35

retrievals, we define appropriate DOFS limiting value to select particular subset of the retrieved CO data. For this analysis, these strict threshold values are applied to MOPITT L2V3 and L2V4 retrieved data to exclude particular subsets of the data and the results are presented and discussed in the following sections. For L2V3, percent a priori CO mixing ratio threshold value taken as 32%. For L2V4, the DOFS threshold value taken as 1.35. Note that these threshold value only applied to daytime measurements for which one can expect greater sensitivity to the lowest layer of the atmosphere.

The methodology then for the results of section 5.2 is to use only data which pass the percent a priori (L2V3) or DOFS (L2V4) to compute the day-night differences for both the L2V3 and L2V4. A city is identified only if a spatially isolated signal specific to the target is observable in both data sets. Examinations of the day data set alone

and of SCIAMACHY NO₂ is used to give additional support to the conclusions. The analysis is applied to one year of CO data i.e. 2007.

5.3 Global Distribution of CO

High levels of CO pollution are found in both hemispheres, essentially above urban areas due to industry, motor vehicle traffic and domestic heating, and over areas where biomass fires occur, either natural, related to agriculture, or deforestation. Elevated amount can also be found long distances from the CO source regions, as the atmospheric lifetime of CO is long enough (from a few weeks to several months) that long-range transport can occur.

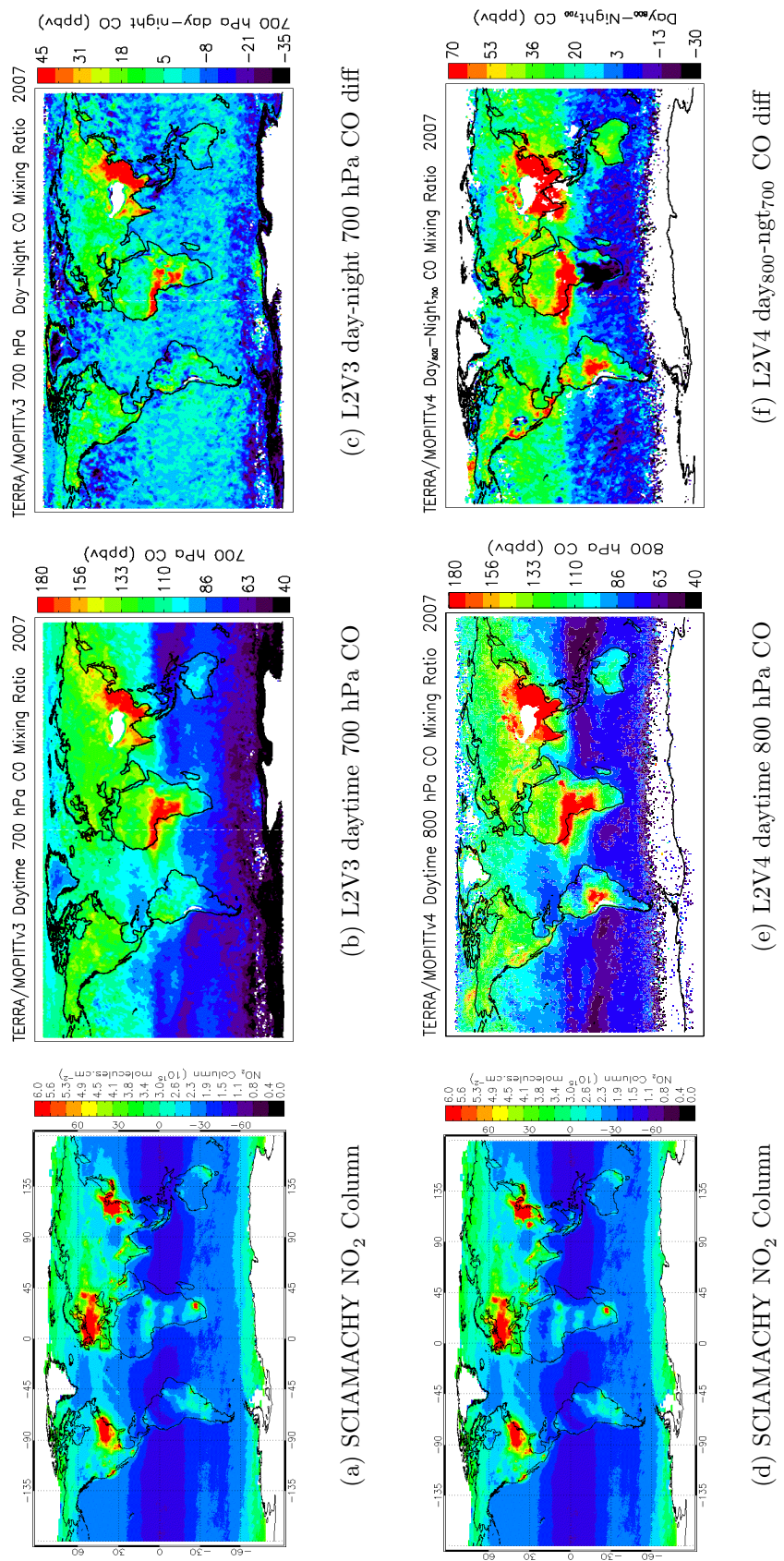
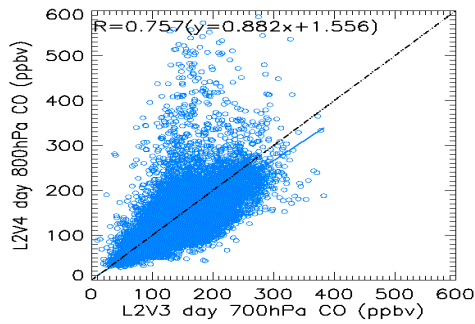


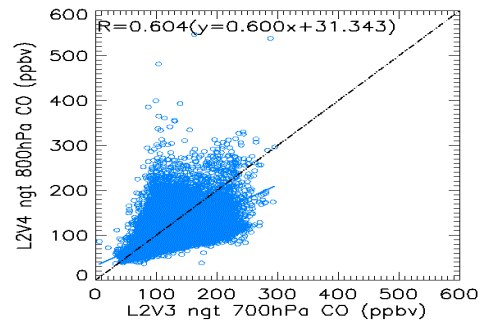
Figure 5.1: (a) SCIAMACHY 0.25 deg. gridded NO₂ total column ($\times 10^{15}$ molecules.cm⁻²); (b) MOPITT L2V3 0.5 degree gridded daytime 700 hPa CO mixing ratios; (c) MOPITT L2V3 0.5 degree gridded 700 hPa day-night difference CO mixing ratios; (d) Same as (a); (e) MOPITT L2V4 0.5 degree gridded daytime 800 hPa CO mixing ratios; (f) MOPITT L2V4 0.5 degree gridded day₈₀₀-ngt₇₀₀ difference CO mixing ratios.

Figure 5.1 compares the global SCIAMACHY NO₂ column distribution to (i) MOPITT L2V3 daytime 700 hPa and 700 hPa day-night difference CO mixing ratios; (ii) MOPITT L2V4 daytime 800 hPa and day₈₀₀-ngt₇₀₀ difference CO mixing ratios, for the year 2007. The SCIAMACHY data is averaged over 0.25°×0.25° grid and MOPITT data is averaged over 0.5°×0.5° grid. Strong gradients can be seen in both the NO₂ and CO distributions. In particular, there are several areas of localised enhancements in the CO, which are also seen in the corresponding NO₂ distribution. Note that there are some differences in detail between the NO₂ and CO distributions, over central-south africa, along the south eastern coast and over north eastern coast. A direct one-to-one correlation between NO₂ and CO may not always be expected because of differences in the sources and their lifetimes [Buchwitz et al., 2007]. Interestingly, a good correlation, especially for IG basin and China, is observed between the L2V3 700 hPa day-night difference CO (or L2V4 day₈₀₀-ngt₇₀₀) and NO₂ concentrations, with the highest positive day-night CO differences observed where the higher NO₂ levels occurs. This supports the idea that day-night differences can be used to sketch possible CO enhancements in the lowermost layer of the atmosphere. In the next section, we present two-fold comparison between SCIAMACHY NO₂ and MOPITT CO for selected most interesting cities, some of them are reported by Clerbaux et al. [2008] and some are not.

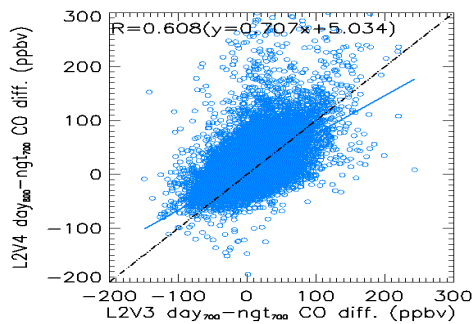
Figure 5.2 shows the correlation between MOPITT L2V3 and L2V4 retrieved CO data. From Fig. 5.2(c), it is clearly evident that both the L2V3 and L2V4 day-night CO differences are strongly correlated, suggesting utility of day-night difference to understand CO enhancements in the lowermost layer of atmosphere. Similarly for total column, one can see considerable utility to day-night total columns.



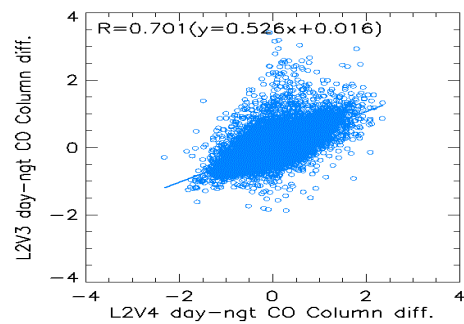
(a) V3 700hPa vs V4 800hPa day CO



(b) V3 700hPa vs V4 800hPa ngt CO



(c) V3 diff vs V4 diff CO



(d) V3 CO col. vs V4 CO col. diff.

Figure 5.2: Correlation results for (a) L2V3 700 hPa daytime CO Vs L2V4 700 hPa daytime CO; (b) Same as (a) except for nighttime; (c) L2V3 700 hpa day-night difference Vs day₈₀₀-ngt₇₀₀ difference; (d) L2V3 CO column Vs L2V4 CO column, for the year 2007.

5.4 CO from Urban Centres

5.4.1 A City-Specific Analysis

In this section, the possibility of using satellite-derived observations to monitor city-specific pollution sources is investigated with respect to some particularly interesting outcomes of the analysis. Figure 5.3 and 5.4 compares SCIAMACHY NO_2 total column, L2V3 daytime 700 hPa CO, L2V3 700 hPa day-night CO differences, L2V4 daytime 800 hPa CO, and L2V4 $\text{day}_{800\text{-ngt}_{700}}$ CO differences, over key regions such as Houston (Fig. 5.3(a-e)), Miami (Fig. 5.3(f-j)), Cairo (Fig. 5.3(k-o)), and Birmingham and Wales (Fig. 5.4(a-e)).

In Fig. 5.3(a-e), the enhancements of CO can clearly be detected over Houston, either above the city, or in general vicinity, enhancements in NO_2 are observed over this region supporting this analysis. The greatest enhancements in day-night CO difference can be seen in vicinity of Houston region, confirming presence of elevated CO in the lowermost layer of the atmosphere. Additionally, 5.5(a-c) indeed show a very good correlation between L2V3 and L2V4 calculated day-night differences and the individual with NO_2 total column, further indicating that day-night difference is a good identification of individual plumes from large urban centres or megacities. Note again that a direct one-to-one correlation between CO and NO_2 may not always be expected because of differences in the sources and their lifetimes. For Houston, some indication is observed in the day signals, but the effect is not as evident in the day-night data.

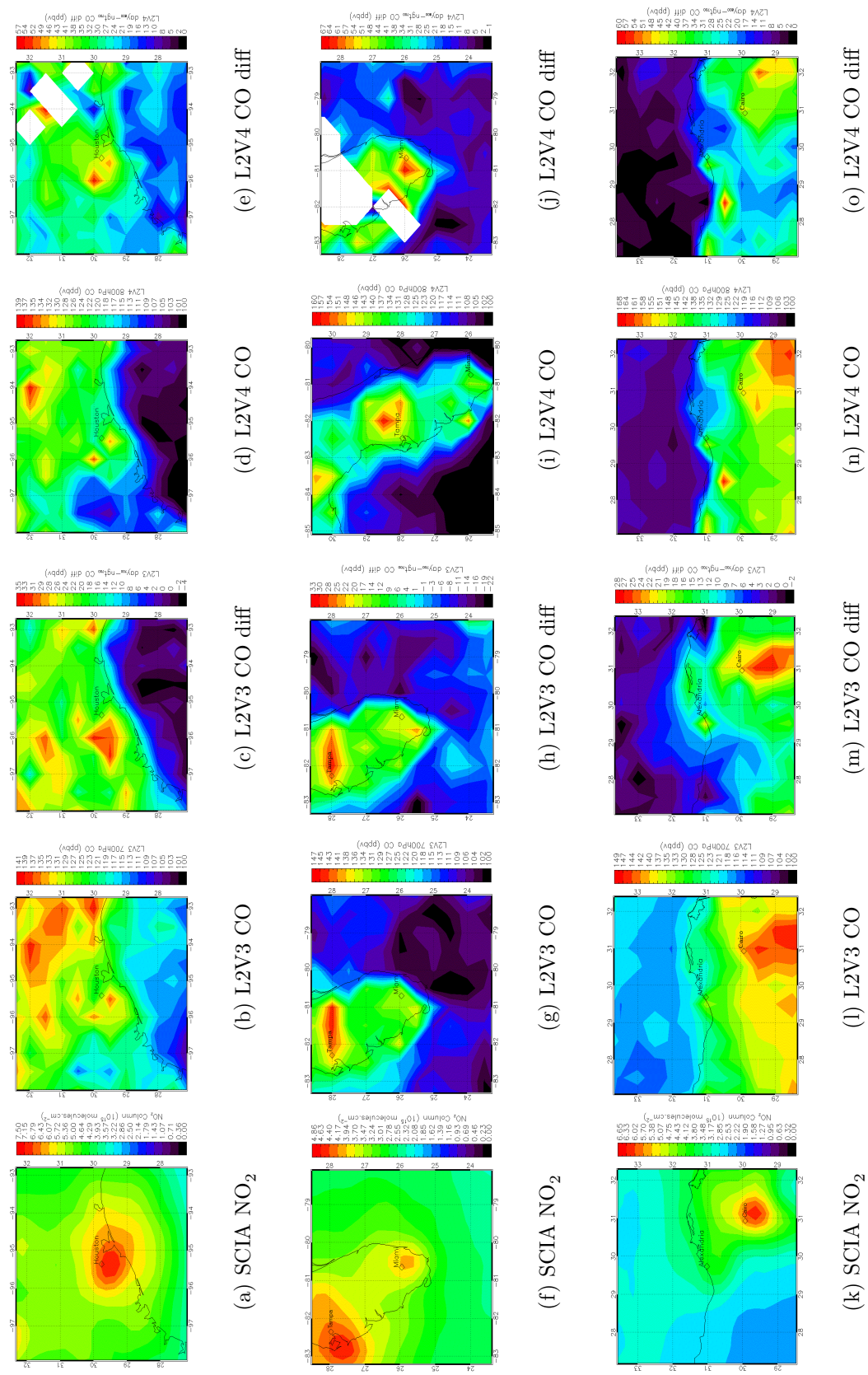


Figure 5.3: SCIAMACHY NO₂, MOPITT L2V3 daytime 700 hPa CO mixing ratios, MOPITT L2V3 700 hPa day-night difference CO mixing ratios, MOPITT L2V4 daytime 800 hPa CO mixing ratios, and MOPITT L2V4 day800-ngt700 difference CO mixing ratios, over striking cities. Houston (top row), Florida(middle row), Cairo(bottom row).

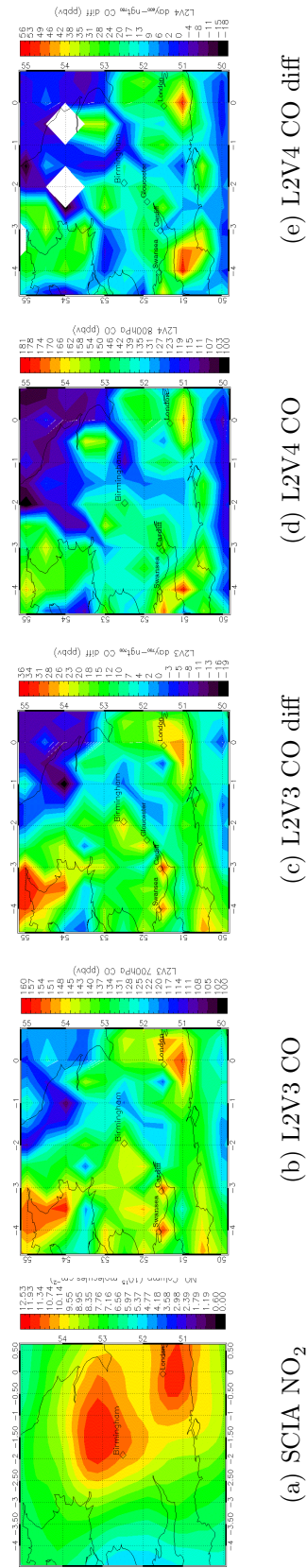
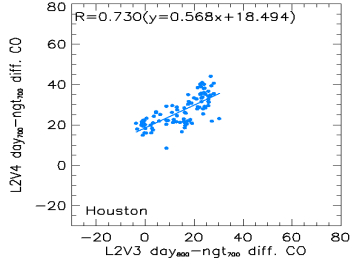
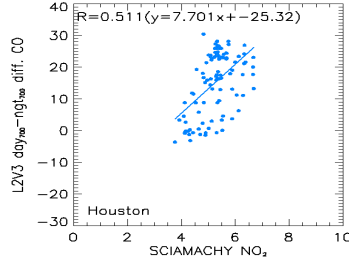


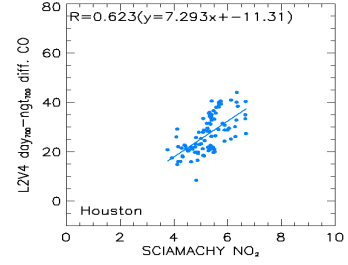
Figure 5.4: SCIAMACHY NO₂, MOPITT L2V3 daytime 700 hPa CO mixing ratios, MOPITT L2V3 700 hPa day-night difference CO mixing ratios, MOPITT L2V4 daytime 800 hPa CO mixing ratios, and MOPITT L2V4 day₈₀₀-ngt₇₀₀ difference CO mixing ratios, over Birmingham and Wales.



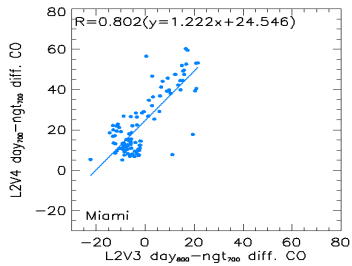
(a) L2V3 Vs L2V4 CO diff



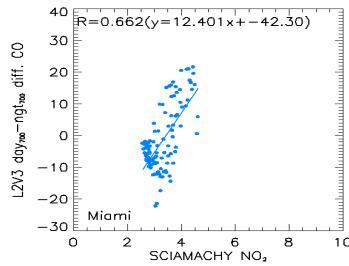
(b) NO₂ Vs V3 diff CO



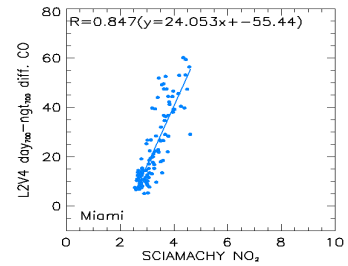
(c) NO₂ Vs V4 day CO



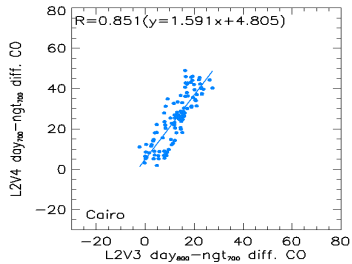
(d) L2V3 Vs L2V4 CO diff



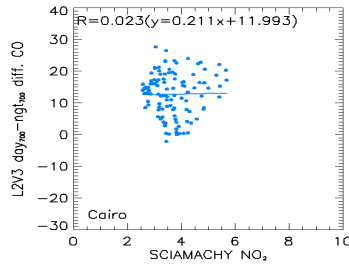
(e) NO₂ Vs V3 diff CO



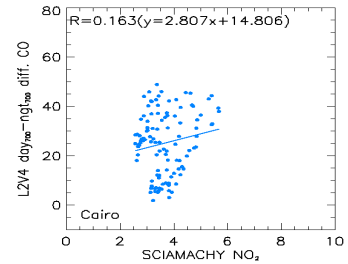
(f) NO₂ Vs V4 day CO



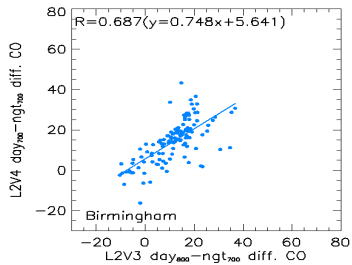
(g) L2V3 Vs L2V4 CO diff



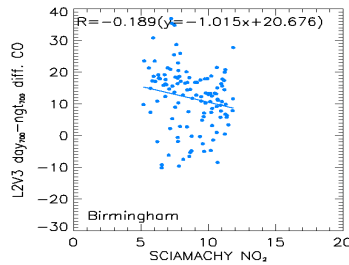
(h) NO₂ Vs V3 diff CO



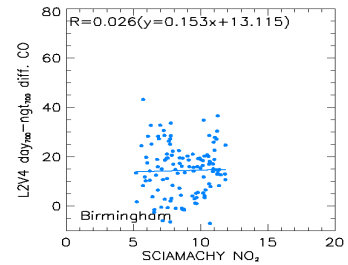
(i) NO₂ Vs V4 day CO



(j) L2V3 Vs L2V4 CO diff



(k) NO₂ Vs V3 diff CO



(l) NO₂ Vs V4 day CO

Figure 5.5: Correlation results for (i) L2V3 CO diff. vs L2V4 CO diff.; (ii) SCIAMACHY NO₂ vs L2V3 CO diff.; and (iii) SCIAMACHY NO₂ vs L2V4 CO diff. for (a-c) Houston, (d-f) Florida, (g-i) Cairo, (j-l) Birmingham respectively.

Figure 5.3(f-j) compares SCIAMACHY NO₂ with MOPITT L2V3 and L2V4 retrieved CO data over Florida region, identifying Tampa area and Miami. The enhancements of CO and NO₂ can be seen over the Tampa region and less clearly for Miami CO. Similar extended enhancements can be seen in day-night differences, in the general vicinity of city area. The Miami identification is much more convincing in day-night difference. This is more similar to Houston region and more convincing of the use of day-night difference to identify individual CO plumes from large urban centres or megacities. It should be noted that neither of these two surrounded by mountains where pollution is trapped and can thus can be detected using MOPITT observations as suggested by Clerbaux et al. [2008]. Hence the methodologies applied in this thesis seem effective to indicate specific sensitivity to lowermost atmosphere. Moreover, Fig. 5.5(d-f) show a very good correlation between L2V3 and L2V4 day-night differences with NO₂ total column, suggesting a really good identification of enhanced CO in the lowermost layer of the atmosphere.

Figure 5.3(k-o) as well shows similar comparisons over Cairo region identifying Alexandria and Cairo. A strong elevated NO₂ plume can be observed over Cairo. The enhancements of CO in the vicinity of Cairo, southward plume, can be seen clearly in the daytime and day-night differences map for both the L2V3 and L2V4. Interestingly, isolated plume of enhanced positive day-night differences can be identified over Alexandria in both the L2V3 and L2V4, which is less significant in the daytime data alone. Moreover, Fig. 5.5(g) also show a very good correlation between L2V3 and L2V4 day-night differences, confirming presence of elevated CO concentration in the lowermost layer of the atmosphere over Alexandria. A correlation between day-night differences and NO₂ is not promising in this region, possibly either due to differences in sources or their lifetimes.

Figure 5.4(a-e) compares SCIAMACHY NO₂ total column with MOPITT L2V3 and L2V4 daytime and day-night differences CO mixing ratios over Birmingham and Wales region. A strong wide-spread plume of NO₂ over Birmingham and London clearly evident. However, individual plumes of CO can be identified from large cities e.g. Birmingham, and poorly from others such as Cardiff, and Swansea. The day-night differences indeed help to mark out individual CO plumes from large cities which are densely populated and close to each other. Fig. 5.5(j) indeed show a very good correlation between L2V3 and L2V4 day-night differences. It is worth noting

that these key cities were not identified by Clerbaux et al. [2008] work and thus it is more convincing to use day-night difference along with methodologies described in chapter 3 and 4 to identify strong individual plumes from each large city across the globe.

The results shown here indicate a good use of day-night differences for isolating city signals over a year of data. These signals are often present but less highly in the daytime CO and for the stronger sources, but not always are well correlated with NO₂. In the next section, a global analysis has been performed for number of large cities.

5.4.2 Global Analysis

In this section, a global survey has been done to identify pollution plumes from large cities or megacities across the globe. Figure 5.6, 5.7, 5.8 and 5.9 compares SCIAMACHY NO₂ total column and MOPITT L2V3 and L2V4 daytime and day-night differences over few selected, most promising, large cities across the globe. In general, the enhancements in CO and highest day-night differences, for both the L2V3 and L2V4, can be clearly seen over city or in vicinity of city except that amplitude of day-night differences is slightly reduced in case of L2V4 data. Even if the CO signature arising from cities might be amplified by the specific dynamic and thermal conditions occurring over urban areas (heat island effect), high CO and good thermal contrast conditions likely to facilitate to detect CO pollution from the urban areas using the MOPITT observations, the region does not necessarily need to be surrounded by mountains as pointed out by Clerbaux et al. [2008]. These results, thus, support the work presented in chapter 3 and 4 which demonstrate that there is real sensitivity to lowermost atmosphere CO where day-night differences are positive.

It is also worth noting that Clerbaux et al. [2008] did not detect notable polluted Lagos city (Africa) by averaging daytime surface CO data over long time period due to this region often under the outflow coming from region biomass burning activity. However, this analysis clearly show CO enhancements over or in general vicinity of Lagos city using yearly mean CO data. Moreover, day-night differences are also highest and positive in this region, confirming presence of elevated CO concentrations in the lowermost layer of the atmosphere (refer to Fig. 5.7(1-o)).

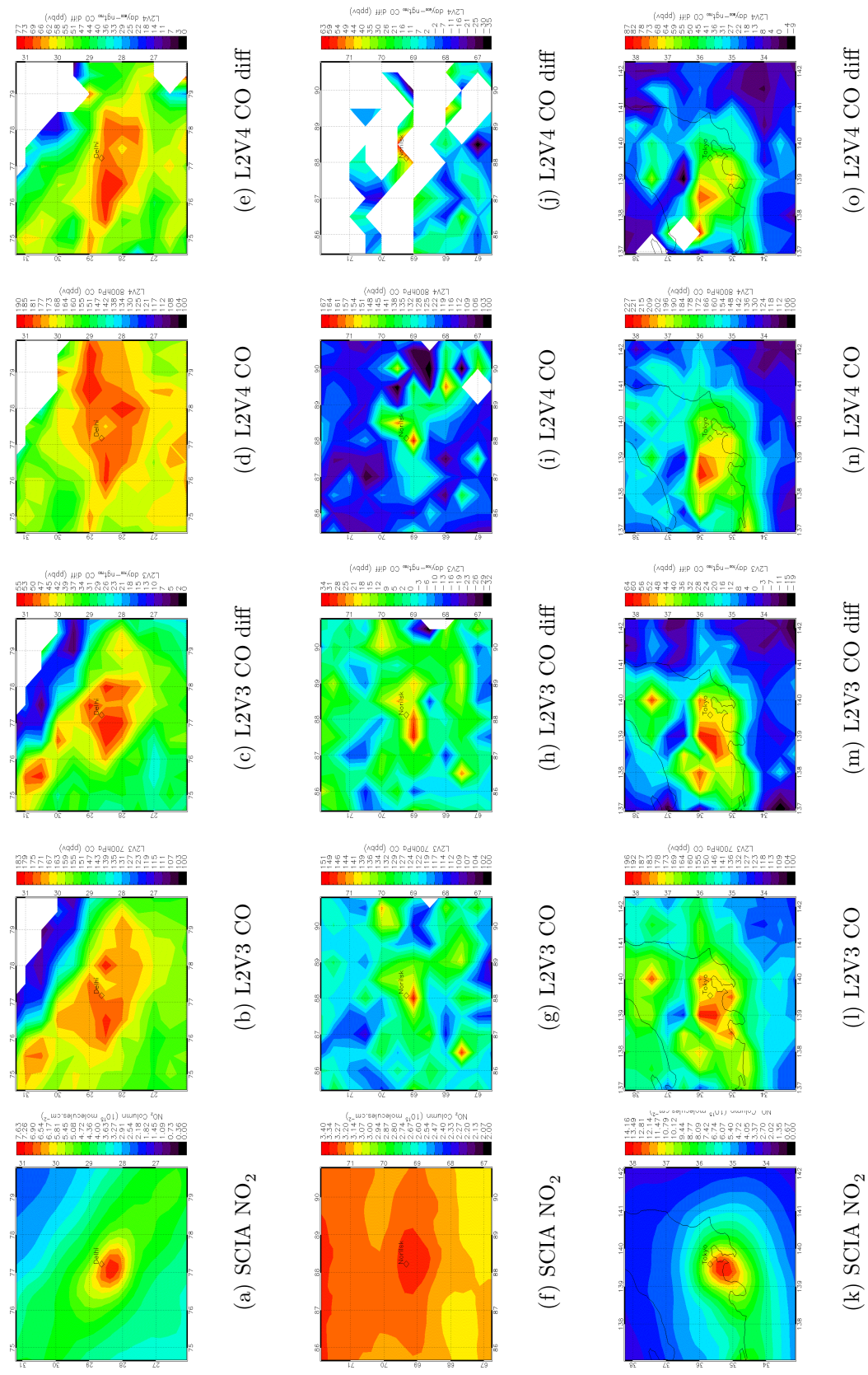


Figure 5.6: SCIAMACHY NO₂, MOPITT L2V3 daytime 700 hPa CO mixing ratios, MOPITT L2V3 700 hPa day-night difference CO mixing ratios, MOPITT L2V4 daytime 800 hPa CO mixing ratios, and MOPITT L2V4 day800-ngt700 difference CO mixing ratios, over striking cities. Delhi(top row), Norilsk(middle row), Tokyo(bottom row).

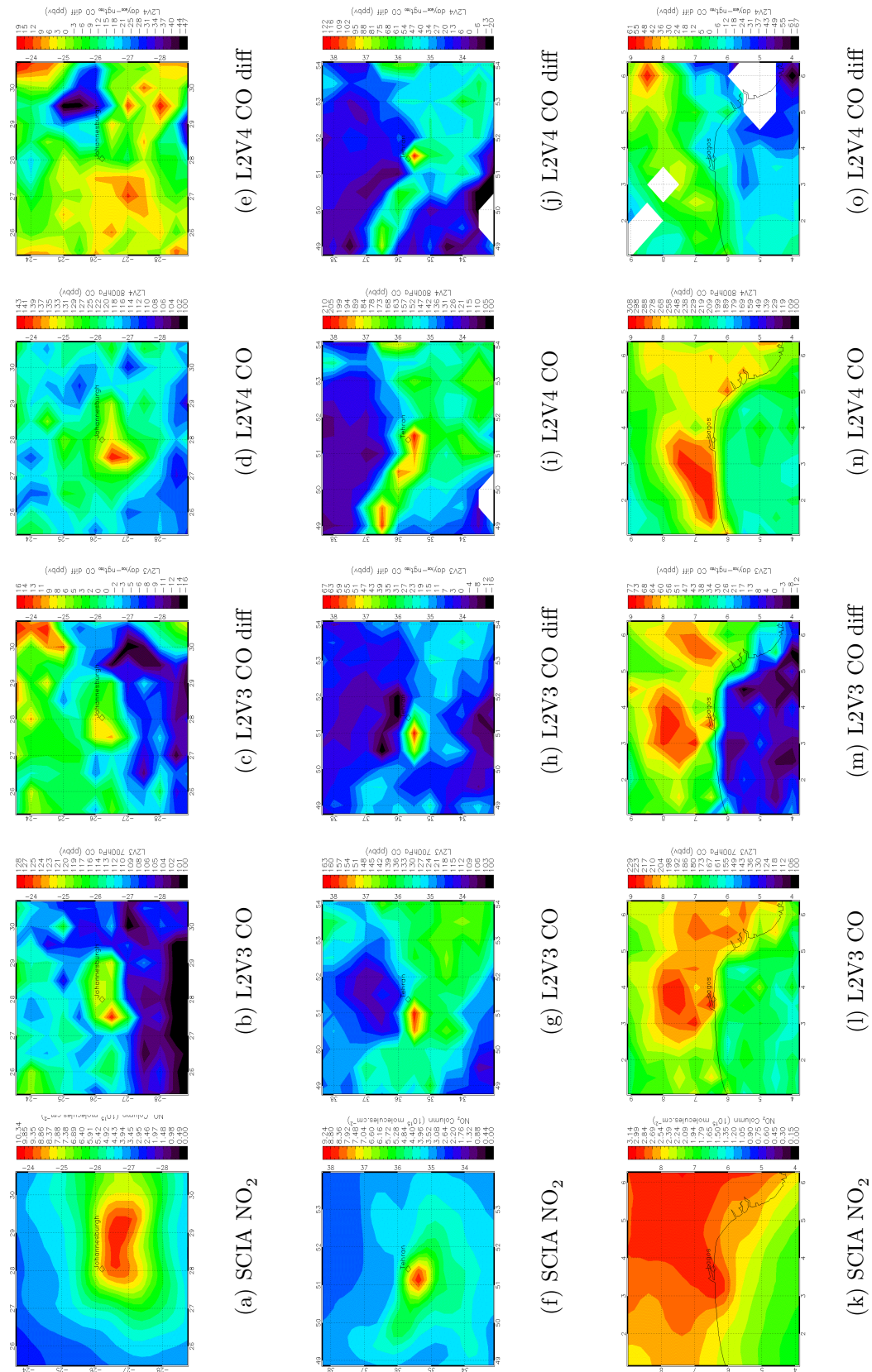


Figure 5.7: SCIAMACHY NO₂, MOPITT L2V3 daytime 700 hPa CO mixing ratios, MOPITT L2V3 700 hPa day-night difference CO mixing ratios, MOPITT L2V4 daytime 800 hPa CO mixing ratios, and MOPITT L2V4 day800-ngt700 difference CO mixing ratios, over striking cities. Johannesburg(top row), Teheran(middle row), Lagos(bottom row).

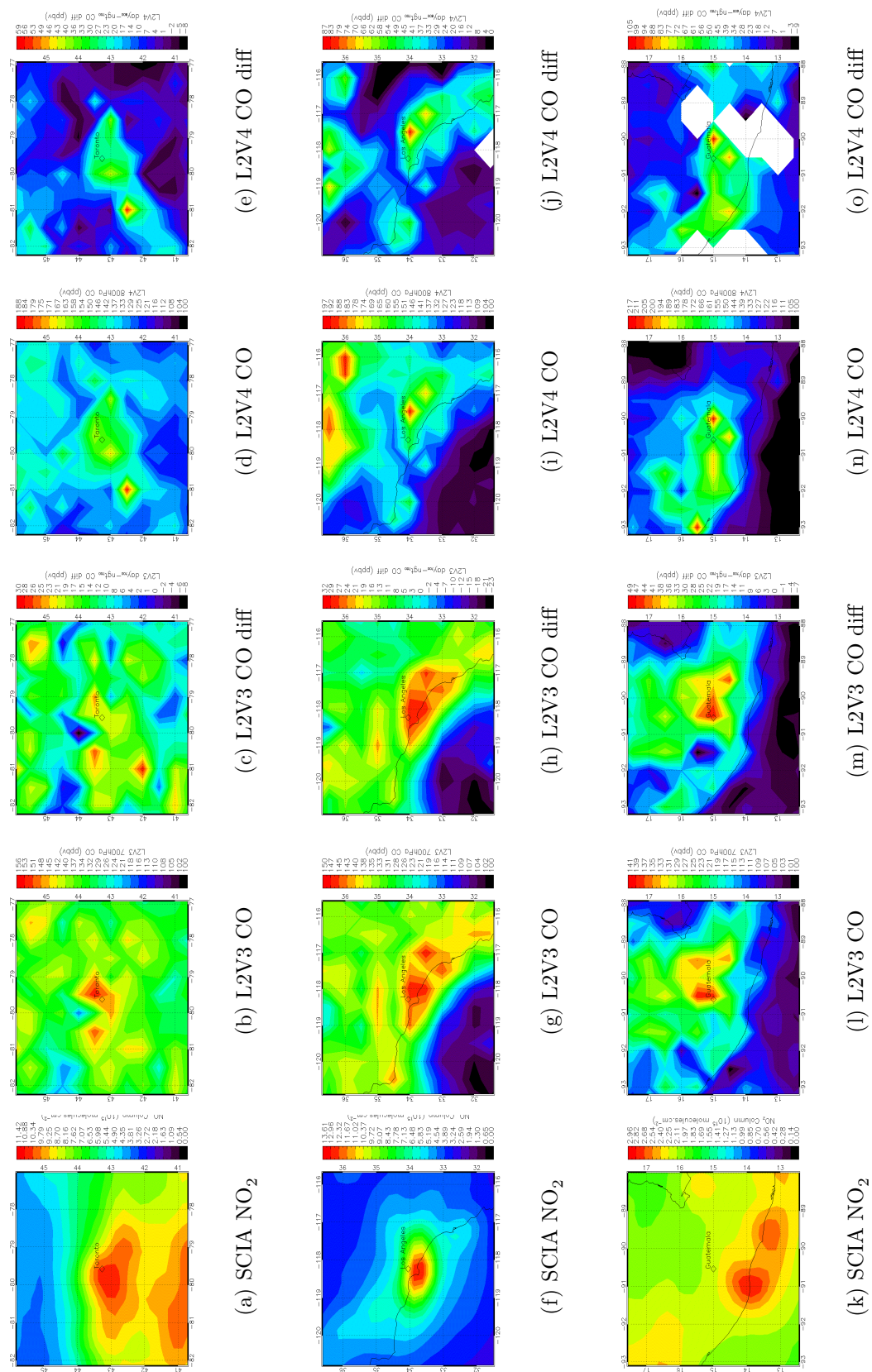


Figure 5.8: SCIAMACHY NO₂, MOPITT L2V3 daytime 700 hPa CO mixing ratios, MOPITT L2V3 700 hPa day-night difference CO mixing ratios, MOPITT L2V4 daytime 800 hPa CO mixing ratios, and MOPITT L2V4 day_{800-ngt700} difference CO mixing ratios, over striking cities. Toronto(top row), Los Angeles(middle row), Guatemala(bottom row).

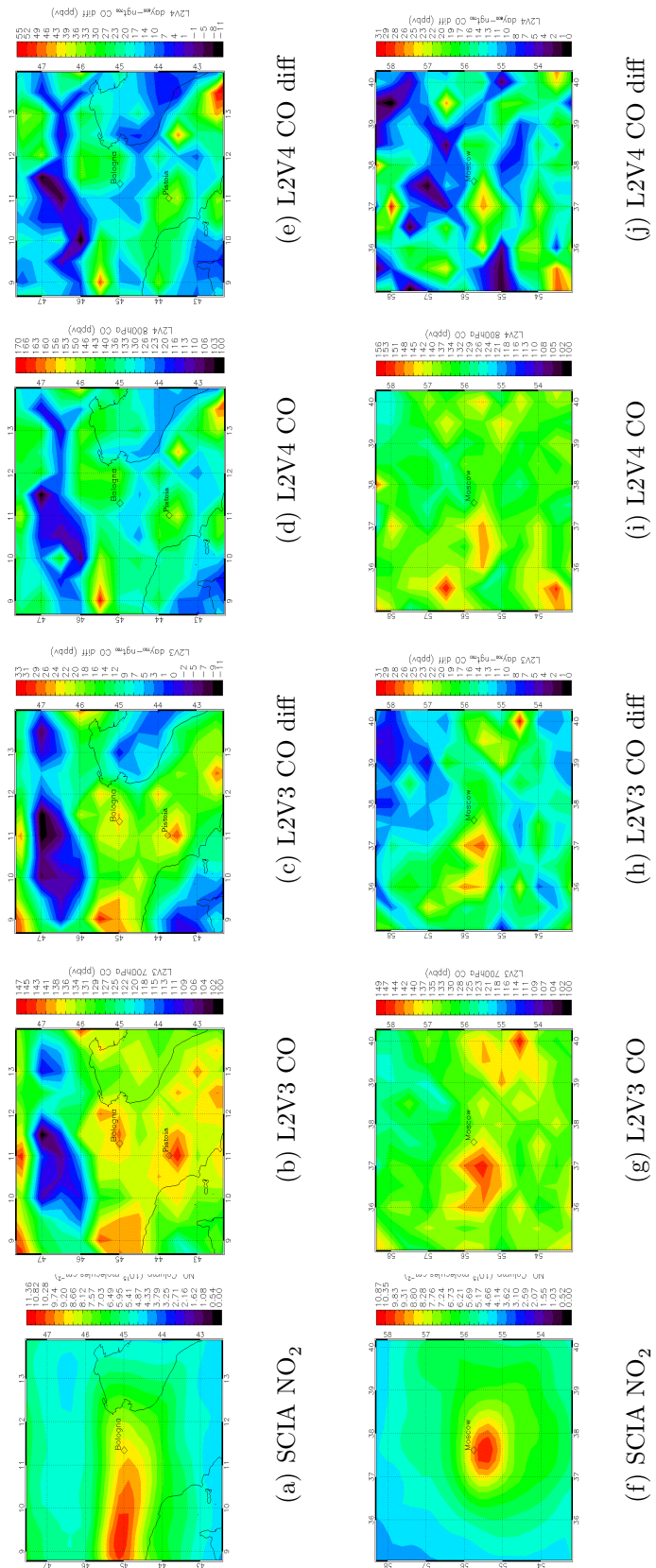


Figure 5.9: SCIAMACHY NO₂, MOPITT L2V3 daytime 700 hPa CO mixing ratios, MOPITT L2V3 700 hPa day-night difference CO mixing ratios, MOPITT L2V4 daytime 800 hPa CO mixing ratios, and MOPITT L2V4 day₈₀₀-ngt₇₀₀ difference CO mixing ratios, over striking cities. Bologna(top row), Moscow(bottom row).



Figure 5.10: Map showing large cities found in this analysis.

Specifically, this analysis was tested for 100+ large cities across the globe and it is found about 87 large cities or megacities, this includes all the cities identified by Clerbaux et al. [2008], can be detected using MOPITT observations to monitor pollution sources.

5.5 Summary of Chapter 5

In this chapter, the possibility of using IR instrument (e.g. MOPITT) to detect the CO signature of megacities or urban centres has been investigated. Satellites could complement the in-situ ground stations network for air pollution monitoring and air quality forecasts. This could be a step forward in our ability to observe CO emissions at key (at most) locations across the globe and also demonstrates the information available in current satellite sensors.

A comparison between SCIAMACHY NO_2 total column and L2V3 and L2V4 CO data has been presented. The elevated levels of CO over many urban areas or megacities can be detected when averaging one year of satellite data compared to recent studies which shows that elevated CO for some of the cities can be detected using 3 years of SCIAMACHY NIR nadir observations [Buchwitz et al., 2007] and 7 years of MOPITT IR nadir observations [Clerbaux et al., 2008]. It is also shown that day-night CO difference indeed offers very useful information on CO from the lowermost layer of the atmosphere which is unlikely to be obtained using daytime data

alone (e.g. Houston, Cairo, Florida, Birmingham and Wales). This analysis clearly shows a strong improvement to information on CO in the lowermost atmosphere. The major steps forward seen to be the use of day-night differences for two different analyses L2V3 and L2V4, the use of thresholds for higher DOFS retrievals, and the use of non-surface retrieval levels with less tie to a priori (L2V3).

Chapter 6

Conclusions and Future Scope

Atmospheric CO is one of the most abundant and widely distributed air pollutant and is a very important atmospheric gas via its reaction with OH radical which in turn controls the oxidising capacity of the troposphere. Our present understanding of the global CO distribution is mainly a result of the increasing availability of CO observations from local to global scale. A number of different techniques exist to measure CO in the troposphere. The early studies of CO were driven by an interest to better understand the underlying mechanisms of the variability in CO concentrations that has been observed in multiple scales and dimensions (i.e. local to global, ground-based network, airborne and space-based, short to long term atmospheric observations as well as laboratory and field flux measurements). Satellites measurements provide the opportunity to achieve global distribution of CO on a daily basis over long periods of time and possibly give a complete picture of CO in the atmosphere. Specifically, the MOPITT instrument CO data have offered the first opportunity to study horizontal and vertical distribution of CO in the troposphere. However, satellite data are still uncertain for several reasons (e.g. vertical sensitivity, insufficient signal due to reflection from the ocean, etc.). It is therefore of crucial importance to understand how satellite data can be interpreted correctly to identify and determine various natural and anthropogenic sources contributing to the tropospheric CO distribution. It has been shown in this thesis that MOPITT can, possibly, differentiate CO into layers and it indeed likely to have greatest sensitivity to the CO in the lowermost atmosphere and most likely the planetary boundary layer, certainly when there is good thermal contrast, elevated CO, and probably high boundary layer height.

6.1 Conclusions

6.1.1 Chapter 3: Sensitivity of MOPITT Observations of Tropospheric CO

In chapter 3, it is shown that MOPITT retrievals have significant sensitivity to CO in the lowermost layer of the atmosphere. MOPITT retrieved averaging kernels have large variability, particularly in the upper troposphere over a given region which has fairly uniform underlying surface properties (land vs ocean, surface temperature) and atmospheric properties (CO, temperature profile). Over land, daytime thermal contrast conditions appear to often produce significant sensitivity to lower tropospheric CO. Simulations have been conducted using selected 'typical' MOPITT averaging kernels to investigate the ability of the instrument to detect plumes of enhanced CO for different surface and atmospheric properties. In particular over the Indian subcontinent, the 'simulated' day-night CO differences can effectively delineate the strong surface source regions in summer as well as in winter.

The main conclusions of this study of the Indian subcontinent in 2007 are:

1. MOPITT L2V3 retrieval averaging kernels vary considerably, particularly from day to night and over land.
2. DOFS analysis shows greater sensitivity to lower atmosphere in daytime than of nighttime observations as expected, with greater DOFS in daytime.
3. For the selected Indian regions, the DOFS is well correlated to upper-troposphere (i.e. 350 hPa) percent a priori CO mixing ratios as expected.
4. The percent a priori CO mixing ratio is a useful parameter to understand uncertainty of the retrieved CO (at each retrieval level) as a percentage of a priori variability. The strong correlation between DOFS and percent a priori CO mixing ratio suggests one can use percent a priori instead DOFS which has to be calculated for each retrieved profile in L2V3 and it is time consuming process.

5. The daytime and nighttime DOFS exhibits a bi-modal DOFS for all selected Indian regions. A similar distribution can be seen in thermal contrast.
6. It is also shown that day-night could give a more sensitive indicator to the monthly averaged component of lower atmosphere enhancements, at the price of a loss of data and assumptions on variations of CO on monthly timescales. This finding is consistent with [Richards, N. A. D., 2004] thesis.
7. An analysis demonstrate for the first time that 700 hPa day-night differences gives a closer differentiation of lowermost CO than other measures for MOPITT data.
8. It can further shown that 700 hPa day-night difference is clearly superior to (850/350) CO ratio in demonstrating lowermost atmosphere enhancement.
9. Similarly for columns, a considerable utility to day-night columns difference which further provide confidence in adopted robust methodology.
10. For Indian subcontinent, this analysis confirms the pollution pools at the extremes of the Indo-Gangetic basin ("Bihar Pollution Pool" reported by [Kar et al., 2008]). A more extensive CO pollution loading in the west coast and southern tip of India are also observed. Small enhancements in NO₂ are also observed in these regions supporting this analysis.

6.1.2 Chapter 4: MOPITT L2V3 and L2V4 Simulation Comparison Study

In this chapter, two-fold evidence that MOPITT retrievals indeed have sensitivity to the boundary layer CO is presented which mostly depends upon the thermal contrast conditions, boundary layer height and elevated CO. The MOPITT L2V3 and L2V4 retrievals show that it is possible to use day-night differences in retrieved CO data to detect lowermost and high altitude enhancements which indeed help to localised CO pollution and later to study of transport to long distances from source regions. The results also indicate that in order to determine the vertical structure of CO using MOPITT profile data, a selection methodology for 'typical' averaging kernel is required. The method developed in this thesis primarily for MOPITT L2V3 and later applied to recently released (April 2009) L2V4 retrievals is thought to be reasonable and appropriate for this kind of analysis. Moreover, the simulation tests for more realistic TOMCAT model CO profile further enhance our knowledge about CO and build-up confidence in this methodology.

The main conclusions of this study are -

1. Similar to L2V3 retrievals, the L2V4 retrievals averaging kernels also vary considerably, particularly from day to night and from land to water surfaces. However, the L2V4 retrieval averaging kernels likely to provide 2 pieces of profile shape information for the retrieved CO profile, averaging kernel peaking at 800 hPa, 500 hPa and 300 hPa retrieval level.
2. The L2V4 retrievals also show greater sensitivity to lower atmosphere in daytime that of nighttime observations as expected, with greater DOFS in daytime. The L2V4 DOFS are always superior to L2V3 DOFS.
3. The daytime and nighttime DOFS exhibits a bi-modal DOFS for all selected Indian regions similar to L2V3 retrievals.
4. In this chapter, it is shown in L2V4 data that $\text{day}_{800}\text{-night}_{700}$ differences gives a closer differentiation of lowermost CO, showing greatest sensitivity to 800 hpa retrieval level for the daytime measurements having large planetary boundary layer height.

5. For Indian subcontinent, an analysis confirms the elevated lower layer CO concentrations over extremes of the Indo-Gangetic basin (i.e. Bihar), Delhi, west coast (i.e. Mumbai) and southern tip of India (i.e. Coimbatore) in the month of May and December owing to variability of the sensitivity in these regions as observed in chapter 3 work.
6. It is likely that the MOPITT L2V4 a priori has significant influence on profile shape information for the retrieved CO profile. However, it need further more rigorous analysis to fully asses a priori influence on L2V4 retrievals.

6.1.3 Chapter 5: Signature of CO from Megacities

Atmospheric air pollution resulting from fossil and bio fuel combustion is an important problem, especially for countries with increasing fuel consumption such as China and India. CO contributes significantly to air quality problem because it is toxic in large concentrations, acts as a precursor to tropospheric ozone and via OH it largely determines the self-cleansing efficiency of the troposphere. CO is highly variable in space and time and accurate measurements of its spatial pattern and time evolution is required especially for air pollution monitoring and forecasting applications in highly populated areas. It is worth noting that MOPITT satellite sensor offers CO measurements over extended periods of time (nearly a decade) and it does indeed allow the examination of the impact of intense urban pollution sources on continental and global scale air quality

The work presented in chapter 3 and 4 has outlined methodologies which demonstrate that there is real sensitivity to lowermost atmosphere CO where day-night differences are positive and one could exploit day-night differences and daytime CO as a guide to investigate possibility of using MOPITT observations to detect CO enhancements over large urban centres or megacities, by averaging data over a year time.

The main conclusions of this study are -

1. From the work presented in chapter 3 and 4, it is clearly more informative to use available information content thresholds to exclude particular subsets of the data
2. A very good correlation between L2V3 and L2V4 day-night differences and with NO₂ total column confirms that day-night difference is a good identification of individual plumes from large urban centres or megacities.
3. Positive day-night differences often appear over large urban centres, suggesting elevated CO concentrations in the lowermost layer of the atmosphere. Interestingly the enhancements are not clearly visible in the daytime data alone with careful plotting and do not in themselves are not proof of lowermost atmosphere enhancements. There is a clear utility to day-night differences to mark out CO over or in general, in vicinity of urban centres.

4. It is worth noting that MOPITT can detect large cities which are not, in particular, surrounded by mountains where pollution is trapped and can thus be detected using MOPITT observations as suggested by Clerbaux et al. [2008].
5. It is clear that the advanced detection presented here arises from more 3 points from conclusions of chapter 5.
6. The major steps forward seen to be the use of day-night differences for two different analyses L2V3 and L2V4, the use of thresholds for higher DOFS retrievals, and the use of non-surface retrieval levels with less tie to a priori
7. This analysis could be a step forward in our ability to observe CO emissions over urban centres or megacities across the globe and offers utility to the information available in current satellite sensors.

6.2 Future Scope

This thesis demonstrated, in general, a closer differentiation of lowermost CO in the troposphere using MOPITT L2V3 and L2V4 retrieved CO profile data. The simulation results are presented for May and December months of the year 2007. It would be useful to perform simulations for different time periods to examine seasonal variability in the characteristics of MOPITT retrievals. The fuller understanding of seasonal or interannual variability in the retrieved CO profile data would probably facilitate future efforts to examine long term trends in the CO data despite the fact that a variety of effects besides instrument noise influence individual retrieved CO profiles.

The simulation study could be extended further to investigate the ability of day-night differences to explore the altitude of CO enhancement. It would probably be helpful to determine the source of upper tropospheric CO enhancements over a wide range of latitudes.

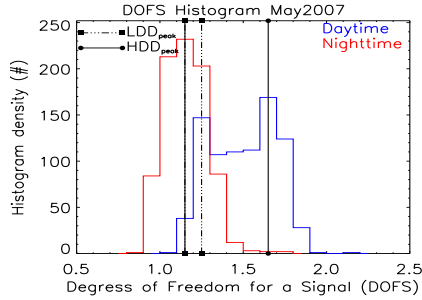
The analysis demonstrate that there is real sensitivity to lowermost atmosphere CO where day-night differences are positive, particularly over land. It is necessary to understand the significance of day-night differences over the ocean to study long-range transport of pollution.

The work presented in chapter 5 demonstrate that MOPITT is able to detect CO signatures from large cities or urban centres using methodologies outlines in chapters 3 and 4 by averaging data over one year. It would be further possible to investigate the possibility of MOPITT instrument to detect CO signatures from urban centres on monthly averaged data, at the price of a loss of data and assumptions on variations of CO on monthly timescales.

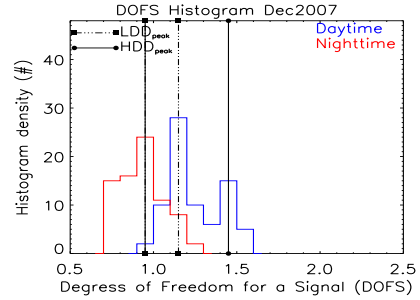
The use of day-night differences suggest that the advantage and in parts on design of geostationary instruments should be explored. The advantage of using geostationary satellites is that they can view the whole earth, rather than a small subsection, and therefore they scan the same area very frequently (typically every 30 to 60 minutes). This makes them ideal for meteorological applications.

Chapter 7

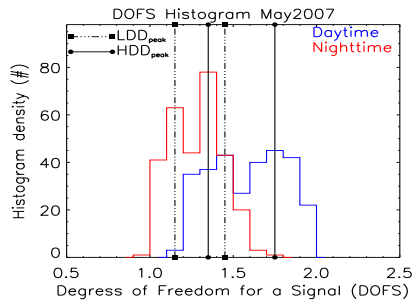
Appendix-I



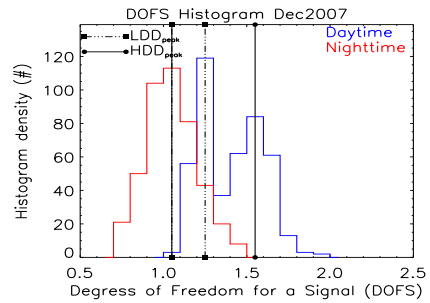
(a) Delhi - May



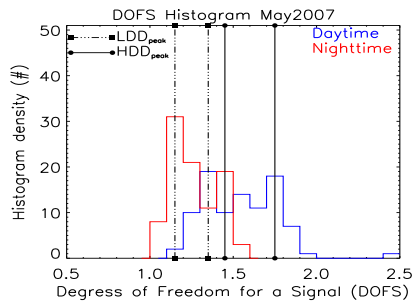
(b) Delhi - Dec



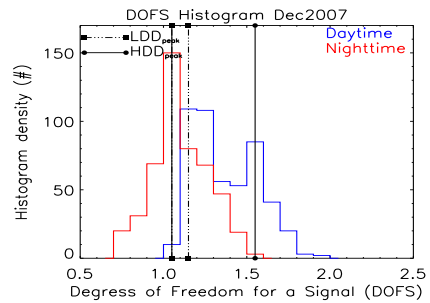
(c) Mumbai - May



(d) Mumbai - Dec



(e) Coimbatore - May



(f) Coimbatore - Dec

Figure 7.1: (a) Histogram for daytime and nighttime DOFS, over Delhi box, for May 2007; (b) Same as (a) except for December 2007; (c) Same as (a) except for Mumbai; (d) Same as (a) except for Mumbai and December 2007; (e) Same as (a) except for Coimbatore; (f) Same as (a) except for Coimbatore and December 2007.

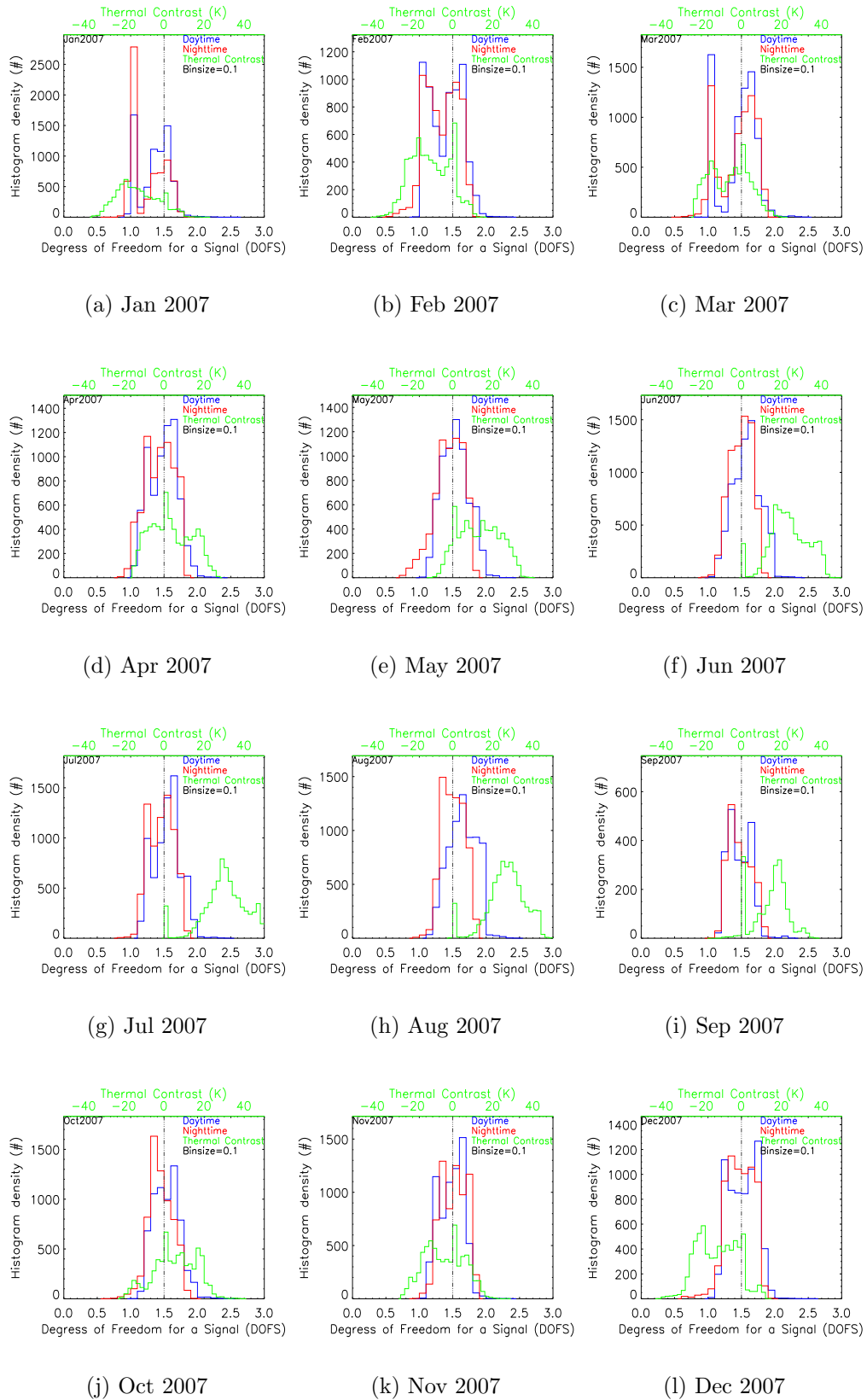


Figure 7.2: Histogram of DOFS and thermal contrast calculated for Northern Hemisphere tropical region for each month of the year 2007.

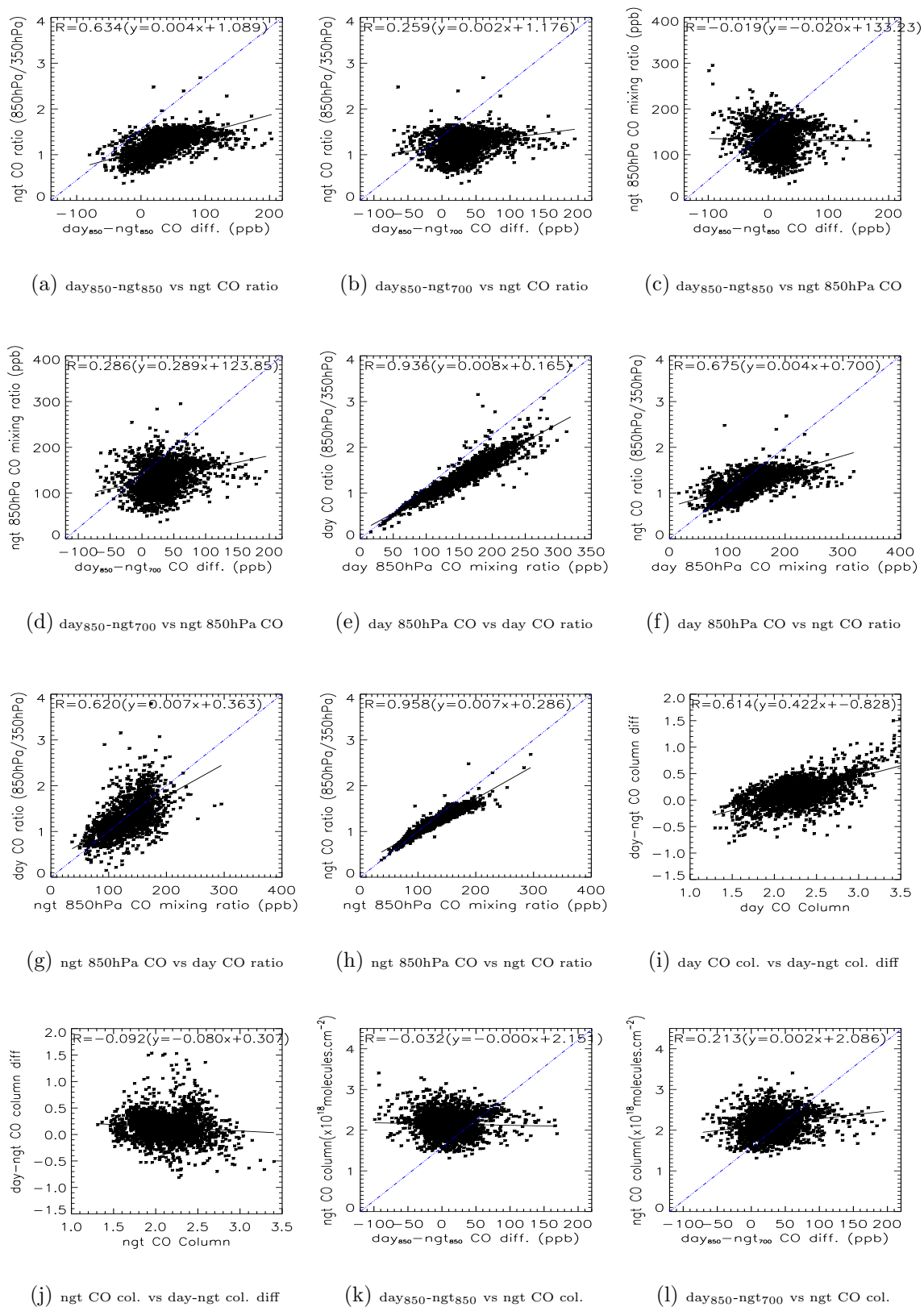


Figure 7.3: Correlation results between MOPITT L2V3 retrieved CO data and considered diagnostics in this study in the month of May 2007.

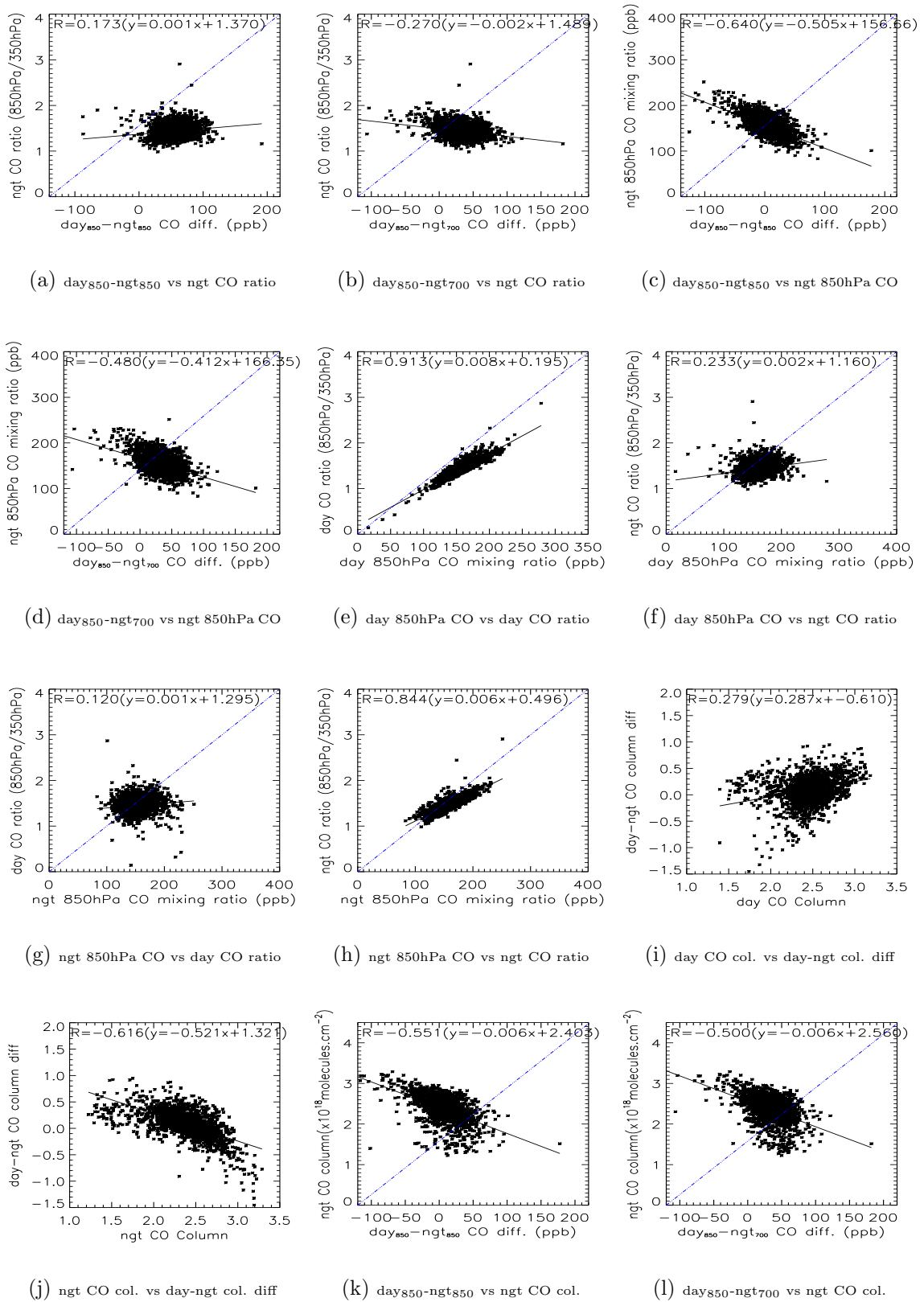
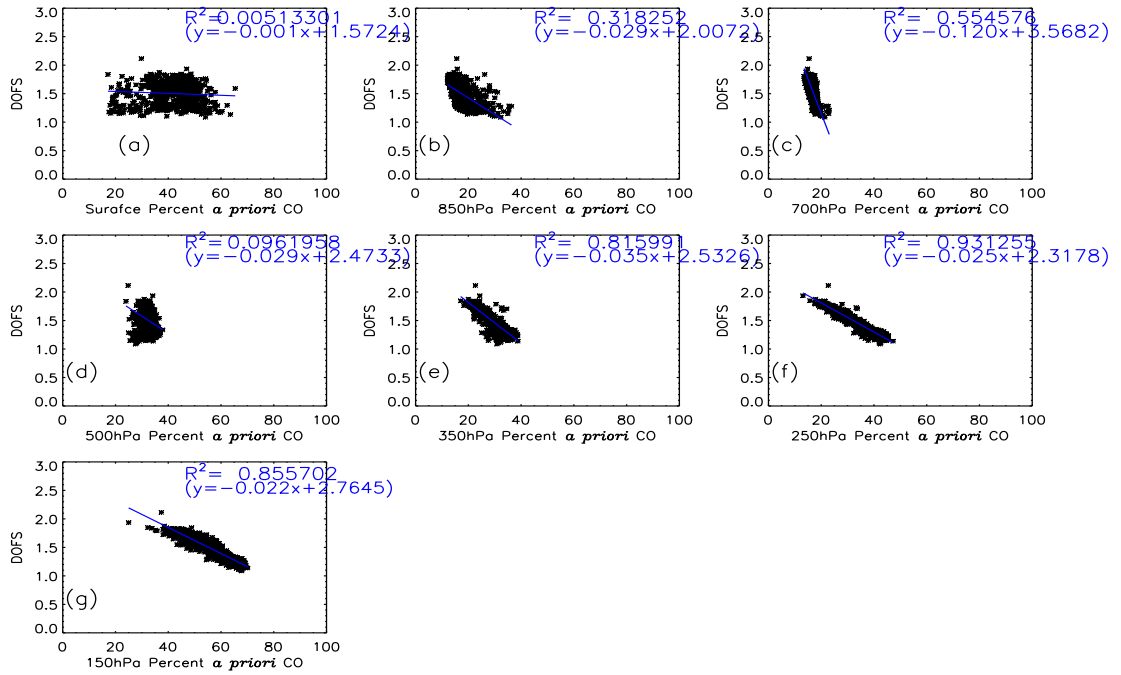
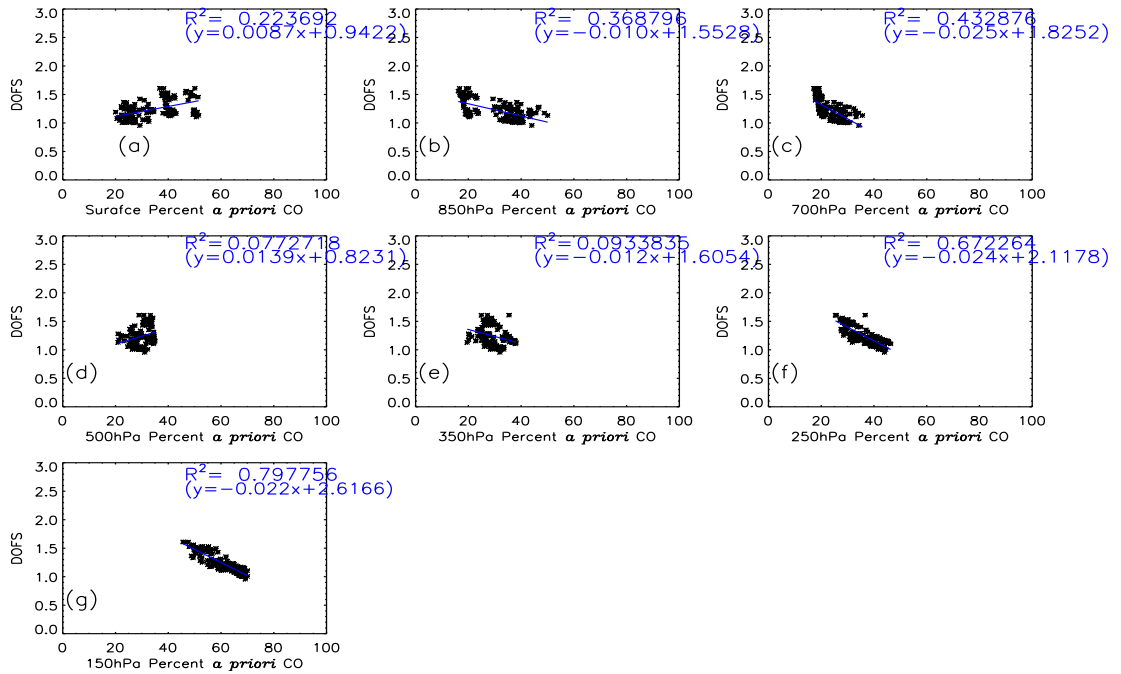


Figure 7.4: Correlation results between MOPITT L2V3 retrieved CO data and considered diagnostics in this study in the month of December 2007.

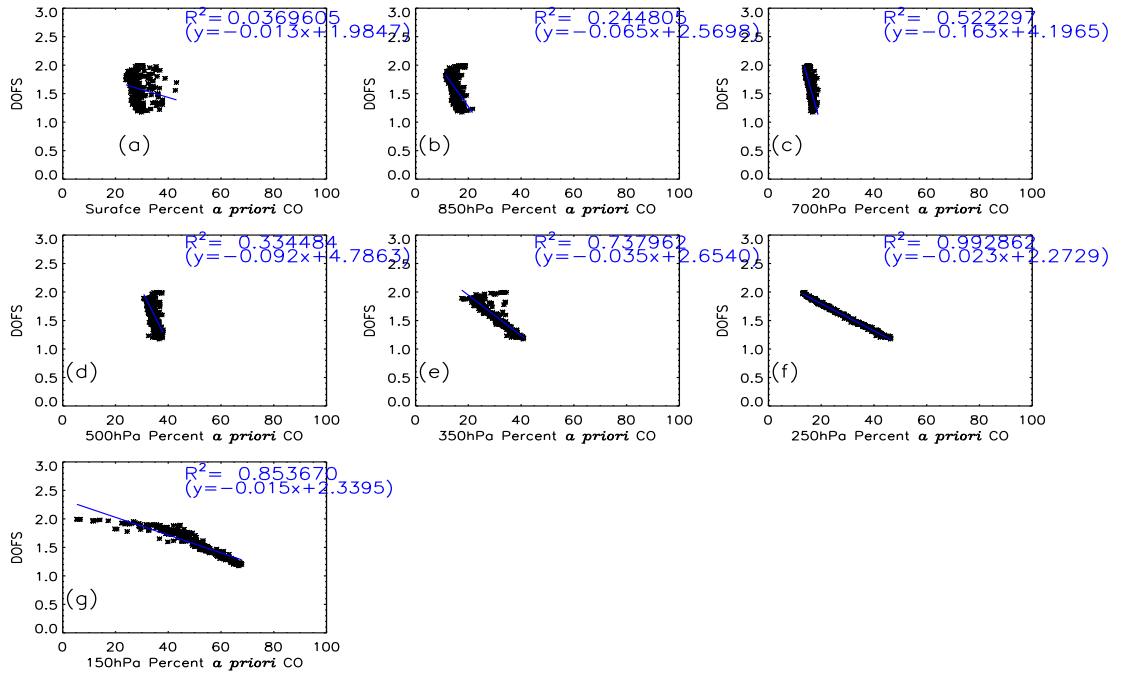


(a) Delhi - May

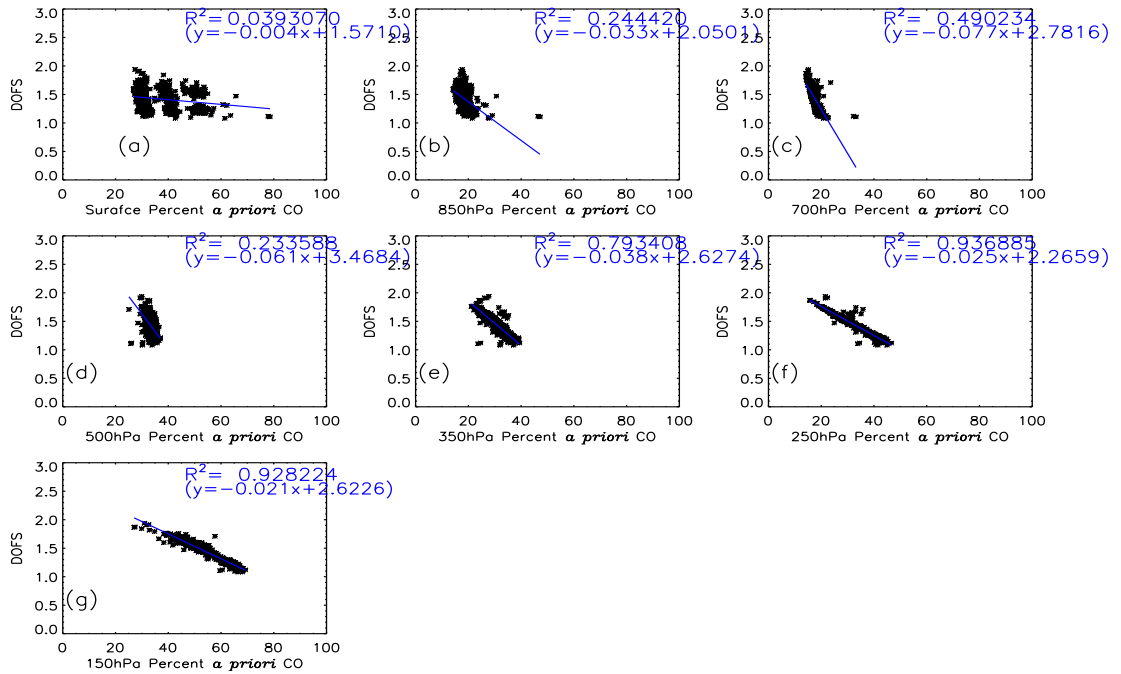


(b) Delhi - December

Figure 7.5: Correlation between DOFS and percent a priori CO mixing ratio, over Delhi region, in the month of May and December 2007.

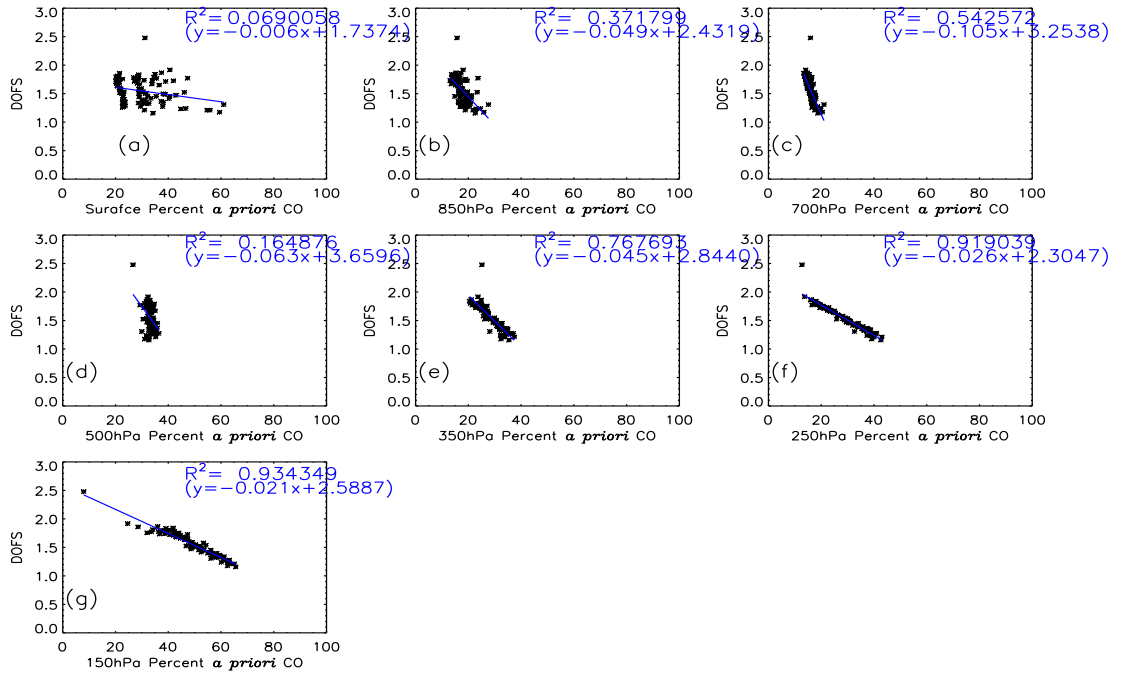


(a) Mumbai - May

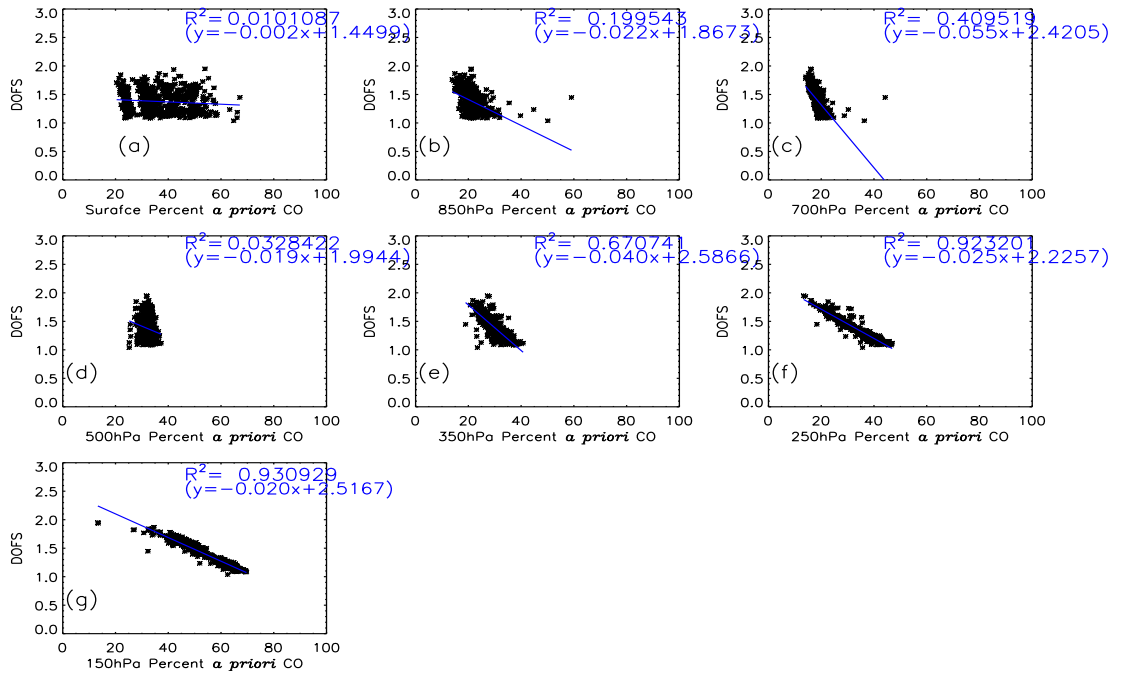


(b) Mumbai - December

Figure 7.6: Correlation between DOFS and percent a priori CO mixing ratio, over Mumbai region, in the month of May and December 2007.



(a) Coimbatore - May



(b) Coimbatore - December

Figure 7.7: Correlation between DOFS and percent a priori CO mixing ratio, over Coimbatore region, in the month of May and December 2007.

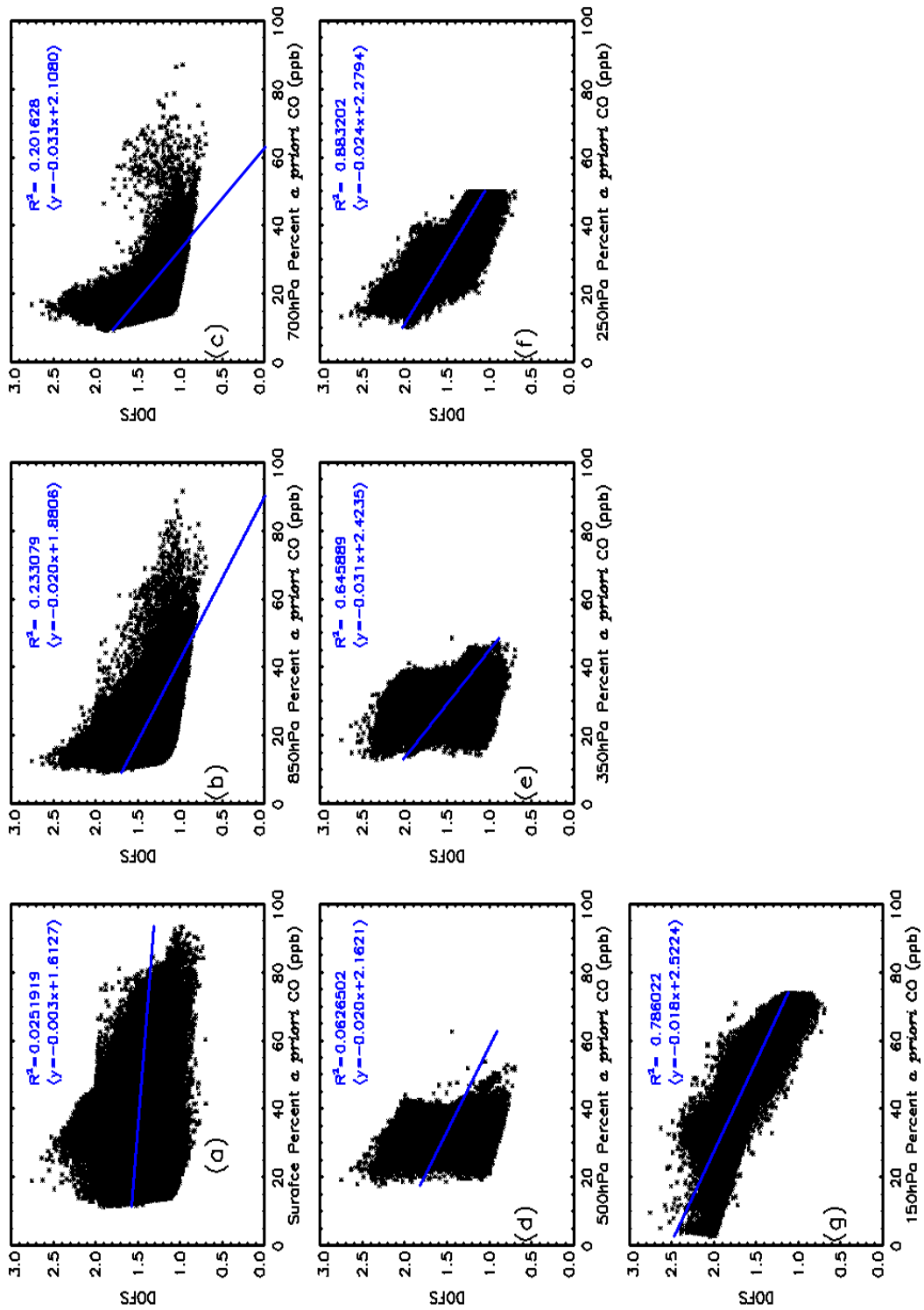


Figure 7.8: Correlation between DOFS and percent a priori CO mixing ratio for global land data in the month of May 2007.

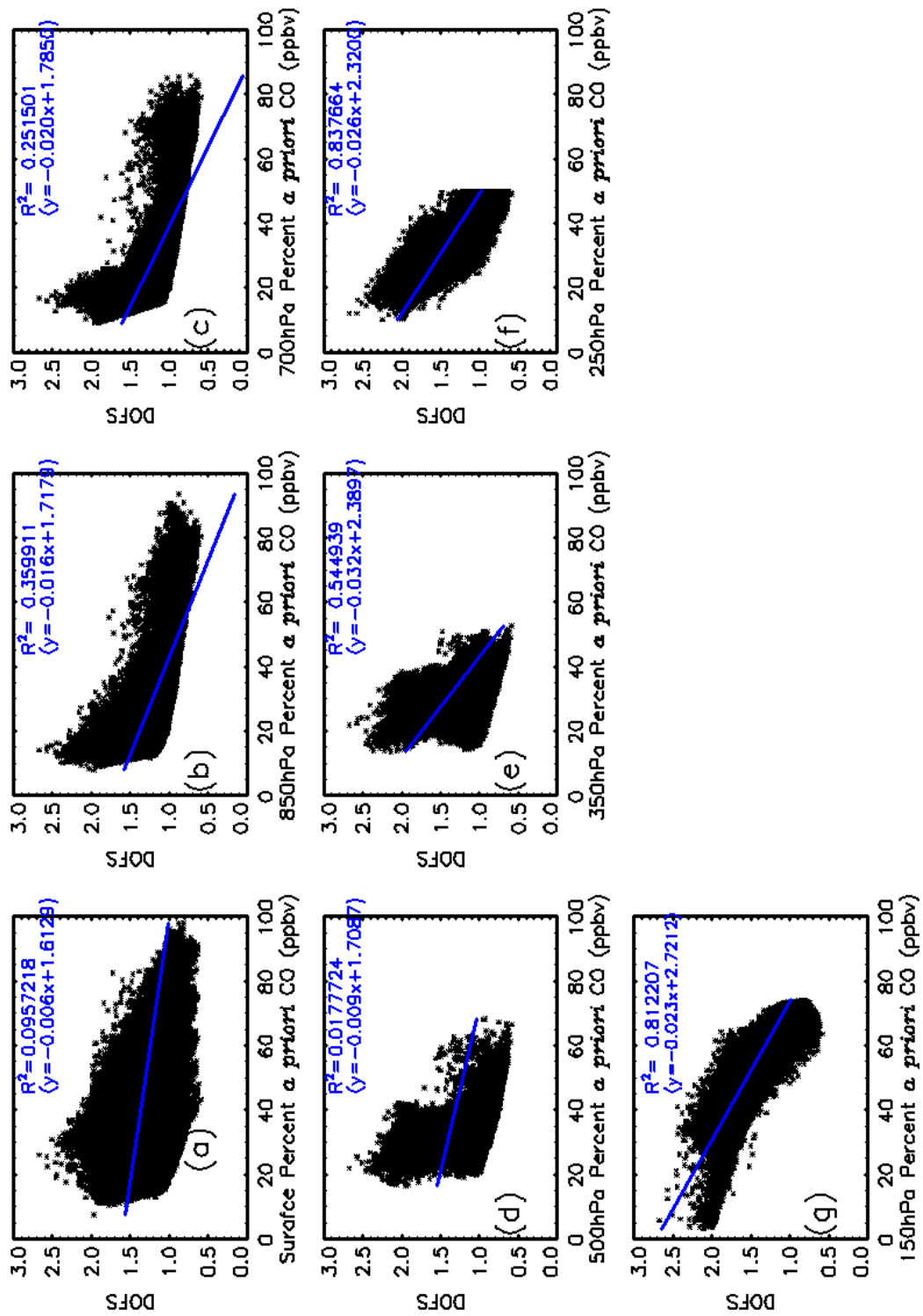
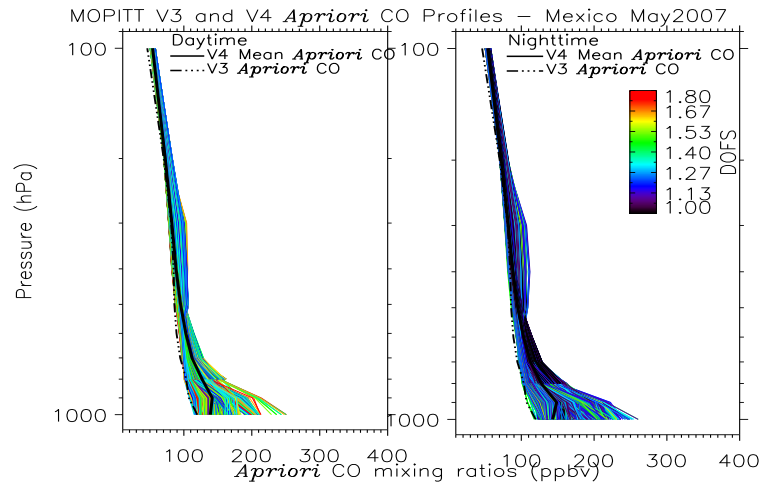


Figure 7.9: Correlation between DOFS and percent a priori CO mixing ratio for global land data in the month of Dec 2007.

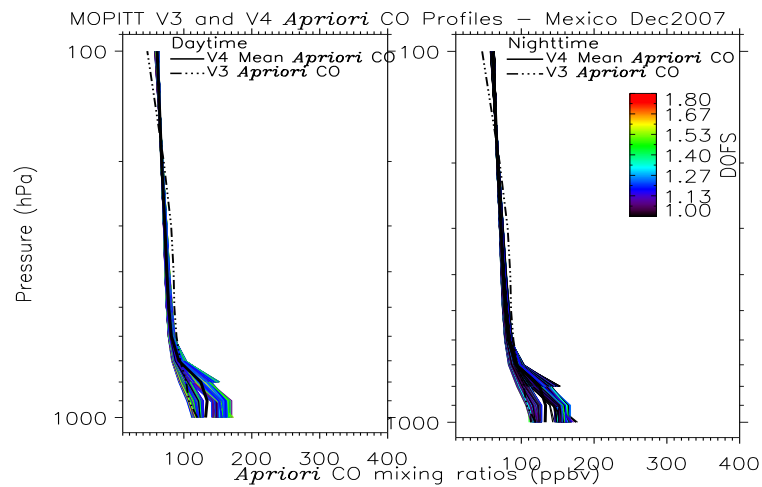
Chapter 4

7.1 A Case Study of Mexico City

7.1.1 L2V3 and L2V4 Simulations

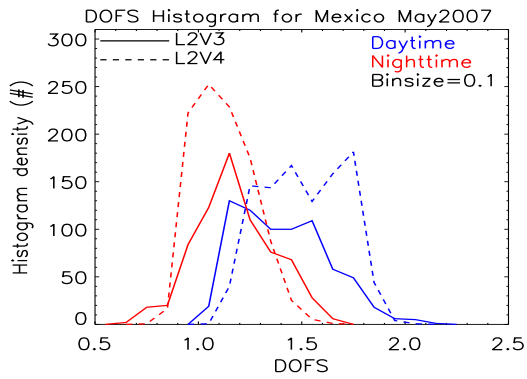


(a) L2V3 and L2V4 a priori CO - May

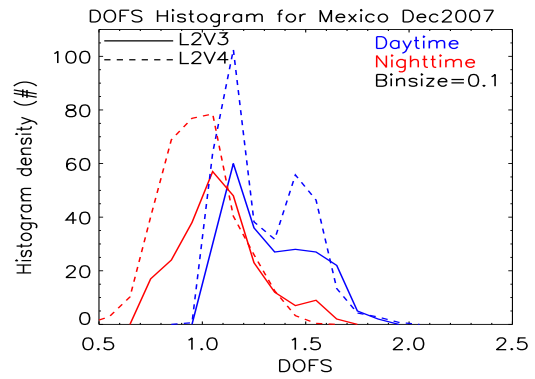


(b) L2V3 and L2V4 a priori CO - Dec

Figure 7.10: (a) MOPITT L2V3 and L2V4 retrievals a priori CO mixing ratio profile(s), over Mexico region, in the month of May 2007; (b) Same as (a) except for December 2007.

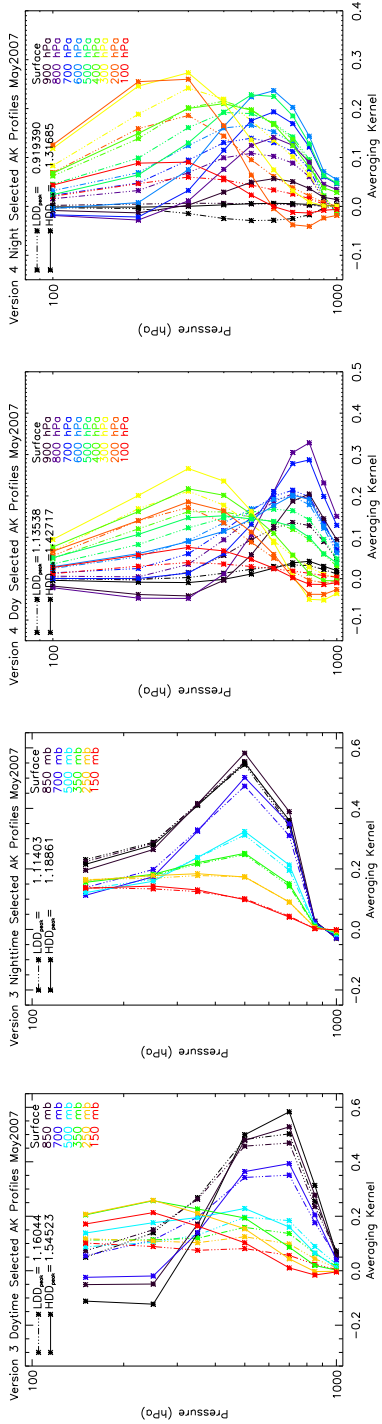


(a) L2V3 and L2V4 DOFS - May



(b) L2V3 and L2V4 DOFS - Dec

Figure 7.11: (a) MOPITT L2V3 and L2V4 DOFS histogram plot, over Mexico region, in the month of May 2007; (b) Same as (a) except for December 2007.

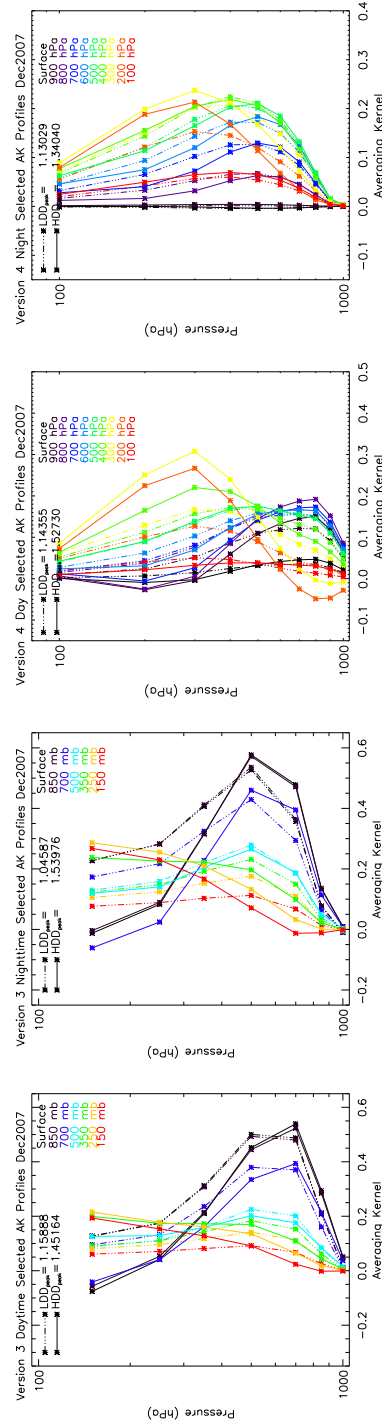


(a) L2V3 - Day AK

(b) L2V3 - Night AK

(c) L2V4 - Day AK

(d) L2V4 - Night AK



(e) L2V3 - Day AK

(f) L2V3 - Night AK

(g) L2V4 - Day AK

(h) L2V4 - Night AK

Figure 7.12: (a) MOPITT L2V3 selected daytime 'typical' averaging kernel, over Mexico region, in the month of May 2007; (b) Same as (a) except for nighttime; (c) MOPITT L2V4 selected daytime 'typical' averaging kernel, over Mexico region, in the month of May 2007; (d) Same as (c) except for nighttime; (e-f) Same as (a-d) except for December 2007.

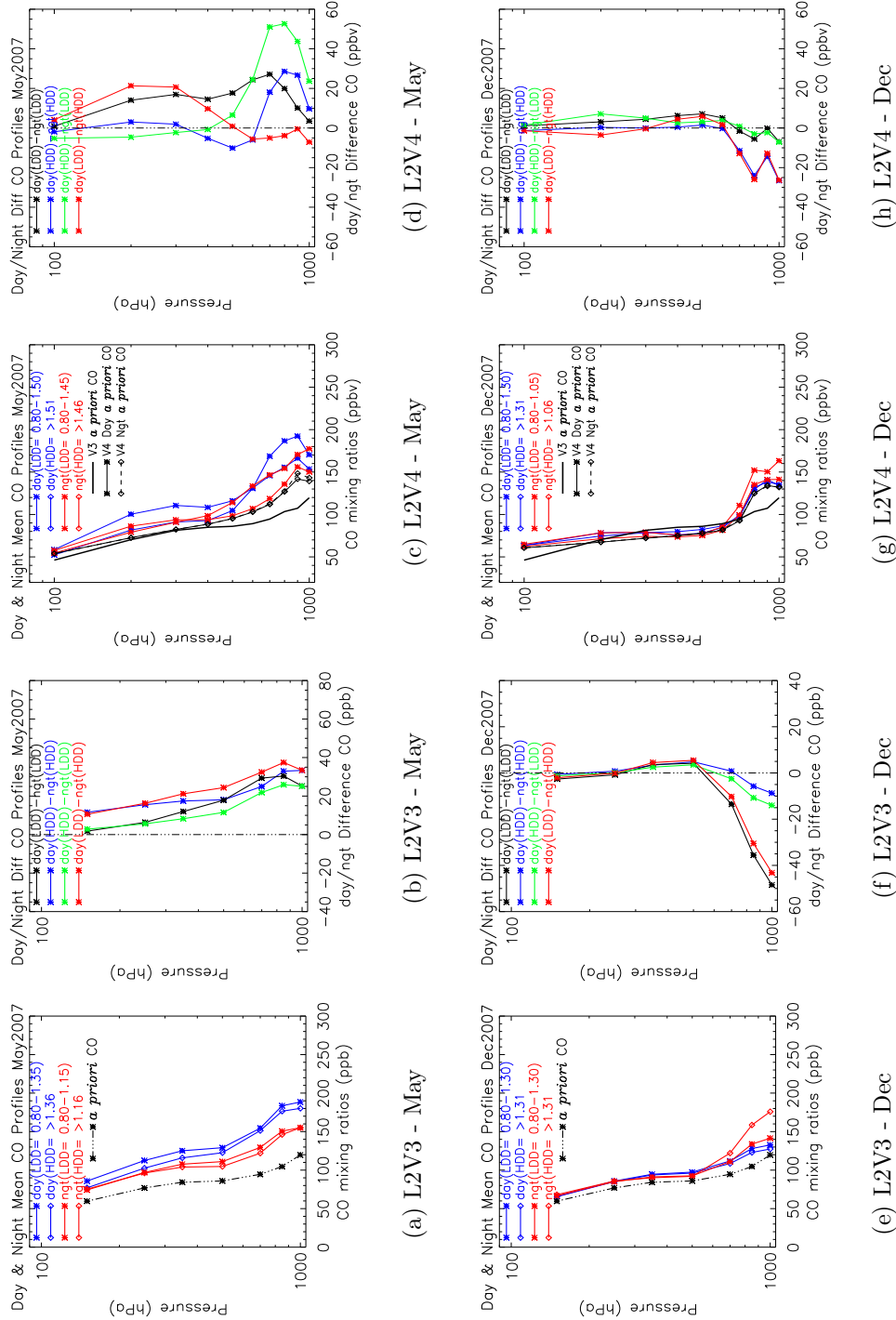
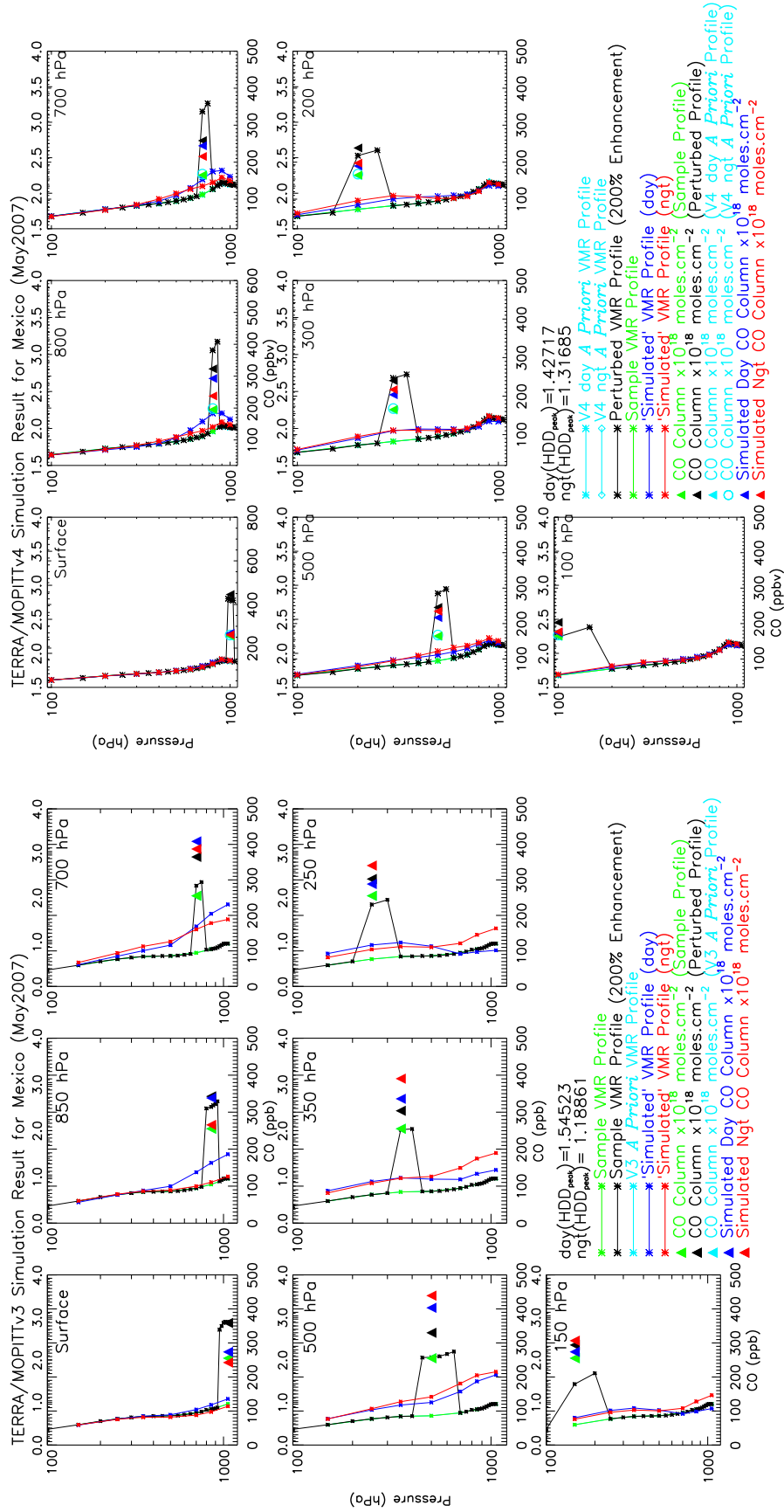


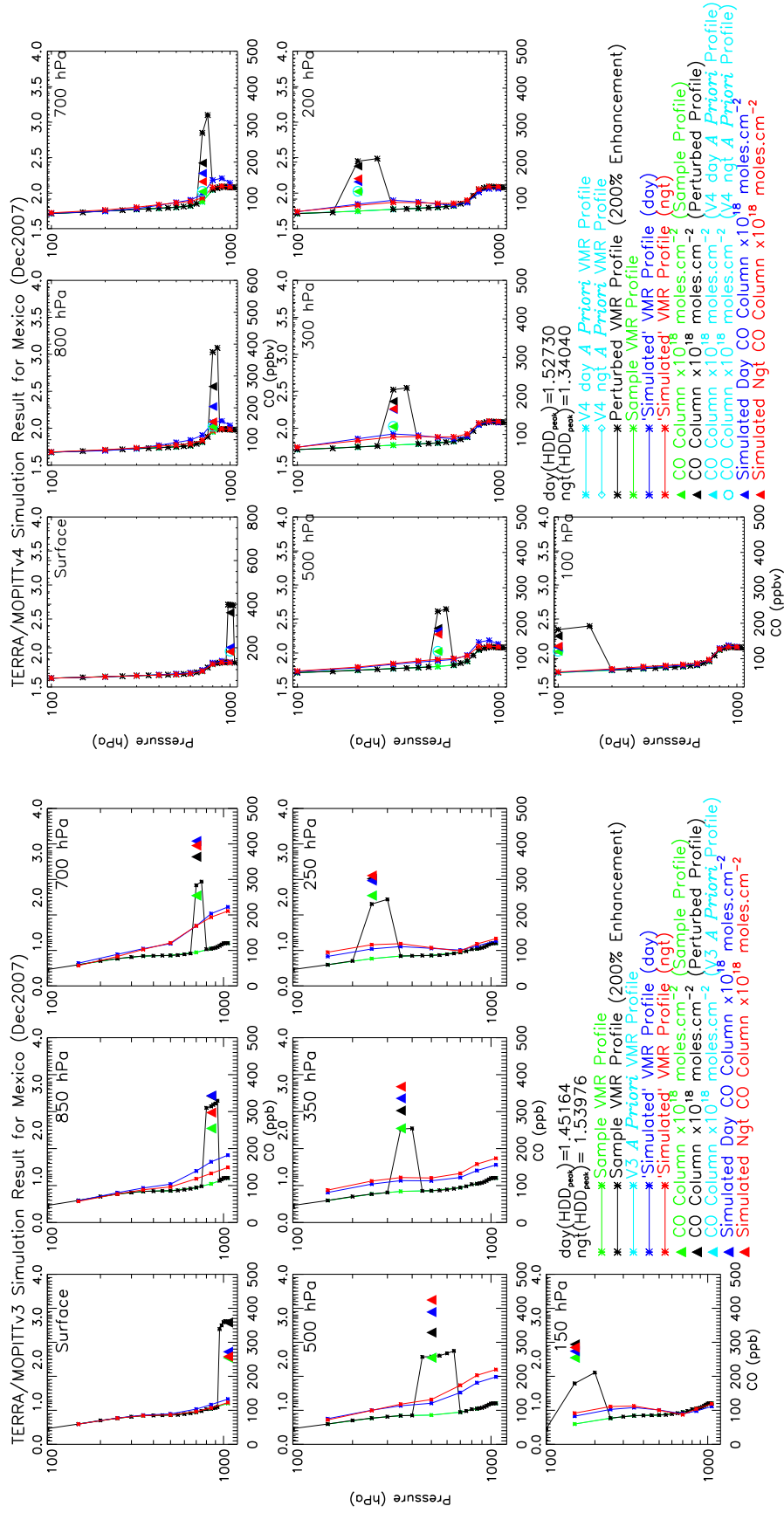
Figure 7.13: (a) MOPITT L2V3 retrieved mean daytime and nighttime CO profiles, over Mexico box, for May 2007; (b) Mean day-night difference CO profiles, over Mexico box, for combination of LDD and HDD; (c) Same as (a) except for MOPITT L2V4; (d) Same as (b) except for MOPITT L2V4; (e) Same as (a) except for December 2007; (f) Same as (b) except for December 2007; (g) Same as (c) except for December 2007; (h) Same as (d) except for December 2007;



(a) L2V3 - May

(b) L2V4 - May

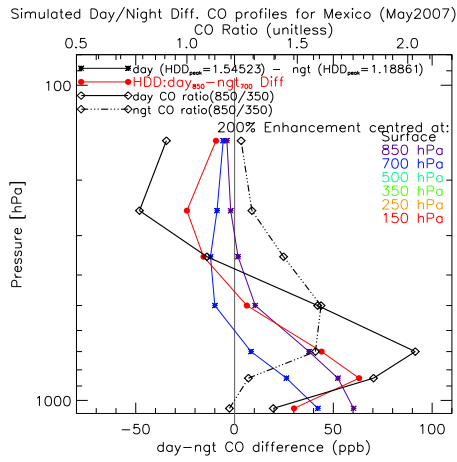
Figure 7.14: (a) MOPITT L2V3 'simulated' daytime and nighttime CO profiles for HDD $_{peak}$ over Mexico, for May 2007; (b) Same as (a) except for MOPITT L2V4. The green, black, cyan, blue, and red line indicates the considered sample CO profile, perturbed CO profile, a priori CO profile, 'simulated' day CO profile, and 'simulated' night CO profile. The green, black, cyan, blue, and red triangles show calculated total column values for corresponding CO VMR profiles. The total column has unit 10 18 molecules.cm $^{-2}$.



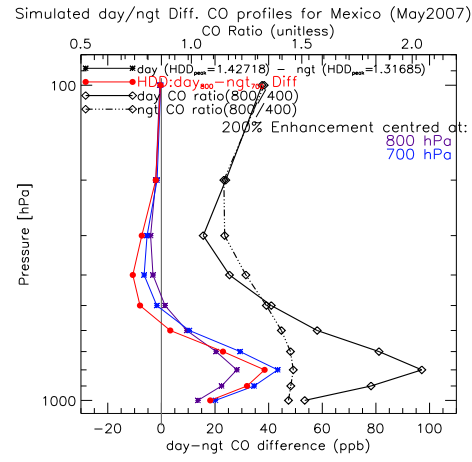
(a) L2V3 - Dec

(b) L2V4 - Dec

Figure 7.15: (a) MOPITT L2V3 ‘simulated’ daytime and nighttime CO profiles for HDD_{peak}, over Mexico, for December 2007; (b) Same as (a) except for MOPITT L2V4. The green, black, cyan, blue, and red line indicates the considered sample CO profile, perturbed CO profile, a priori CO profile, ‘simulated’ day CO profile, and ‘simulated’ night CO profile. The green, black, cyan, blue, and red triangles show calculated total column values for corresponding CO VMR profiles. The total column has unit 10¹⁸ molecules.cm⁻².

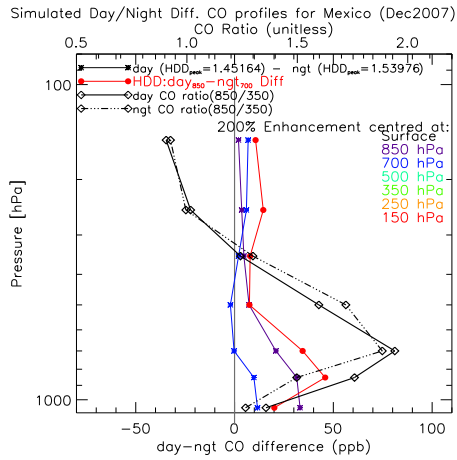


(a) L2V3 - May

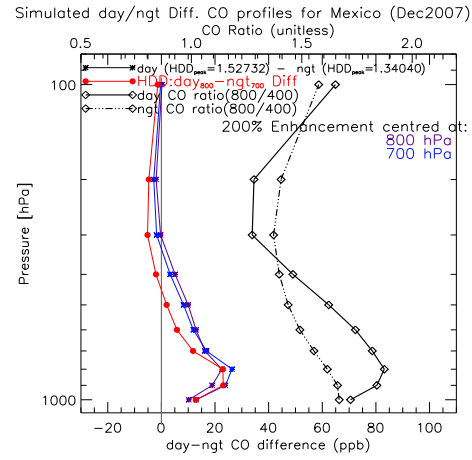


(b) L2V4 - May

Figure 7.16: (a) MOPITT L2V3 ‘simulated’ key day-night difference CO profiles for HDD_{peak} , over Mexico, for May 2007; (b) Same as (a) except for MOPITT L2V4.



(a) L2V3 - Dec



(b) L2V4 - Dec

Figure 7.17: (a) MOPITT L2V3 ‘simulated’ key day-night difference CO profiles for HDD_{peak} , over Mexico, for December 2007; (b) Same as (a) except for MOPITT L2V4.

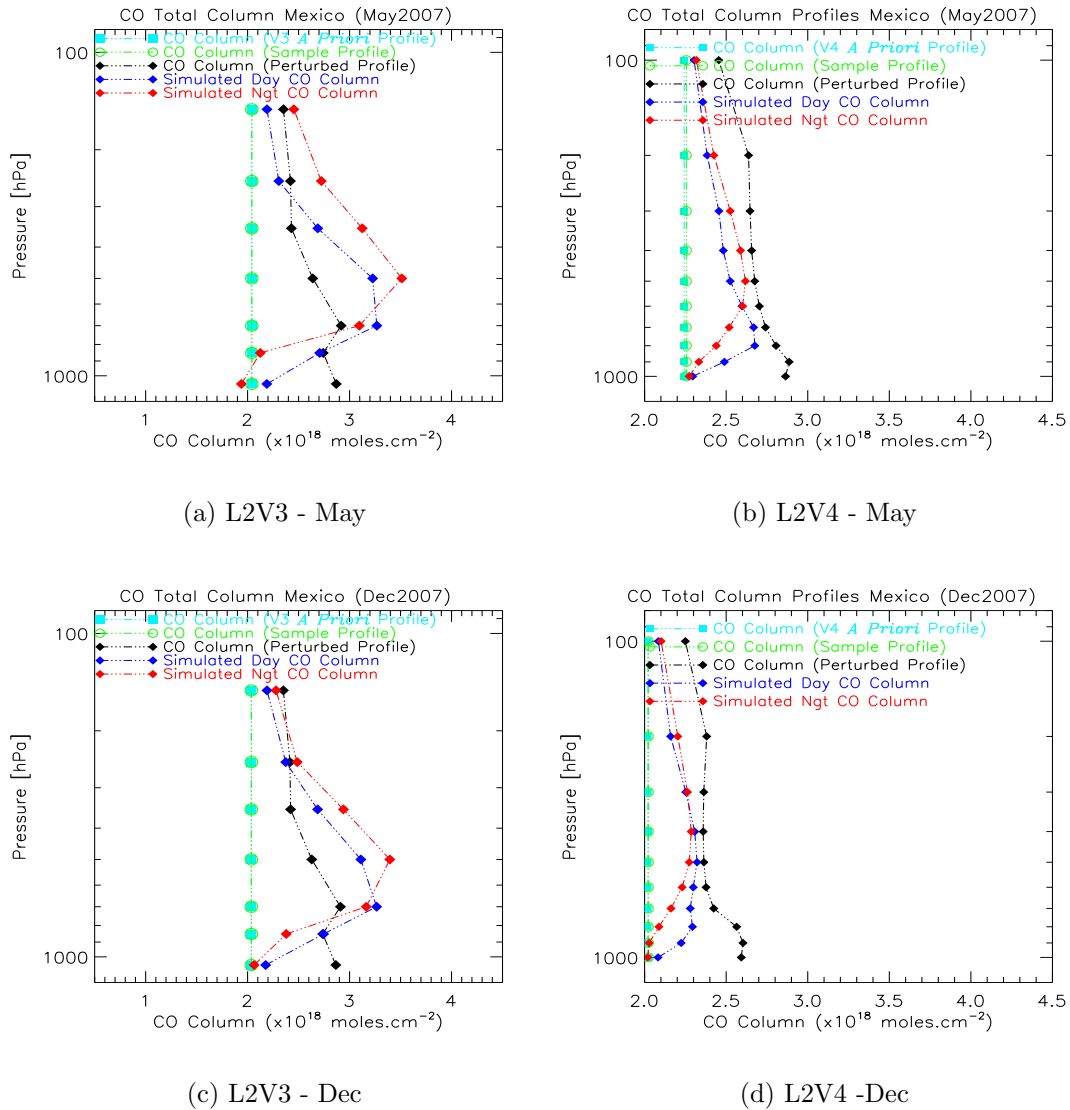


Figure 7.18: MOPITT L2V3 and L2V4 retrieval calculated total column values for i) a priori CO profile (cyan), ii) 7 individual sample profiles (green), iii) 7 individual perturbed sample profile (black), and iv) 7 individual simulated day (blue) and night (red) CO profiles, over Mexico, for May (top panel) and December (bottom panel) 2007; Note that these are not considered as profiles. For proper understanding the total column values plotted at corresponding perturbed retrieval level (layer) for each CO VMR profile.

7.1.2 TOMCAT Model CO Profile Simulation

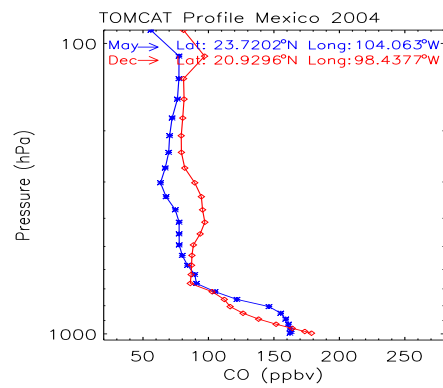
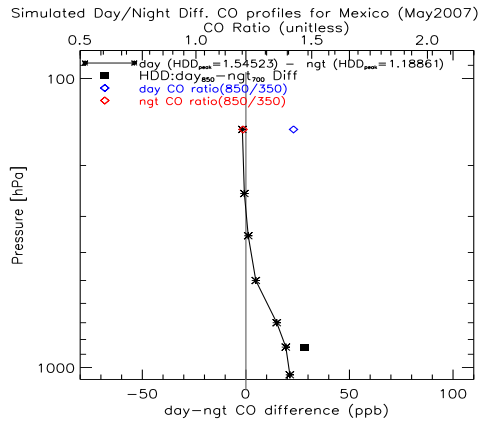
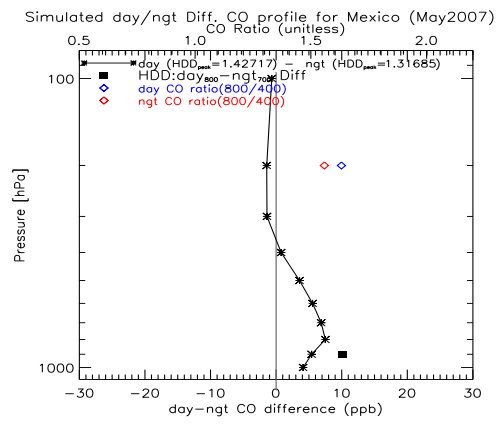


Figure 7.19: Selected TOMCAT model CO profiles, over Mexico box, for May 2004 (blue) and December 2004 (red).



(a) L2V3 - May

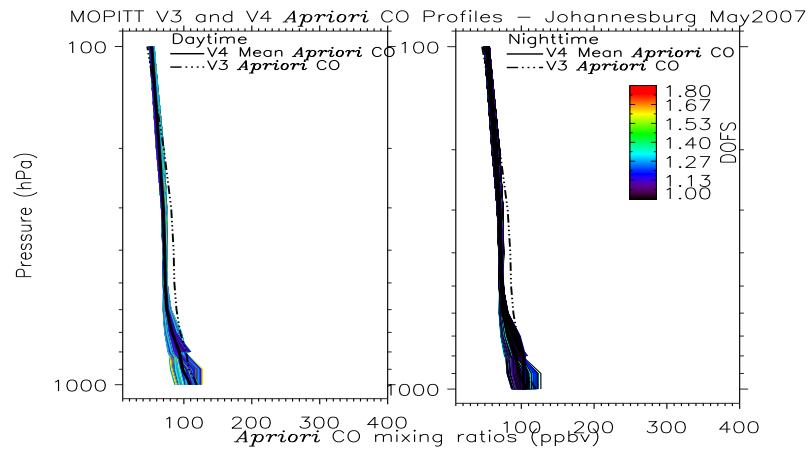


(b) L2V4 - May

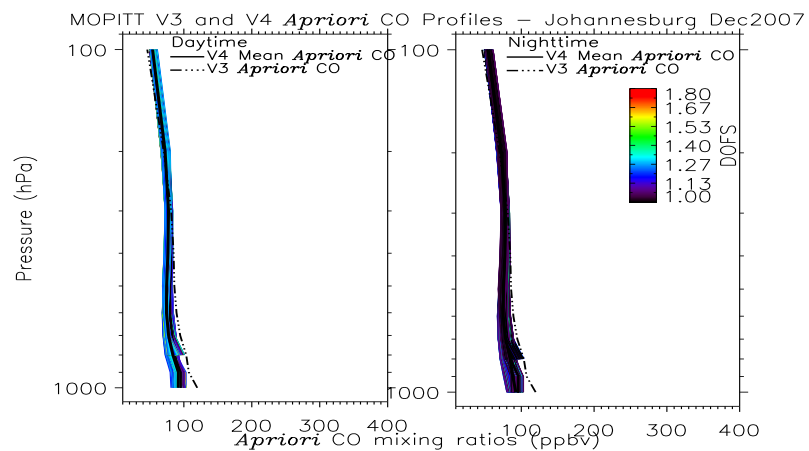
Figure 7.21: (a) MOPITT L2V3 ‘simulated’ day-night difference CO profile for HDD_{peak} , over Mexico, for May 2007; (b) Same as (a) except for MOPITT L2V4.

7.2 A Case Study of Johannesburg

7.2.1 L2V3 and L2V4 Simulations

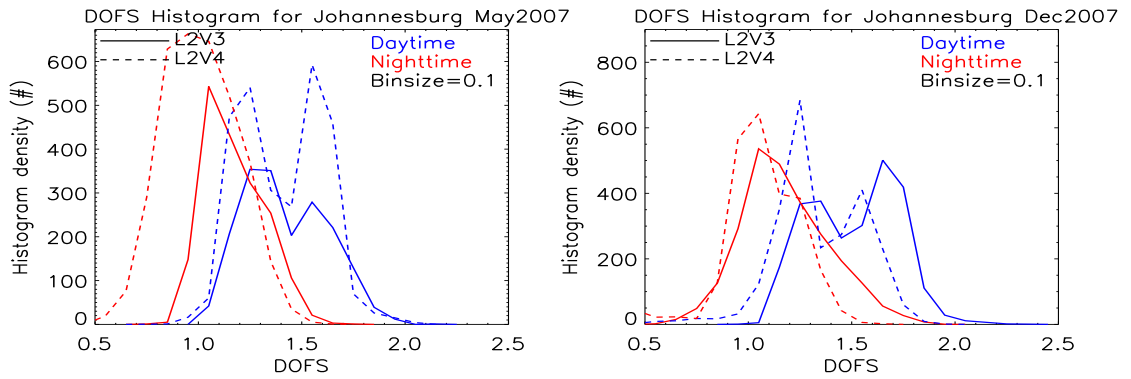


(a) L2V3 and L2V4 a priori CO - May



(b) L2V3 and L2V4 a priori CO - Dec

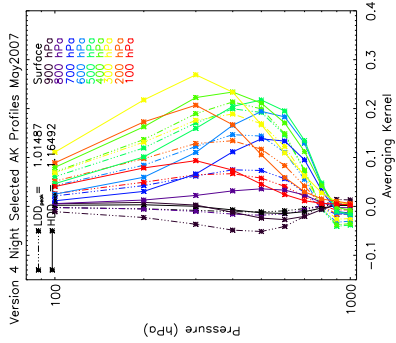
Figure 7.22: (a) MOPITT L2V3 and L2V4 retrievals a priori CO mixing ratio profile(s), over Johannesburg region, in the month of May 2007; (b) Same as (a) except for December 2007.



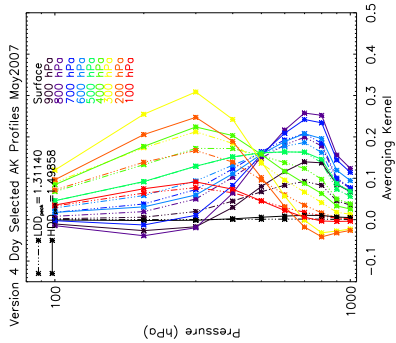
(a) L2V3 and L2V4 DOFS - May

(b) L2V3 and L2V4 DOFS - Dec

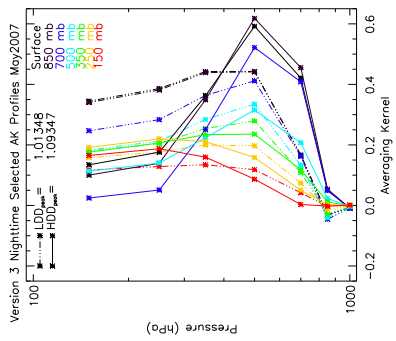
Figure 7.23: (a) MOPITT L2V3 and L2V4 DOFS histogram plot, over Johannesburg region, in the month of May 2007; (b) Same as (a) except for December 2007.



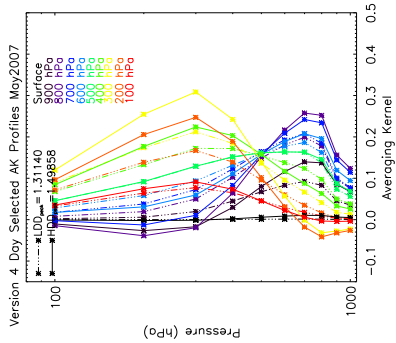
(a) L2V3 - Day AK



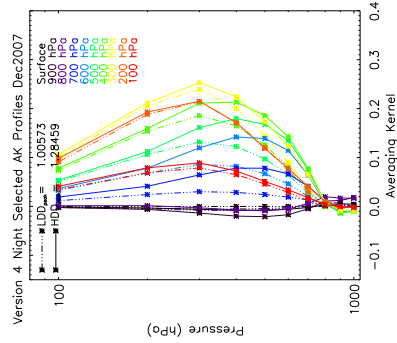
(b) L2V3 - Night AK



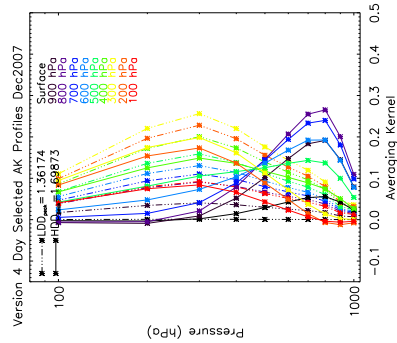
(c) L2V4 - Day AK



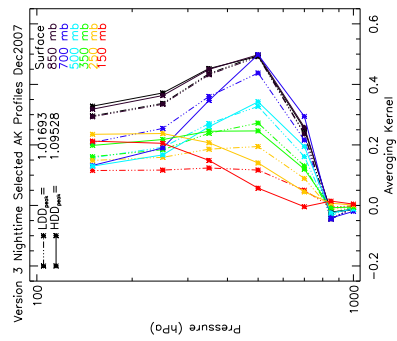
(d) L2V4 - Night AK



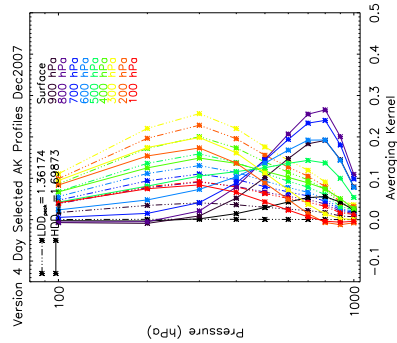
(e) L2V3 - Day AK



(f) L2V3 - Night AK



(g) L2V4 - Day AK



(h) L2V4 - Night AK

Figure 7.24: (a) MOPITT L2V3 selected daytime 'typical' averaging kernel, over Johannesburg region, in the month of May 2007; (b) Same as (a) except for nighttime; (c) MOPITT L2V4 selected daytime 'typical' averaging kernel, over Johannesburg region, in the month of May 2007; (d) Same as (c) except for nighttime; (e-f) Same as (a-d) except for December 2007.

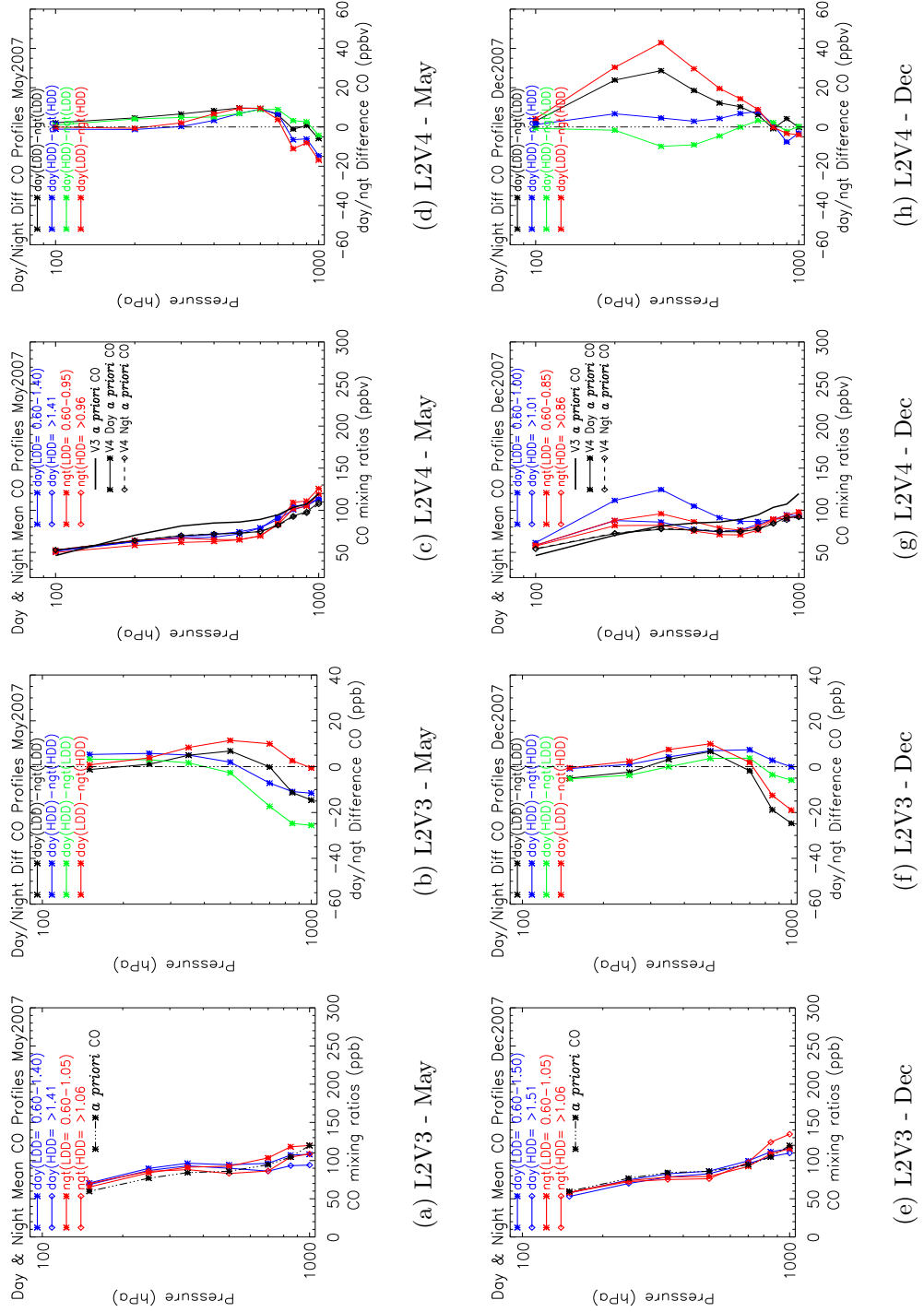
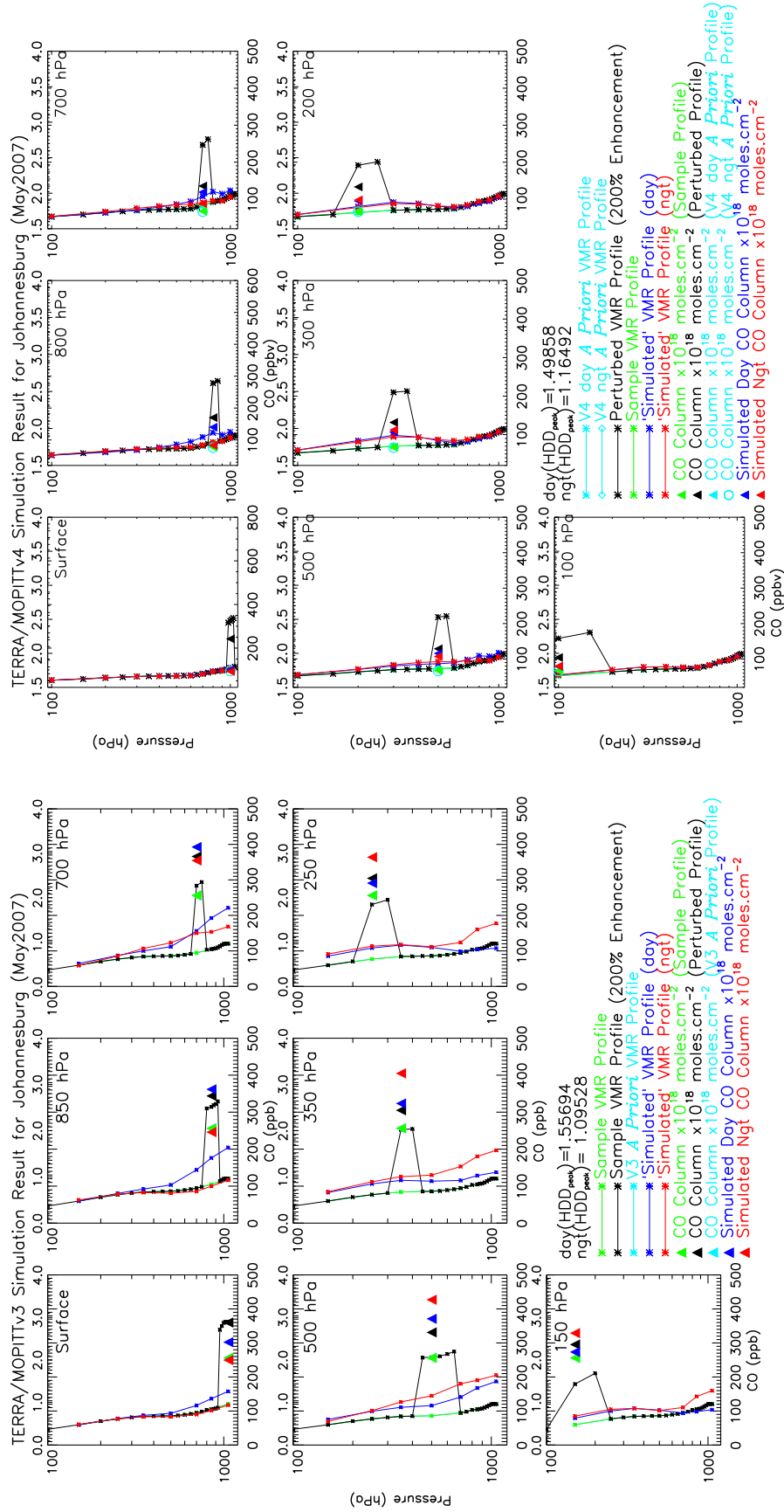


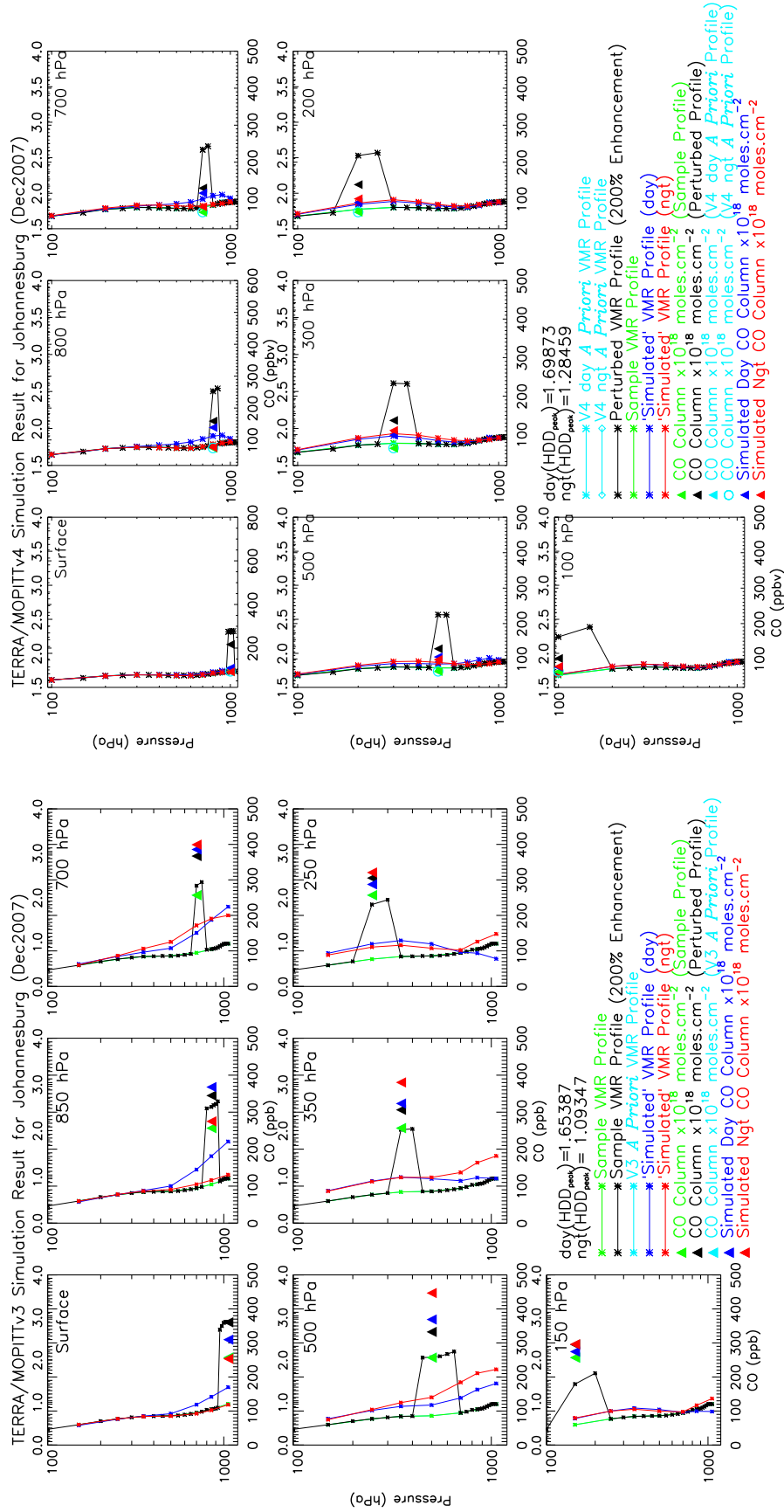
Figure 7.25: (a) MOPITT L2V3 retrieved mean daytime and nighttime CO profiles, over Johannesburg box, for May 2007; (b) Mean day-night difference CO profiles, over Johannesburg box, for combination of LDD and HDD; (c) Same as (a) except for MOPITT L2V4; (d) Same as (b) except for MOPITT L2V4; (e) Same as (a) except for December 2007; (f) Same as (b) except for December 2007; (g) Same as (c) except for December 2007; (h) Same as (d) except for December 2007;



(a) L2V3 - May

(b) L2V4 - May

Figure 7.26: (a) MOPITT L2V3 'simulated' daytime and nighttime CO profiles for HDD_{peak}, over Johannesburg, for May 2007; (b) Same as (a) except for MOPITT L2V4.



(a) L2V3 - Dec

(b) L2V4 - Dec

Figure 7.27: (a) MOPITT L2V3 'simulated' daytime and nighttime CO profiles for HDD_{peek}, over Johannesburg, for December 2007; (b) Same as (a) except for MOPITT L2V4.

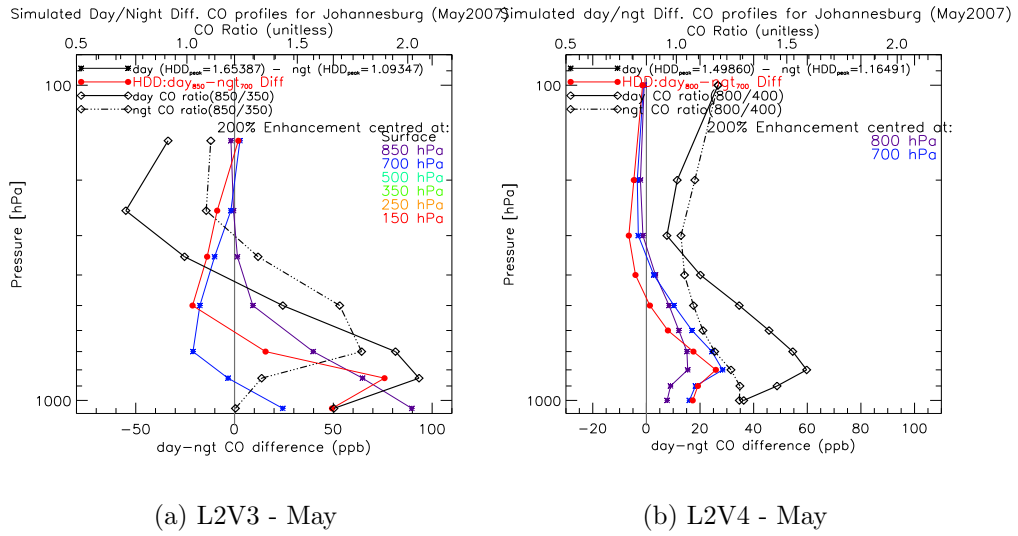


Figure 7.28: (a) MOPITT L2V3 ‘simulated’ key day-night difference CO profiles for HDD_{peak} , over Johannesburg, for May 2007; (b) Same as (a) except for MOPITT L2V4.

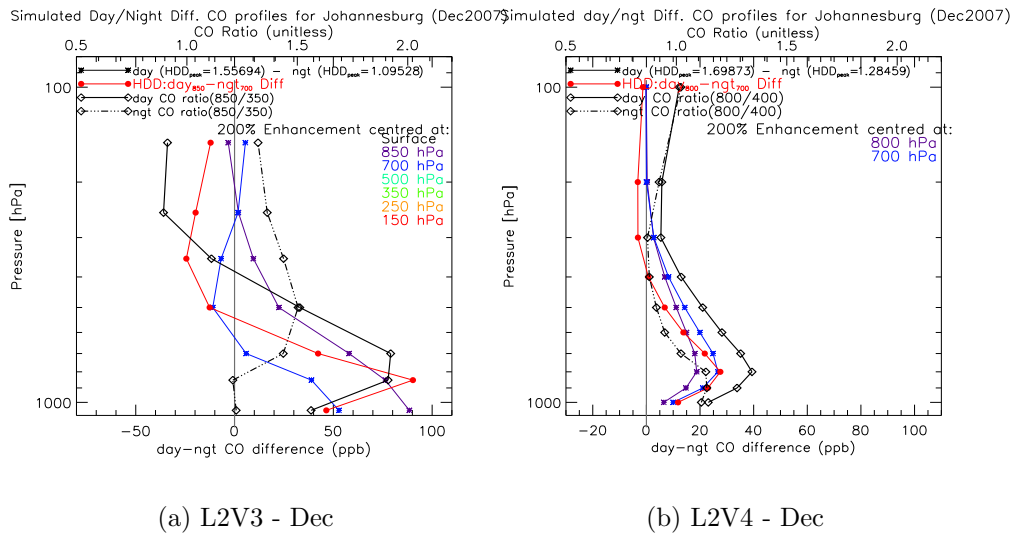


Figure 7.29: (a) MOPITT L2V3 ‘simulated’ key day-night difference CO profiles for HDD_{peak} , over Johannesburg, for December 2007; (b) Same as (a) except for MOPITT L2V4.

7.2.2 TOMCAT Model CO Profile Simulation

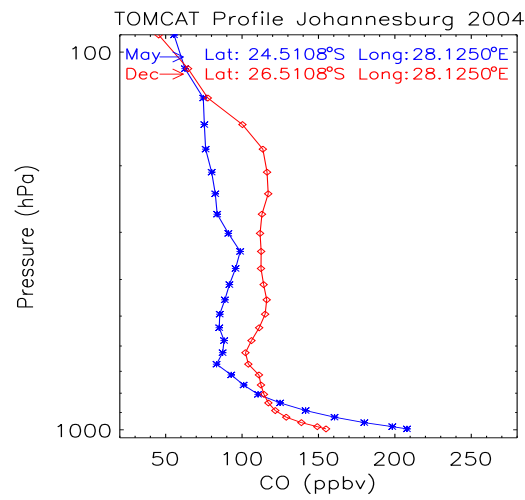
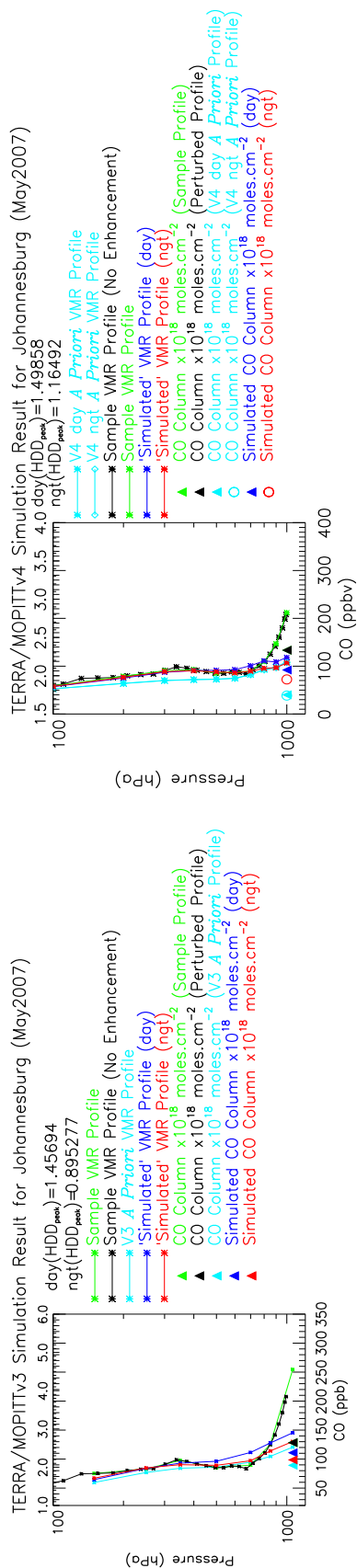
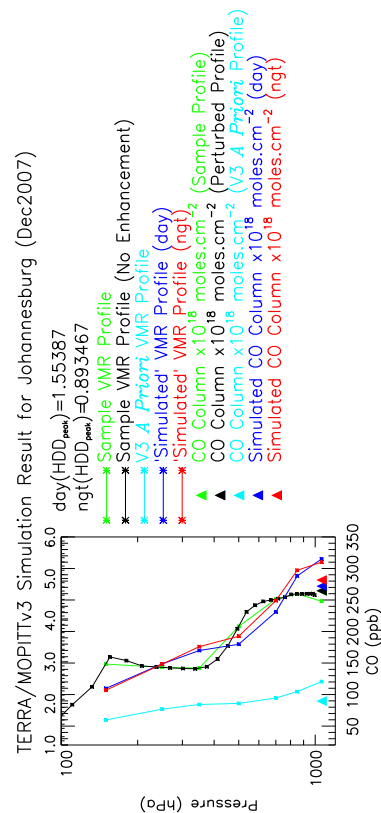


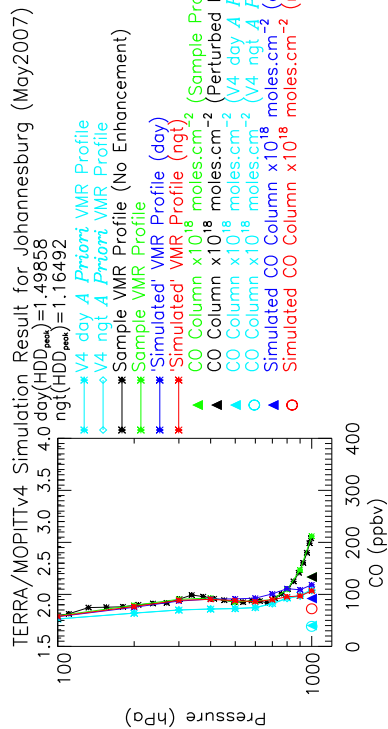
Figure 7.30: Selected TOMCAT model CO profiles, over Johannesburg box, for May 2004 (blue) and December 2004 (red).



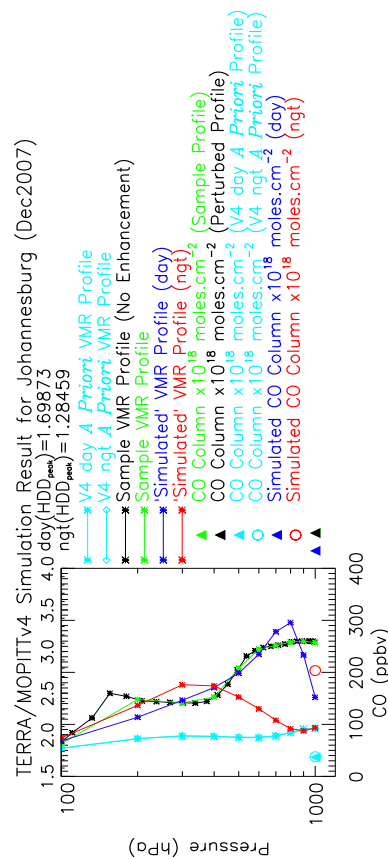
(a) L2V3 - May



(c) L2V3 - Dec

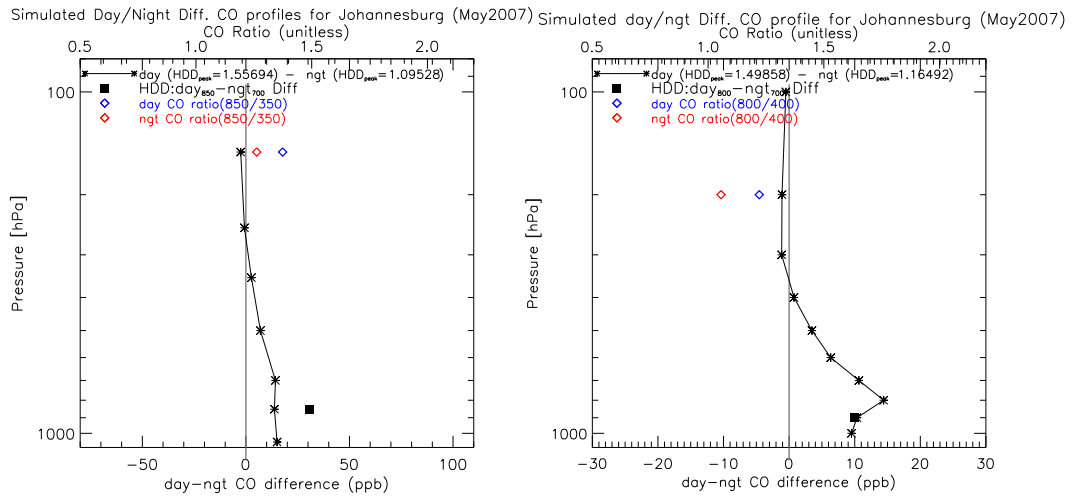


(b) L2V4 - May



(d) L2V4 - Dec

Figure 7.31: (a)MOPITT L2V3 ‘Simulated’ daytime and nighttime CO profiles for TOMCAT model selected base CO profile, over Johannesburg, for May 2007; (b) Same as (a) except for MOPITT L2V4; (c) Same as (a) except for December 2007; (d) Same as (a) except for MOPITT L2V4 and for December 2007.



(a) L2V3 - May

(b) L2V4 - May

Figure 7.32: (a) MOPITT L2V3 ‘simulated’ day-night difference CO profile for HDD_{peak} , over Johannesburg, for May 2007; (b) Same as (a) except for MOPITT L2V4.

Bibliography

- Akimoto, H. [2003], ‘Global air quality and pollution’, *Science*, **302**, 1716–1719.
- Allen, D. J., Kasibhatla, P., Thompson, A. M., Rood, R. B., Doddridge, B. G., Pickering, K. E., Hudson, R. D. and Lin, S. J. [1996], ‘Transport-induced interannual variability of carbon monoxide determined using a chemistry and transport model’, *J. Geophys. Res.*, **101**(D22), 28655–28669.
- Apel, E. C., Emmons, L. K., Karl, T., Flocke, F., Hills, A. J., Madronich, S., Lee-Taylor, J., Fried, A., Weibring, P., Walega, J., Richter, D., Tie, X., Mauldin, L., Campos, T., Sive, B., Kleinman, L., Springston, S., Zaveri, R., Ortega, J., Voss, P., Blake, D., Baker, A., Warneke, C., Welsh-Bon, D., de Gouw, J., Zheng, J., Zhang, R., Rudolph, J., Junkermann, W. and Riemer, D. D. [2009], ‘Chemical evolution of volatile organic compounds in the outflow of the Mexico City Metropolitan area’, *Atmos. Chem. Phys. Discuss.*, **9**, 24085–24143.
- Arellano, A. F. and Hess, P. G. [2006], ‘Sensitivity of top-down estimates of CO sources to GCTM transport’, *Geophys. Res. Lett.*, **32**(L21).
- Arnold, S. R., Chipperfield, M. P. and Blitz, M. A. [2005], ‘A three-dimensional model study of the effect of new temperature-dependent quantum yields for acetone photolysis’, *J. Geophys. Res.*, **110**(D22).
- Bakwin et al. [1994], ‘in Summary Report 1993, Rep. 22, edited by J. T. Peterson and R. M. Rosson’, Carbon Cycle Division, Clim. Monit. and Diagnostics Lab., ERL/NOAA, Boulder, Colo.
- Bates, T. S., Kelly, K. C., Johnson, J. E. and Gammon, R. [1995], ‘Regional and seasonal variations in the flux of oceanic carbon to the atmosphere’, *J. Geophys. Res.*, **100**(11).

- Bauer, K., Seiler, W. and Geihl, H. [1974], ‘Dispersion of tracers in the atmosphere and ocean: survey and comparison of experimental data’, *J. Geophys. Res.*, **79**, 789–795.
- Beig, G. and Ali, K. [2006], ‘Behavior of boundary layer ozone and its precursors over a great alluvial plain of the world: Indo-Gangetic Plains’, *Geophys. Res. Lett.*, **33**(L24), L24.1–L24.4.
- Belward, T. and Loveland, T. [1996], ‘The DIS 1-km land cover data set’, IGBP NewsletterF.
- Bergamaschi, P., Hein, R., Heimann, M. and Crutzen, P. J. [2000], ‘Inverse modeling of the global CO cycle, 1. Inversion of CO mixing ratios’, *J. Geophys. Res.*, **105**(D2), 1909–1927.
- Berman, R., Duggan, P., Flohic, M. P. L., May, A. D. and Drummond, J. R. [1993], ‘Spectroscopic technique for measuring the temperature and pressure cycle of a pressure modulator radiometer’, *Appl. Opt.*, **32**, 6280–6283.
- Boissard, C., Bonsang, B., Kanikidou, M. and Lambert, G. [1996], ‘TROPOZ II: Global distributions and budgets of methane and light hydrocarbons’, *J. Atmos. Chem.*, **25**(2), 115–148.
- Bovensmann, H., Burrows, J. P., Buchwitz, M., J. Frerick, A. S. N., Rozanov, V. V., Chance, K. V. and Goede, A. P. H. [1999], ‘SCIAMACHY: Mission Objectives and Measurement Modes’, *J. Atmos. Sci.*, **56**(2), 127–150.
- Bowman, K. P. [2006], ‘Transport of carbon monoxide from the tropics to the extratropics’, *J. Geophys. Res.*, **111**(D02).
- Brasseur, G. and Solomon, S. [1986], *Aeronomy of the Middle Atmosphere*, Reidel Publishing Company, Netherlands.
- Brunke, E. G., Scheel, H. and Seiler, W. [1990], ‘Trends of tropospheric carbon monoxide, nitrous oxide and methane as observed at Cape Point, South Africa’, *Atmos. Environ.*, **24A**(D12), 585–595.

- Buchwitz, M., Khlystova, I., Bovensmann, H. and Burrows, J. P. [2007], ‘Three Years of global carbon monoxide from SCIAMACHY: comparison with MOPITT and first results related to the detection of enhanced CO over cities’, *Atmos. Chem. Phys.*, **7**, 2399–2411.
- Butler, T. M., Lawrence, M. G., Gurjar, B. R., van Aardenne, J., Schultz, M. and Lelieveld, J. [2008], ‘The representation of emissions from megacities in global emission inventories’, *Atmos. Environ.*, **42**, 703–719.
- Chipperfield, M. P. [2006], ‘New version of the TOMCAT/SLIMCAT off-line chemical transport model: Intercomparison of stratospheric tracer experiments’, *Q. J. R. Meteorol. Soc.*, **132**(617), 1179–1203.
- Chipperfield, M. P., Cariolle, D., Simon, P., Ramaroson, R. and Lary, D. J. [1993], ‘A three-dimensional modelling study of trace species in the Arctic lower stratosphere during winter 1989–90’, *J. Geophys. Res.*, **98**, 7199–7218.
- Clerbaux, C., Boynard, A., Clarisse, L., George, M., Lazaro, J., Herbin, H., Hurtmans, D., Pommier, M., Razavi, A., Turquety, S., Wespes, C. and Coheur, P. F. [2009], ‘Monitoring of atmospheric composition using the thermal infrared IASI/MetOp sounder’, *Atmos. Chem. Phys. Discuss.*, **9**, 8307–8339.
- Clerbaux, C., Edwards, D., Deeter, M., Emmons, L., Lamarque, J., Tie, X., Massie, S. and Gille, J. [2008], ‘Carbon monoxide pollution from cities and urban areas observed by the Terra/MOPITT mission’, *Geophys. Res. Lett.*, **35**(L03), L03.1–L03.6.
- Conrad, R. and Seiler, W. [1985], ‘Influence of temperature, moisture, and organic carbon on the flux of H₂ and CO between soil and atmosphere. Field Studies in subtropical regions’, *J. Geophys. Res.*, **90**, 5699–5709.
- Conrad, V. S., Gormsen, B. B., Nolf, S. and Jr., H. G. R. [1999], ‘Spaceborne observations of the global distribution of carbon monoxide on the middle troposphere during April and October 1994’, *J. Geophys. Res.*, **104**(D17).
- Crutzen, P. [1973], ‘A discussion of the chemistry of some minor constituents in the stratosphere and troposphere’, *Pure Appl. Geophys.*, **106**(1), 1385–1399.

- Crutzen, P. J. and Andreae, M. O. [1990], ‘Biomass burning in the tropics: Impact on atmospheric chemistry and biogeochemical cycles’, *Science*, **250**(4988), 1669–1678.
- Crutzen, P. J. and Zimmermann, P. H. [1991], ‘The changing photochemistry of the troposphere’, *Tellus*, **43**, 136–151.
- Deeter, M. N. [2009], ‘MOPITT (Measurements of Pollution in the Troposphere) Provisional Version 4 Product User’s Guide’, MOPITT Algorithm Development Team.
- Deeter, M. N., Edwards, D. P., Gille, J. C. and Drummond, J. R. [2007], ‘Sensitivity of MOPITT observations to carbon monoxide in the lower troposphere’, *J. Geophys. Res.*, **112**(D24).
- Deeter, M. N., Edwards, D. P., Gille, J. C. and Drummond, J. R. [2009], ‘CO retrievals based on MOPITT near-infrared observations’, *J. Geophys. Res.*, **114**(D04).
- Deeter, M. N., Emmons, L. K., Edwards, D. P., Gille, J. C. and Drummond, J. R. [2004], ‘Vertical resolution and information content of CO profiles retrieved by MOPITT’, *Geophys. Res. Lett.*, **32**(L15).
- Deeter, M. N., Emmons, L. K., Francis, G. L., Edwards, D. P., Gille, J. C., Warner, J. X., Khattatov, B., Ziskin, D., Lamarque, J.-F., Ho, S.-P., Yudin, V., Atti, J.-L., Packman, D., Chen, J., Mao, D. and Drummond, J. R. [2003], ‘Operational carbon monoxide retrieval algorithm and selected results for the MOPITT instrument’, *J. Geophys. Res.*, **108**(D14), 4399–4410.
- DeMore, W. B., Sander, S. P., Golden, D. M., Hampson, R. F., Kurylo, M. J., Howard, C. J., Ravishankara, A. R., Kolb, C. E. and Molina, M. J. [1994], ‘Chemical kinetics and photochemical data for use in stratospheric modeling’, JPL Publication, Report 94–26.
- Di Girolamo, L., Bond, T. C., Bramer, D., Diner, D. J., Fettingner, F., Kahn, R. A., Martonchik, J. V., Ramana, M. V., Ramanathan, V. and Rasch, P. J. [2004], ‘Analysis of multi-angle imaging spectroradiometer (MISR) aerosol optical depths over greater India during winter’, *Geophys. Res. Lett.*, **31**(L23), L23.1–L23.5.

- Dlugokencky, E. J., Dutton, E. G., Novelli, P. C., Tans, P. P., Masarie, K. A., Lantz, K. O. and Mardronich, S. [1996], ‘Changes in CH₄ and CO growth rates after the eruption of Mt. Pinatubo and their link with changes in tropical tropospheric UV flux’, *Geophys. Res. Lett.*, **23**(20), 2761–2764.
- Drummond, J. R. [1989], ‘Novel correlation radiometer: The lengthmodulated radiometer.’, *Appl. Opt.*, **28**, 2451–2452.
- Drummond, J. R. [1992], ‘Measurements of Pollution in the Troposphere (MOPITT), in The use of EOS for Studies of Atmospheric Physics, edited by J. C. Gille and G. Visconti, North Holland, Amsterdam’.
- Drummond, J. R. [1993], The Measurements of Pollution in the Troposphere (MOPITT) Instrument, *in* ‘SPIE Proceedings’, Vol. 1939.
- Drummond, J. R. [1996], ‘MOPITT Mission Description Document, University of Toronto Internal Report’.
- Duncan, B. N., Logan, J. A., Bey, I., Megretskaia, I. A., Yantosca, R. M., Novelli, P. C., Jones, N. B. and Rinsland, C. P. [2007], ‘Global budget of CO, 1988–1997: Source estimates and validation with a global model’, *J. Geophys. Res.*, **112**(D22), D22.1–D22.29.
- Duncan, B. N., Martin, R. V., Staudt, A. C., Yevich, R. and Logan, J. A. [2003], ‘Interannual and seasonal variability of biomass burning emissions constrained by satellite observations’, *J. Geophys. Res.*, **108**(D2), ACH1.1–ACH1.22.
- Edwards, D. [1999], ‘GENLN2: A general line-by-line atmospheric transmittance and radiance model: version 3.0 description and users guide’, *Rep. NCAR/TN-367+STR, Natl. Cent. for Atmos. Res.* .
- Edwards, D., Halvorson, C. and Gille, J. [1999], ‘Radiative transfer modeling for the EOS Terra satellite Measurement of Pollution in the Troposphere (MOPITT) instrument’, *J. Geophys. Res.*, **104**(14), 16755–16775 .
- Edwards, D. P., Emmons, L. K., Gille, J. C., Chu, A., Atti, J.-L., Giglio, L., Wood, S. W., Haywood, J., Deeter, M. N., Massie, S. T., Ziskin, D. C. and Drummond,

- J. R. [2006], ‘Satellite-observed pollution from southern hemisphere biomass burning’, *J. Geophys. Res.*, **111**(D14), D14.1–D14.9.
- Edwards, D. P., Emmons, L. K., Hauglustaine, D. A., Chu, D. A., Gille, J. C., Kaufman, Y. J., Petron, G., Yurganov, L. N., Giglio, L., Deeter, M. N., Yudin, V., Ziskin, D. C., Warner, J., Lamarque, J. F., Francis, G. L., Ho, S. P., Mao, D., Chen, J., Grechko, E. I. and Drummond, J. R. [2004], ‘Observations of carbon monoxide and aerosols from the Terra satellite: Northern Hemisphere variability’, *J. Geophys. Res.*, **109**(D24), D24.1–D24.17.
- Ehhalt, D. H., Dorn, H. P., and Hofzumahaus, A. [1994], The measurement of OH radicals in the troposphere, *in* ‘in J. G. Calvert (ed.) Blackwell Scientific Publications, London,’ pp. 157–173.
- Emmons, L. K., Deeter, M. N., Gille, J. C., Edwards, D. P., Attie, J.-L., Warner, J., Ziskin, D., Francis, G., Khattatov, B., Yudin, V., Lamarque, J.-F., Ho, S.-P., Mao, D., Chen, J. S., Drummond, J., Novelli, P., Sachse, G., Coffey, M. T., Hannigan, J. W., Gerbig, C., Kawakami, S., Kondo, Y., Takegawa, N., Schlager, H., Baehr, J. and Ziereis, H. [2004], ‘Validation of Measurements of Pollution in the Troposphere (MOPITT) CO retrievals with aircraft in situ profiles’, *J. Geophys. Res.*, **109**(D03), D03.1–D03.13 .
- Emmons, L. K., Edwards, D. P., Deeter, M. N., Gille, J. C., Campos, T., Nedelec, P., Novelli, P. and Sachse, G. [2009], ‘Measurements of Pollution In The Troposphere (MOPITT) validation through 2006’, *Atmos. Chem. Phys.*, **9**, 1795–1803.
- Emmons, L. K., Pfister, G. G., Edwards, D. P., Gille, J. C., Sachse, G., Blake, D., Wofsy, S., Gerbig, C., Matross, D. and Nedelec, P. [2007], ‘Measurements of Pollution in the Troposphere (MOPITT) validation exercises during summer 2004 field campaigns over North America’, *J. Geophys. Res.*, **112**(D12), D12.1–D12.7.
- Etheridge, D., Pearman, G. and de Silva, F. [1988], ‘Atmospheric trace gas variations as revealed by air trapped in an ice core from Law Dome, Antarctica’, *Annals of Glaciology*, **10**, 28–33.
- Fishman, J., Hoell, J. M., Bendura, R. D., McNeal, R. J. and Kirchhoff, V. [1996],

- ‘NASA GTE TRACE A experiment (September October 1992): Overview’, *J. Geophys. Res.*, **101**(D19), 23865–23879.
- Francis, G. L., Edwards, D. and Gille, J. [1999], Channel radiance calculations for MOPITT forward modeling and operational retrievals, *in* ‘SPIE’.
- Fraser, P., Coram, S. and Derek, N. [1994], Program reports 4.12: Atmospheric methane, carbon monoxide and carbon dioxide by gas chromatography, *in* ‘In: Baseline Atmospheric Program (Australia) 1991, A.L. Dick and J.L. Gras(eds)’, Vol. 212, Bureau of Meteorology and CSIRO Division of Atmospheric Research, Melbourne, Australia.
- Fraser, P., Hyson, P. and Coram, S. [1986a], Carbon monoxide in the Southern Hemisphere, *in* ‘In: Proceedings of the Seventh World Clean Air Congress, H.F. Hartmann (ed.)’, Vol. 2, Clean Air Society of Australia and New Zealand.
- Fuchs, R. J., Brennan, E., Chamie, J., Fu-chen, L. and Juha, U. [1994], *Mega-city growth and the future*.
- Gautam, R., Hsu, N. C., Kafatos, M. and Tsay, S. C. [2007], ‘Influences of winter haze on fog/low cloud over the Indo-Gangetic plains’, *J. Geophys. Res.*, **112**(D05), D05.1–D05.14.
- Gerhardt, P., Poppe, D. and Marenco, A. [1989], ‘Ozone, CO and NO_x distribution in the troposphere during STRATOZ III, in Ozone in the Atmosphere, edited by R. D. Bojkov and P. Fabian’.
- Ghude, S. D., Fadnavis, S., Beig, G., Polade, S. D. and van der A, R. J. [2008], ‘Detection of surface emission hot spots, trends, and seasonal cycle from satellite-retrieved NO₂ over India’, *J. Geophys. Res.*, **113**.
- Giannakopoulos, C., Chipperfield, M. P., Law, K. S. and Pyle, J. A. [1999], ‘Validation and intercomparison of wet and dry deposition schemes using Pb-210 in a global three-dimensional off-line chemical transport model’, *J. Geophys. Res.*, **104**, 23761–23784.

- Gulluk, T., Slemr, F. and Stauffer, B. [1998], ‘Simultaneous measurements of CO₂, CH₄ and N₂O in air extracted by sublimation from Antarctica ice cores: confirmation of the data obtained using other extraction techniques’, *J. Geophys. Res.*, **102**(D13), 15971–15978.
- Hamilton, J. F., Allen, G., Watson, N. M., Lee, J. D., Saxton, J. E., Lewis, A. C., Vaughan, G., Bower, K. N., Flynn, M. J., Crosier, J., Carver, G. D., Harris, N. R. P., Parker, R. J., Remedios, J. J. and Richards, N. A. D. [2008], ‘Observations of an atmospheric chemical equator and its implications for the tropical warm pool region’, *J. Geophys. Res.*, **113**(D20), D20.1–D20.12.
- Harriss, R. C., Wofsy, S. C., Bartlett, D. S., Shipham, M. C., Jacob, D. J., Hoell, J. M., Bendura, R. J., Drewry, J. W., McNeal, R. J., Navarro, R. L., Gidge, R. N. and Rabine, V. E. [1992], ‘The Arctic Boundary Layer Expedition (ABLE 3A): July August 1988’, *J. Geophys. Res.*, **97**(15), 16383–16394.
- Harriss, R. C., Wofsy, S. C., Hoell, J. M., Bendura, R. J., Drewry, J. W., McNeal, R. J., Pierce, D., Rabine, V. and Snell, R. L. [1994], ‘The Arctic Boundary Layer Expedition (ABLE 3B): July August 1990’, *J. Geophys. Res.*, **99**(D1), 1635–1643.
- Hauglustaine, D. A., Brasseur, G. P., Walters, S., Rasch, P. J., Muller, J. F., Emmons, L. K. and Carroll, M. A. [1998], ‘MOZART, a global chemical transport model for ozone and related chemical tracers: 2. Model results and evaluation’, *J. Geophys. Res.*, **103**(D21), 28291–28335.
- Heald, C. L., Jacob, D. J., Jones, D. B. A., Palmer, P. I., Logan, J. A., Streets, D. G., W. Sachse, G., Gille, J. C., Hoffman, R. N. and Nehr Korn, T. [2004], ‘Comparative inverse analysis of satellite (MOPITT) and aircraft (TRACE-P) observations to estimate Asian sources of carbon monoxide’, *J. Geophys. Res.*, **109**(D23), D23.1–D23.17.
- Heimann, M. [1996], ‘The global atmospheric tracer model TM2’, Tech. Rep. 10.
- Ho, S. P., Edwards, D. P., Gille, J. C., Chen, J., Ziskin, D., Francis, G. L., Deeter, M. N. and Drummond, J. R. [2005], ‘Estimates of 4.7 m surface emissivity and their impact on the retrieval of tropospheric carbon monoxide by Measurements

- of Pollution in the Troposphere (MOPITT)', *J. Geophys. Res.* **110**(D21), D21.1–D21.13.
- Ho, S. P., Gille, J. C., Edwards, D. P., Attie, J. L., Deeter, M. N., Warner, J., Francis, G. L. and Ziskin, D. [2002b], 'Validation of the retrieval of surface skin temperature and surface emissivity from MOPITT measurements and their impacts to the retrievals of tropospheric carbon monoxide profiles'.
- Hoell, J. M., Davis, D. D., Jacob, D. J., Rodgers, M. O., Newell, R. E., Fuelberg, H. E., McNeal, R. J., Raper, J. L. and Bendura, R. J. [1999], 'Pacific Exploratory Mission in the tropical Pacific: PEM Tropics A, August–September 1996', *J. Geophys. Res.*, **104**(D5), 5567–5583.
- Holloway, T., H. L. I. and Kasibhatla, P. [2000], 'Global distribution of carbon monoxide', *J. Geophys. Res.*, **105**(D10), 12123–12148.
- Houghton, J., Callander, B. and Varney, S. [1992], 'Climate Change 1992: The Supplementary Report to the IPCC Scientific Assessment', Intergovernmental Panel on Climate Change, Cambridge University Press, Cambridge, Great Britain,.
- Houghton, J. T., Taylor, F. W. and Rodgers, C. D. [1986], *Remote sounding of atmospheres*, Cambridge University Press.
- IPCC [2001], 'Climate Change 2001: The Science Basis, Contribution of Working Group I to the Third Assessment Report of the Intergovernmental Panel on Climate Change'.
- IPCC [2007], 'Climate Change 2007: The Science Basis, Contribution of Working Group I to the Fourth Assessment Report of the Intergovernmental Panel on Climate Change'.
- Irie, H., Sudo, K., Akimoto, H., Richter, A., Burrows, J., Wagner, T., Wenig, M., Beirle, S., Kondo, Y., Sinyakov, V. and Goutail, F. [2005], 'Evaluation of long-term tropospheric NO₂ data obtained by GOME over East Asia in 1996–2002', *Geophys. Res. Lett.*, **32**(L11), L11.1–L11.4.

- Jacob, D. J., Crawford, J. H., Kelb, M. M., Connors, V. S., Bendura, R. J., Raper, J. L., Sachse, G. W., Gille, J. C., Emmons, L. and Heald, C. L. [2003], ‘Transport and chemical evolution over the pacific (TRACE-P) aircraft mission: design, execution, and first results’, *J. Geophys. Res.*, **108**(D20), D20.1–D20.19.
- Jacob, D. J., Logan, J. A. and Murti, P. P. [1999], ‘Effect of rising Asian emissions on surface ozone in the United States’, *Geophys. Res. Lett.*, **26**(14), 2175–2178.
- Jaffe, D., Bertsch, I., Jaeglé, L., Novelli, P., Reid, J. S., Tanimoto, H., Vingarzan, R. and Westphal, D. L. [2004], ‘Long-range transport of Siberian biomass emissions and impact on surface ozone in western North America’, *Geophys. Res. Lett.*, **31**(L16), L16.1–L16.4.
- Jethva, H., Satheesh, S. K. and Srinivasan, J. [2005], ‘Seasonal variability of aerosols over the Indo-Gangetic plains’, *J. Geophys. Res.*, **110**(D21), D21.1–D21.17.
- Kanakidou, M., Dentener, F., Brasseur, G., Bernsten, T., Collins, W., Hauglustaine, D., Houweling, S., Isaksen, I., Krol, M., Lawrence, M., Müller, J.-F., Poisson, N., Roelofs, G., Wang, Y. and Wauben, W. [1999], ‘3-D global simulations of tropospheric CO distributions-Results of the GIM/IGAC inter-comparison 1997 exercise’, *Chemosphere: Global Change Sci.*, **1**, 263–282.
- Kar, J., Bremer, H., Drummond, J. R., Rochon, Y. J., Jones, D. B. A., Nichitiu, F., Zou, J., Liu, J., Gille, J. C., Edwards, D. P., Deeter, M. N., Francis, G., Ziskin, D. and Warner, J. [2004], ‘Evidence of vertical transport of carbon monoxide from Measurements of Pollution in the Troposphere (MOPITT)’, *Geophys. Res. Lett.*, **31**(L23), L23.1–L23.4.
- Kar, J., Jones, D. B. A., Drummond, J. R., Attie, J. L., Liu, J., Zou, J., Nichitiu, F., Seymour, M. D., Edwards, D. P., Deeter, M. N., Gille, J. C. and Richter, A. [2008], ‘Measurement of Low Altitude CO over the Indian subcontinent by MOPITT’, *J. Geophys. Res.*, **113**(D16), D16.1–D16.13.
- Khalil, M. A. K. and Rasmussen, R. A. [1988], ‘Carbon monoxide in the Earth’s atmosphere: indications of a global increase’, *Nature*, **332**, 242–245.
- Khalil, M. A. K. and Rasmussen, R. A. [1990], ‘Atmospheric carbon monoxide: latitudinal distribution of sources’, *Geophys. Res. Lett.*, **17**(11), 1913–1916.

- Khalil, M. and Rasmussen, R. [1994], ‘Global decrease in atmospheric carbon monoxide concentration’, *Nature*, **370**, 639–641.
- King, G. M. [2000], ‘Land use impact on atmospheric carbon monoxide consumption by soils’, *Global Biogeochem. Cycles.*, **14**, 1161–1172.
- King, G. M. and Crosby, H. [2002], ‘Impacts of plant roots on soil CO cycling and soil-atmosphere CO exchange’, *Global Change Bio.*, **8**, 1085–1093.
- Langenfelds, R. L., Francey, R. J., Pak, B. C., Steele, L. P., Lloyd, J., Trudinger, C. M. and Allison, C. E. [2002], ‘Interannual growth rate variations of atmospheric CO₂ and its $\delta^{13}C$, H₂, CH₄, and CO between 1992 and 1999 linked to biomass burning’, *Global Biogeochem. Cycles*, **16**(3), 1048.
- Law, K. S., Plantevin, P. H., Shallcross, D. E., Rogers, H. L., Pyle, J. A., Grouhel, C., Thouret, V. and Marenco, A. [1998], ‘Evaluation of modeled O₃ using Measurements of Ozone by Airbus In-Service Aircraft (MOZAIC) data’, *J. Geophys. Res.*, **103**, 25721–25737.
- Levine, J. S. [1991], ‘Biomass Burning: Atmospheric, Climatic and Biospheric Implications’, MIT Press, Cambridge, MA.
- Levine, J. S. [1996], ‘Biomass Burning and Global Change’, MIT Press, Cambridge, MA.
- Levy II, H. [1971], ‘Normal atmosphere: Large radical and formaldehyde concentrations predicted’, *Science*, **173**, 141–143.
- Logan, J. A., Prather, M. J., Wofsy, S. C. and McElroy, M. B. [1981], ‘Tropospheric chemistry: a global perspective’, *J. Geophys. Res.*, **86**, 7210–7254.
- Lowe, D., Brenninkmeijer, C., Brailsford, G., Lassey, K. and Gomez, A. [1994], ‘Concentration and ^{13}C records of atmospheric methane in New Zealand and Antarctica: Evidence for changes in methane sources’, *J. Geophys. Res.*, **99**(D08), 16913–16925.
- Ludwig, C. B., Griggs, M., Mailmus, W. and Bartle, E. R. [1974], ‘Measurement of air pollutants from satellites, Part-1, Feasibility considerations’, *Appl. Opt.*, **13**(6), 1494–1509.

- Mage, D., Ozolins, G., Peterson, P., Webster, A., Orthofer, R., Vandeweerd, V. and Gwynne, M. [1996], ‘Urban air pollution in megacities of the world’, *Atmos. Environ.*, **30**(5), 681–686.
- Mahieu, E., Zander, R., Delbouille, L., Demoulin, P., Roland, G. and Servais, C. [1997], ‘Observed trends in total vertical column abundances of atmospheric gases from IR solar spectra recorded at the Jungfraujoch’, *J. Atmos. Chem.*, **28**, 227–243.
- May, R. D., McCleese, D. J., Rider, D. M., Schofield, J. T. and Webster, C. R. [1988], ‘Tunable diode laser spectral diagnostic studies of a pressure modulator radiometer’, *Appl. Opt.*, **27**, 3591–3593.
- Mickley, L. J., Murti, P. P., Jacob, D. J., Logan, J. A., Rind, D. and Koch, D. [1999], ‘Radiative forcing from tropospheric ozone calculated with a unified chemistry-climate model’, *J. Geophys. Res.*, **104**(D23), 30153–30172.
- Molina, M. J. and Molina, L. T. [2004], ‘Critical Review: Megacities and Atmospheric Pollution’, *J. Air Waste Manage. Assoc.*, **54**(6), 644–680.
- Muller, J. F. and Brasseur, G. P. [1995], ‘IMAGES: A three-dimensional chemical transport model of the global troposphere’, *J. Geophys. Res.*, **100**, 16445–16490.
- Muller, J. F. and Stavrou, T. [2005], ‘Inversion of CO and NO_x emissions using the adjoint of the IMAGES model’, *Atmos. Chem. Phys.*, **5**, 1157–1186.
- Nair, V. S., Moorthy, K. K., Alappattu, D. P., Kunhikrishnan, P. K., George, S., Nair, P. R., Babu, S. S., Abish, B., Satheesh, S. K., Tripathi, S. N., Niranjana, K., Madhavan, B. L., Srikant, V., Dutt, C. B. S., Badarinath, K. V. S. and Reddy, R. R. [2007], ‘Wintertime aerosol characteristics over the IG Plain (IGP): Impacts of local boundary layer processes and long-range transport’, *J. Geophys. Res.*, **112**(D13), D13.1–D13.15.
- Newell, R. E., Wu, Z. X., Zhu, Y., Hu, W., Browell, E. V., Gregory, G. L., Sachse, G. W., Collins, J. E., Kelly, K. K. and Liu, S. C. [1996], ‘Vertical fine-scale atmospheric structure measured from NASA DC-8 during PEM-West A’, *J. Geophys. Res.*, **101**(D01), 1943–1960.

- Novelli, P. C., Connors, V. S., Reichle, H. G., Anderson, B. E., Brenninkmeijer, C. A. M., Brunke, E. G., Doddridge, B. G., Kirchhoff, V. W. J. H., Lam, K. S., Masarie, K. A., Matsuo, T., Parrish, D. D., Scheel, H. E. and Steele, L. P. [1998a], ‘An internally consistent set of globally distributed atmospheric carbon monoxide mixing ratios developed using results from an intercomparison of measurements’, *J. Geophys. Res.*, **103**(D15), 19285–19293.
- Novelli, P. C., Masarie, K. A. and Lang, P. M. [1998b], ‘Distributions and recent changes of carbon monoxide in the lower troposphere’, *J. Geophys. Res.*, **103**(D15), 19015–19033.
- Novelli, P. C., Masarie, K. A., Lang, P. M., Hall, B. D., Myers, R. C. and Elkins, J. W. [2003], ‘Reanalysis of tropospheric CO trends: Effects of the 1997 1998 wildfires’, *J. Geophys. Res.*, **108**(D15), D15.1–D15.14.
- Novelli, P. C., Masarie, K. A., Tans, P. P. and Lang, P. M. [1994], ‘Recent Changes in atmospheric carbon monoxide’, *Science*, **263**, 1587–1590.
- Olivier, J. G. J. and Berdowski, J. J. M. [2001], ‘Global emissions sources and sinks. In: Guicherit, R., Heij, B.J. (Eds.)’, *The Climate System*. Balkema Publishers/Swets, Zeitlinger Publishers, Lisse, The Netherlands.
- Pak, B. C., Langenfelds, R. L., Fransey, R. J., Steele, L. P. and Simonds, I. [1996], ‘A climatology of trace gases from the Cape Grim overflights, 1992–1995’, in *Baseline Atmospheric Program (Australia) 1994–5*, edited by R. J. Fransey, A. L. Dick, and N. Derek.
- Palmer, P. I., Suntharalingam, P., Jones, D. B. A., Jacob, D. J., Streets, D. G., Fu, Q., Vay, S. A. and Sachse, G. [2006], ‘Using CO₂:CO correlations to improve inverse analyses of carbon fluxes’, *J. Geophys. Res.*, **111**(D12), D12.1–D12.14.
- Pan, L., Edwards, D. P., Gille, J. C., Smith, M. W. and Drummond, J. R. [1995], ‘Satellite remote sensing of tropospheric CO and CH₄ : forward model studies of the MOPITT instrument’, *Appl. Opt.*, **34**, 6976–6988.
- Pan, L., Gille, J., Edwards, D. P., Bailey, P. L. and Rodgers, C. D. [1998], ‘Retrieval of carbon monoxide for the MOPITT instrument’, *J. Geophys. Res.*, **103**(D24), 32277–32290.

- Petron, G., Granier, C., Khattatov, B., Yudin, V., Lamarque, J. F., Emmons, L., Gille, J. and Edwards, D. P. [2004], ‘Monthly CO surface sources inventory based on the 2000 2001 MOPITT satellite data’, *Geophys. Res. Lett.*, **31**(L21), L21.1–L21.5.
- Potter, C. S., Klooster, S. A. and Chatfield, R. B. [1996], ‘Consumption and production of carbon monoxide in soils: A global model analysis of spatial and seasonal variation’, *Chemosphere*, **33**, 1175–1193.
- Reichle, H. G., J., Connors, V., Holland, J., Hypes, W., Wallio, H., Casas, J., Gormsen, B., Saylor, M. and Hesketh, W. [1986], ‘Middle and upper tropospheric carbon monoxide mixing ratios as measured by a satellite-borne remote sensor during November 1981’, *J. Geophys. Res.*, **91**, 10865–10887.
- Reichle, H. J., Connors, V., Holland, J., Sherrill, R., Wallio, H., Casas, J., Condon, E., Gormsen, B. and Seiler, W. [1990], ‘The distribution of middle tropospheric carbon monoxide during early October 1984’, *J. Geophys. Res.*, **95**(D07), 9845–9856.
- Reif, F. [1965], *Fundamentals of Statistical and Thermal Dynamics*, McGraw-Hill Book Company.
- Richards, N. A. D. [2004], Characteristics of Tropospheric Carbon Monoxide Profiles Retrieved from MOPITT Measurements, PhD thesis, PhD Thesis, University of Leicester.
- Richter, A., Burrows, J., Nues, H., Granier, C. and Niemeijer, U. [2005], ‘Increase in tropospheric nitrogen dioxide over China observed from space’, *Nature*, **437**, 129–130.
- Rinsland, C. P., Luo, M., Logan, J. A., Beer, R., Worden, H., Kulawik, S. S., Rider, D., Osterman, G., Gunson, M., Eldering, A., Goldman, A., Shephard, M., Clough, S. A., Rodgers, C., Lampel, M. and Chiou, L. [2006], ‘Nadir measurements of carbon monoxide distributions by the Tropospheric Emission Spectrometer instrument onboard the Aura Spacecraft: Overview of analysis approach and examples of initial results’, *Geophys. Res. Lett.*, **33**(L22), L22.1–L22.6.

- Rodgers, C. D. [2000], *Inverse Methods for Atmospheric Sounding: Theory and Practice*.
- Roscoe, H. K. and Wells, R. J. [1989], ‘The variation of pressure, temperature and transmission within a pressure modulator: Measurements with a high-compression modulator’, *J. Quant. Spectros. Radiat. Transfer*, **41**, 259–285.
- Roy, S., Beig, G. and Jacob, D. [2008], ‘Seasonal distribution of ozone and its precursors over the tropical Indian region using regional chemistry-transport model’, *J. Geophys. Res.*, **113**(D21).
- Scheel, H., Brunke, E. G. and Seiler, W. [1990], ‘Trace gas measurements at the monitoring station Cape Point, South Africa, between 1978 and 1988’, *J. Atmos. Chem.*, **11**, 197–210.
- Scheel, H., Sladkovic, R. and Brunke, E. G. [2001], ‘Temporal variations of O₃ and CO at mid-latitude sites in the northern and southern hemispheres, In: Extended Abstracts of Papers Presented at the WMO-IGAC Conference on the Measurement and Assessment of Atmospheric Composition Change, Beijing, China, WMO/TD-NO’.
- Seiler, W. [1974], ‘The cycle of atmospheric CO’, *Tellus*, **26**, 116–135.
- Seiler, W. and Junge, C. [1970], ‘Carbon monoxide in the atmosphere’, *J. Geophys. Res.*, **75**, 2217–2226.
- Shindell, D. T., Faluvegi, G., Stevenson, D. S., Krol, M. C., Emmons, L. K., Lamarque, J.-F., Ptron, G., Dentener, F. J., Ellingsen, K., Schultz, M. G., Wild, O., Amann, M., Atherton, C. S., Bergmann, D. J., Bey, I., Butler, T., Cofala, J., Collins, W. J., Derwent, R. G., Doherty, R. M., Drevet, J., Eskes, H. J., Fiore, A. M., Gauss, M., Hauglustaine, D. A., Horowitz, L. W., Isaksen, I. S. A., Lawrence, M. G., Montanaro, V., Mller, J.-F., Pitari, G., Prather, M. J., Pyle, J. A., Rast, S., Rodriguez, J. M., Sanderson, M. G., Savage, N. H., Strahan, S. E., Sudo, K., Szopa, S., Unger, N., van Noije, T. P. C. and Zeng, G. [2006], ‘Multimodel simulations of carbon monoxide: Comparison with observations and projected near-future changes’, *J. Geophys. Res.*, **111**(D19), D19.1–D19.24.

- Simmonds, P. G., Manning, A. J., Derwent, R. G., Ciais, P., Ramonet, M., Kazan, V. and Ryall, D. [2005], ‘A burning question. Can recent growth rate anomalies in the greenhouse gases be attributed to large scale biomass burning events?’, *Atmos. Env.*, **39**, 2513–2517.
- Singer, S. F. [1970], ‘Global Effects of Environmental Pollution’, American Association for the Advancement of Science.
- Singh, R. P., Dey, S., Tripathi, S. N., Tare, V. and Holben, B. [2004], ‘Variability of aerosol parameters over Kanpur, northern India’, *J. Geophys. Res.*, **109**(D23), D23.1–D23.14.
- Solomon, S., Qin, D., Manning, M., Chen, Z., Marquis, M., Averyt, K. B., Tignor, M. and Miller, H. L. [2007], ‘Climate Change 2007: The Physical Science Basis. Contribution of Working Group I to the Fourth Assessment Report of the Intergovernmental Panel on Climate Change’.
- Stephens, G. L. [1994], *Remote Sensing of the Lower Atmosphere - An Introduction*, Oxford University Press.
- Stockwell, D. Z. and Chipperfield, M. P. [1999], ‘A tropospheric chemical transport model: Development and validation of the model transport schemes’, *Q. J. R. Meteorol. Soc.*, **125**, 1747–1783.
- Streets, D., Bond, T. C., Carmichael, G. R., Fernandes, S. D., Fu, Q., He, D., Klimont, Z., Nelson, S. M., Tsai, N. Y., Wang, M. Q., Woo, J.-H. and Yarber, K. F. [2003], ‘An inventory of gaseous and primary aerosol emissions in Asia in the Year 2000’, *J. Geophys. Res.*, **108**(D21), D21.1–D21.23.
- Talbot, R. W., Dibb, J. E., Lefer, B. L., Bradshaw, J. D., Sandholm, S. T., Blake, D. R., Blake, N. J., Sachse, G. W., Collins, J. E., Heikes, B. G., Merrill, J. T., Gregory, G. L., Anderson, B. E., Singh, H. B., Thornton, D. C., Bandy, A. R. and Poeschel, R. F. [1997], ‘Chemical characteristics of continental outflow from Asia to the troposphere over the western Pacific Ocean during February–March 1994: Results from PEM-West B’, *J. Geophys. Res.*, **102**(D23), 28255–28274.
- Taylor, F. W. [1983], *Pressure modulator radiometry. Spectroscopic Techniques*, G. A. Vanasse, Ed., Academic Press.

- Tripathi, S. N., Tare, V., Chinnam, N., Srivastava, A. K., Dey, S., Agarwal, A., Kishore, S., Lal, R. B., Manar, M., Kanawade, V., Chauhan, S. S. S., Sharma, M., Reddy, R. R., Gopal, K. R., Narasimhulu, K., Reddy, L., Gupta, S. and Lal, S. [2006], 'Measurement of atmospheric parameters during ISRO-GBP Land Campaign II at a typical location in Ganga Basin: Part-I-Physical and optical properties', *J. Geophys. Res.*, **111**(D23).
- Van der Werf, G. R., Randerson, J. T., Giglio, L., Collatz, G. J. and P. S. Kasibhatla, A. A. F. A. J. [2006], 'Interannual variability in global biomass burning emissions from 1997 to 2004', *Atmos. Chem. Phys.*, **6**, 3423–3441.
- Wang, J., Gille, J. C., Bailey, P. L., Pan, L., Edwards, D. and Drummond, J. R. [1999], 'Retrieval of Tropospheric Carbon Monoxide Profiles from High-Resolution Interferometer Observations: A New Digital Gas Correlation (DGC) Method and Applications', *J. Atmos. Sci.*, **56**, 219–232.
- Wang, Y., Jacob, D. and Logan, J. [1998], 'Global simulation of tropospheric O₃-NO_x-hydrocarbon chemistry, 1. Model formulation', *J. Geophys. Res.*, **103**(D09), 10713–10725.
- Wang, Y. X., McElroy, M. B., Wang, T. and Palmer, P. I. [2004], 'Asian emissions of CO and NO_x: Constraints from aircraft and Chinese station data', *J. Geophys. Res.*, **109**(D24), D24.1–D24.26.
- Warneck, P. [1988], 'Chemistry of the Natural Atmosphere', Academic Press, San Diego.
- Warner, J., Gille, J., Edwards, D. P., Ziskin, D., Smith, M., Bailey, P. and Rokke, L. [2001], 'Cloud detection and clearing for the Earth Observing System Terra satellite Measurements of Pollution in the Troposphere (MOPITT) experiment', *Appl. Opt.*, **40**(8), 1269–1284.
- Wayne, R. P. [1991], 'Chemistry of the Atmospheres', Second Edition, Clarendon Press, Oxford.
- Wilber, A. C., Kratz, D. P. and Gupta, S. K. [1999], 'Surface emissivity maps for use in satellite retrievals of longwave radiation, NASA Tech', Pap. 1999-209362.

- WMO [2003], 'Scientific assessment of ozone depletion:2002', Global Ozone Research and Monitoring Project Report No. 47.
- WMO [March 2009], 'WDCGG Data Summary No. 33, Global Atmosphere Watch data Volume IV - Greenhouse Gases and Other Atmospheric Gases'.
- Wofsy, S. C. [1976], 'Interaction of CH₄ and CO in the Earth's atmosphere', *Annual Rev. Earth Pl. Sc.*, **4**, 441–468.
- Yurganov, L. [1993], 'Long-term variations of some tropospheric trace gases in the 1980s: an influence of stratospheric ozone', *J. Ecol. Chem.*, **4**, 274–278.
- Zander, R., Demoulin, P., Ehhalt, D., Schmidt, U. and Rinsland, C. [1989], 'Secular increase of total column abundance of carbon monoxide above central Europe since 1950', *J. Geophys. Res.*, **94**, 11021–11028.